ASSESSMENT MODELS IN SUPPORT OF THE HAZARD ASSESSMENT HANDBOOK

ARTHUR D. LITTLE, INCORPORATED

PREPARED FOR
COAST GUARD

JANUARY 1974

The work reported herein was accomplished for the U. S. Coast Guard's Office of Research and Development, Marine Safety Technology Division, as part of its program in Cargo Safety Technology.

The contents of this report reflect the views of the author(s) who are responsible for the facts and the accuracy of the data presented herein. The contents do not necessarily reflect the official views or policy of the Coast Guard. This report does not constitute a standard, specification, or regulation.

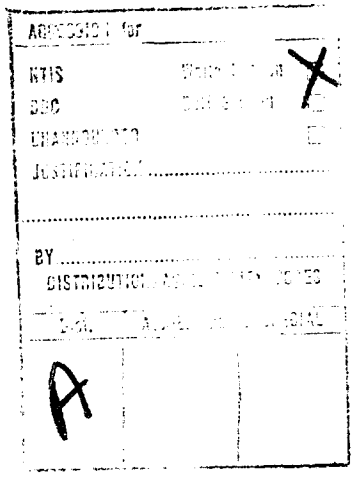

Reviewed By: J. M. CECE,
Project Officer

Submitted By: E. L. JONES, CDR, USCG
Chief, Marine Safety Projects Branch

Released By: C. J. GLASS, CAPT, USCG
Chief, Marine Safety Technology Division
Office of Research and Development
U. S. Coast Guard Headquarters
Washington, D. C. 20590

TECHNICAL REPORT STANDARD TITLE PAGE

1. Report No.	2. Government Accession No.	3. Recipient's Catalog No.
CG-D-65-74		AD-776617

4. Title and Subtitle	5. Report Date
Assessment Models in Support of the Hazard Assessment Handbook	January 1974
	6. Performing Organization Code
7. Author(s)	8. Performing Organization Report No.
Phani P. K. Raj and Ashok S. Kalelkar	74685-40
9. Performing Organization Name and Address	10. Work Unit No.
Arthur D. Little, Inc. Acorn Park Cambridge, Mass. 02140	4151
	11. Contract or Grant No.
	DOT-CG-24,655A
12. Sponsoring Agency Name and Address	13. Type of Report and Period Covered
Department of Transportation United States Coast Guard Washington, D. C. 20590	Technical Report
	14. Sponsoring Agency Code

15. Supplementary Notes

16. Abstract

Analytical models are derived to describe the hazards caused by the accidental release of chemicals into the atmosphere or spills onto water. The models encompass a variety of physical phenomena that can occur such as dispersion of vapor in the atmosphere, dispersion of liquid in water, spreading on water, burning of a liquid pool, radiation from flame, etc. Analyses include the modeling of the phenomenon, solution to the governing equations, and detailed workings of specific examples.

17. Key Words	18. Distribution Statement
Hazard Assessment	Document is available to the public through the National Technical Information Service, Springfield, VA 22151

19. Security Classif. (of this report)	20. Security Classif. (of this page)	21. No. of Pages	22. Price
Unclassified	Unclassified	253	$6.50-1.45

Form DOT F 1700.7 (8-69)

ACKNOWLEDGMENT

The authors wish to acknowledge the contribution made by other members of the ADL staff including John Hagopian, W. David Lee and Sami Atallah who participated in the development and computerization of some of the mathematical models. We also acknowledge the contributions made by Professor Robert C. Reid of MIT in the development of several important models and for the help provided by Professor Donald R. J. Harleman of MIT in the formulation of water dispersion models.

This report has been written under the CHRIS program for which Mr. Donald S. Allan is the ADL project director. The work was performed for the Office of Research and Development, U. S. Coast Guard under the close technical supervision of LCDR John Lindak and Dr. John Cece.

TABLE OF CONTENTS

TABLE OF CONTENTS (Continued)

TABLE OF CONTENTS (Continued)

TABLE OF CONTENTS (Continued)

TABLE OF CONTENTS (Continued)

TABLE OF CONTENTS (Continued)

TABLE OF CONTENTS (Continued)

TABLE OF CONTENTS (Continued)

TABLE OF CONTENTS (Continued)

TABLE OF CONTENTS (Continued)

LIST OF FIGURES

LIST OF FIGURES (Continued)

LIST OF FIGURES (Continued)

LIST OF FIGURES (Continued)

LIST OF TABLES

LIST OF TABLES (Continued)

1.0 INTRODUCTION

This report contains details of the analytical models (and their derivations) used in the CHRIS manual 3 for assessing the hazards caused by the spill of chemicals on water. The report is presented in two parts. Part I contains those models that have been based on the existing information in the literature, while Part II contains detailed derivations for each of the models that were developed. In general, Part II contains more sophisticated information. This report also includes discussions of the applicability of each of the analytical models to the different branches of the hazard assessment events chart (Figure 1.1).

Each model is given in a separate chapter and each chapter contains the following sections.

- Aim
- Introduction
- Assumptions and Principles
- Data Required
- Details of the Model
- Computational Algorithm
- Specific Example
- Discussions
- Conclusions
- References
- List of Symbols
- Appendix

The models are explained by first giving the principle on which the derivations are based and the major physical assumptions used. A specific example of each model is then presented to highlight the calculation procedure and to indicate the order of magnitude of the numerical values obtained. All the calculations are carried out in SI* units and main results are indicated in tables and graphs. The list of symbols includes the definitions and values (or formulas) of the common symbols used in the text. In many cases the symbols are defined in the text also and their physical meanings indicated. The discussion phase includes the analysis of the assumptions and their effects on the answers and also the extent to which the results could be used with confidence to describe the real system in nature. In general, the assumptions made are such that a conservative estimate of the hazard follows from using the model.

* International System of Units.

PART I

MODELS BASED ON EXISTING INFORMATION IN THE LITERATURE

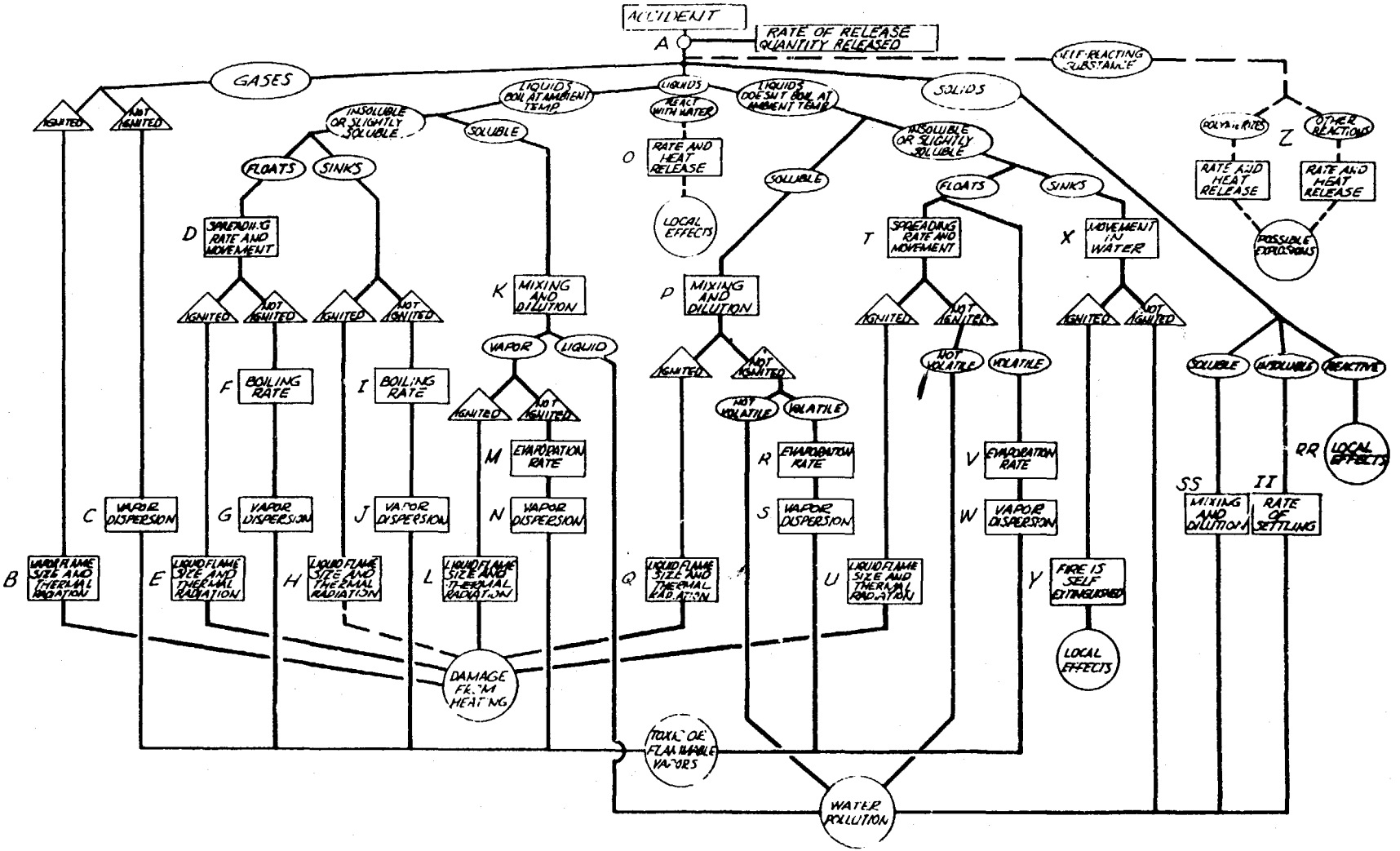

FIGURE 1.1 HAZARD ASSESSMENT TREE: (EVENTS CHART)

2.0 VENTING RATE (A)*

2.1 AIM

The aim of the derivations given below is to obtain the time history of the tank conditions and the venting rates of gas and/or liquid subsequent to a rupture in the tank wall.

2.2 INTRODUCTION

Vital information needed to evaluate consequences of the physical phenomena occurring after a spill of a chemical includes the amount of material spilled or its rate of spill. The analytical models presented here indicate the methods of calculations. The equations derived are all standard relations obtainable from any of the text books on thermodynamics. [1,2]

2.3 PRINCIPLES AND ASSUMPTIONS

Basic thermodynamic principles are used in the derivations. It is assumed that the gases behave as ideal gases and that equilibrium thermodynamic relationships are applicable. While this is true in most cases (liquid venting, slow gas venting, rupture area in the tank small compared to tank cross-sectional area), there are cases in which the dynamics of venting become as important as the thermodynamics. The latter situations occur when a highly pressurized vessel containing a cryogen suddenly bursts open. Only two tank wall thermal conditions are considered; namely, adiabatic and isothermal. It is expected that the results for other wall conditions will lie somewhere between the results obtained for adiabatic and isothermal conditions.

2.4 DATA REQUIRED

- Initial tank conditions (temperature, pressure), tank volume (and approximate geometry), and initial mass of content;
- Properties of the chemical (physical and thermodynamic); and
- Size and location of the rupture.

*Letters in the parentheses correspond to the events nomenclature provided in the "Hazard Assessment Events Chart." The models given are applicable to the events.

2.5 DETAILS OF THE MODEL:[1]*

In the derivations given below, it is assumed that the tank contains only pure vapor and pure liquid in equilibrium with each other. No other component is present.

With reference to Figure 2.1 we write the following equations.

2.5.1 Venting Rates

(1) *Liquid Venting:* Liquid is vented from the tank when the vent hole is below the liquid vapor interface; that is, liquid is vented when

$$H_L > H_h. \tag{2.1}$$

Then,

$$W_L = A_h C_d \rho_L \sqrt{2g\rho_L (H_L - H_h) + (p - p_a)2} \tag{2.2}$$

where

W_L = instantaneous liquid venting rate,

H_L = height of liquid column at that instant, and

p = tank pressure at that instant.

(2) *Gas Venting:* If the tank contains only gas, or if the vent hole is above liquid surface, only gas is vented; that is, if,

$$H_h > H_L \tag{2.3}$$

then only gas is vented.

If the pressure inside the tank is high, then it is likely that a sonic condition will occur at the hole. Then the flow is said to be "choked," and this represents the maximum flow attainable under those conditions.

Flow is said to be "choked" if,

$$\frac{p}{p_a} > \left(\frac{k+1}{2}\right)^{\frac{k}{k-1}} \tag{2.4a}$$

*Number in the parentheses used as superscripts refer to the references given at the end of each section.

Then flow rate is:

$$W_v = A_h \frac{c\ p}{\sqrt{T}} \tag{2.5a}$$

where

$$c = C_d \sqrt{\frac{k}{R_v}\left[\frac{2}{k+1}\right]^{\frac{k+1}{k-1}}}$$

If the *flow* is not *choked*, i.e., if

$$\frac{p}{p_a} \leq \left(\frac{k+1}{2}\right)^{\frac{k}{k-1}} \tag{2.4b}$$

then

$$W_v = A_h C_d Y \sqrt{2\left(p - p_a\right)\rho_v} \tag{2.5b}$$

where

$$Y = \sqrt{\left(\frac{p_a}{p}\right)^{\frac{2}{k}}\left(\frac{k}{k-1}\right)\left[\frac{1-(p_a/p)^{\frac{k-1}{k}}}{1-(p_a/p)}\right]}$$

The venting rates can be calculated from Eq. (2.2) or (2.5) if the tank conditions are known.

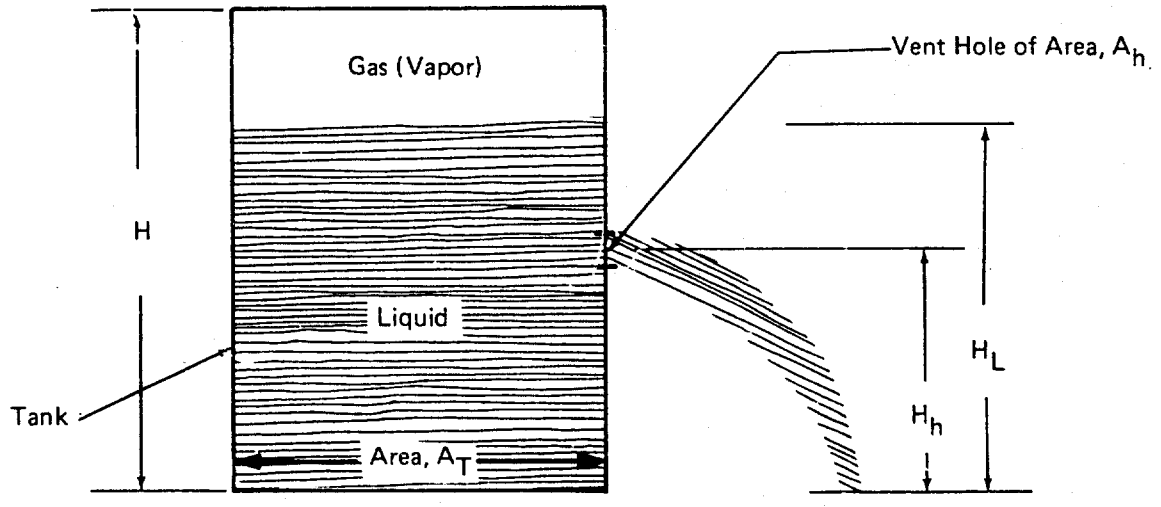

FIGURE 2.1 SCHEMATIC DIAGRAM OF THE TANK WITH A VENT HOLE ON THE SIDE WALL

2.5.2 Relationships Among the Thermodynamic Properties of the Substance in the Tank

(1) *Pressure-Temperature Relationships:* If all the mass in the tank were in the form of vapor, then:

$$P = \frac{m}{V} R_V T \tag{2.6}$$

However, if liquid is present in the tank, then:

$$P = P_{sat}(T) = a\, e^{-\frac{b}{T}} \tag{2.7}$$

If liquid is present in the tank, then the following inequality is satisfied:

$$\frac{m}{V} R_V T > P_{sat}(T) \tag{2.8}$$

(2) *Vapor Weight Fraction:*

$$\rho_V = \frac{P}{R_V T} \tag{2.9a}$$

Now

$$V = \frac{m}{\rho_L}(1-X) + \frac{m}{\rho_V} X \tag{2.9b}$$

hence

$$X = \frac{\left(\frac{V}{m} - \frac{1}{\rho_L}\right)}{\left(\frac{1}{\rho_V} - \frac{1}{\rho_L}\right)} \tag{2.9c}$$

X = 1 means that the tank contains only gas.

(3) *Vapor Fraction-Temperature-Pressure Relationship* (Energy equation)

—: Adiabatic Tank Wall: —

If the tank is adiabatic and the tank contains only gas (X = 1), then

$$\frac{T}{T_i} = \left(\frac{P}{P_i}\right)^{\frac{k}{k-1}} \tag{2.10a}$$

If the tank *contains liquid,* but the *gas is vented,* then it can be shown by simply using the energy conservation law that:

$$m(T_i - T)\left(X\, c_{pg} + (1-X)c_L\right) = \lambda\left[m_i(1-X_i) - m(1-X)\right] + V(P_i - P) \tag{2.10b}$$

and if *liquid only is vented:*

$$m(T_i - T)\left(X c_{pg} + (1-X)c_L\right) = \lambda\left(mX - m_i X_i\right) + V(P_i - P) \tag{2.10c}$$

—; Isothermal Tank Wall: —

When the wall is maintained at constant temperature (at T_i), the pressure inside the tank is a constant at the saturated pressure (see Eq. (2.7)) if there is liquid present. In the absence of liquid, the pressure decreases with venting because of mass loss and can be calculated using Eq. (2.6).

2.6 ALGORITHM FOR COMPUTATION

Given the initial tank conditions, such as the initial mass m_i, temperature T_i, pressure P_i, the information on the presence of liquid, and the geometric conditions such as the tank volume, wall thermal property, and the size and location of the vent hole, it is desired to calculate at any instant:

a) The phase which is being vented;

b) The rate of venting;

c) The thermodynamic conditions of the tank (pressure, temperature, mass fraction of vapor, etc.); and

d) The total mass of material vented up to that instant.

The flow chart given in Figure 2.2 illustrates the algorithm for calculations. A computer program can also be written, based on Figure 2.2.

2.7 SPECIFIC EXAMPLE

Tank Dimensions:

Tank volume, $V = 1250\ m^3$

Tank cross-sectional area, $A_T = 250\ m^3$

$\therefore$ Tank height, $H = 5m$

Hole area, $A_h = 6.5 \times 10^{-3}\ m^2$ ($65\ cm^2$)

Height of hole on the side wall, $H_h = 2\ m$

Coefficient of discharge, $C_d = 0.8$

Tank Conditions:

Material in the tank = liquid natural gas

Initial pressure, $p_i = 220\ kN/m^2$

Initial temperature, $T_i = 122\ °K$

Initial mass, $m_i = 510 \times 10^3\ kg$

Properties:

Liquid density, $\rho_L = 425\ kg/m^3$

Specific heat of liquid, $C_{pL} = 4.186\ kJ/kg\ °K$

Specific heat of vapor, $C_{pg} = 2.344\ kJ/kg\ °K$

Molecular weight of LNG, $M = 17.05\ kg/kmole$

Specific heat ratio of vapor, $k = 1.305$

Gas constant for natural gas, $R_v = 489.1\ J/kg\ °K$

Latent heat of vaporization, $\lambda = 510.79\ kJ/kg$

Atmospheric pressure, $p_a = 101.325\ kN/m^2$

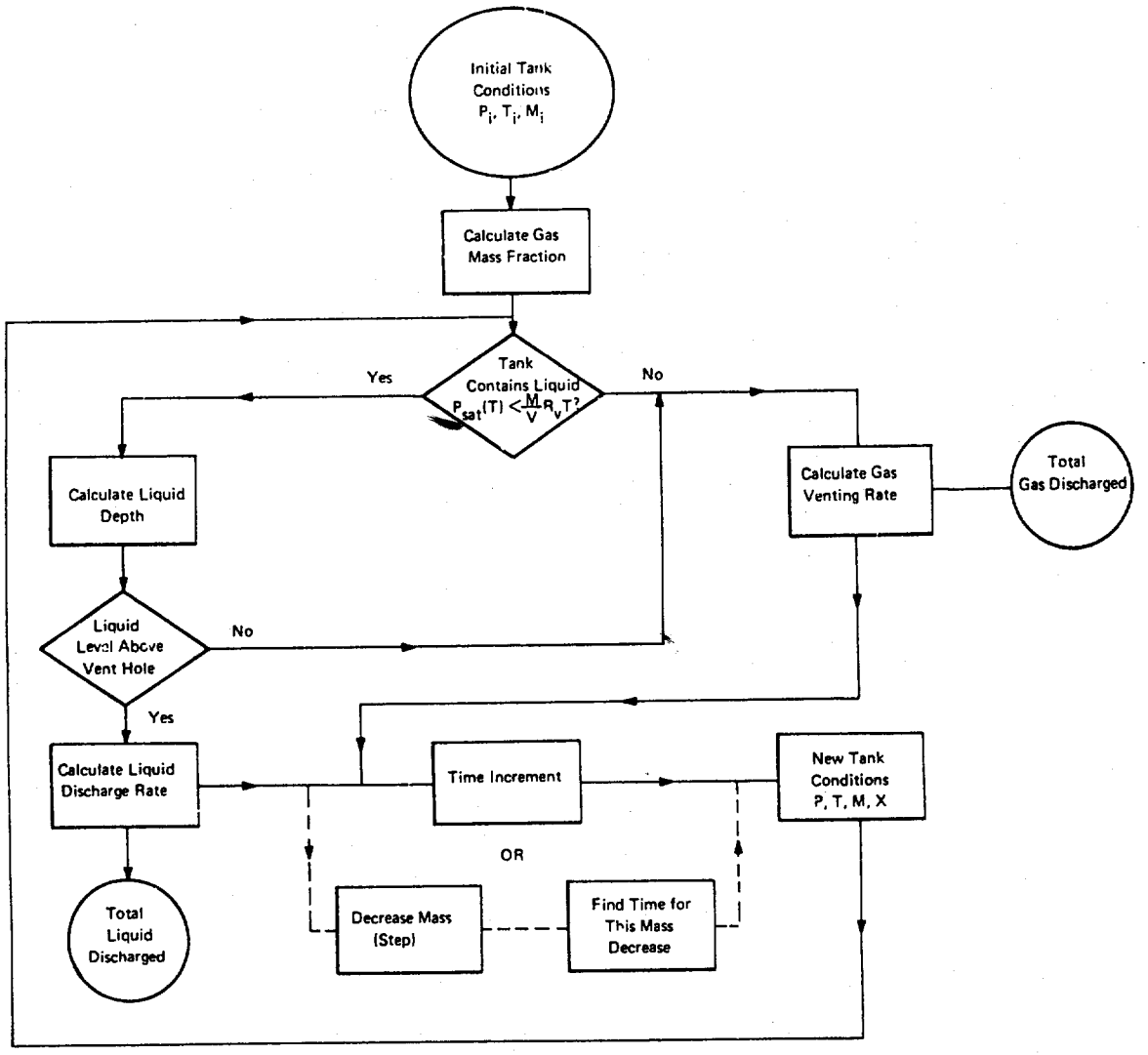

FIGURE 2.2 FLOW DIAGRAM FOR CALCULATION OF DISCHARGE RATE FOR VENTING FROM A TANK

Calculations:

Initial vapor density $\rho_{i,v} = \dfrac{p_i}{R_v T_i} = 3.687$ kg/m³

Now: $\dfrac{m_i}{V} R_v T_i = 24345.4$ kN/m²

Since this pressure is far in excess of the saturated liquid pressure at 122°K, we can say with certainty that there is liquid present in the tank. From Eq. (2.9):

Initial vapor mass fraction =

$$X_i = \frac{\left(\frac{v}{m} - \frac{1}{\rho_L}\right)}{\left(\frac{1}{\rho_v} - \frac{1}{\rho_L}\right)} = 3.61 \times 10^{-4}$$

Venting rates:

For hole at the top of the tank gas is vented

$$p/p_a = 2.171;$$

Also $\left[\dfrac{k+1}{2}\right]^{\left(\frac{k}{k-1}\right)} = 1.835$

Hence, from Eq. (2.4a), flow is "choked":

$$c = 0.8\sqrt{\frac{1.305}{489.1} \times \left(\frac{2}{2.305}\right)^{\frac{2.305}{0.305}}} = 0.02417$$

Initial gas discharge rate:

$$W_v = \frac{6.5 \times 10^{-3} \times 0.02417 \times 220 \times 10^3}{\sqrt{122}} = 3.13 \text{ kg/s}$$

If the wall is *isothermal,* the same discharge rate is maintained until all the liquid has been vaporized and only gas remains in the tank. This requires about 45¼ hours.

If the wall is *adiabatic* and time step increments are used for calculations, then (first, the mass in the tank at the end of the time step is calculated as follows):

Time step = 5 minutes, for example

$\therefore$ mass in the tank at the end of one time step = m

$$m = m_i - W_v \times (5 \times 60)$$

$$= 509.061 \times 10^{-3} \text{ kg}$$

Now an iterative procedure is used to find the tank condition. The steps are illustrated below:

i) First, a liquid temperature is assumed, say, $T = T_i - 5°K$;

ii) Saturation pressure is calculated from Eq. (2.7);

iii) Vapor density, and hence vapor mass fraction, is calculated from Eq. (2.9);

iv) These are substituted in Eq. (2.10b) and T is then calculated;

v) The calculated T and assumed T in (i) are compared;

vi) If the absolute difference between the above values is greater than a preset error limit (say, 1% of the calculated value), a mean temperature between assumed and calculating value is used and steps i through vi repeated until proper convergence is achieved.

The results of the calculations so done for adiabatic tank conditions for three positions of the hole are shown in Tables 2.1a, 2.1b, and 2.1c and are plotted in Figures 2.3a, 2.3b, and 2.3c, respectively. Results of similar calculations performed with isothermal conditions are given in Tables 2.2a, 2.2b, and 2.2c and are shown plotted in Figures 2.3a, 2.3b, and 2.3c, respectively.

2.8 DISCUSSIONS

It is seen that when liquid is present in the tank the tank pressure and temperature are uniquely related (by the Clausius-Clayperon equation). Also most of the mass in the tank is present in the liquid phase for tank pressures far below the critical pressure. This is because of the relatively large density of liquid compared to the vapor density. For the same reason the mass vented is relatively large when a liquid leaks as compared to a gas leak. Also it is seen that the tank wall condition has a relatively small effect on the liquid venting, but has considerable influence on the gas venting rate. An adiabatic walled tank with a puncture hole in the vapor volume area presents the least hazard among all the possible hazards.

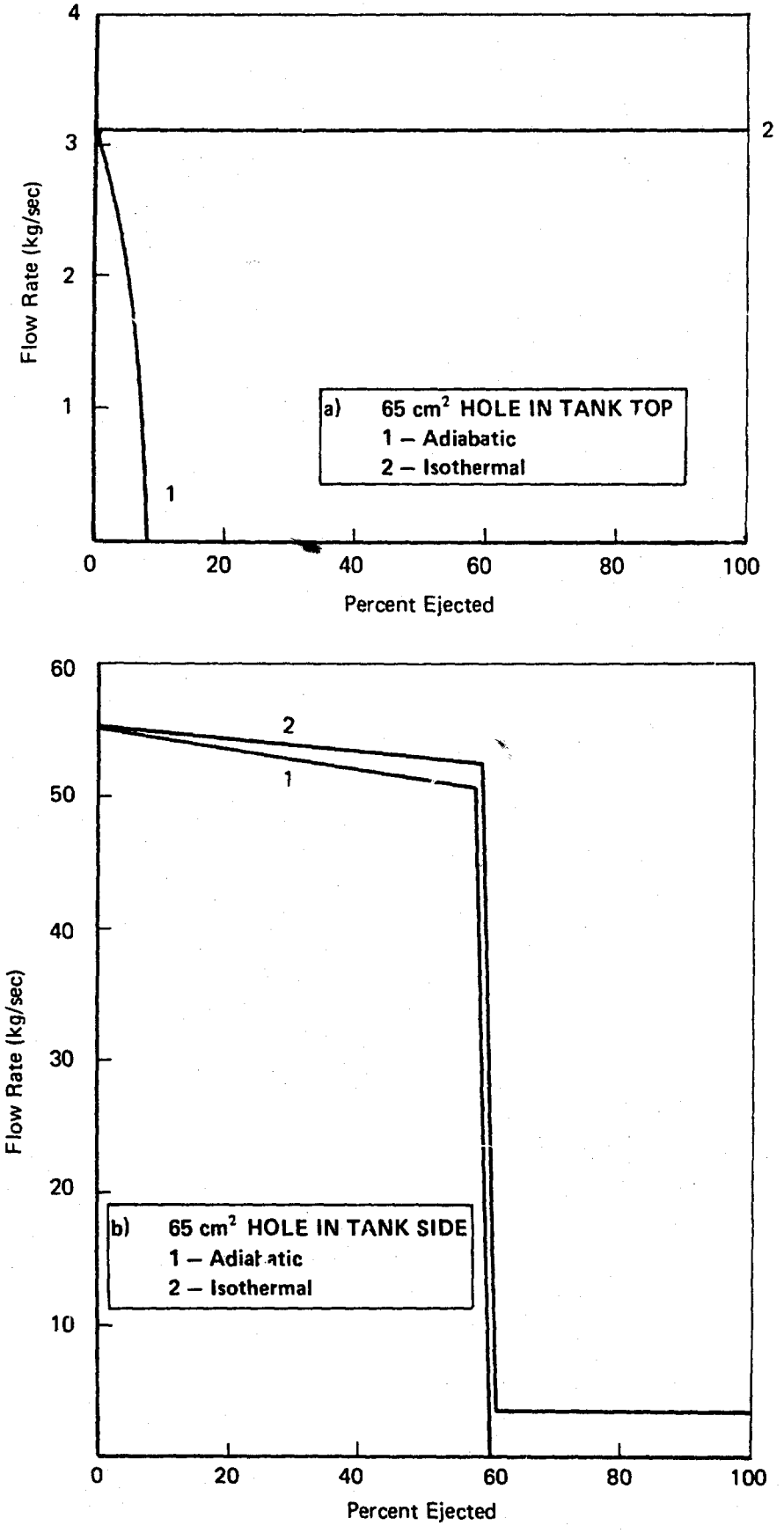

FIGURE 2.3 VENTING RATE AS A FUNCTION OF TIME FOR ISOTHERMAL AND ADIABATIC TANK WALL CONDITIONS FOR THREE POSITIONS OF A 65-cm² HOLE IN THE TANK

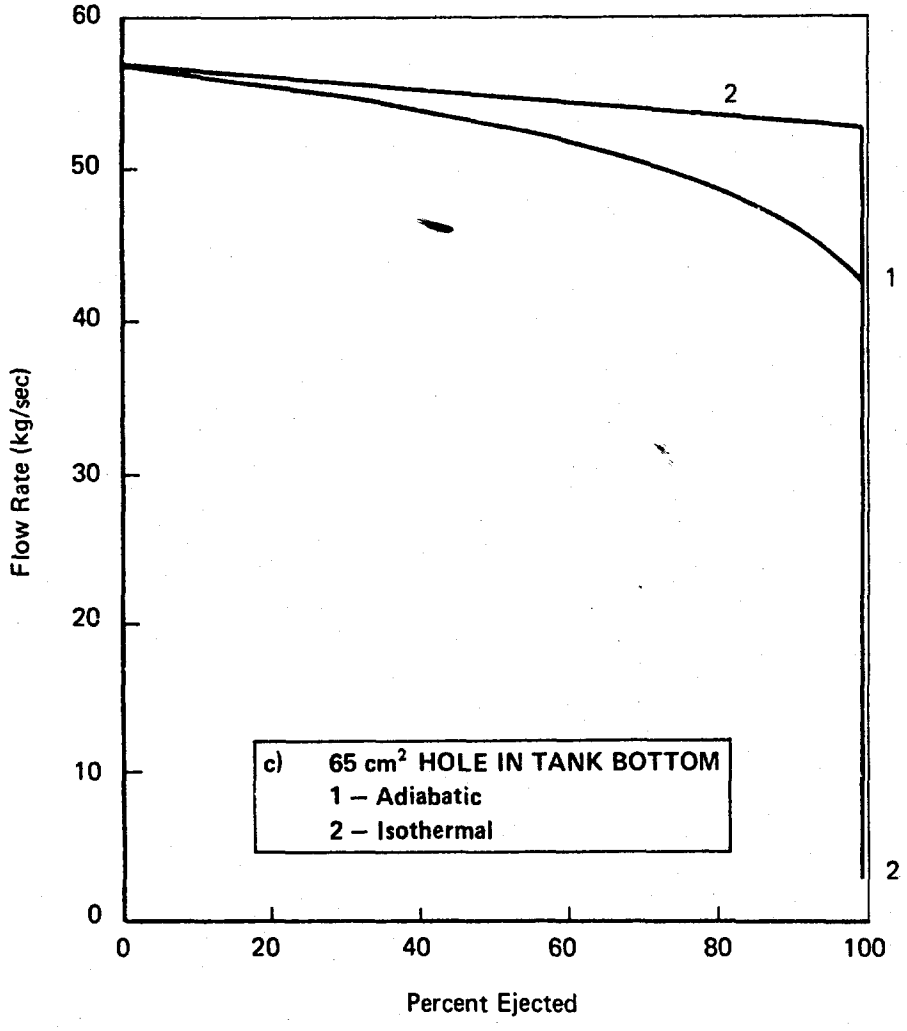

FIGURE 2.3 VENTING RATE AS A FUNCTION OF TIME FOR ISOTHERMAL AND ADIABATIC TANK WALL CONDITIONS FOR THREE POSITIONS OF A 65-cm^2 HOLE IN THE TANK

The primary limitation of the model presented lies in the assumption of thermodynamic equilibrium at all times. This is hardly true in cases where the contents of a tank are spilled in a relatively short time (as can occur in a sudden rupture), or when a cryogenic liquid flashes, caused by the sudden release of pressure. In both cases the dynamics of emptying are almost (in some cases, more) as important as the thermodynamics involved. The model was also predicated on the position of the hole relative to the ground level (or sea level) remaining fixed. This condition may not always exist (say, in the case in which a barge tilts after a collision).

The model presented, however, is useful in predicting, as a first approximation, the liquid or gaseous discharge of hazardous cargo. These calculations are useful in predicting further effects of such a discharge.

2.9 CONCLUSIONS

A method of calculating the time history of the venting rates and tank conditions has been given. Applicability of thermodynamic relations (local thermodynamic equilibrium) is assumed. A brief algorithm and a specific example are given to illustrate the method of calculation. The limitations of the method due to the omission of non-equilibrium processes and those governed by the dynamics of rupture are discussed.

2.10 REFERENCES

1) Zemanaky, M. W., "Heat and Thermodynamics"; 4th edition; McGraw-Hill Co., N.Y. 1957.

2) Keenan, J. H. "Thermodynamics," MIT Press, Cambridge, Mass., March 1970.

2.11 NOMENCLATURE

Symbol	Description	Value	Units
a	= constant in the Clausius-Clayperon equation (2.7) for saturated vapor pressure		N/m^2
A_T	= tank cross-sectional area		m^2
A_h	= area of vent hole		m^2
b	= constant in Clausius-Clayperon equation (2.7)		°K
C_d	= coefficient of discharge of the vent		

Symbol	Description	Value	Units
C_{pg}	= specific heat at constant pressure of gas (vapor)		J/kg °K
C_L	= specific heat at constant pressure of liquid		J/kg °K
g	= acceleration due to gravity	9.81	m/s^2
k	= specific heat ratio for the vapor		
M	= molecular weight of the substance		kg/kmole
p	= pressure in the tank		N/m^2
p_a	= atmospheric pressure	$101.325 \times 10^{+3}$	N/m^2
$p_{sat}(T)$	= saturated vapor pressure at temperature, T		N/m^2
R	= universal gas constant	8.314×10^{-3}	J/kmole °K
R_v	= vapor gas constant		J/kg °K
T	= temperature inside the tank		°K
V	= volume of tank		m^3
W	= mass flow rate from vent hole		kg/s
X	= mass fraction of vapors in the tank		
ρ	= density of material		kg/m^3
λ	= latent heat of vaporization of liquid		J/kg

Subscripts

i	= initial condition
L	= liquid
v	= vapor
h	= hole

TABLE 2.1a

ADIABATIC
(65 cm^2 Hole in the Tank Top)

% Original Mass Released	Physical State of Venting Material	Vapor Fraction in the Tank	Temperature (°K)	Pressure (kN/m^2)	Flow Rates (kg/sec)	Time (min)
1	Vapor	.000428	121.0	203.7	2.88	27.5
2	Vapor	.000477	119.7	186.5	2.65	57.0
3	Vapor	.000516	118.4	170.1	2.42	89.1
4	Vapor	.000546	117.1	154.9	2.17	124.2
5	Vapor	.000568	115.9	140.5	1.89	163.3
6	Vapor	.000582	114.5	127.1	1.55	208.4
7	Vapor	.000589	113.2	114.5	1.13	263.1
8	Vapor	.000589	111.9	102.8	.38	338.3

TABLE 2.1b

ADIABATIC VENTING
(65 cm^2 Hole in the Tank Side)

% Original Mass Released	Physical State of Venting Material	Vapor Fraction in the Tank	Temperature (°K)	Pressure (kN/m^2)	Flow Rates (kg/sec)	Time (min)
1	Liquid	.000461	122.2	221.6	55.03	1.6
10	Liquid	.001383	122.1	220.3	54.37	15.5
20	Liquid	.002638	122.0	218.9	53.63	31.3
30	Liquid	.004237	121.9	217.4	52.88	47.2
40	Liquid	.006352	121.8	215.0	52.12	63.4
50	Liquid	.009271	121.7	214.0	51.23	79.8
60	Vapor	.007733	113.0	112.3	1.03	172.5

TABLE 2.1c

ADIABATIC VENTING
(65 cm^2 Hole in the Tank Bottom)

% Original Mass Released	Physical State of Venting Material	Vapor Fraction in the Tank	Temperature (°K)	Pressure (kN/m^2)	Flow Rates (kg/sec)	Time (min)
1	Liquid	.000461	122.2	221.6	56.7	1.5
10	Liquid	.001383	122.1	220.3	56.1	15.1
20	Liquid	.002638	122.0	218.9	55.4	30.3
30	Liquid	.004237	121.9	217.4	54.7	45.7
40	Liquid	.006352	121.8	216.0	53.9	61.4
50	Liquid	.009271	121.7	214.0	53.1	77.2
60	Liquid	.013485	121.4	209.7	51.7	93.5
70	Liquid	.020413	121.1	205.5	50.3	110.1
80	Liquid	.034043	120.8	200.8	48.7	127.2
90	Liquid	.073632	120.2	193.3	46.4	145.0
99	Liquid	.762036	119.3	181.2	42.9	162.0

TABLE 2.2a

ISOTHERMAL VENTING
(65 cm^2 Hole in the Tank Top)

% Original Mass Released	Physical State of Venting Material	Vapor Fraction in the Tank	Temperature (°K)	Pressure (kN/m^2)	Flow Rates (kg/sec)	Time (min)
1	Vapor	.000461	122.2	221.8	3.12	27.5
10	Vapor	.000139	122.2	221.8	3.12	272.6
20	Vapor	.000267	122.2	221.8	3.12	545.1
30	Vapor	.000431	122.2	221.8	3.12	817.5
40	Vapor	.000650	122.2	221.8	3.12	1089.9
50	Vapor	.009572	122.2	221.8	3.12	1362.3
60	Vapor	.014173	122.2	221.8	3.12	1634.7
70	Vapor	.021843	122.2	221.8	3.12	1907.1
80	Vapor	.037183	122.2	221.8	3.12	2179.5
90	Vapor	.083202	122.2	221.8	3.12	2451.9
99	Vapor	.911780	122.2	221.8	3.12	2697.1

TABLE 2.2b

ISOTHERMAL VENTING
(65 cm^2 Hole in the Tank Side)

% Original Mass Released	Physical State of Venting Material	Vapor Fraction in the Tank	Temperature (°K)	Pressure (kN/m^2)	Flow Rates (kg/sec)	Time (min)
1	Liquid	.000461	122.2	221.8	55.1	1.6
10	Liquid	.001391	122.2	221.8	54.7	15.5
20	Liquid	.002669	122.2	221.8	54.3	31.1
30	Liquid	.004312	122.2	221.8	53.8	46.8
40	Liquid	.006504	122.2	221.8	53.4	62.7
50	Liquid	.009572	122.2	221.8	53.0	78.6
60	Vapor	.014173	122.2	221.8	3.12	146.0
70	Vapor	.021843	122.2	221.8	3.12	418.4
90	Vapor	.037183	122.2	221.8	3.12	690.8
99	Vapor	.911780	122.2	221.8	3.12	1208.4

TABLE 2.2c

ISOTHERMAL VENTING
(65 cm^2 Hole in the Tank Bottom)

% Original Mass Released	Physical State of Venting Material	Vapor Fraction in the Tank	Temperature (°K)	Pressure (kN/m^2)	Flow Rates (kg/sec)	Time (min
1	Liquid	.000461	122.2	221.8	56.77	1.5
10	Liquid	.001391	122.2	221.8	56.40	15.0
20	Liquid	.002669	122.2	221.8	55.99	30.1
30	Liquid	.004312	122.2	221.8	55.58	45.4
40	Liquid	.006504	122.2	221.8	55.16	60.7
50	Liquid	.009572	122.2	221.8	54.73	76.2
60	Liquid	.014173	122.2	221.8	54.31	91.8
70	Liquid	.021843	122.2	221.8	53.88	107.5
80	Liquid	.037183	122.2	221.8	53.41	123.3
90	Liquid	.083202	122.2	221.8	53.01	139.3
99	Liquid	.911780	122.2	221.8	3.12	153.8

3.0 SPREADING OF A LIQUID ON WATER (T)

3.1 AIM

The aim of the model presented in this section is to obtain the extent of spread and mean thickness of film at any given time after the spill of a certain amount of liquid.

3.2 INTRODUCTION

It is well known that when a water-immiscible, lighter-than-water liquid is spilled on the surface of a water body, it starts to spread. This spreading is caused in the initial stages by the hydrostatic pressure difference between the water and liquid. When the liquid has spread to form a thin film, the spreading thereafter is mainly caused by surface tension.

Abbot[1], Hoult and Suchon[2], Fay[3], and Fannelop and Waldman[4] have all developed theories to explain oil spreading on water, and all of their theories are based on considerations of equilibria between the spreading and resisting forces. The model presented here follows from the work of Fannelop and Waldman. The equations describe the spreading of a highly viscous liquid (such as crude oil) on a water surface. The model does not include the effects of either heat transfer or dissolution. Spread models for very low viscosity fluids and those incorporating the effects of heat transfer and mass loss by dissolution are given in Part II of this report.

3.3 ASSUMPTIONS

The principal assumption on which this model is based is that all of the liquid is spilled in a very short time ["instantaneously"]. The properties of the spreading liquid and the total mass of the liquid in the "slick" are assumed to be constant during the spread. The derivations are based on the principle of balancing a spreading force and a resisting force.

3.4 DATA REQUIRED

- Quantity (volume or mass) of liquid spilled on the water surface;
- Physical properties of the liquid and water.

3.5 MODEL

The physical processes involved in spreading are elegantly illustrated by Fay[5]. The following results are taken from the paper of Fannelop and Waldman[4]. The durations for which the spreading is in various regimes and the equations that apply are summarized in Tables 3.1 and 3.2.* The results in Table 3.2 are non-dimensional representations of the results in Table 3.1. Generally $1500 \leqslant \Gamma_w \leqslant 15{,}000$ and $10 \leqslant \Sigma_w \leqslant 50$ based on a 10,000-ton maximum spill.

*List of symbols is given at the end of the Section.

Figure 3.1 is a plot of the equations in Table 3.2 for the radial spread case, within the ranges of the Γ_w and Σ_w indicated.

3.6 ALGORITHM FOR COMPUTATION

Since the formulas are simple, the calculation procedure is straightforward. For any given time, first, the regime of spread is determined and, with the suitable formula, the extent of spread is then calculated. A flow chart illustrating the procedure is given in Figure 3.2.

3.7 SPECIFIC EXAMPLE

To illustrate the calculation procedure and to indicate the order of magnitude of the numbers involved, the following example has been worked out.

Liquid spilled = heavy crude oil
Mass of spill, m = 5000 metric tons
Density of oil, ρ_L = 950 kg/m^3
Viscosity of oil, μ_L = 0.1 N s/m^2
Surface tension, σ_L = 0.03 N/m
Density of water, ρ_w = 1000 kg/m^3
Viscosity of water (18°C), $\mu_w = 10^{-6}$ N s/m^2
Kinematic viscosity of water, $\nu_w = 1 \times 10^{-6}$. m^2/s

It is to be noted that $\mu_L \gg \mu_w$ and $\rho_L < \rho_w$. Let us assume that the spill occurs in a channel; hence one-dimenstional spread.

Width of channel (assumed), W = 500 m.

Description	Formula	Symbol	Value
Volume of spill	$= m/\rho_L$	$= V$	5263.15 m^3
Effective gravity	$= g\left(1-\frac{\rho_L}{\rho_w}\right)$	$= G$	0.49 m/s^2
Characteristic initial volume per unit channel width	$= V/2W$	$= A$	5.263 m^2
First critical time (for changeover from gravity-inertia to gravity-viscous regime)	$= \left[\frac{A^4}{G^2 \nu_w^3}\right]^{\frac{1}{7}}$	$= t_1$	1180.55 s
Second critical time (for changeover from gravity-viscous regime to viscous-surface tension regime)	$= 0.989\left[\frac{G^{\frac{1}{2}} \nu_w^{\frac{1}{4}} A \rho_w}{\sigma}\right]^{\frac{4}{3}}$	$= t_2$	60395.13 s

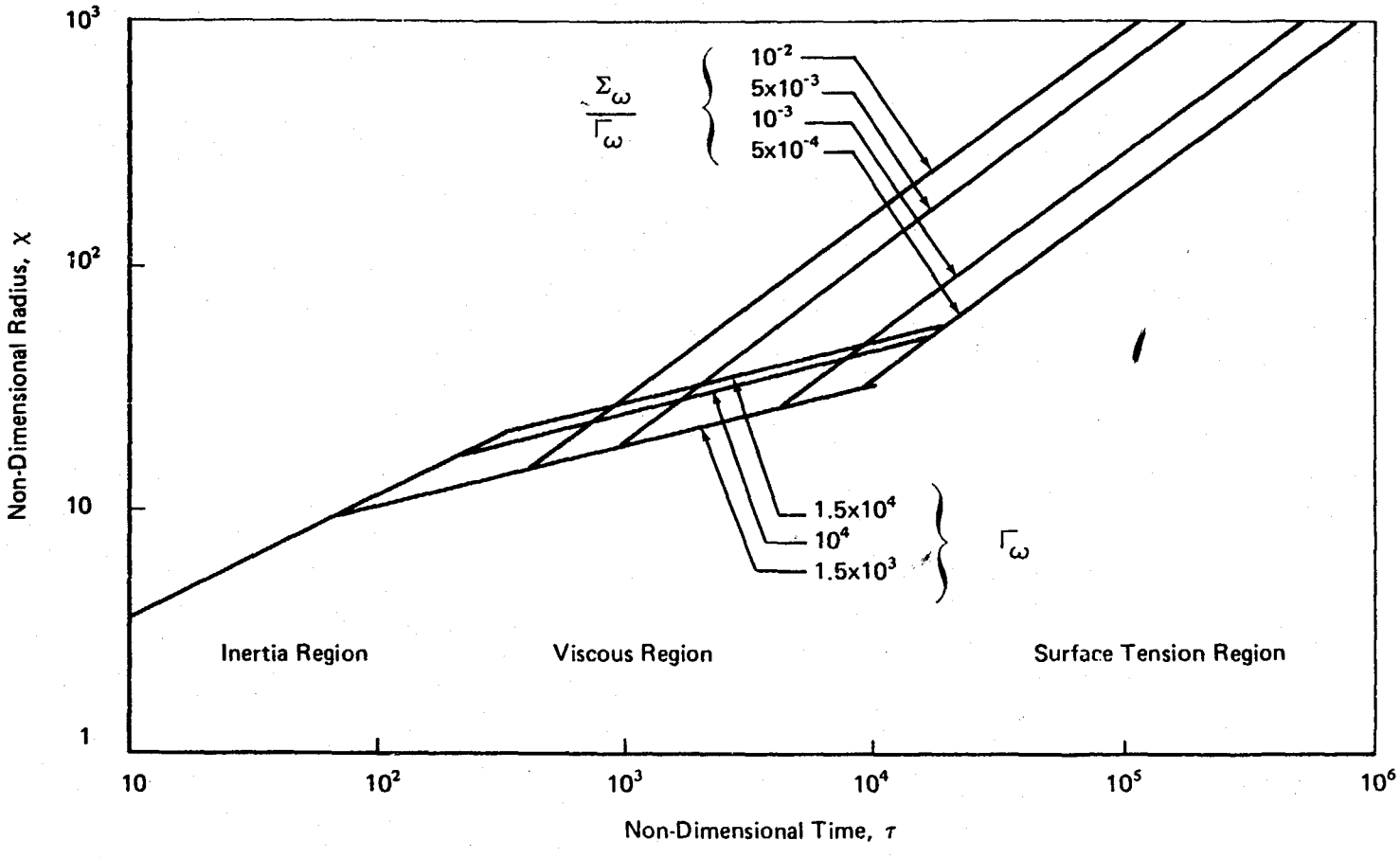

FIGURE 3.1 RADIAL SPREADING OF HIGH VISCOUS LIQUID ON WATER

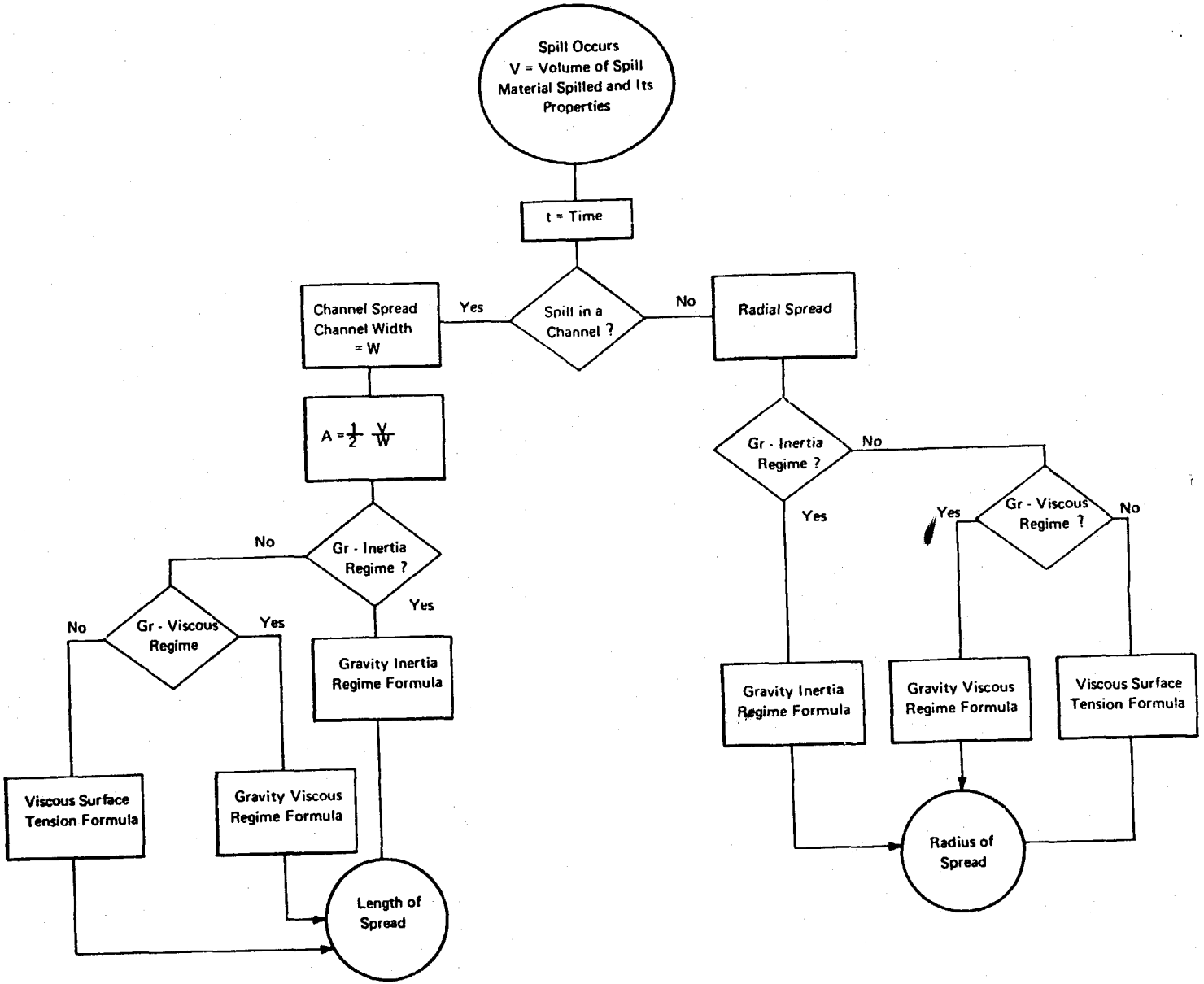

FIGURE 3.2 FLOW CHART FOR THE CALCULATION OF THE EXTENT OF SPREAD OF A HIGH VISCOSITY LIQUID ON WATER

Description	Formula	Symbol	Value
Time at which extent of spread is to be calculated	=	t	10,000 s
Half width of spread	$= 1.39\left[\frac{G A^2}{\sqrt{\nu_w}}\right]^{\frac{1}{4}} t^{\frac{3}{8}} =$	x	1125.0 m
Length of spread	= 2 x		2250.0 m

3.8 DISCUSSIONS

The model indicated gives a simple method of obtaining the extent of spread of a high-viscosity liquid on water. The equations shown have been tested on laboratory-scale experiments (Hoult and Suchon,[2] Fay,[3]) and, in a general sort of way, on large-scale spills. They are found to be adequately accurate in correlating the data.

The equations presented are plotted in Figure 3.1. It is seen that the extent of spread during the gravity-viscous regime is relatively insensitive to the volume of spill. In fact a 10-fold increase in spill causes only a factor of 2 increase in the radius of the spread when measured in non-dimensional units (comparison is made at the same non-dimensional time). This relative insensitivity of radius to the volume of spill can be attributed to the dependence of the radius on the one-third power of the volume. Also it should be observed that in the surface tension regime of spread, the radius of spread is independent of the volume of spill (see Table 3.1).

The greatest limitation of the model lies in its assumption of calm water on which the liquid is spilled. For a spill of oil on the sea, this would hardly be true. Physically, the most important assumption underlying the analysis (which is most likely to be violated in real life) is the absence of wind effects, tidal currents, and waves on the spill. It is known that wind shear plays an important role in moving oil slicks on the sea. To take into account the effects of wind and current, it has been proposed that the analysis presented could be utilized if the center of the spill were moved with a velocity given by the vectorial addition of the current velocity and 3% of the wind velocity. However, it is to be noted that wind and tidal currents also produce a relative shearing motion in the plane of water surface, deforming the shape of the slick from those simple shapes expected on calm water. Such distortion is commonly observed and is most likely to limit the usefulness of spreading laws proposed. These effects are very difficult to predict or even describe, and there is little empirical evidence on which to base an estimate of their importance.

It has been noted in real life that slicks cease to spread after some time. Fay[5] contends that this cessation is caused by the evaporation of some oil fractions which reduces the spreading coefficient to zero. Based on diffusion of oil fractions in sea water, Fay gives the following estimate for the maximum slick size:

$$\text{Spread area in } m^2 = 10^5 \times [\text{spill volume in } m^3]^{\frac{3}{4}}.$$

The thickness of the film at this stage is of the order of 1 mm.

3.9 CONCLUSIONS

Theoretical formulas have been given to estimate the extent of spread of a high-viscous, water-immiscible liquid on a water surface. The formulas have been based on the physical processes that are involved in spreading one liquid over another. An illustrative example has been worked to show the calculation procedure. The limitations and extensions of the formulas to some other cases have been discussed.

3.10 REFERENCES

1) Abbot, M. B., "On the Spreading of One Liquid over Another," Part II, La Houille Blanche, 6, Dec. 1961, pp. 928-46.

2) Hoult, D. P., and Suchon, W, "The Spread of Oil in a Channel," Fluid Mechanic Lab Report; MIT, 1970.

3) Fay, J. A., "The Spread of Oil Slicks on a Calm Sea," in *Oil on the Sea*, edited by D. P. Hoult; Plenum Press, N. Y., 1969, pp. 53-63.

4) Fannelop, T. K., and Waldman, G D., "Dynamics of Oil Slicks," AIAA Journal, Vol. 10, No. 4, April 1972, pp. 506-510.

5) Fay, J. A., "Physical Process in the Spread of Oil on a Water Surface," in Prevention and Control of Oil Spills, American Petroleum Institute, Washington, D. C., 1971, pp. 463-467.

3.11 NOMENCLATURE

Symbol	Description	Formula or Value	Units
A	half spill volume per unit channel width		m^2
g	acceleration due to gravity	9.8	m/s^2
G	effective gravity	$g\,(1 - \rho_L/\rho_w)$	m/s^2
L	characteristic scale length	$V^{\frac{1}{3}}$ or $A^{\frac{1}{2}}$	m
m	mass of liquid spilled		kg
r	spread radius at any time		m
t	time		sec.

Symbol	Description	Formula or Value	Units
T	characteristic time	$\sqrt{\frac{L}{G}}$	sec.
V	spill volume		m^3
W	channel width		m
x	semi-length of spill in 1-D spread = total spill extent/2		m
Greek Letters			
Γ_w	non-dimensional viscosity	$[L^3 G/\nu_w^2]^{1/4}$	
μ	absolute viscosity		$N\ s/m^2$
ν	kinematic viscosity		m^2/s
ρ	density		kg/m^3
σ	interfacial tension between spreading liquid and water		N/m
Σ_w	non-dimensional surface tension	$\sigma/\mu_w \sqrt{GL}$	
τ	non-dimensiona time		
χ	non-dimensional distance to the spread front	r/L or x/L	
Subscripts			
L	spreading liquid		
w	water.		

TABLE 3.1

DIMENSIONAL EQUATIONS OF SPREAD WITH HIGH VISCOSITY

Spread Regimes → / Geometry of Spread ↓	Gravity – Inertia	Gravity – Viscous	Viscous – Surface Tension
One-Dimensional	$0 < t < \left[\frac{A^4}{G^2 \nu_w^3}\right]^{1/7}$	$\left[\frac{A^4}{G^2 \nu_w^3}\right]^{1/7} \leqslant t \leqslant 0.989 \left\{\frac{\sqrt{G}\, \nu_w^{1/4} A \rho_w}{\sigma}\right\}^{4/3}$	$t > 0.989 \left[\frac{G^{1/2} \nu_w^{1/4} A \rho_w}{\sigma}\right]^{4/3}$
	$x = 1.39 (GA)^{1/3} t^{2/3}$	$x = 1.39 \left[\frac{G^2 A^4}{\nu_w}\right]^{1/8} t^{3/8}$	$x = 1.43 \left[\frac{\sigma}{\sqrt{\mu_w \rho_w}}\right]^{1/2} t^{3/4}$
Radial	$0 < t < 0.546 \left[\frac{V}{G \nu_w}\right]^{1/3}$	$0.546 \left[\frac{V}{G \nu_w}\right]^{1/3} \leqslant t \leqslant 0.375 \frac{\rho_w}{\sigma} \left[G^2 V^4 \nu_w^2\right]^{1/6}$	$t > 0.375 \frac{\rho_w}{\sigma} \left[G^2 V^4 \nu_w^2\right]^{\frac{1}{6}}$
	$r = 1.14 (GV)^{1/4} t^{1/2}$	$r = 0.98 \left[\frac{G^2 V^4}{\nu_w}\right]^{1/12} t^{1/4}$	$r = 1.6 \left[\frac{\sigma}{\sqrt{\mu_w \rho_w}}\right]^{1/2} t^{3/4}$

TABLE 3.2

NON-DIMENSIONAL EQUATIONS OF SPREAD WITH HIGH VISCOSITY

Regimes of Spread Geometry	Gravity – Inertia	Gravity – Viscous	Viscous – Surface Tension
One-Dimensional	$0 < \tau < \Gamma_w^{6/7}$	$\Gamma_w^{6/7} \leqslant \tau \leqslant 0.989 \frac{\Gamma_w^2}{\Sigma_w^{4/3}}$	$\tau > 0.984 \frac{\Gamma_w^2}{\Sigma^{4/3}}$
	$\chi = 1.39 \tau^{2/3}$	$\chi = 1.39 \Gamma_w^{1/4} \tau^{3/8}$	$\chi = 1.43 \left(\frac{\Sigma_w}{\Gamma_w}\right)^{1/4} \tau^{3/4}$
Radial	$0 < \tau < 0.546 \Gamma_w^{2/3}$	$0.546 \Gamma_w^{2/3} \leqslant \tau \leqslant 0.375 \frac{\Gamma_w^{4/3}}{\Sigma_w}$	$\tau > 0.375 \frac{\Gamma_w^{4/3}}{\Sigma_w}$
	$\chi = 1.14 \tau^{1/2}$	$\chi = 0.98 \Gamma_w^{1/6} \tau^{1/4}$	$\chi = 1.6 \left(\frac{\Sigma_w}{\Gamma_w}\right)^{1/2} \tau^{3/4}$

4.0 MIXING AND DILUTION (K,P)

4.1 AIM

The aim of this section is to present methods for calculating liquid concentrations in water after the spill of a water-miscible liquid.

4.2 INTRODUCTION

When a water-miscible liquid is spilled on a water surface, mixing takes place, thereby diluting the liquid. The mixing is caused by molecular diffusion in calm water and mass convection (turbulent diffusion) in streams, rivers, estuaries, and the sea. Mixing may take place preferentially in one direction, depending on the flow conditions, flow geometry, water density gradients, and the like. Because of the predominance of certain types of mixing phenomena in different regions of the navigational waters, the latter are divided into four different categories, and are illustrated in Figure 4.1.

In non-tidal rivers the main agency for mixing is stream turbulence. In tidal rivers, estuaries, and also in the open sea, wave action becomes quite important in addition to the stream or current velocity. In estuaries and other regions where a density stratification of water due to salinity is likely to be found, mixing caused by the density-driven circulation becomes extremely important. However, since the velocities involved in these circulations are small and the area influenced by these kinds of flows is generally large, only long-time effects are important. For assessing the hazards caused by a relatively infrequent spill (even though the tonnage of the spill itself may be large) in such areas therefore, the effects of salinity-driven mixing can be ignored.

The phenomenon of mixing is generally described theoretically by the classical diffusion equations with one or more diffusion coefficients. A comprehensive survey of literature and the derivations of the equations from first principles are described in References 1 and 2. The models described are strictly correct for the dispersion of neutrally buoyant liquids only. Several other investigators (Fisher,[3] Holley and Harleman,[4] Thatcher and Harleman,[5] *et al.)* have correlated, from experimental data, the dispersion and turbulent diffusion coefficients for dispersion of pollutants in rivers, estuaries, and other regions. These correlations are presented in Section 4.5.

The equations given are applicable to neutrally buoyant solids – liquids and solids that dissolve in water – and have been arranged according to their regions of applicability.

4.3 ASSUMPTIONS

The following assumptions were made in deriving the equations given below:

- No heat transfer, chemical reaction, or phase change effects were considered; that is, the total mass of the liquid which is mixing with water remains a constant.

- No rapid settling of the liquid due to higher density effects was included.

4.4 DATA REQUIRED

The following data are generally required to estimate the concentration of the liquid mixing with water:

- Geometry of the water region and stream and tidal velocities where needed; and

- Mass of liquid spilled and the location of the spill point.

4.5 DETAILS OF DISPERSION MODELS

The equations given below are grouped under three different categories: dispersion in non-tidal rivers, dispersion in tidal rivers, and dispersion in estuaries.

4.5.1 Dispersion in Non-Tidal Rivers

(1) *Initial stages of dispersion (near-field approximation):* Referring to Figure 4.2 we write the following equations:

a) For an instantaneous spill on the surface of the river at the point (0,a,0):

$$c(x,y,z,t) = \frac{2M}{(4\pi t)^{3/2}\sqrt{e_x e_y e_z}} \exp\left[-\left(kt + \frac{(x-Ut)^2}{4e_x t}\right)\right] \left\{ e^{-\frac{(y-a)^2}{4e_y t}} + e^{-\frac{(y-a-w)^2}{4e_y t}} + e^{-\frac{(y+a-w)^2}{4e_y t}} \right\} \left[e^{-\frac{z^2}{4e_z t}} + e^{-\frac{(z-2d)^2}{4e_z t}} \right] \quad (4.1)$$

Equation (3.1) takes into account the fact that there is no diffusion through the boundaries of the river.

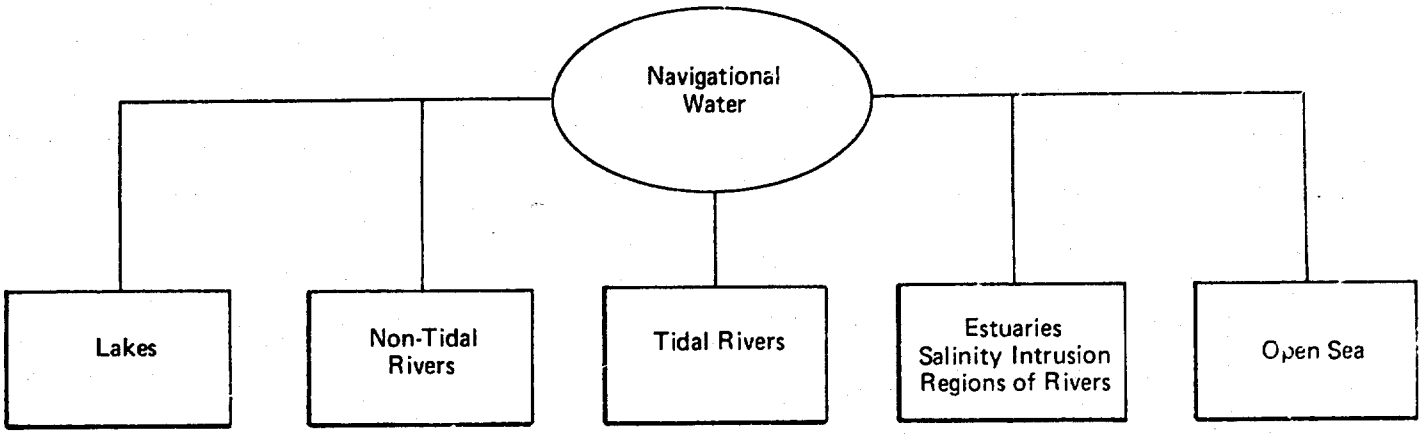

FIGURE 4.1 DIVISION OF WATER REGIONS

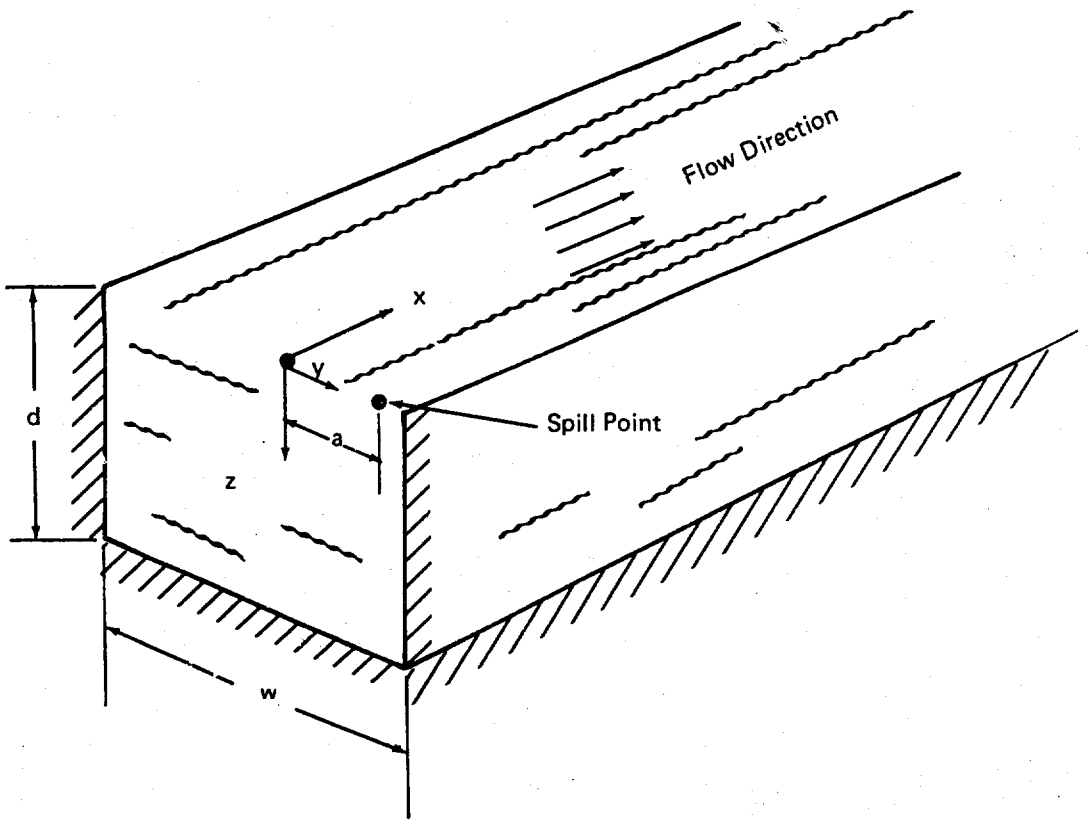

FIGURE 4.2 SCHEMATIC DIAGRAM ILLUSTRATING THE CROSS-SECTION AND SPILL POINT iN A NON-TIDAL RIVER

b) Continuous spill on the surface at (0,a,0) and no longitudinal dispersion:

$$c(x,y,z,t) = \frac{2\,\dot{M}\left(t-\frac{x}{U}\right)}{4\pi x\sqrt{e_y\,e_z}}\;Exp\left[-\frac{U}{4x}\left\{\frac{y^2}{e_y}+\frac{z^2}{e_z}+4k\right\}\right] \qquad (4.2a)$$

Equation (4.2a), which is similar to the vapor dispersion equations, can be shown to be strictly correct only for the case in which the longitudinal diffusion coefficient is vanishingly small. Also Eq. (4.2a) gives a discontinuous concentration with time (as experienced by an observer downstream), as shown in Figure 4.3.

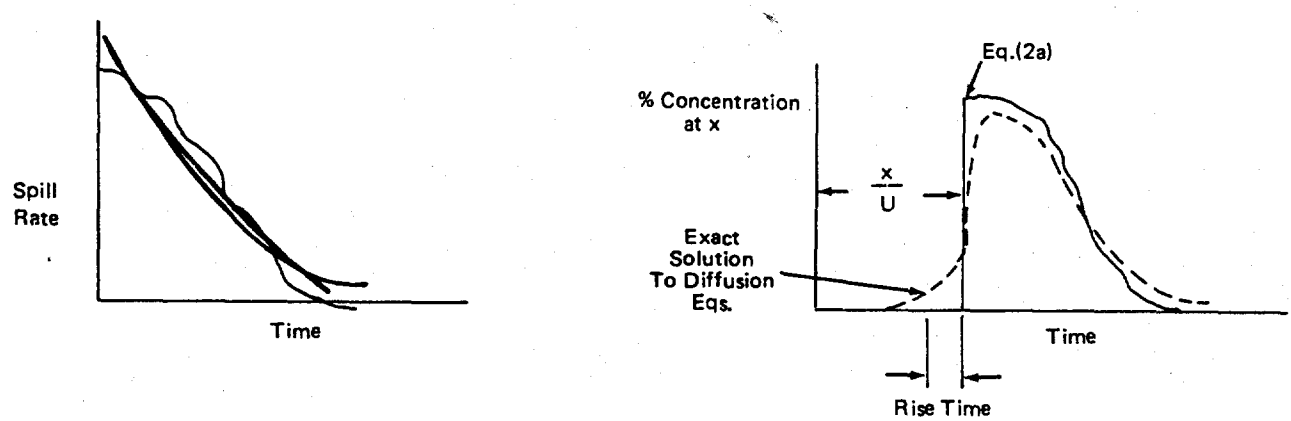

FIGURE 4.3 CONCENTRATION VERSUS TIME DIAGRAMS

If one can neglect the initial rise time with respect to the duration of the concentration experience, then Eq. (4.2a) is sufficiently accurate to describe the phenomenon. An alternative formula suggested by Harleman[6] is:

$$c(x,y,z) = \frac{\dot{M}}{2\pi\sqrt{e_y\,e_z}\,x}\;Exp\left(-\frac{U}{4x}\left[\frac{y^2}{e_y}+\frac{z^2}{e_z}+4k\right]\right) \qquad (4.2b)$$

which is exact for a constant spill rate and in the steady-state conditions. Harleman[6] has suggested the use of the following turbulent diffusion coefficients (for use in Eqs. (4.1) and (4.2) for narrow and wide rivers:*

Diffusion Coefficients	Very wide rivers (w/d > 100)	For narrow rivers (w/d < 100)	Remarks
e_z	$0.067\ u^*d$	$0.067\ u^* R_h$	The e_z value is the mean of the vertical distribution given by $e = 0.4\ u^*d\ (z/d)\ (1 - z/d)$
e_x	$0.1\ e_z$	$0.1\ e_z$	
e_y	$0.1\ e_z$	$0.23\ u^* R_h$	

(4.3)

It is assumed that the above "point source" type of spreading occurs until a measurable concentration can be detected near the river banks. The order of time for this to occur is given by

$$T_c = b^2/e_y \tag{4.4a}$$

The "initial period" T_I is defined as the duration up to which Eqs. (4.1) and (4.2) can be used to predict the concentration:

$$T_I = 0.3T_c \longrightarrow \text{(Eq. 14 of Ref. 4)} \tag{4.4b}$$

However, Eqs. (4.1) and (4.2) could be used for any length of time because of the provision of the image source terms in the equations, which assure that there is no diffusion through the boundaries.

(2) *For time larger than T_I (far-field approximation):* We use one-dimensional analysis to describe mean concentration, the concentration being derived from the equation:

$$\frac{\partial C}{\partial t} + U\frac{\partial C}{\partial x} = \frac{1}{A}\frac{\partial}{\partial x}\left(EA\frac{\partial C}{\partial x}\right) \tag{4.5}$$

where C is the cross-sectional average concentration.

*w/d ≃ 100 which is assumed to be the upper limit for the side banks of the rivers to have any influence on the transverse velocity distribution. However, Holley et al [4] have used w/d ≃ 600 for estuaries in the tidal regions.

a) For an instantaneous spill:

$$C(x,t) = \frac{M}{A\sqrt{4\pi E t}} \; Exp - \left[\frac{(x-Ut)^2}{4Et} + k\,t \right] \qquad (4.6a)$$

where

k = decay rate coefficient, defined by r = k c, and

r = rate of depletion of the specie mass/unit of time

b) Continuous spill:

$$C(x,t) = \frac{\dot{M}}{2\Omega A} e^{\frac{xU}{2E}} \left[e^{\frac{x\Omega}{2E}} \left(erf\left(\frac{x+\Omega t}{\sqrt{4Et}}\right) - 1 \right) - e^{-\frac{x\Omega}{2E}} \left(erf\left(\frac{x-\Omega t}{\sqrt{4Et}}\right) - 1 \right) \right] \qquad (4.6b)$$

where

$$\Omega = \sqrt{U^2 + 2kE}$$

Eq. (4.6b) reduces at large times (when $t \longrightarrow \infty$) to:

$$C(x) = \frac{\dot{M}}{A\,\Omega} Exp\left[\frac{x}{2E}(U-\Omega) \right] \qquad (4.6c)$$

and if $E \ll U^2/2k$,

then

$$C(x) = \frac{\dot{M}}{A\,U} Exp\left(-\frac{x\,k}{U}\right) \qquad (4.6d)$$

c) Determination of E to be used in Eqs. (4.6a) and (4.6b)

Using Elder's equation* we have:[1]

$$E = 63\, n U R_h^{\frac{5}{6}} \qquad \text{for} \quad \frac{w}{d} > 100 \tag{4.7}$$

$$\frac{E}{R_h U^*} = 0.3 \frac{u''^2}{U^{*2}} \left(\frac{b}{R_h}\right)^2 \qquad \text{for} \quad \frac{w}{d} < 100 \tag{4.8a}$$

One of the drawbacks of using Eq. (4.8a) is that a knowledge of the velocity distribution is necessary (i.e., u") to evaluate the dispersion coefficient. Since for most rivers this may not be readily available, the utility of Eq. (4.8a) becomes limited. However, a plot of $E/R_h U^*$ against w/d from the data given in Fischer's paper[3] indicates that this is essentially a constant at about 225. Therefore, it is suggested that in the event of lack of data as to the velocity distribution, we might use as a thumbrule:

$$\frac{E}{R_h u^*} = 225 \tag{4.8b}$$

for all rivers.

4.5.2 Dispersion in Tidal Rivers

The constant density regions of an estuary (where salinity intrusion is minimal) are designated as tidal rivers. Such a nomenclature, it is hoped, indicates the non-steady nature flow in these regions.

The concentration dispersion in such regions could be represented by the following equation.

$$\frac{\partial C}{\partial t} + U(t) \frac{\partial C}{\partial x} = \frac{1}{A(t)} \frac{\partial}{\partial x}\left(A E \frac{\partial C}{\partial x}\right) \tag{4.9}$$

(1) *Pulse injection at the instant of time* τ:

For a constant-area, constant-dispersion coefficient,[1]

$$C(x,t) = \frac{M}{A\sqrt{4\pi E (t-\tau)}} \operatorname{Exp} -\left[\frac{x^2}{4E(t-\tau)} + k(t-\tau)\right] \tag{4.10a}$$

*Note that Eq. (4.7) is a dimensional equation; all the quantities are in SI Units.

where

$$\mathcal{X} = x - \int_{\tau}^{t} U(t')\, dt' \tag{4.11}$$

and the spill occurs at x = 0 at time = τ.

For

$$U(t) = U_f + U_T \sin \sigma (t-\delta) \tag{4.12}$$

we get from Eqs. (4.12), (4.11), and (4.10a):

$$C(x,t) = \frac{M}{A\sqrt{4\pi E t}}\, e^{-\left\{\frac{(x - U_f t) + \frac{U_T}{\sigma}\left[\cos\sigma(t-\delta) - \cos(\sigma\delta)\right]}{\sqrt{4Et}}\right\}^2} \tag{4.10b}$$

where t = 0 is the instant of spill at x = 0 and δ = the time for the next high-water slack.

(2) *Continuous injection:*

$$C(x,t) = \int_0^{t'} \frac{\dot{M}(\xi)\, d\xi}{\sqrt{4\pi E(t'-\xi)}} \exp -\left[\frac{\mathcal{X}^2}{4E(t'-\xi)} + k(t'-\xi)\right] \tag{4.13a}$$

where $t' = t - \tau$ is the instant at which injection starts, and x is defined in Eq. (4.11).

For a *sinusoidal flow velocity* with a superimposed steady flow, we have:

$$C(x,t) = \int_0^{t} \frac{\dot{M}(\xi)\, d\xi}{A\sqrt{4\pi E(t-\xi)}}\, e^{-\left[\frac{x - U_f(t-\xi) + \frac{U_T}{\sigma}\left[\cos(t-\xi-\delta)\sigma - \cos(\sigma\delta)\right]}{\sqrt{4E(t-\xi)}}\right]^2 - k(t-\xi)} \tag{4.13b}$$

Figures 4.4 and 4.5 show the solution of Eq. (4.13b) for some typical values of E and k. The two figures indicate the effect of values of E and k on the solution. It is noticed that for long times (i.e., a few hundred tidal periods) the solution is fairly insensitive to the variation

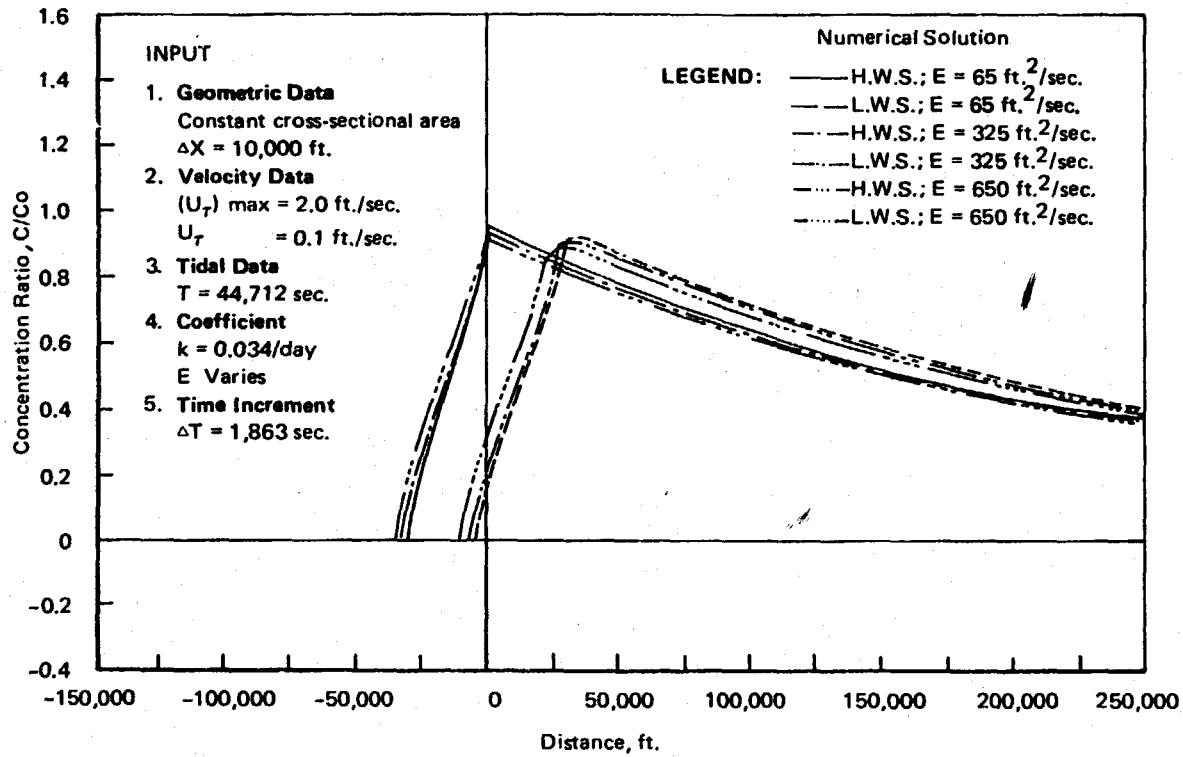

Note: Above figure taken from reference 7.

FIGURE 4.4 SENSITIVITY OF LONGITUDINAL DISPERSION COEFFICIENT IN IDEALIZED CHANNEL OF PROTOTYPE CONDITION

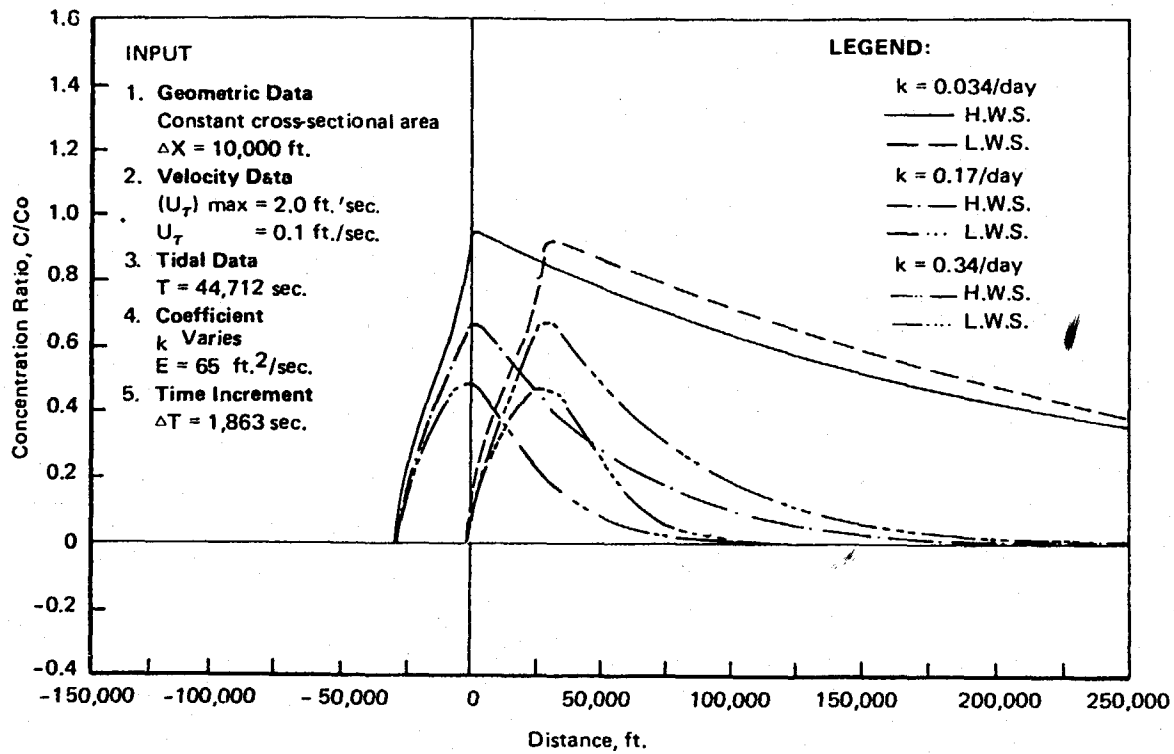

Note: Above figure taken from reference 7.

FIGURE 4.5 SENSITIVITY OF DECAY COEFFICIENTS ON FINITE DIFFERENCE SOLUTION

in E, but is quite sensitive to small changes in k – the decay coefficient. However, for CHRIS manuals, the time of interest is not large (maybe one or two tidal periods) and in such short times the effect of E and k are expected to be about the same on the solution. What this means is that assigning a correct value for E – the dispersion coefficient becomes more important.

Determination of E [for use in Eqs. (4.10) and (4.13)]

The results given below are not applicable to multichanneled or island-studded estuaries. However, these results are reasonably accurate for fairly well defined straight channels. The results are taken from Reference 4 and are presented below.

For $U_f \ll U_T$

E_v = dispersion coefficient predominently affected by vertical velocity gradients;

E_t = dispersion coefficient primarily influenced by transverse velocity variation;

$E_v = 6\, du^*$;

$$\frac{E_t}{E_v} = 0.11 \left(\frac{U_T\, T}{b}\right)^2 \left[\frac{\overline{U''^2}}{\left(\frac{2}{\pi} U_T\right)^2}\right] \tag{4.14}$$

where generally $0.01 < \overline{U''^2}/(2/\pi\, U_T)^2 < 0.04$ and u^* is based on mean oscillating flow velocity $(2\, U_T/\pi)$.

To determine which of the above two dispersion coefficient values to use in Eqs. (4.10) and (4.13), two characteristic time ratios are defined:

T'_v = diffusional time ratio for vertical (depth-wise) spreading = $T/(d^2/e_v)$, and

T'_t = transverse spreading = $T/(b^2/e_v)$.

where T is the tidal period of oscillation.

If $T'_v < 1$, then we use $E = E_v$.

If $T'_v > 1$ (and $T'_t < 0.1$), then we calculate E_t/E_v from Eq. (4.14) using a mean value of 0.02 for the bracketed term). If the E_t/E_v thus calculated is less than 1, then again we use

$E = E_v$. However, if this ratio is greater than 1, then we set $E = E_t$. Holley *et al.*[4] observed a maximum value of 11 for E_t/E_v for several estuaries. It is interesting to compare this to a value of about 1,000 observed by Fischer[3] for non-oscillating flow in rivers. Holley *et al.*[4] also observed the fact that, for continuous releases, the concentrations predicted by using either E_v or E_t for dispersion coefficient differed by less than a few percent of the actual value for times greater than about five tidal periods.

4.5.3 Dispersion in Estuaries

In this section the dispersion in saline regions of the estuary is considered, where both tidal action and the density gradient-driven circulation are important. Essentially one obtains the mean concentration at a particular time and location by solving the following equation:

$$A(x,t)\frac{\partial C}{\partial t} + Q(x,t)\frac{\partial C}{\partial x} = \frac{\partial}{\partial x}\left(A(x,t)\,E(x,t)\frac{\partial C}{\partial x}\right) \qquad (4.15)$$

It is assumed, however, that the A(x,t) and Q(x,t) (the discharge) data are available, in addition to a knowledge of E. In the saline regions the dispersion coefficient is closely related to density-induced circulation. Thatcher[5] feels that this circulation is greatest in the regions where the longitudinal salinity concentration gradients are largest.

To predict the concentration of a pollutant, Eq. (4.15), a real-time equation, has to be solved for C for both given initial and boundary conditions. The effort of knowing the concentrations can be minimized if only an average value (over a tidal period) is needed.

Then Eq. (4.15) can be written as:

$$\bar{Q}(x)\frac{\partial \bar{C}}{\partial x} = \frac{\partial}{\partial x}\left[\bar{A}\,E^{TA}(x)\,\frac{\partial \bar{C}}{\partial x}\right] \qquad (4.16)$$

where

$\bar{Q}$ is the time-averaged discharge,

$\bar{A}(x)$ is the average-over-a-tidal-cycle flow area, and

E^{TA} is the time-averaged-dispersion coefficient.*

*Note this dispersion coefficient is *not* the same as E (x,t) time-averaged over a tidal cycle.

(1) *Solution of Equations (4.15) and (4.16)*

Since the variables in Eqs. (4.15) and (4.16) are peculiar to each estuary, no general solution can be obtained for the differential equations. The only recourse is to numerical techniques. However, the tidal data and the estuary cross-sectional data constitute the information necessary for solution of either Eq. (4.15) or Eq. (4.16).

(2) *Evaluation of Dispersion Coefficients*

The most detailed and recent analysis of the problem of correlating the dispersion coefficient for different estuaries has been done by Thatcher,[5] who has also reviewed the current literature on this subject. His correlations are given below:

$$\frac{K}{U_o L} = f(\mathbb{E}_D) \tag{4.17}$$

where

K = dispersion parameter defined below,

$\mathbb{E}_D$ = estuary stratification parameter,

U_0 = maximum flood velocity at the entrance to the estuary,

L = length of estuary (salinity intrusion region),

$\mathbb{E}_D$ = estuary number defined

$= P_T \mathbb{F}_D^2 / Q_f T$,

P_T = tidal prism = volume of water entering the estuary in flood tide,

$\mathbb{F}_D$ = densimetric Froude number at the entrance to estuary

$= U_0 / \sqrt{g[\Delta\rho/\rho]h}$,

$\Delta\rho$ being the change in density over the entire length of the estuary,

T = tidal period, and

Q_f = fresh water discharge in volume/time.

The dispersion coefficient is evaluated using the equation:

$$E(x,t) = K\left|\frac{\partial \overset{\circ}{S}}{\partial \overset{\circ}{x}}\right| + E_T \tag{4.18}$$

and

$$E^{TA}(x) = K\left|\frac{\partial \overset{\circ}{S}}{\partial \overset{\circ}{x}}\right| + E_T \qquad \text{time averaged over a tidal period} \tag{4.19}$$

where

$\overset{\circ}{S}$ = S/S^0 = dimensionless one-dimensional salinity,

S_0 = salinity at any location,

$\overset{\circ}{x}$ = x/L,

E_T = longitudinal dispersion coefficient in fresh water region or a mixed estuary,

= $63\ n\ UR_h^{5/6}$ (U is average velocity),

K = $.002\ U_0\ L\ (E_D)^{-1/4}$ – (from Reference (5))

It is to be noted that the evaluation of the dispersion coefficient (to be used in Eqs. (4.15) or (4.16) would involve the knowledge of the salinity gradients in the estuary. This can be calculated by knowing the tidal hydraulics of the estuary, or it can be obtained from observed data. In conclusion, one can see that there is no easy way of obtaining the dispersion coefficient. Each estuary has to be treated separately; its dispersion coefficient evaluated and then used for concentration prediction.

4.6 COMPUTATIONAL ALGORITHM

A general mixing-dilution computer program has been written to calculate the concentration given the necessary data. Except for the case of Eq. (3.13b) in which a numerical integration is to be performed, the remaining equations are simple and calculations can be done without much difficulty. Figure 4.6 is a flow chart on which the computer program is based. Essentially the water region in which the spill occurs is established and the appropriate formula is used.

4.7 SPECIFIC EXAMPLE

The following spill situation is considered for illustrating the numerical values obtained for concentration:

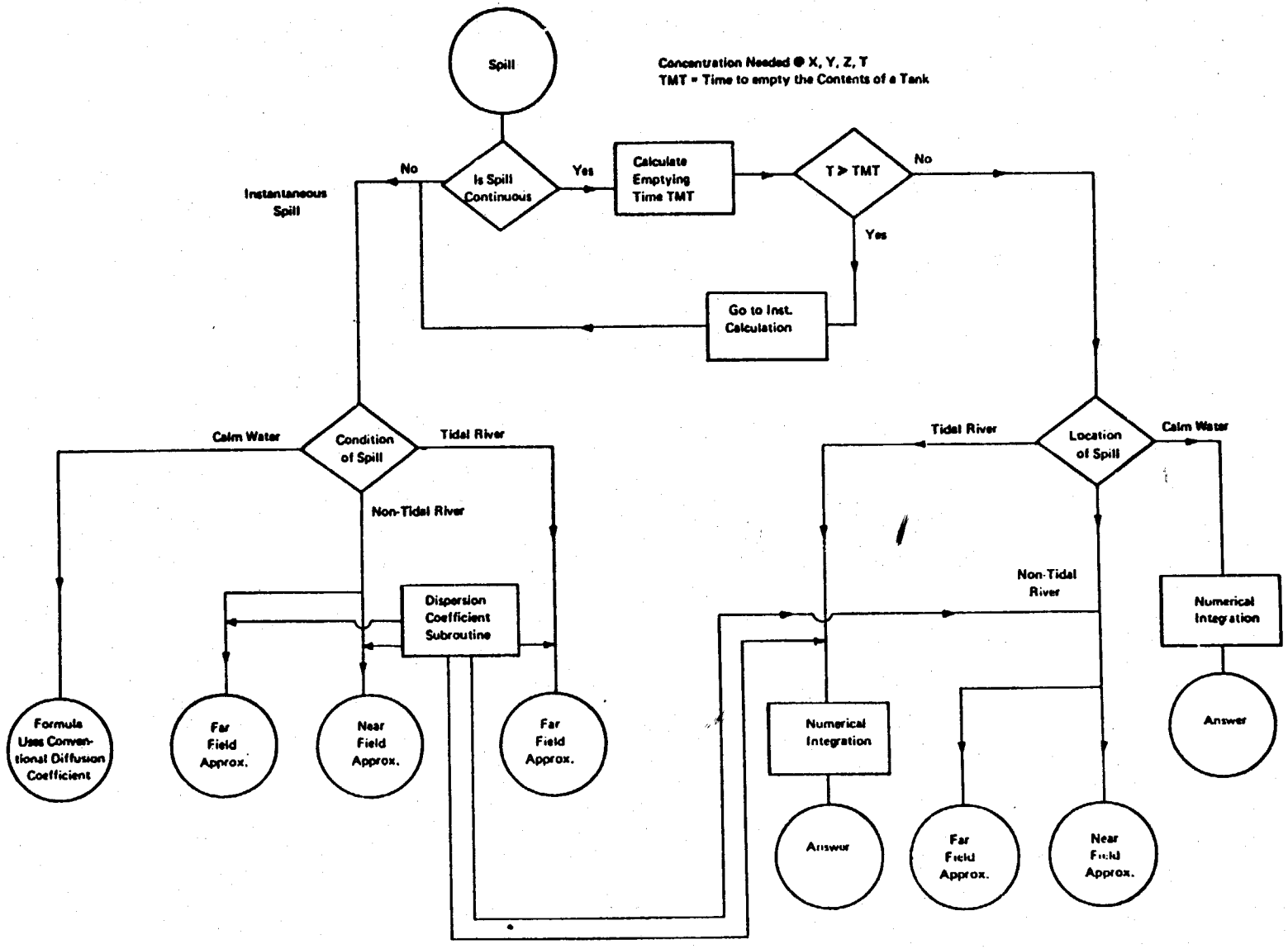

FIGURE 4.6 FLOW CHART FOR THE CONCENTRATION CALCULATION IN A SPILL OF A LIQUID ON WATER

Data

Type of water region	= non-tidal river
Width of river	= 50 m
Depth of river	= 5 m
Average river velocity	= 1 m/s
Spill mass	= 10^6 kg
Time for spill of this mass	= 10^3 s
Downstream observation point (at the mid-stream on the water surface)	x = 10^3 m y = 0 m z = 0 m
River surface roughness coefficient	n = 0.03

4.7.1 Calculations

Now,

w/d = 50/5 < 100; hence the river is a "narrow river":

Hydraulic depth = 5 x 50/(2 x 5 + 50) = 4.17 m

Shear velocity = $u^* = 3.115 \times .03 \times 1/(4.17)^{1/6} = 0.0737$ m/s

From Eq. (4.3) we have

$e_z = 0.067 \times 0.0737 \times 4.17 = 0.0206$ m²/s

$e_x = 0.1 \times 0.0206 = 0.00206$ m²/s

$e_y = 0.23 \times 0.0737 \times 4.17 = 0.0705$ m²/s

Characteristic time of initial period (Eq. 4.4) = $0.3 \times 25^2/0.0705 = 2660$ sec. If an *instantaneous spill* is assumed and this occurs at mid-river, then the peak concentration occurs at the point (x,y,z) at time $t = 10^3/1 = 10^3$ sec. Hence, observation time is less than initial period time. Therefore, this maximum concentration (from equation) is:

$$c_{max} = \frac{2 \times 10^6}{[4\pi\, 10^3]^{1.5}\sqrt{0.00206 \times .0705 \times .0206}} = 821.3 \text{ kg/m}^3$$

This concentration is about 80% of water density.

If the *spill* is assumed to occur *continuously*, then;

Rate of mass spill = $10^6/10^3 = 10^3$ kg/s

Maximum concentration from Eq. (4.2a) =

$$c_{max} = \frac{10^3}{2 \times \pi \times 10^3 \times \sqrt{0.0705 \times .0206}} = 4.18 \text{ kg/m}^3$$

This concentration is about 200 times smaller than the concentration obtained if all of the spill had occurred in a very short time.

4.7.2 Concentrations at 5 km Downstream

The maximum concentration occurs at this location at a time far exceeding the initial period. Hence the "far-field approximation" equations are used.

Since $w/d < 100$, the longitudinal dispersion coefficient (Eq. 4.8b) is

$$E = 225 \times 4.17 \times 0.0737 = 69.15 \text{ m}^2/\text{s}.$$

Hence from (Eq. 4.6a) for instantaneous spill:

$$C_{max} = \frac{10^6}{5 \times 50 \times \sqrt{4 \times \pi \times 69.15 \times 5000}} = 1.92 \text{ kg/m}^3$$

For a continuous spill at the rate of 10^3 kg/s the concentration at t = 5000 sec. is given by (Eq. 4.6b):

$$C_{max} = \frac{10^3}{2 \times 1 \times (5 \times 50)} \left[e^{\frac{5 \times 10^3 \times 1}{69.15}} \left\{ erf\left(\frac{5 \times 10^3 \times 2}{\sqrt{4 \times 69.15 \times 5000}} \right) - 1 \right\} + 1 \right]$$

$$= 1.806 \text{ kg/m}^3$$

4.8 DISCUSSIONS

Several equations have been given, each applicable in a specific context, to predict the concentration history of a pollutant spilled into water. All of these equations are based on the solutions of diffusion equations with constant or variable diffusion coefficients. Except for the simplest types of variations and geometrical configurations, the analytical solution to the diffusion equation is almost impossible. The equations presented are based on two types of spills, viz.; instantaneous and continuous. The continuous-spill formulas are strictly

correct only when the spill is continuous for a long period of time (mathematically infinite time). Hence, when these formulas are used for concentration predictions consequent to a short-duration spill (duration however long compared to "instantaneous"), great care and proper judgment should be exercised. In fact, to solve the problem correctly, in such intermittent or time-varying spill rate cases, a numerical integration procedure should be used.

The value of the concentration predicted is quite sensitive to the type of spill as can be seen from the numerical example. Moreover, the formulas given for estimating the turbulent diffusion coefficients are empirical. These can vary depending on the topography of the locality. For example, if a river is flowing with many bends in its path, or its cross-sectional area is changing rapidly in its path, the diffusion coefficients will be much higher. Similarly, the dispersion coefficients (E's) have been obtained based on limited correlations.

For using some of the equations (Eqs. 4.16, 4.17, . . .), one needs a large amount of information that may not be readily available. This is especially true of estuarine regions where, to use the equations and predict the concentrations, one needs the salinity and hydrographical data of the region in addition to the tidal hydraulic information. Also questions have been raised[6] as to the applicability of estuarine model equations for concentration prediction of the short-time release of a pollutant as would occur in a shipping accident. This doubt has been expressed because of the fact that the dispersion coefficients (E's in Eq. (4.18)) for the salinity-intrusion regions of estuaries have been obtained by taking into account the large-scale motions (induced by salinity gradients) of the order of 100 km or more. It has been suggested,[6] therefore, that ordinary turbulent diffusional mechanisms alone could be used (along with tidal dispersion), even in the case of salinity-intrusion regions of estuaries to predict concentrations of spills caused by a shipping accident.

The major limitation of the model proposed is its inability to handle spills and water mixing of liquids that can react with water, thereby producing vapor or liquids that are so heavy that they have a tendency to settle to the bottom of the water region. In Part II of this report, a simple extension of this model which includes the effects of high vapor pressure of liquid is given.

4.9 CONCLUSION

A simple diffusion-dispersion model is given for predicting the concentration history of a water-miscible chemical spilled on water. The navigational water region is divided into different regions, such as lakes, rivers, tidal rivers and the sea, and equations of dispersion applicable to each region are given. A sample calculation is done to indicate the method of calculation. The limitations of the model are discussed.

4.10 REFERENCES

1) "Estuarine Modeling – An Assessment" by Tracor, Inc. – Austin, Texas; Report prepared for the Water Quality Office of the Environmental Protection Agency. February 1971.

2) Harleman, D. R. F., "Transport Processes in Water Quality Control," MIT course lecture notes, 1972.

3) Fischer, H., "Dispersion Predictions in Natural Streams," Proc. ASCE, J. Sanitary Eng. Division, October 1968, pp. 927-943.

4) Holley, E. R., Harleman, D. R. F., and Fischer, H., "Dispersion in Homogeneous Estuary Flow"; J. Hyd. Div., Proc. ASCE, August 1970, pp. 1691-1709.

5) Thatcher, L., and Harleman, D. R. F., "A Mathematical Model for the Prediction of Unsteady Salinity Intrusion in Estuaries"; Report No. 144, Dept. of Civil Engineering, MIT, February 1972.

6) Harleman, D. R. F., Personal Communication, November 1972.

7) Chok Hung Lee, "One Dimensional Real Time Model for Estuarine Water Quality Prediction," Ph.D thesis, MIT, Civil Engineering Department, 1970.

4.11 NOMENCLATURE

Symbol		Description	Units
A	=	cross-sectional area	m^2
b	=	half-width of the river	m
c	=	local concentration of a pollutant	kg/m^3
C	=	cross-sectional area averaged concentration	kg/m^3
d	=	depth of flow	m
e_y, e_z	=	turbulent diffusion coefficients in y and z directions	m^2/s
E(x,t)	=	dispersion coefficient (local value)	m^2/s
E_L	=	longitudinal dispersion coefficient	m^2/s

Symbol		Description	Units
E_T	=	dispersion coefficient for the fresh water or well mixed region of the estuary	m^2/s
E_D	=	estuary stratification parameter (based on densimetric Froude number) = $P_T F_D^{\,2}/(Q_f T)$	
F_D	=	densimetric Froude number = $U_0/\sqrt{gh\,\Delta\rho/\rho}$	
g	=	acceleration due to gravity	m/s^2
h	=	depth of flow (or average depth)	m
k	=	decay rate coefficient	
K	=	dispersion parameter	
L	=	length of estuary	m
M	=	mass of pollutant released	kg
$\overset{\circ}{M}$	=	rate of mass release of the pollutant	kg/s
n	=	manning roughness factor $0.01 < n < .04$	
P_T	=	tidal prism = volume of water entering the estuary in flood tide	
Q_f	=	fresh water volumetric flow	m^3/s
R_h	=	hydraulic radius = cross-sectional flow area/wetted perimeter	m
s	=	salinity in ppm	
S_0	=	salinity concentration in the ocean. Also slope of the river bed.	
$\overset{\circ}{S}$	=	non-dimensional salinity – S/S_0	
t	=	time	s
T	=	tidal period	s
T'_v	=	characteristic vertical mixing time ratio	

Symbol		Description	Units
T_t'	=	characteristic, transverse mixing time ratio	
u	=	instantaneous velocity	m/s
u*	=	shear velocity $= \sqrt{\tau_0/\rho} = 3.115\ n\ U/R_h^{1/6}$	m/s
U_0	=	maximum flood velocity at the estuary entrance	m/s
U	=	average velocity of cross-section	m/s
U_f	=	fresh water velocity	m/s
U_T	=	peak oscillating velocity (amplitude)	m/s
W	=	width of river	m
x	=	longitudinal coordinate	m
y	=	lateral coordinate	m
z	=	depth-wise coordinate	m

Greek Symbols

δ	=	phase lag (to the next high water slack)	s
ρ	=	density of fluid	kg/m^3
ρ_w	=	density of water	kg/m^3
$\Delta\rho$	=	change in density over the entire length of estuary	kg/m^3
τ_0	=	wall shear stress	N/m^2

5.0 VAPOR DISPERSION (C,G,J,N,S,W)

5.1 AIM

The object of the derivations and equations given below is to obtain the vapor concentration at any position in space and at any time after a hazardous vapor cloud is released into the atmosphere.

5.2 INTRODUCTION

Of the many chemicals transported on water, quite a few are cryogenic liquids which vaporize when heated to atmospheric temperatures. Some liquids are highly reactive with water and produce toxic gases. Therefore, it is imperative that one has knowledge of the extent of dispersion of these released gases to assess their inherent hazard. A model is given here to enable the prediction of vapor concentrations at various locations and times.

The primary agent that will disperse a vapor cloud released into the atmosphere is the atmospheric turbulence. Molecular diffusion caused by concentration gradients represents a much smaller effect compared to turbulent mixing. Therefore wind conditions and the air temperature gradient (in effect, the local meteorological conditions) have considerable influence on the dilution of the cloud. The uncertain and unpredictable character of the atmospheric condition, the differences in topography of a particular locale, and the differences in the physical properties of the vapor released make it difficult to give a general dispersion model applicable to all circumstances and locations. However, some models have been proposed in the literature,* all of which have their roots in the Fickian diffusion equation based on turbulent diffusion coefficients. In almost all of the models the vapor released is assumed to have the same density as the local air (neutrally buoyant), and it is further assumed that during the dispersion process neither the wind direction, not its velocity, nor other meteorological conditions change. In most cases the effects of heat transfer from the surrounding air and ground are neglected. [For a discussion of the other effects, such as particulate settling, wash out by rain, etc., see Reference 1.]

The models presented here are the ones most widely used in practice for concentration predictions. Point sources (gas leak from a tank) and area sources (liquid spreading on water surface and evaporating) are considered separately. Both instantaneous and continuous vapor releases are considered. At the end of this section a discussion is given about the applicability of some of the atmospheric parameters obtained (from specif. experiments) from the literature.

*For an extensive discussion of the various types, see Reference 1.

5.3 ASSUMPTION

In using the equations given below, the following assumptions have to be noted:

a) The vapor that is diffusing is neutrally buoyant; that is, there is no gross movement of the vapor cloud caused by either gravity or buoyancy;

b) Mixing with air is uniform throughout the cloud; and

c) The concentration obtained is time-averaged.

5.4 DATA REQUIRED

- The atmospheric condition;
- The wind velocity and direction;
- The coordinates (with respect to the vapor source) of the point at which the concentration is to be calculated;
- The mass of vapor released (or the rate of release in the case of a continuous release); and
- The area of the source (not needed if point source formulas are used).

5.5 DETAILS OF THE MODEL

The models presented are based on the Gaussian diffusion models of Pasquill and others.[1] The origin of the x, y, z coordinates is on the ground directly beneath the source point (and, in the case of area sources, it is the center of the area on the ground). The x direction is defined as the direction of the wind and z is the vertical direction (see Figure 5.1).

5.5.1 Point Source

For vapor released *instantaneously* the following equation is used:

$$C(x,y,z,t) = \frac{m}{(2\pi)^{\frac{3}{2}}\sigma_x\sigma_y\sigma_z} \text{Exp}-\left[\frac{(x-Ut)^2}{2\sigma_x^2}+\frac{y^2}{2\sigma_y^2}\right]\times\left[\text{Exp}-\frac{(z-h)^2}{2\sigma_z^2}+\text{Exp}-\frac{(z+h)^2}{2\sigma_z^2}\right] \quad (5.1)$$

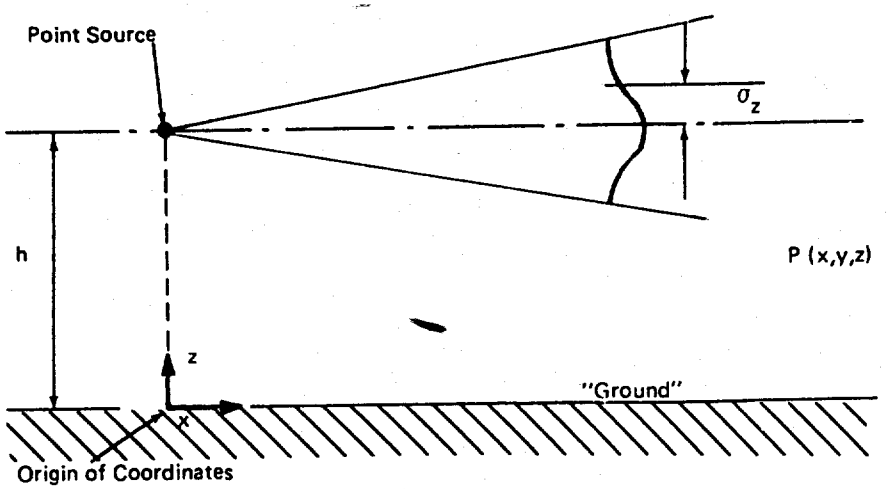

FIGURE 5.1a SCHEMATIC DIAGRAM OF A CONTINUOUS POINT SOURCE

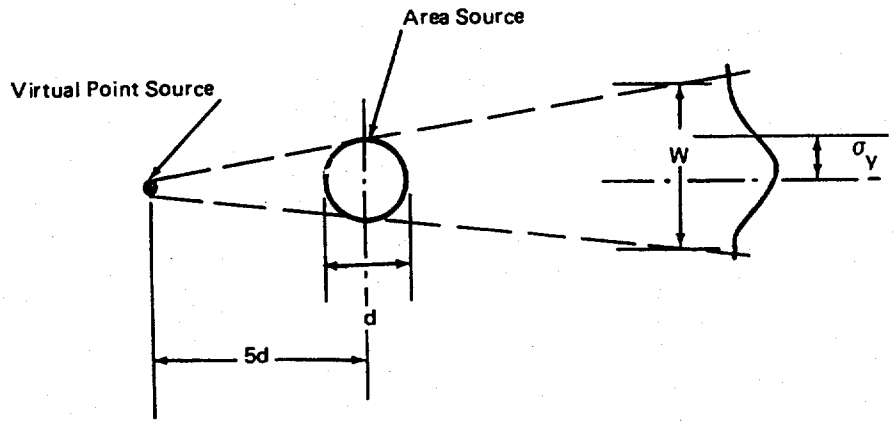

FIGURE 5.1b SCHEMATIC DIAGRAM OF A CONTINUOUS AREA SOURCE

where

σ_x, σ_y, σ_z = variances of the Gaussian concentration profiles in the respective directions.

The terms σ_y and σ_z are shown in Figure 5.2 as functions of downwind distance. For use in Eq. (5.1) we assume $\sigma_x = \sigma_y$.

For vapor released *continuously* at a *constant rate* the following equation is used:

$$C(x,y,z,t) = \begin{cases} \dfrac{\dot{m}}{2\pi u \sigma_y \sigma_z} e^{-\frac{y^2}{2\sigma_y^2}} \left[Exp - \left[\dfrac{(z-h)^2}{2\sigma_z^2} \right] + Exp - \left[\dfrac{(z+h)^2}{2\sigma_z^2} \right] \right] & \text{for } x \leq Ut \quad (5.2a) \\ 0 & \text{for } x > Ut \quad (5.2b) \end{cases}$$

If the concentration is expressed in mole fraction (C_f) of the air vapor mixture, then:

$$C_f = \frac{1}{\left[1 + \dfrac{\rho_a}{C} \dfrac{M_v}{M_a} \right]} \quad (5.3)$$

where ρ_a = the density of air at standard conditions (15°C, 1 atm).

5.5.2 Area Sources

The proper procedure for obtaining the concentration at any point due to an area source is to add the contributions from each infinitesimal point source in the area toward the concentration. This is illustrated by Eq. (5.4).

$$C_a(x,y,z,t) = \frac{m}{A} \int_{\bar{x},\bar{y} \text{ over the source area A}} C_p(x-\bar{x}, y-\bar{y}, z, t-\frac{\bar{x}}{U}) \, d\bar{x} \, d\bar{y} \quad (5.4)$$

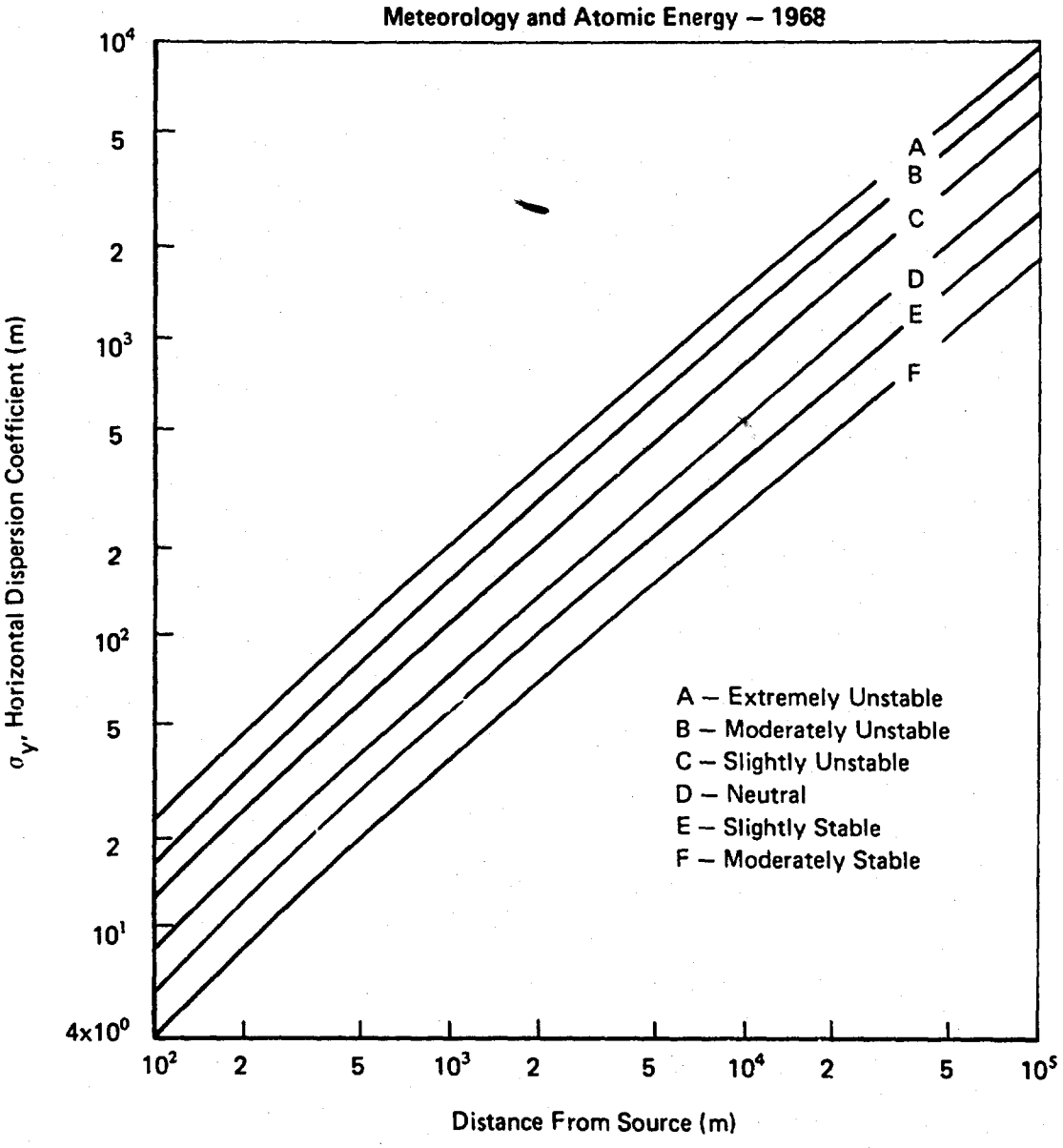

FIGURE 5.2a LATERAL DIFFUSION, σ_y, VERSUS DOWNWIND DISTANCE FROM SOURCE FOR PASQUILL'S TURBULENCE TYPES

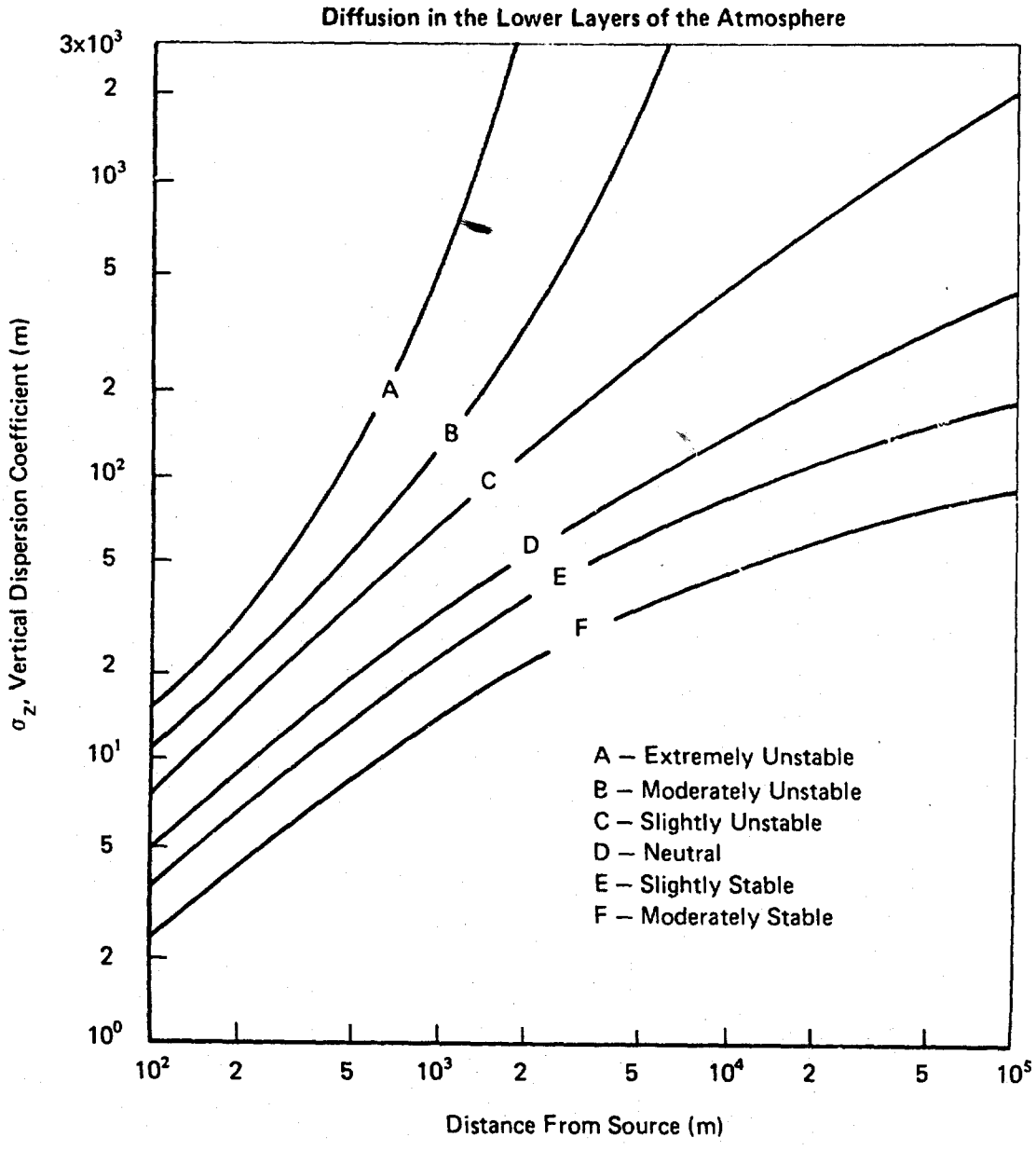

FIGURE 5.2b VERTICAL DIFFUSION, σ_z, VERSUS DOWNWIND DISTANCE FROM SOURCE FOR PASQUILL'S TURBULENCE TYPES

where

C_a = concentration at (x, y, z) due to area source;

C_p = concentration at the same point due to a point source at $\bar{x}$, $\bar{y}$; and

A = area of source.

In general, the evaluation of the above integral is difficult. However, for estimating the concentration at large distances (greater than two equivalent diameters of the source area) the following simple analysis suffices for most engineering purposes.

The area source is replaced by a virtual point source of the same total strength, but displaced upwind by a suitable distance. It is found that this "suitable distance" is a function of the concentration itself. However, a reasonable estimate of this upwind origin-shift distance is about 5 diameters. Hence, for area source calculations we use:

$$x' = x + 5d \tag{5.5a}$$

and substitute this x' in Eq. (5.1), instead of x, to obtain the concentration at point x.

For *continuous area sources* also a similar procedure is used (as described above). Use is made of Eqs. (5.5a) and (5.2) to obtain the downwind concentrations. In Reference 4 a more sophisticated model is presented for the case in which the source area is changing with time as in the case of an expanding and evaporating liquid pool (say, on water). This is based on the evaluation of the integral given in Eq. (5.4).

5.5.3 Plume Width

From the equations given above, it is easy to calculate the width of the vapor plume (at the source level) to any specified concentration C*.

Let $C_0(x,t)$ = peak concentration at point x and at any time (this is obtained by putting y = 0 and z = h in the equations given above).

Then it can be shown that

$$W(C^*) = \text{Plume width} = 2\sqrt{2}\,\sigma_y \sqrt{\ln\left(\frac{C_0(x,t)}{C^*}\right)} \tag{5.5b}$$

5.6 ALGORITHM FOR COMPUTATIONS

Since the formulas presented are straightforward, the algorithm for computation is very simple. Once the type of the source is established, the proper formula is used. The algorithm is best illustrated by the example worked out.

5.7 SPECIFIC EXAMPLE

Type of vapor dispersing = natural gas

Atmospheric condition = neutral

Total mass of vapor released = m = 1000 tons.

If this mass of LNG is spilled on water, the maximum pool radius* $R_{max} \simeq 125$ m.

Mean pool radius $R_{mean} \simeq R_{max}/\sqrt{2} = 88$ m

Time for complete evaporation $t_e \simeq 450$ s

Wind velocity $\simeq 2.5$ m/s.

Position of the observation point $\begin{cases} x = 1.0 \text{ m} \\ y = 0.0 \text{ m} \\ z = 0.0 \text{ m} \end{cases}$

Therefore from Figure 5.2 for atmosphere D $\begin{cases} \sigma_y = 70 \text{ m} \\ \sigma_z = 32 \text{ m} \end{cases}$

5.7.1 Instantaneous Point Source

If all of the above mass is released at a point instantaneously, then (Eq. (5.1)):

$$C_0 (1 \text{ km}, 0, 0, t') \simeq 2m/(2\pi)^{3/2} \sigma_z \sigma_y^2 = 0.81 \text{ kg/m}^3.$$

The time at which this maximum concentration occurs = $t^1 = x/u = 400$ s.

*See Part II – "Simultaneous Spreading and Evaporation on Water," Chapter 9.

From Eq. (5.3) we have mole fraction concentration:

$$C_f = \frac{1}{[1 + 1.22/0.81 \times 17/28.9]} = 0.53$$

Hence, the width of 5% mole concentration = $2\sqrt{2}\ \sqrt{\ell n(53/5)}\ \sigma_y = 304$ m

5.7.2 Continuous Area Source:

Displacement distance = 5 x (2 x 88) = 880 m

Mean evaporation rate = $10^6/450 = 2222.2$ kg/s

$x^1 = x + 880 = 1880$ m

$\sigma_y\ (x^1) = 120$ m

$\sigma_z\ (x^1) = 48$ m

From Eq. (5.2):

$$C_o = \frac{\dot{m}}{\pi\ \sigma_y\ \sigma_z\ U} = \frac{2222.2}{\pi \times 2.5 \times 120 \times 48} = 0.049 \ \text{kg/m}^3.$$

$$C_f = \frac{1}{1 + 1.22/0.049 \times 17/28.9} = 0.064$$

Therefore, the width of 5% mole concentration $\simeq$ 98 m.

5.8 DISCUSSION

The equations given in this section provide a means of estimating the concentration of vapor at any location at any time, provided the wind and other meteorological data are available. The model is based on the Gaussian diffusion model and uses two experimentally determined parameters σ_y and σ_z. These have been measured by Pasquill under different

atmospheric conditions. These curves (as a funciton of downwind distance) are reproduced in Figure 5.2 from Reference 1. These variance values were measured for continuous discharges of a specific vapor. Whether the same values apply to the dispersion of a puff (suddenly released vapor mass) is debatable. It can be argued that since these values represent, in a way, a scale of atmospheric turbulence, and since we assume that the effect of a large amount of vapor release has but little influence on the local atmospheric dynamics, σ_y and σ_z given in Figure 5.2 should be almost universal and should not depend on the nature of vapor release. However, limited data obtained from measurements of σ_y from instantaneous sources seem to indicate[2] that the above contention is not justified. The σ_y's measured from instantaneous source experiments are smaller than those obtained from continuous source experiments. Also the assumption of $\sigma_x = \sigma_y$ does not seem to be proper. The σ_x measurements[2] for instantaneous sources indicate that they are higher than σ_y values. However, since the data given in Reference 2 have not been verified for many cases of instantaneous sources, and since Pasquill's curves have withstood the tests of time, it is suggested for the purposes of usage at the present time that σ_y and σ_z values given in Figure 5.2 to be used until such time as more refined experimental data are available.

It should be noted that the models given do not take into account the disturbances caused by obstruction or wind direction change or wind velocity change. In the real case all these phenomena are definitely present and cause the vapor to disperse over a wider area (therefore in lower concentration than predicted by the equations). Since there is no quantitative way in which these effects can be included in the equations and since these are quite important, one should not attach too much importance to the concentration values predicted by using the equations given. In fact, these numbers should be considered only as a guide to evaluating the hazards. The equations presented do not include the effects of the vapor being heated by the ground or air and the consequent rise of the plume although the literature[3] does contain some information on the rise of the plume. However, since no rational basis is provided for calculating these rise velocities, they are not incorporated in the equations presented.

5.9 CONCLUSIONS

Equations are given for calculating the downwind concentrations (of vapor) consequent to a release of a vapor cloud to the atmosphere. A method of treating an area source by an equivalent virtual point source is presented. Limitations of the models are discussed in detail. An illustrative example is worked out to indicate the procedure of calculations and to indicate the values of numbers that can be expected.

5.10 REFERENCES

1) "Meteorology and Atomic Energy"; U.S. Atomic Energy Commission, Division of Technical Information, Slade, D.H., Editor. July 1968, Ch. 3, pp. 65-116.

2) Beals, G.A., "Guide to Local Diffusion of Air Pollutants"; Technical Report No. 214 U.S.A.F. Air Weather Service (MAC), Scott AFB, Illinois, May 1971, p. 37.

3) Humbert, B.R., and Montet, A., "Flammable Mixture Penetration in the Atmosphere from Spillage of LNG"; 3rd International Conference and Exhibition on LNG; Washington, D.C., Sept. 24-28, 1972, Section VI, pp. 1-34 (paper in French).

4) Arthur D. Little, Inc., "A Report on LNG Safety Research – Vol. II," prepared for American Gas Association, Jan. 1971, pp. 62-65.

5.11 NOMENCLATURE

Symbol	Description	Formula or Value	Units
C	concentration of vapor		kg/m^3
C_f	molar vapor concentration		fraction or %
d	equivalent diameter of area source		m
h	height of source above the ground		m
m	mass of vapor released		kg
$\dot{m}$	rate of release of vapor		kg/s
M_a	molecular weight of air	28.9	kg/kmole
M_v	molecular weight of vapor		kg/kmole
t	time		s
U	wind velocity		m/s
W	width of vapor plume at any point		m
x	downwind distance		m
y	crosswind distance		m
z	vertical distance		m
ρ_a	density of air at 15°C, 1 atm	1.22	kg/m^3
$\sigma_x, \sigma_y, \sigma_z$	variances of Gaussian concentration profile		m

6.0 FLAME SIZE (B, E, H, L, Q, U, Y)

6.1 AIM

The object of the flame size models is to obtain the length, diameter, and inclination of flames, during the burning of a gas or a liquid burning from a pool.

6.2 INTRODUCTION

Many of the chemicals transported over water are combustible. To assess the radiation damage to nearby structures caused by the flame of a burning chemical, one must know the flame size, its shape, and its orientation, in addition to its equivalent blackbody temperature. The models given below predict the flame size and orientation for two kinds of burning processes. In the first case the burning of a jet of gas issuing from a hole in a pressurized tank is considered. In the second case the flame size on a liquid pool is considered.

Hawthorne, Waddell, and Hottel,[1] and Hottel[2] have investigated the flame lengths from turbulent gas jets. They have also developed a model in which the flame length is derived by applying the laws of conservation of mass and momentum and an equation of state, together with the assumption that the flame shape is an inverted right circular cone (i.e., the angular spread of flame is a constant). This equation is given in a later section. The size prediction by this equation has been tested experimentally by NASA[3] and found to be reasonably accurate. Pool burning of liquids has been investigated by various people (Thomas,[4] Blinov and Khudiakov,[5] et al.). Correlations to the flame height and angular tilt have been obtained in terms of wind velocity and the burning rate. However, these relationships have been obtained with only laboratory size flames.

6.3 ASSUMPTIONS

In the case of burning of a gas jet it is assumed that the flow in the jet is turbulent and that the plume is like a cone with constant angle opening. It is also assumed that the buoyancy does not affect the flame in any way (since the velocity of jet is quite high, this is generally true) and also wind blowing has little effect on bending the flame.

6.4 DATA REQUIRED

To predict the flame length and tilt because of the wind, the following data are needed:

Jet burning

- Adiabatic flame temperature of the gas

- Chemical composition of the gas in the jet
- Molecular weight of the gas.

Pool burning

- Liquid burning rate
- Diameter of the pool
- Wind velocity

6.5 DETAILS OF EQUATIONS

Burning jet

The following equation is suggested for flame length:[2]

$$\frac{L}{D} = \frac{k_f}{c}\sqrt{c + (1-c)\frac{M_a}{M_f}\frac{T_F}{\alpha T_o}} \qquad (6.1)$$

$$c = \frac{1}{\left[1 + r\frac{M_f}{M_a}\right]} \qquad (6.2)$$

where

k_f = a factor ($\simeq 5.3$) which depends on the Froude number,

r = stoichiometric air-fuel ratio = $\frac{\text{kg of air}}{\text{kg of fuel}}$,

M_f, M_a = molecular weights of gas and air, respectively,

α = $\frac{\text{moles of reactants}}{\text{moles of products}}$ for stoichiometric combustion,

T_F = adiabatic flame temperature, °K, and

T_0 = ambient temperature, °K,

and r can be calculated from the chemical reaction equation for complete combustion.

The exhaust angle θ is between 10 to 20 deg. (see Figure 6.1).

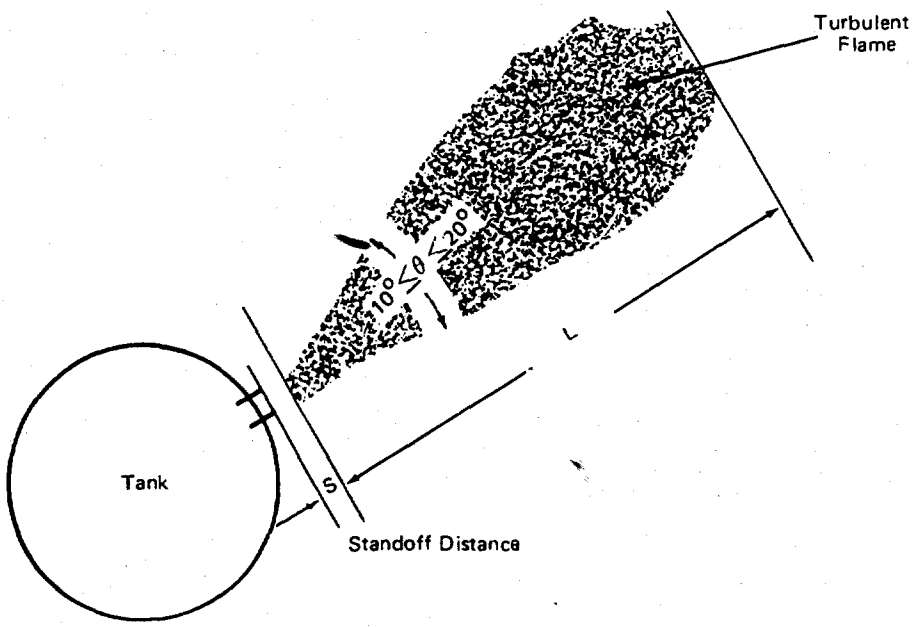

FIGURE 6.1 STANDOFF FLAME IN A TURBULENT JET

The diameter of an equivalent cylindrical flame (for radiation calculations) is:

$$\frac{D_e}{D} = \left(\sec \frac{\theta}{2} + \frac{L}{D} \sin\frac{\theta}{2} \sec^2 \frac{\theta}{2} \right) \tag{6.3}$$

Pool burning

Thomas[6] suggests the following flame-height correlation:

$$\frac{L}{D} = 42 \left[\frac{\dot{m}''}{\rho_a \sqrt{gD}} \right]^{0.61} \tag{6.4}$$

and for the flame tilt angle θ with vertical

$$\cos\theta = 0.7 \left[\frac{U}{\left(\frac{\dot{m}''}{\rho_a} g D \right)^{1/3}} \right]^{-0.49} \tag{6.5}$$

An alternative equation suggested by Welker and Sliepcevich[7] is:

$$\frac{\tan\theta}{\cos\theta} = 3.3 \left(\frac{D U}{\nu_a} \right)^{0.07} \left(\frac{U^2}{g D} \right)^{0.8} \left(\frac{\rho_g}{\rho_a} \right)^{-0.6} \tag{6.6}$$

It is known that the length of the flame is not affected to any measurable degree by wind velocity. This is probably due to the wind stretching and increased turbulent mixing effects counteracting each other.

6.6 COMPUTATIONAL ALGORITHM

No algorithm is given because of the simplicity of the equations. Depending on the nature of the burning (gas jet or pool), the appropriate formula is used.

6.7 SPECIFIC EXAMPLE

Jet burning:

Fuel in the gas jet = methane (CH_4)

Molecular weight = 16 ⟷ kg/kmole

Adiabatic flame temperature = 2065°C or 2338°K

Diameter of hole = 0.15 m

Ambient air temperature = 300°K.

r = stoichiometric air-fuel ratio = $\frac{64}{16 \times 0.233} = 17.17$

α = reactant product molar ratio = $\frac{3}{3} = 1$

$$C = \frac{1}{1 + 17.17 \frac{16}{28.9}}$$

Hence, from Eq. (6.1):

$$\frac{L}{D} = \frac{5.3}{0.095} \sqrt{\left\{0.095 + (1 - 0.095) \frac{28.9}{16}\right\} \frac{2338}{300}} = 204.8.$$

Hence, length of flame, L = 204.8 x 0.15 = 30.72 m,

assuming flame cone angle = 20 deg.

Equivalent cylindrical flame diameter:

$$D_e = (0.15 \times 1.015 + 30.72 \times 0.1736 \times 1.031) = 5.65 \text{ m}$$

Table 6.1 gives results for a few of the common gases.

Pool burning:

Pool liquid = LNG

Density of liquid = 425 kg/m^3

Burning rate = 10 mm/min

Diameter of dike = 10 m

Wind velocity = 3 m/s

Therefore:

$$\dot{m}'' = \text{burning rate} = 10 \times 10^{-3}/60 \times 425 = 0.07083 \text{ kg/m}^2 \text{ s}$$

$$= 1.3 \times \sqrt{9.8 \times 10} = 12.869 \text{ kg/m}^2 \text{ s}$$

Therefore, from Eq. (6.4):

$$\frac{L}{D} = 42\ \frac{.07083^{.61}}{12.869} = 1.76,$$

and therefore height of flame = 17.58 m.

The flame height for other diameters is indicated in Figure 6.2. Using Eq. (6.5) the flame angle is estimated to be

$$\cos\theta = 0.7 \left[\frac{3}{\left[\frac{(9.8 \times 10)\ \ .07083}{1.3}\right]^{1/3}} \right]^{-0.49} = 0.537$$

Therefore flame tilt with vertical = 57.5 deg. Equation (6.6) gives a value of $\theta = 42.2$ deg.

6.8 DISCUSSIONS

The equations given for the flame length and tilt due to wind are the best available information in the literature. However, it should be noted that in recent times more and more large-scale experiments – particularly with LNG – are being conducted and it is suggested that, as and when new correlations are obtained, they be incorporated into the CHRIS program.

Equation (6.1) has been obtained by Hawthorne et al. for the burning of fuel in a ramjet. It is noted here that the jet is highly turbulent in these cases. Also the pressure differential between the tank and the ambient does not seem to matter as far as the length of the flame is concerned. This is probably due to the fact that a higher pressure differential (before the throat attains sonic condition) gives a higher discharge velocity, causing increased turbulence leading to better mixing and, hence, shorter time for complete burning (diffusion flame). The product of this time and the velocity seems to remain approximately a constant, giving a pressure insensitive flame length. Hottel's paper[1] contains a comparison between Eq. (6.1) and experimental data with various gases. The equation and the data agree very well.

Thomas'[4] equation (6.4) for the flame height in pool burning is also an empirical equation based on simple dimensional analysis and extensive experimental data. The correlation has been tested against data for burning of heavy industrial fuels up to a pool size of 23 meters in diameter. Thomas feels that the correlation would give an overestimate of the flame height for very large pool sizes. The equation does not take into account the possibility of stretching of flame by wind. However, experimental observations seem to indicate that this wind stretching is minimal – again possibly due to increased turbulence.

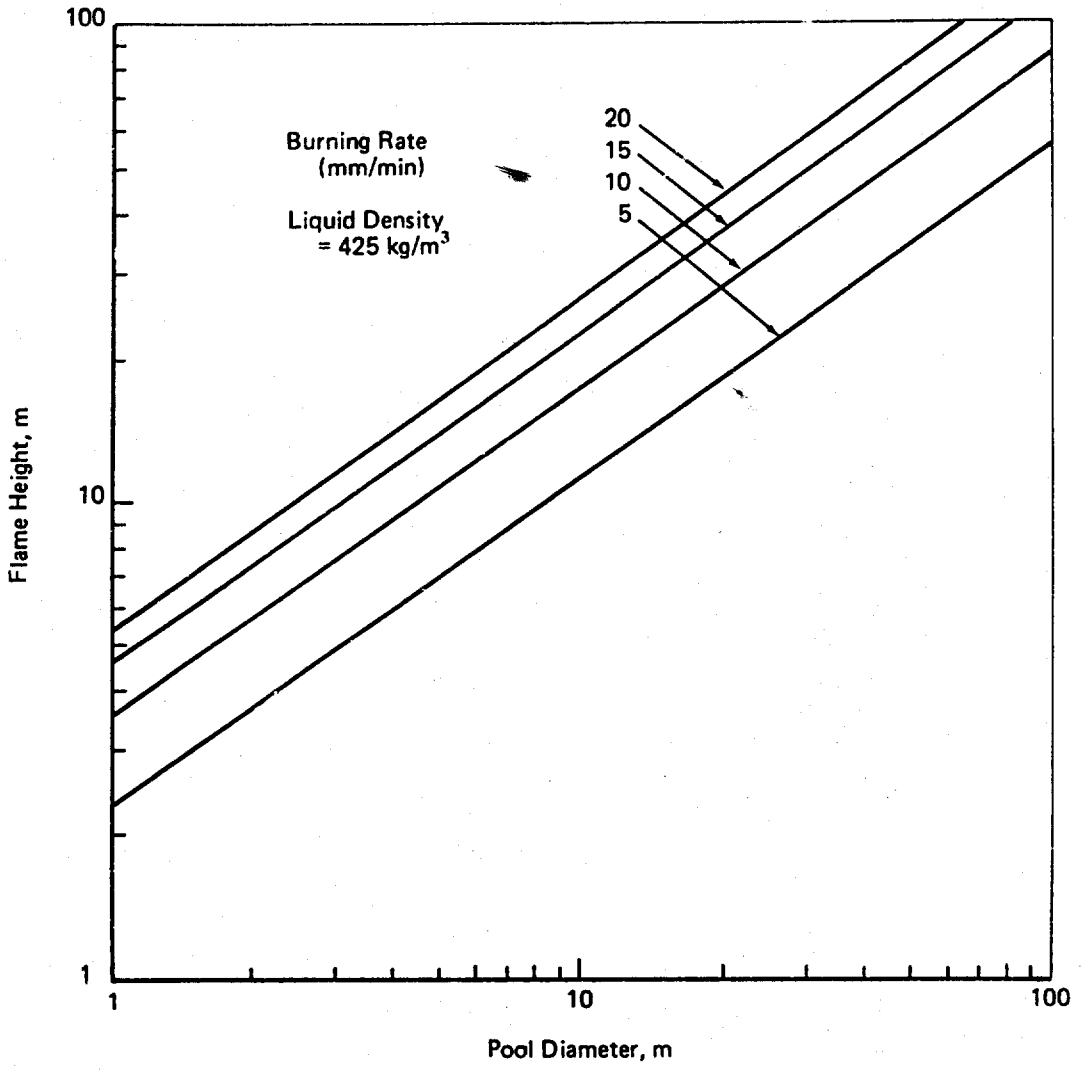

FIGURE 6.2 PLOT OF EQUATION 6.4

Equations (6.5) and (6.6) are flame-tilt correlations obtained from laboratory experiments. It is doubtful whether these can be extended to give the flame tilts for very large flames. The turbulence in a wind tunnel is quite different from the turbulence in the atmosphere. Also large flames themselves cause radially inward winds up to 2 m/s (because of the large convection flux). They also tend to act like solid cylinders in air stream, which causes air to deflect around the sides of the flame. Again, as before, lack of field data constrains us to use these correlations at the present time. Because of the slightly improved correlation provided by Eq. (4.6), it is suggested that this formula be used for CHRIS calculations for the present.

6.9 CONCLUSIONS

Formulas have been provided that predict the flame length for burning of a gas jet of a pool of liquid. Also provided are equations to calculate the flame tilt caused by wind. Several aspects of the formulas are discussed and their limitations explained. Suggestions have been made for the appropriate use of the formulas.

6.10 REFERENCES

1) Hottel, H.C., "Burning in Laminar and Turbulent Fuel Jets"; 4th International Symposium on Combustion, 1953, pp. 97-113.

2) Hawthorne, W.R., Waddell, D.S., and Hottel, H.C., "Mixing and Combustion in Turbulent Gas Jets"; 3rd International Symposium on Combustion, Flame and Explosion Phenomena, Williams and Wilkins, Baltimore, 1949, pp. 266-280.

3) "NES Exhaust Plume Scale Model Measurements and Full-Scale Predictions," NERVA Program Report No. RN-S-0168 to NASA, Aerojet General Corp, November 1964.

4) Thomas, P.H., "The Size of Flames from Natural Fires"; 9th Symposium (International) on Combustion, Academic Press, New York, 1963, pp. 844-859.

5) Blinov, V.I., and Khudiakov, G.N., "Certain Laws Governing Diffusive Burning of Liquids," Doklady Alcademii Naud., USSR, Vol. 113, No. 5, May 1957, pp. 1094-1097.

6) Thomas, P.H., "Fire Spread in Wooden Cribs – Part III: The Effect of Wind," Fire Res. Note No. 600, Fire Research Station, Boreham Wood, England, June 1965.

7) Welker, J.R., and Sliepovich, C.M., "The Effect of Wind on Flames," Technical Report No. 2, Contract OCD-OS-62-89, University of Oklahoma Research Institute, Norman, Oklahoma, November 1965.

6.11 LIST OF SYMBOLS

Symbol	Description	Value or Formula	Units
D	diameter of dike or diameter of jet hole		m
D_c	equivalent diameter of a cylindrical flame	Eq. (6.3)	m
g	acceleration due to gravity	9.8	m/s^2
L	flame length or height		m
$\dot{m}''$	burning rate		$kg/m^2 s$
M_a	molecular weight of air	28.9	kg/kmole
M_f	molecular weight of fuel		kg/kmole
r	stoichiometric air-fuel ratio		kg of air/kg of fuel
T_F	adiabatic flame temperature		°K
T_0	ambient air temperature		°K
U	wind velocity		m/s
Greek Letters			
α	Stoichiometric ratio of moles of reactants to moles of products		
θ	angle of tilt of flame with vertical		radian
ρ_a	density of air	1.3	kg/m^3

TABLE 6.1

TURBULENT FLAME LENGTH FOR VARIOUS COMMON GASEOUS FUELS

Type of Gas	Chemical Formula	Mol. Wt (kg/kmole)	Adiabatic Flame Temp (°K)	Air Fuel Ratio, r	Reactant Product Mole Ratio, α	L/D	D_e/D for 20 Deg Angle
Methane	CH_4	16	2338	17.17	1.0	204.8	37.68
Propane	C_3H_8	44	2390	15.61	0.857	327.8	59.7
Hydrogen	H_2	2	2485	34.33	1.5	136.0	25.37
Acetylene	C_2H_2	26	2905	13.20	1.167	206.4	38.0

7.0 THERMAL RADIATION FROM FLAMES

7.1 AIM

The aim of this section is to provide formulas and correlations to predict the radiant heat transfer from the flames of different fuels.

7.2 INTRODUCTION

The damage to nearby objects due to a fire is caused mainly by thermal radiation. Depending on the intensity of radiation and the nature of the objects, the hazard can be serious. Welker et al.[1] suggest the use of the radiant flux levels given in Table 7.1 to assess the damage to different objects.

Thermal radiation interchange between two objects depends, to a large extent, on the amount of the surface area of one that the other can "see." In addition, the heat flux exchange also depends on the absolute temperatures of the surfaces, their relative orientation, the emissivity and absorptivity of the two surfaces, and emission or absorption by the intervening gaseous medium. In the case of radiation from a flame to an object outside of it, the radiant energy received by the object depends on the flame temperature, the "view factor," and the flame emissivity. Emissivity of the flame is a function of the flame size (diameter) and its luminosity (which itself depends on the type of fuel burning). Atallah[2] has discussed in detail the emissivity of luminous flames and the problems involved in measuring the emissivity of fires. The emissivities are expressed in terms of an absorption coefficient (k) which is a measure of the distance (through the fire) in which considerable radiation is absorbed. For "optically thick" fires this distance is much smaller than the characteristic flame dimension.

Effective flame temperatures for radiation depend on the type of fuel and the size of flame. Several workers (Canfield and Russel[3], and Maezawa[4]) have measured temperatures inside flames and found them to vary over a wide range, both radially and vertically. Rasbash et al.[5] measured the effective flame temperatures and emissivities. The results are given in Table 7.2.

The calculation of the view factor between a flame and an infinitesimal plane on the ground have been performed by Rein et al.[6] and Merriam.[7] These calculations are based on the numerical integration of the "view factor" integral. An improved calculation, based on analytical methods of view factor calculation, is given in Part II of this report.

7.3 ASSUMPTIONS

The main assumption made in calculating the radiant heat transfer from the flame to a body outside it is to treat the flame as a cylindrical object of uniform temperature. This cylindrical plume may be inclined to the vertical.

7.4 DATA REQUIRED

a. Flame diameter, length, and the inclination with respect to the vertical;

b. Flame emissivity and temperature (or, alternatively, the type of fuel that is burning from which these can be estimated); and

c. Position of the observer, the orientation of the observation plane, and absorptivity of the material.

7.5 MODEL DETAILS

The heat flux received by the observer from a flame is:

$$Q = F\ \alpha \tau \epsilon \sigma T_f^4 \tag{7.1}$$

where α, F, τ, ϵ, σ, and T_f are, respectively, the object absorptivity, view factor, the atmospheric transmissivity, the flame emissivity, Stefan-Boltzamann constant and the equivalent blackbody flame temperature.

7.5.1 Emissivity (ϵ)

$$\epsilon = 1 - e^{-\kappa d} \tag{7.2}$$

where κ is the emission coefficient (also called the attenuation coefficient) obtained from Table 7.2, and d is the characteristic thickness dimension of the flame.

7.5.2 Transmissivity (τ)

The main medium of absorption in the atmosphere is the water vapor, though carbon dioxide also absorbs (but this absorption is small compared to that of water vapor). The following method has been suggested by Sarofim[8] to calculate the mean transmissivity of water vapor:

$$\tau_\omega = \exp\left[\frac{-\frac{s_\omega}{d} U}{\sqrt{1 + \frac{s_\omega}{4b_\omega} U}}\right] \tag{7.3}$$

where

τ_ω = transmissivity for a radiation of wave number

$s_\omega = \int_{\omega'=-\infty}^{\infty} \kappa\ (\omega, \omega')\, d\,\omega'$ = mean integrated line intensity

κ_ω = attenuation coefficient for a single line – centered at ω

d_ω = mean distance of separation of spectral lines of wave number ω.

b_ω = mean line half width at wave number ω.

$U = \int_{y=0}^{x} p\, dy$ = partial pressure (of water vapor) length (x) integral.

The values of s/d and b/d are given as functions of temperatures for each of the wave number intervals by General Dynamics.[9] The mean transmittance is then calculated using:

$$\tau_{avg} = \frac{\int_0^\infty \tau_\omega\, E_\omega\, d\omega}{\int_0^\infty E_\omega\, d\omega} \tag{7.4}$$

where

E_ω = emissive power of the source at the wave number "ω" in units of W/m

$$= C_1 \left(\frac{\omega}{T}\right)^3 \Bigg/ \left[e^{\left(\frac{C_2\,\omega}{T}\right)} - 1 \right]$$

C_1 = First Planck Constant = 3.7418×10^{-16} W/m^2

C_2 = Second Planck Constant = 1.4388×10^{-2} m°K

The integration in the numerator of Eq. (7.4) is carried out numerically while the denominator has the value.

$$\int_0^\infty E_\omega d\,\omega = \sigma\, T^4$$

7.5.3 View Factor

The view factor between a body and an infinitesimal surface (of surface area dA_1) is calculated by the formula:

$$F_{1\to 2} = \int_{\overline{A}_2} dA_2 \frac{\cos\theta_1 \cos\theta_2}{\pi r^2} \tag{7.5}$$

where

$\overline{A}_2$ = area "seen" by the infinitesimal surface 1

r = magnitude of the distance between the centers of areas dA_1 and dA_2

θ_1 = angle between the r vector and the outward normal to dA_1

θ_2 = angle between the r vector and the outward normal to dA_2

The integration of Eq. (7.5) is carried out numerically, the details of which are given below in Section 7.6.

7.6 COMPUTATIONAL ALGORITHM

The main features of the algorithm are illustrated by the flow diagrams in Figures 7.1, 7.2, and 7.3. Figures 7.2 and 7.3 are the algorithms to evaluate numerically the transmissivity of water vapor and the view factor.

7.7 SPECIFIC EXAMPLE

The following values are used for illustrating the method of calculations:

Type of fuel	= natural gas
Flame diameter	= D = 6 m
Flame length	= L = 18 m
Flame tilt with respect to vertical	= θ = 60 deg.
Flame temperature	= T = 900°C = 1173°K

Observation plane position

Distance from flame center on the ground	= s = 24 m

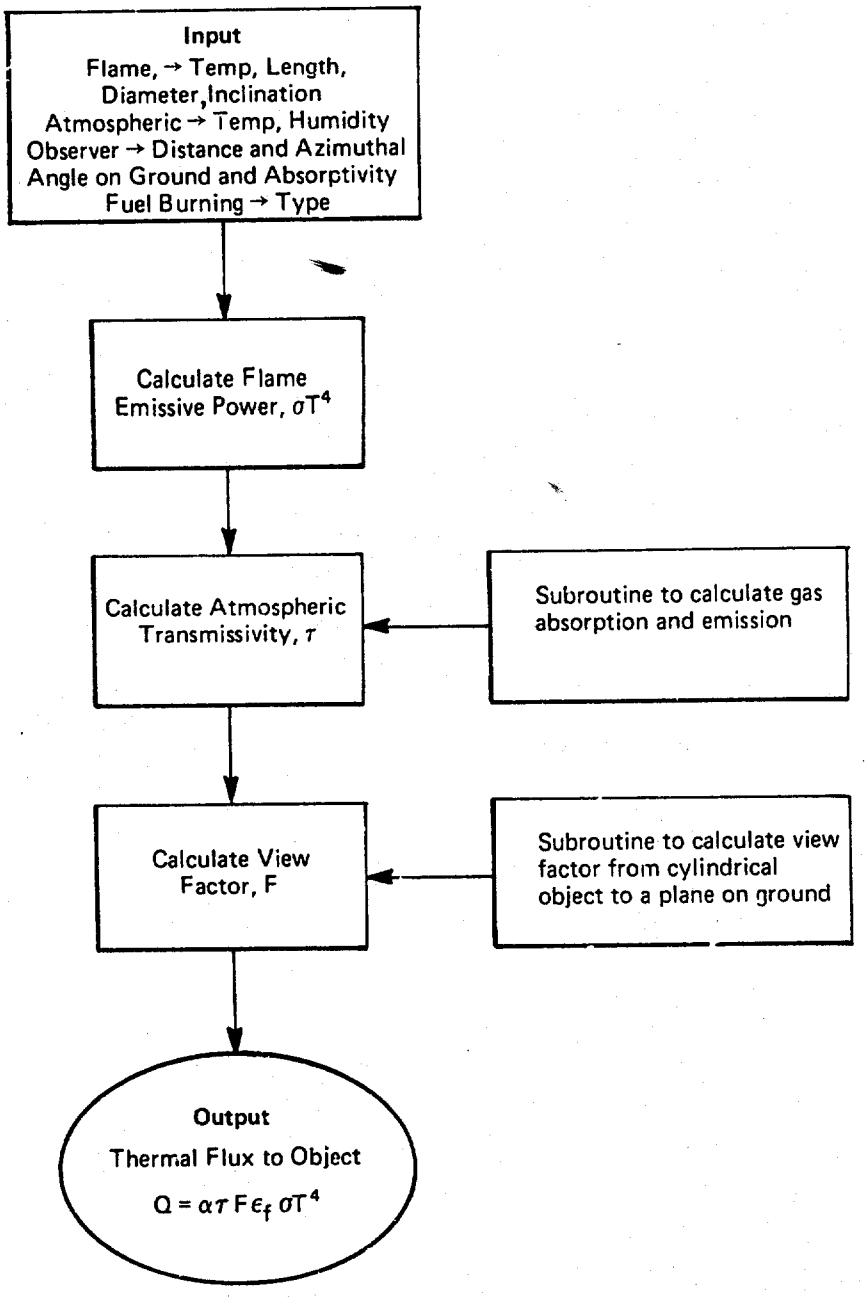

FIGURE 7.1 FLOW CHART FOR THERMAL FLUX CALCULATION

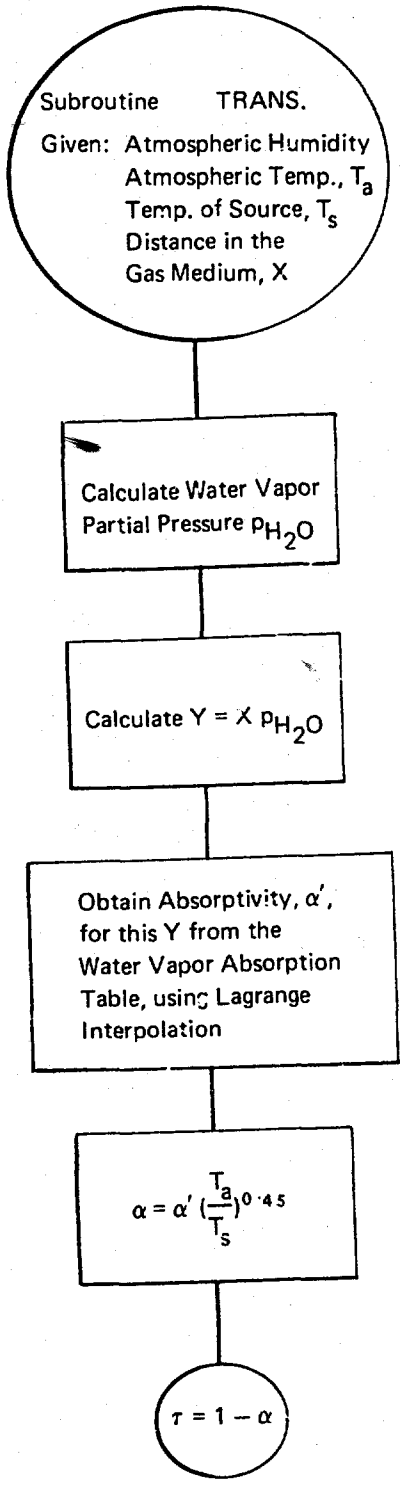

FIGURE 7.2 FLOW CHART FOR THE CALCULATION OF WATER VAPOR TRANSMISSIVITY

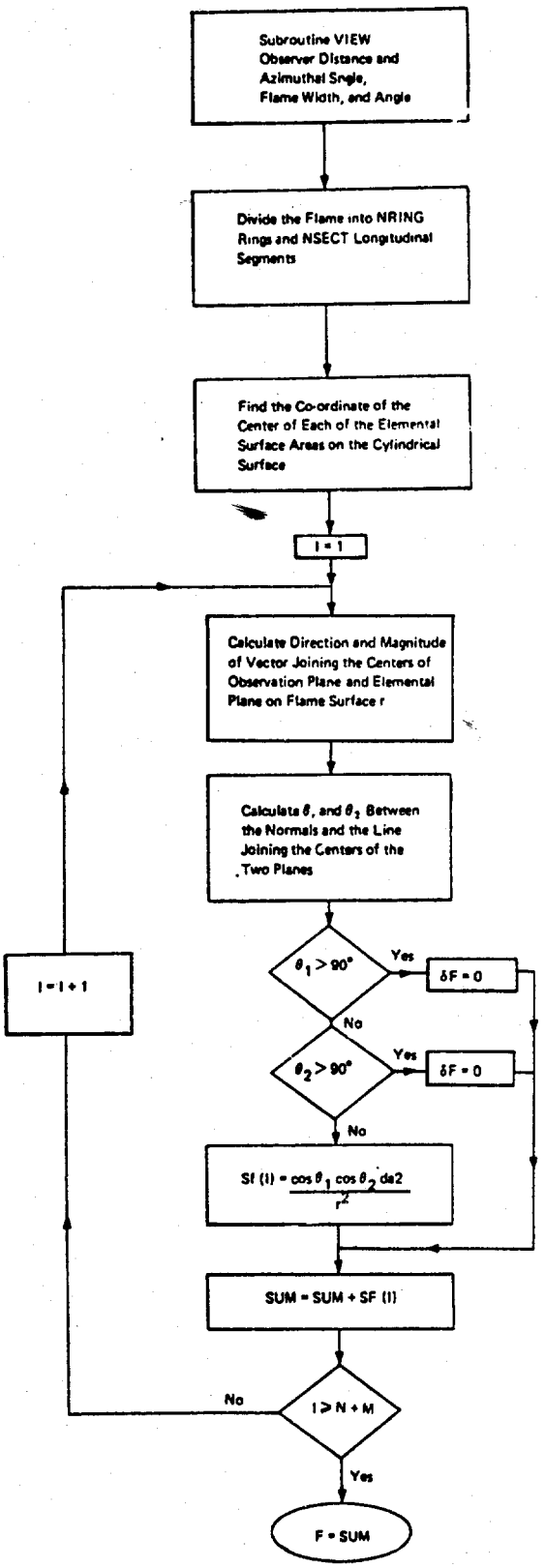

FIGURE 7.3 FLOW CHART FOR THE CALCULATION OF THE VIEW FACTOR

Azimuthal angle (with the flame inclination direction as the initial line)	$= \phi = 0°$
Atmospheric temperature =	$= T_a = 15.5°C$
Atmospheric relative humidity	$= RH = 50\%$
Attenuation coefficient (from Table 7.2)	$= \kappa = 0.5\ m^{-1}$
Stefan-Boltzmann constant	$= \sigma = 5.6696 \times 10^{-8}\ W/m^2\ °K^4$
Hence:	
Flame emissivity	$= \epsilon_f = (1 - e^{-0.5 \times 6}) = 0.9552$

For the given atmospheric conditions and the distance of (24 – D/2) = 21 m, the transmissivity of water vapor τ is obtained from the computer result:

$$\tau = 0.7994$$

Similarly the view factor to a vertical plane on the ground at 24 m from the flame center is obtained from the computer result:

$$F = 0.0463.$$

Hence the heat flame to the element on the ground at 24 m from flame center is (with element absorptivity $\alpha = 1$) (refer to Eq. (7.1)):

$$Q = 1 \times 0.0463 \times 0.7994 \times 0.9552 \times 5.6696 \times 10^{-8} \times (1173)^4 = 3794.7\ W/m^2$$

7.8 DISCUSSIONS

A radiation view factor-based model has been given which treats the flame as a cylindrical object radiating heat to the surroundings. However, it is known that large size flames in the atmosphere are quite turbulent and can hardly be described as cylinders. In fact, the radiating surface area of flames is much larger (because of folding surfaces) than that of an equivalent cylinder. However, because these folded surfaces "see" each other, the effective radiative surface area for radiation to the surroundings is nearly equal to the area of the equivalent cylinder. The flame shape also depends on the pool geometry. Should the burning emanate from a narrow but long ditch, the flame is more likely to be a planar flame rather than cylindrical.

The emissivity values given in Table 7.2 are only the mean values. The emissivity also depends on the flame dimension. The physical meaning of the attenuation coefficient is seen from the reciprocal of the K value. This gives a distance inside the flame within which the radiation intensity is reduced by 37% of its original value by absorption effected by the gaseous products inside the flame. For some flames (such as heavy hydrocarbon fuel fires) the emissivity is very low because of the predominance of soot in the flame. However, it should be remembered that wind action sometimes exposes the hot portions in the flame. Therefore, in assessing the hazards due to such flames a higher emissivity is to be used than the values quoted.

Water vapor in the atmosphere is a very good absorber of the infrared radiation. In fact, it can be shown that at 21°C and 80% RH about 62% of radiation is absorbed in a distance of 150 m (flame temperature 800°C). The higher the humidity or longer the distance, the greater is the absorption. Carbon dioxide also is a good absorber of thermal radiation. However, only traces of CO_2 are present in the atmosphere and, hence, it does not contribute to the absorption of radiation from flames.

Burgess and Zabetakis[10] and May and McQueen[11] have reported that only a fraction of the total heat released by the combustion process is radiated to the surroundings, the rest of the heat being convected away by the hot combustion product gases. This fraction varies from as low as 0.1 to as high as 0.35, depending on the fuel, flame emissivity, and such.

7.9 CONCLUSIONS

A method has been given to calculate the heat flux between a flame and a surface on the ground. This method is based on a view factor radiation model in which the flame is considered to be a cylinder. Principles of the methods of calculation of the view factor and the atmospheric transmissivity are given. Water vapor in the atmosphere and relative position and orientation (with respect to the flame of the heat-receiving object) were found to be quite important in determining the extent of heat received by the surface.

7.10 REFERENCES

1. Welker, J.R., Wesson, H.R., and Sliepcevich, C.M., "LNG Spills: To Burn or Not to Burn!," Presented at the Distribution Conference, Operating Section, American Gas Association, Philadelphia, May 1969.

2. Atallah, S., "A Preliminary Study of the Radiative Properties of Town Gas Diffusion Flames"; Fire Res. Note #670, Fire Research Station, Borehamwood, England, July 1967.

3. Canfield, J.A., and Russel, L.H.; "Measurements of the Heat Flames within a Luminous Aviation Fuel Flame," Presented at the Eastern Section of the Combustion Institute, September 1969.

4. Maezawa, M., "Experiments on Fire Hazards of Liquefied Flammable Gases," Japan Society of Safety Engineering, May 1973.

5. Rasbash, D.J., Rogawski, Z.W., and Stark, G.W.V., "Properties of Fires of Liquids," Journal of Fuel Science, Vol. 25, No. 1, January 1956. pp. 94-107.

6. Rein, R.G., Siepcevich, C.M., and Welker, J.R., "Radiation View Factors for Tilted Cylinders," Journal of Fire and Flammability, No. 1, 1970, pp. 140-153.

7. Merriam, R.L., "View Factor between an Inclined Cylinder and a Plane-Numerical Technique," Internal Report, Arthur D. Little, Inc., 1972.

8. Sarofim, A., Personal Communication.

9. Ludwig, C.B., et al., "Study on Exhaust Plume Radiation Prediction," NASA, CR-61222, 1968.

10. Burgess, D., and Zabetakis, N. G. "Fire and Explosion Hazards Associated with Liquefied Natural Gas," Bureau of Mines Report #9099, U.S. Department of Interior, 1962.

11. May, W.G., and McQueen, W., "Radiation from Large LNG Fires," LNG Importation and Terminal Safety Conference Proceedings, Boston, Mass., June 1972, pp. 106-121.

7.11 LIST OF SYMBOLS

Symbol	Description	Value	Units
b_ω	mean half-width of line at wave number ω		m
c_1	First Planck Constant	3.7418×10^{-16}	$W\,m^2$
c_2	Second Planck Constant	1.4388×10^{-2}	$m\,°K$
d_ω	mean separation distance of spectral lines at wave number ω		m
D	diameter of flame		m
E_ω	emissive power of a blackbody in the interval ω and $\omega + d\omega$	σT^4	W/m
F	view factor between flame and observation element		

Symbol	Description	Value	Units
L	flame length		m
p	partial pressure of water vapor in the atmosphere		atm
Q	heat flux received by the object		W/m^2
r	magnitude of the vector joining the object plane to any point on the flame surface		m
s	distance of observation plane from flame center on the ground		m
T_a	ambient temperature		°K
T_f	flame blackbody temperature		°K

Greek Letters

α	absorptivity of the object		
ϵ_f	flame emissivity	Eq. (7.2)	
$\theta_{1\ (2)}$	angle made by the normal vector to observation surface (or flame surface with the vector joining the plane with any point on the flame surface)		radian
θ	flame tilt to vertical		radian
κ	attenuation coefficient for the flame	Eq. (7.2)	m^{-1}
κ_ω	attenuation coefficient of the atmosphere for a single line centered at ω		m/atm
σ	Stefan-Boltzmann Constant	5.6696×10^{-8}	$W/m^2\ °K^4$
τ	atmospheric transmissivity		
ϕ	azimuthal angle of the position of the observation plane		radian
ω	wave number		m^{-1}

TABLE 7.1[1]

HEAT FLUX DATA FOR SOME COMMON HAZARDS

Material	Exposure Time (min)	Heat Flux (Btu/hr ft^2)
Pilot ignition of blackened pine	1.0	12,000
Ignition of blackened pine	5.0	7,000
Minimum ignition level for wood		4,000
Blistering of human skin	0.5	1,500

TABLE 7.2[5]

EMISSIVITY AND EMISSION COEFFICIENTS OF FLAMES

	Emissivity ϵ_f	Flame Width cm D	Emission Coefficient K cm^{-1}	Effective Flame Temperature °C
Alcohol	0.066	18	0.0037	1218
Gasoline	0.36	22	0.020	1026
Kerosene	0.37	18	0.026	980
Benzole				
after 2 min burning	0.59	22	0.039	
after 5 min burning	0.70	29	0.041	921
after 8 min burning	0.72	30	0.042	

Note: $\epsilon_f = (1 - e^{-KD})$

PART II

NEW MODELS DEVELOPED

8.0 SPREADING OF A LOW-VISCOSITY LIQUID ON A HIGH-VISCOSITY LIQUID

8.1 AIM

The aim of the derivations given in this chapter is to obtain expressions for the extent of spread at any time after a sudden spill of a low-viscosity liquid on a high-viscosity liquid.

8.2 INTRODUCTION

In Chapter 3 the spreading formulas were given for the spread of a high-viscosity liquid, such as oil, on a low-viscosity liquid, such as water. However, there are a whole series of liquids that are lighter than water and also with viscosities considerably less than that of water. Many of these liquids are transported by ships and barges and, therefore, a spread model is needed to predict the hazard caused by spills of these liquids. Models to predict the spread of such low-viscosity liquids on water are not available in the literature, hence the following development.

The model derived is strictly correct for the spread of a liquid on a solid surface ($\mu_\ell/\mu_s \longrightarrow 0$). However, we assume that the same result could be utilized to describe the spread of a low-viscosity liquid on water also, without incurring too much error.

8.3 ASSUMPTIONS

In deriving the equations for the spread the following have been assumed:

- The total mass of the spilled liquid remains the same during the spread; that is, there are no evaporative or dissolution effects, nor does the liquid react with water.
- The physical properties of the liquid and water do not change.
- The liquid is lighter than water, has very low viscosity, and is immiscible with water.
- The spill occurs instantaneously.

8.4 DATA REQUIRED

To obtain the extent of spread, the following have to be known:

- Physical properties of the liquid, such as density, viscosity, interfacial tension with water,

- Density of water, and
- Volume of spill.

8.5 DETAILS OF THE MODEL

The spreading phenomenon takes place in three distinct regimes. In the first regime ("gravity-inertia regime") the spreading force is basically the hydrostatic pressure due to the film thickness. This force is resisted by the inertia of the spreading mass. In the second regime ("gravity-viscous regime") the gravitational spreading force is resisted by the viscous friction brought about by the motion of the top liquid on the bottom liquid. The third regime of spread ("surface tension – viscous regime") occurs when the thickness of the film of the spreading liquid is very small. The spreading force is primarily the interfacial tension between the two liquids. Each of these regimes is discussed below, separately and in detail for the case of "*radial* spreading *only*." The results of both radial and one-dimensional spreading are summarized in Table 8.1.

8.5.1 Radial Spreading

(1) *Gravity-Inertia Regime*

Since viscosity of liquid has no effect on the spread rates in this regime, the equations are the same as given in Chapter 3. For radial spread this is:*

$$R = 1.14\,(G\,V)^{1/4}\,t^{1/2}, \tag{8.1a}$$

and in non-dimensional form

$$\xi = 1.14\,\tau^{1/2} \tag{8.1b}$$

(2) *Gravity-Viscous Regime*

The conservation equations of mass and momentum are written for the spreading liquid along with the boundary conditions at the interface between the two liquids. Based on these equations expressions are obtained for film velocity and film thickness.

Referring to Figures 8.1 and 8.2 we write the following mass-continuity equations:

Local continuity:

$$\frac{1}{r}\int_{y=0}^{h} r\,u\,dy + \left(\frac{\partial h}{\partial t}\right)_r = 0 \tag{8.2}$$

*For definition of symbols, see "List of Symbols."

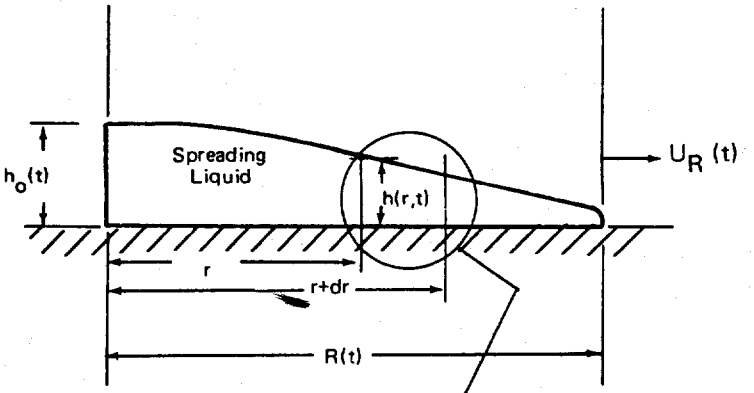

FIGURE 8.1

DETAILS OF THE SPREADING MODEL

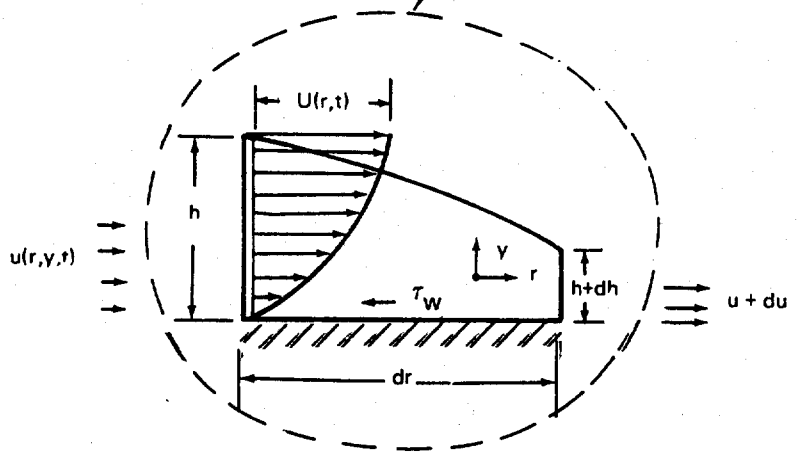

FIGURE 8.2 CONTROL VOLUME

Global conservation:

$$\text{Initial volume of liquid} = V = 2\pi \int_0^R r\, h\, dr = \text{constant} \tag{8.3}$$

Momentum equations:

$$\frac{\partial P}{\partial y} = -\rho_\ell G \tag{8.4a}$$

$$\frac{\partial P}{\partial r} = \mu_\ell \frac{\partial^2 u}{\partial y^2} \tag{8.4b}$$

where G is the effective gravity given by*

$$G = g(1 - \rho_\ell/\rho_\omega) \tag{8.5}$$

Pressure gradient:

The radial pressure gradient arises due to the change in the film thickness. Therefore:

$$\frac{\partial P}{\partial r} = \rho_\ell G \frac{\partial h}{\partial r} \tag{8.6}$$

Boundary conditions:**

$$u(r,o,t) = 0 \tag{8.7a}$$
$$u(o,y,t) = 0 \tag{8.7b}$$
$$\partial u(r,h,t)/\partial y = 0 \text{ (no shear at the top of the liquid)} \tag{8.7c}$$
$$h(r,t) = 0 \tag{8.7d}$$

and the shear stress continuity across the interface of the two liquids, at all radii and times. (8.7e)

*For the spreading of a liquid on a solid surface G = g.

**The condition (8.7a) is strictly correct only for the spread of a liquid on a solid surface. However, if $\mu_\ell/\mu_\omega \longrightarrow 0$, the approximation becomes better and better.

There are sufficient equations and conditions to obtain the radius of spread R as a function of time and also to obtain the shape of the film thickness as a function of r and time t. The procedure is given below.

Substituting Eq. (8.6) in Eq. (8.4b) and rearranging, we get:

$$G \frac{\partial h}{\partial r} = \nu_\ell \frac{\partial^2 u}{\partial y^2} \tag{8.8}$$

The LHS of Eq. (8.8) is independent of y and therefore it follows that RHS also is independent of y; that is, the curvature of the velocity profile through the film thickness is a constant.

Utilizing the above condition and Eqs. (8.7a) and (8.7c), we can show that

$$u = U\left[2\frac{y}{h} - \left(\frac{y}{h}\right)^2\right] \tag{8.9}$$

where

U = velocity at the top of the film at any radius and time

From Eq. (8.8) and (8.9), after some simplifications, we get:

$$\frac{G}{6\nu_\ell}\frac{\partial^3 h}{\partial r} + U = 0 \tag{8.10}$$

Substituting Eq. (8.9) and for U from Eq (8.10) in the continuity eq. (9.2) after the integration and simplification, we get:

$$\left(\frac{\partial h}{\partial t}\right)_r = \frac{G}{12\nu_\ell}\frac{1}{r}\left[\frac{\partial}{\partial r} r\left(\frac{\partial h^4}{\partial r}\right)\right]_t \tag{8.11}$$

Equation (8.11) is a non-linear partial differential equation for the film thickness as a function of radius and time. This equation is to be solved subject to the following initial boundary conditions.

$$h = \text{Delta function at } t = 0 \tag{8.12a}$$

$$(\partial h/\partial r) = 0 \text{ at } r = 0 \text{ for all time.} \tag{8.12b}$$

$$h(R) = 0 \text{ for all time.} \tag{8.12c}$$

and the Global conservation equation (8.3).

We now define the following quantities:

$$\left.\begin{aligned} L_1 &= [V/2\pi]^{1/3} \\ T_1 &= (12\nu_\ell/GL) \\ \tau_1 &= t/T_1 \\ \text{and} \quad \chi_1 &= \chi_1(\tau_1) = R(t)/L_1 \end{aligned}\right\} \tag{8.13a}$$

Further the following local similarity variables are defined:

$$\xi = \xi(r,t) = \frac{r}{R(t)} \quad ; \quad \delta_1 = \delta_1(\xi,\tau) = \frac{h(r,t)}{L_1} \tag{8.13b}$$

using the definitions of Eq. (8.13), Eq. (8.11) can be rewritten in dimensionless form* as:

$$\frac{1}{\chi_1^2}\left[\frac{\partial}{\partial\xi}\left(\xi\frac{\partial\delta_1^4}{\partial\xi}\right)\right]_{\tau_1} = \left(\frac{\partial\delta_1}{\partial\tau_1}\right)_\xi - \frac{\xi}{\chi_1}\left(\frac{d\chi_1}{d\tau_1}\right)\left(\frac{\partial\delta_1}{\partial\xi}\right)_{\tau_1} \tag{8.14}$$

and the globl conservation Eq. (8.2) as:

$$\chi_1^2 \int_0^1 \xi\,\delta_1\,d\xi = 1 \tag{8.15}$$

Eq. (8.14) and (8.15) are two equations in two unknowns, namely, χ_1 and δ_1.

*Note that if F is a function F = F (r,t), then

$$\left(\frac{\partial F}{\partial r}\right)_t = \frac{1}{R(t)}\left(\frac{\partial F}{\partial \xi}\right)_t$$

and

$$\left(\frac{\partial F}{\partial t}\right)_r = \left(\frac{\partial F}{\partial t}\right)_\xi - \frac{\xi}{R}\frac{dR}{dt}\left(\frac{\partial F}{\partial \xi}\right)_t$$

Solution:

Let

$$\delta_1(\xi,\tau) = f(\xi)\tau_1^n. \tag{8.16}$$

Therefore, from Eq. (8.12b) and (8.12c):

$$\left(\frac{\partial f}{\partial \xi}\right)_{\xi=0} = 0 \tag{8.17}$$

and

$$f(1) = 0$$

Substituting Eq. (8.16) into Eq. (8.15), we get:

$$\chi_1 = \frac{1}{\sqrt{C}}\ \tau_1^{-\frac{n}{2}} \tag{8.18a}$$

where

$$C = \int_0^1 \xi\, f(\xi)\ d\xi \tag{8.18b}$$

Substituting Eqs. (8.16) and (8.18) in Eq. (8.14) and rearranging and equating the powers of τ on both sides of the equation yields:

$$n = -\frac{1}{4} \tag{8.19}$$

$$C\,\frac{1}{\xi}\,\frac{d}{d\xi}\left(\xi\frac{df}{d\xi}\right)^4 + \frac{f}{4} + \frac{\xi}{8}\,\frac{df}{d\xi} = 0 \tag{8.20}$$

This equation with its boundary conditions (8.17) is solved in Appendix A. The solution is:

$$f = \left[\frac{3}{64\,C}\right]^{\frac{1}{3}}(1-\xi^2)^{\frac{1}{3}} \tag{8.21}$$

Equations (8.21) and 8.18b), after simplification, give:

$$C = 3/(2^{15/4}) = 0.223.$$

Hence

$$\chi_1(\tau_1) = 2.1177\ \tau_1^{\frac{1}{8}} \tag{8.22a}$$

$$\delta_1(\xi,\tau) = 0.5946\,(1-\xi^2)^{\frac{1}{3}}\ \tau_1^{-\frac{1}{4}} \tag{8.22b}$$

and

$$R(t) = 0.8412 \left[\frac{G V^3}{\nu_\ell}\right]^{\frac{1}{8}} \tag{8.22c}$$

$$\chi(\tau) = 0.8412\, \Gamma_\ell^{\frac{1}{4}}\, \tau^{\frac{1}{8}} \tag{8.22d}$$

(3) *Surface Tension-Viscous Regime*

Total surface tension force on the spreading film:

$$F_\sigma = 2\pi R \sigma \tag{8.23}$$

and the viscous resistance to spread is

$$F_\psi = 2\pi \int_o^R r \chi \, dr \tag{8.24}$$

where

$$\psi = \psi(r,t) = -\mu_\ell (\partial u/\partial y)_{y=o}.$$

= shear stress at the interface of the two liquids.

Using Eq. (8.9), it can be shown that

$$\psi = 2\mu_\ell U/h. \tag{8.25}$$

substituting the film velocity distribution [Eq. (8.9)] in local continuity [Eq. (8.2)] and integrating, the following is obtained:

$$\frac{2}{3}\ \frac{1}{r}\left[\frac{\partial}{\partial r}(r U h)\right]_t + \left(\frac{\partial h}{\partial t}\right)_r = 0 \tag{8.26a}$$

and Eq. (8.26a) in non-dimensional form is:

$$\frac{2}{3}\ \frac{1}{\chi}\left[\frac{1}{\xi}\frac{\partial}{\partial \xi}\xi v \hat{\delta}\right]_\tau + \left(\frac{\partial \delta}{\partial \tau}\right)_\xi - \frac{\xi}{\chi}\ \frac{d\chi}{d\chi}\left(\frac{\partial \delta}{\partial \xi}\right)_\tau \tag{8.26b}$$

where

$$\left.\begin{aligned} L &= V^{1/3} \\ T &= \sqrt{L/G} \\ \xi &= r/R \\ \chi &= R/L \\ \delta &= h/L \\ \tau &= t/T \\ v &= UT/L \text{ and} \\ \Sigma_\ell &= \sigma T/L\mu_\ell \end{aligned}\right\} \tag{8.27}$$

The law of spread in this regime is obtained by equating the spreading and resisting force:

$$F_\sigma = F_\chi .$$

Using Eqs. (8.23), (8.24), (8.25), and (8.27), we have:

$$\chi \int_{\xi=0}^{1} \frac{\xi v}{\delta} \, d\xi = \frac{\Sigma_\ell}{2} \tag{8.28}$$

Also the global continuity Eq. (8.3) becomes:

$$2\pi \chi^2 \int_{\xi=0}^{1} \xi \delta \, d\xi = 1 \tag{8.29}$$

Equations (8.26b), (8.28), and (8.29) are three equations for solving three unknowns, viz., $\delta(\xi,\tau)$, $\chi(\tau)$, and $v(\xi,\tau)$. These are to be solved subject to the following conditions.

Initial condition:

δ = A delta function at $\tau = 0$
$\chi = 0$ at $\tau = 0$

Boundary condition:

$v = 0$ at $\xi = 0$ for all τ
δ = finite for all ξ and $\tau > 0$
$\partial\delta/\partial\xi = 0$ at $\xi = 0$ for all time, τ

(8.30)

Solution:

We seek a similarity solution of the type:

$$\delta(\xi,\tau) = f(\xi)\, \Upsilon(\tau) \tag{8.31}$$

where f is a function of local similarity distance variable ξ only and Υ is a function of dimensionless time only.

Substituting Eq. (8.31) in Eq. (8.26b) and multiplying the resulting equation with ξ, integrating with respect to ξ, and then simplifying, we get (after utilizing the boundary condition $v = 0$ at $\xi = 0$):

$$\xi v f(\xi) = \frac{2}{3}\left[\chi' \int_{z=0}^{\xi} z^2 f(z)\, dz - \chi \frac{\tau'}{\tau} \int_{z=0}^{\xi} z\, f(z)\, dz\right]$$

where the primes on the functions denote differentiation with respect to the respective arguments [time τ in the case of χ and Υ and z or ξ in the case of f].

Rewriting Eq. (8.28) in the form (in view of Eq. (8.31)):

$$\frac{\chi}{\Upsilon}\int_{\xi=0}^{1}\frac{\xi f v}{f^2}\,d\xi \;=\; \frac{\Sigma_\ell}{2} \tag{8.32}$$

and substituting Eq. (8.32) for ξfv and substituting for χ^2 and $\chi\chi'$ from Eq. (8.29), we get the following final equation:

$$-\frac{\Upsilon'}{\Upsilon^3}\,D \;=\; \Sigma_\ell \tag{8.33}$$

where

$$D = \frac{3}{2\pi}\int\frac{d\xi}{\left[f(\xi)\right]^2}\left\{\frac{\frac{1}{2}\int_{z=0}^{\xi} z^2 f'(z)\,dz}{\int_{z=0}^{1} z f(z)\,dz} + \frac{\int_{z=0}^{\xi} z\,f(z)\,dz}{\int_{z=0}^{1} z\,f(z)\,dz}\right\}$$

i.e.,

$$D = \frac{3}{4\pi}\,\frac{\int_0^1 \frac{\xi^2}{f(\xi)}\,d\xi}{\int_0^1 \xi f(\xi)\,d} \tag{8.34}$$

Integrating Eq. (8.33), we get:

$$\Upsilon(t) = \sqrt{\frac{3}{8\pi\Sigma_\ell}\int_{\xi=0}^{1}\frac{\xi^2\,d\xi}{f(\xi)\int_0^1 zf\,dz}} \tag{8.35}$$

It should be noticed that $f(\xi)$, remains undetermined, because by the definition of Eq. (8.31), we introduced an additional function which gave us four unknown functions and three equations to solve them.

Using Eqs. (8.29), (8.31), and (8.35), it can be shown that

$$\delta(\xi,\tau) = \sqrt{\frac{3}{8\pi\Sigma_\ell}\int_0^1 \frac{\xi^2\, d\xi}{f(\xi)\int_0^1 z\, f(z)\, dz}} \tag{8.36a}$$

and

$$\chi^2(\tau) = \sqrt{\frac{2}{3\pi}}\,\frac{1}{\left[\int_0^1 \frac{\xi^2}{f} d\xi \int_0^1 \xi f\, d\xi\right]^{\frac{1}{2}}} \tag{8.36b}$$

The table below illustrates the nature of the solution for various choices of f(ξ) (for details of integration, see Reference 1).

f(ξ)	$\int_0^1 \frac{\xi^2}{f} d\xi$	$\int_0^1 f\, d\xi$	Value of C in Equation $\chi = C\,\Sigma^{1/4}\tau^{1/4}$	Remarks
1	1/3	1/2	1.0623	Constant film thickness
$(1-\xi^2)^p$	$\frac{\Gamma(3/2)\,\Gamma(1-p)}{2\times\Gamma(5/2-p)}$	$\frac{1}{2(p+1)}$		p = 1 gives a logarithmic singularity at the spread front
with				
p = ¼	0.479256	0.4000	0.9749	
p = ½	0.785398	0.3333	1.0539	f(ξ) vs ξ is a circle of unit radius.
p = ¾	1.748038	0.2857	1.2386	

Hence, we can use:

$$\chi = 1.05\,\Sigma_\ell^{\frac{1}{4}}\,\tau^{\frac{1}{4}} \tag{8.37a}$$

i.e.,

$$R(t) = 1.05\left[\frac{\sigma V}{\mu_\ell}\right]^{\frac{1}{4}} t^{\frac{1}{4}} \tag{8.37b}$$

8.5.2 One Dimensional Spread

(1) *Gravity-Intertia Regime*

Because the viscosity of liquid has no effect on the spreading in the inertia regime, the equation given below is the same as the one given in Chapter 3:

$$S = 1.39\,(GA)^{1/3}\quad t^{2/3} \tag{8.38a}$$

or, in dimensionless form:

$$\chi = 1.39\,\tau^{2/3} \tag{8.38b}$$

(2) *Gravity-Viscous Regime*

As in the case of radial spread, we write the conservation equations of mass and momentum.

Local continuity equation:

$$\frac{\partial}{\partial x}\int_0^h u\,dy + \frac{\partial h}{\partial t} = 0 \tag{8.39a}$$

Global conservation equation:

$$\int_0^S h\,dx = A \tag{8.40a}$$

Momentum equation:

$$\frac{\partial p}{\partial x} = \frac{\partial^2 u}{\partial y^2} \tag{8.41a}$$

$$\frac{\partial p}{\partial y} = -\rho_\ell G \tag{8.41b}$$

Also

$$\frac{\partial \bar{p}}{\partial x} = \rho_\ell G \frac{\partial h}{\partial x} \tag{8.42}$$

The no-slip condition* at the interface and the continuity of shear stress across the liquid interface are to be imposed. Using this condition and the fact that x direction pressure gradient is independent of y, we can show:

$$\frac{u}{U} = 2\frac{y}{h} - \left(\frac{y}{h}\right)^2 \tag{8.43}$$

Equating (8.41a) and (8.42) and using Eq. (8.43) and simplifying and substituting the results in the conservation equations, we get:**

Local continuity:

$$\frac{1}{\chi^2}\frac{\partial}{\partial\xi}\left(\frac{\partial\delta}{\partial\xi}\right)^4_{\tau_1} = \left(\frac{\partial\delta}{\partial\tau_1}\right)_{\xi} - \frac{d\xi}{d\chi}\frac{\chi}{\tau_1}\left(\frac{\partial\delta}{\partial\xi}\right)_{\tau_1} \tag{8.39b}$$

Global conservation:

$$\chi\int\delta\, d\xi = 1 \tag{8.40b}$$

Equations (8.39b) and (8.40b) form two equations in two unknowns: $\delta(\xi,\tau_1)$ and $\chi(\tau_1)$

Solution:

Let $$\delta(\xi,\tau_1) = f(\xi)\,\tau_1^n \tag{8.44}$$

Substituting Eq. (8.44) in Eqs. (8.39b) and (8.40b) and simplifying, we get:

$$n = -1/5 \tag{8.45a}$$

and

$$c^2\frac{d^2f^4}{d\xi^2} + \frac{\xi}{5}\frac{df}{d\xi} + \frac{f}{5} = 0 \tag{8.45b}$$

where

$$c = \int_0^1 f(\xi)\, d\xi \tag{8.45c}$$

Equation (8.45b) is solved*** with the following boundary conditions.

at $\xi = 0;\ \partial f/\partial\xi = 0$

$\xi = 1:\ f = 0$

to get

$$f(\xi) = \left[\frac{3}{40\,c^2}\right]^{\frac{1}{3}}(1-\xi^2)^{\frac{1}{3}}$$

and

$$c = \left(\frac{3}{40}\right)^{0.2}\left[\frac{\pi}{2}\,\frac{\Gamma(1+\frac{1}{3})}{\Gamma(1+\frac{5}{6})}\right]^{0.6} = 0.5372$$

*The condition (8.7a) is strictly correct only for the spread of a liquid on a solid surface. However, if $\mu_\ell/\mu_\omega \to 0$, the approximation becomes better and better.

**For the definition of the non-dimensional quantities, see list of symbols.

***See Appendix B.

Hence:

$$\delta(\xi,\tau) = 1.049\,\Gamma_l^{-\frac{1}{10}}\,\tau^{-\frac{1}{5}}\,(1-\xi^2)^{\frac{1}{3}} \tag{8.46a}$$

$$\chi(\tau) = 1.132\,\Gamma_l^{\frac{1}{10}}\,\tau^{\frac{1}{5}} \tag{8.46b}$$

and

$$s(t) = 1.132\left[\frac{G\,A^3}{\nu_l}\right]^{\frac{1}{5}}\,t^{\frac{1}{5}} \tag{8.46c}$$

(3) *Surface Tension – Viscous Regime:*

Surface tension force/unit width of

$$\text{Spread front} = F_\sigma = \sigma \tag{8.47}$$

$$\text{Shear stress/unit width} = F_\psi = \int_0^s \psi\,dx \tag{8.48}$$

The law of spread in this regime is obtained by equating the surface tension spreading force to the viscous resistance. Hence:

$$\sigma = \int_0^s \psi\,dx$$

Since the distribution of velocity in the film is given by Eq. (8.43), we have:

$$\psi = \mu_l\left(\frac{\partial u}{\partial y}\right)_{y=0} = \frac{2\mu_l U}{h}$$

Hence the law of spreading is:

$$\sigma = 2\mu_l\int\frac{U}{h}\,dx \tag{8.49a}$$

and, in dimensionless form:

$$\frac{\Sigma_l}{2} = \chi\int_{\xi=0}^{1}\frac{v}{\delta}\,d\xi \tag{8.49b}$$

Substituting Eq. (8.43) in the local continuity equation (8.39a), we get,

$$\frac{2}{3}\frac{\partial}{\partial x}(\dot{\delta} U h) + \frac{\partial h}{\partial t} = 0 \qquad (8.50a)$$

which in non-dimensional form is:

$$\frac{2}{3}\frac{1}{\chi}\left[\frac{\partial}{\partial \xi}(v\delta)\right]_{\tau} + \left(\frac{\partial \delta}{\partial \tau}\right)_{\xi} - \frac{d\xi}{d\chi}\frac{\chi}{\tau}\left(\frac{\partial \delta}{\partial \xi}\right)_{\tau} = 0 \qquad (8.50b)$$

Equations (8.40b), (8.49b), and (8.50b) represent three equations in three unknowns, viz. v, δ, and χ. These are to be solved subject to the following conditions:

Initial condition:

δ = A Delta function at $\tau = 0$

$\chi = 0$ at $\tau = 0$

Boundary condition:

$v = 0$ at $\xi = 0$ for all τ
δ = finite for all ξ for $\tau > 0$

Solution: $\partial\delta/\partial\xi = 0$ at $\xi = 0$ for all τ

We seek a similarity solution of the type

$$\delta(\xi, \tau) = f(\xi)\ \gamma(\tau) \qquad (8.51)$$

Substituting Eq. (8.51) in the local continuity Eq. (8.50b), integrating with respect to ξ, and simplifying (utilizing b.c., $v = 0$ at $\xi = 0$),

we get:

$$v f(\xi) = \frac{3}{2}\left[\chi' \int z f'(z)\, dz - \chi \frac{\gamma'}{\gamma}\int f(z)\, dz\right] \qquad (8.52)$$

Substituting Eq. (8.52) in Eq. (8.49b) and rearranging, we get:

$$\frac{\Sigma_e}{2} = \frac{3}{2}\frac{\chi}{\gamma}\int_0^1 \frac{d\xi}{[f(\xi)]^2}\left\{\chi' \int_0^{\xi} z f'(z)\, dz - \frac{\chi\gamma'}{\gamma}\int_0^{\xi} f(z)\, dz\right\} \qquad (8.53)$$

Using the global continuity equation:

$$\chi \int \delta \, d\xi = 1 \tag{8.54}$$

and Eqs. (8.53) and (8.31), we get (after getting $\chi\chi^1$ and χ^2 from Eq. (8.54) after some simplification:

$$\frac{\Sigma_\ell}{3} = -D \cdot \frac{\tau'}{\tau^4}$$

where

$$D = \frac{\int \frac{\xi}{f(\xi)} d\xi}{\left\{\int f(\xi)\, d\xi\right\}^2} \tag{8.55}$$

Integrating we get:

$$\tau(\tau) = \left(\frac{D}{\Sigma_\ell}\right)^{\frac{1}{3}} \tau^{-\frac{1}{3}} \tag{8.56}$$

Therefore:

$$\delta(\xi,\tau) = \left(\frac{D}{\Sigma_\ell}\right)^{\frac{1}{3}} f(\xi)\ \tau^{-\frac{1}{3}} \tag{8.57a}$$

and

$$\chi(\tau) = \frac{1}{D^{\frac{1}{3}} \int_0^1 f\, d\xi}\ \Sigma_\ell^{\frac{1}{3}}\ \tau^{\frac{1}{3}} \tag{8.57b}$$

Again, as in the radial case, we have solutions for various f profiles. These are indicated in the table below

$f(\xi)$	$\int_0^1 \frac{\xi}{f(\xi)} d\xi$	$\int_0^1 f(\xi)\, d\xi$	Value of C in the Equation $\chi = C \Sigma_\ell^{1/3} \tau^{1/3}$	Remarks
1	½	1	1.2600	Constant film thickness
$(1-\xi^2)^p$ $p < 1$	$\frac{1}{2(1-p)}$	$\frac{1}{2}\frac{\Gamma(\frac{1}{2})\,\Gamma(1+p)}{\Gamma(3/2+p)}$		$p = 1$ gives a logarithmic singularity at the spread front
$p = \frac{1}{4}$	0.6667	0.8740	1.9727	
$p = \frac{1}{2}$	1.0000	0.7854	1.08385	f vs ξ is a unit radius circle
$p = \frac{3}{4}$	2.0000	0.7189	0.88600	

Therefore, we use

$$\chi(\tau) = 1.2\, \Sigma_\ell^{\frac{1}{3}}\, \tau^{\frac{1}{3}} \tag{8.58a}$$

or

$$s(t) = 1.2 \left[\frac{\sigma A}{\mu_\ell}\right]^{\frac{1}{3}} t^{\frac{1}{3}} \tag{8.58b}$$

The final results of the above derivations for both radial and one-dimensional spread are summarized in Tables 8.1 and 8.2. The latter contains the non-dimensional results. Figure 8.3 is a plot of the dimensionless spread radius in the case of radial spread for the various regimes.

8.6 COMPUTATIONAL ALGORITHM

The algorithm for calculating the extent of spread in both one-dimensional and radial cases is quite simple. For any given properties of the spreading liquid the times t_1 and t_2 (see Table 8.1) are calculated. The extent of spread is then calculated at the given time by first comparing this time with t_1 and t_2 and thereby establishing the regime of spread. Once this is fixed the appropriate formula given in Table 8.1 is used. A flow chart indicating the algorithm is provided in Figure 8.4.

8.7 SPECIFIC EXAMPLE

The method of calculation is illustrated by the following example.

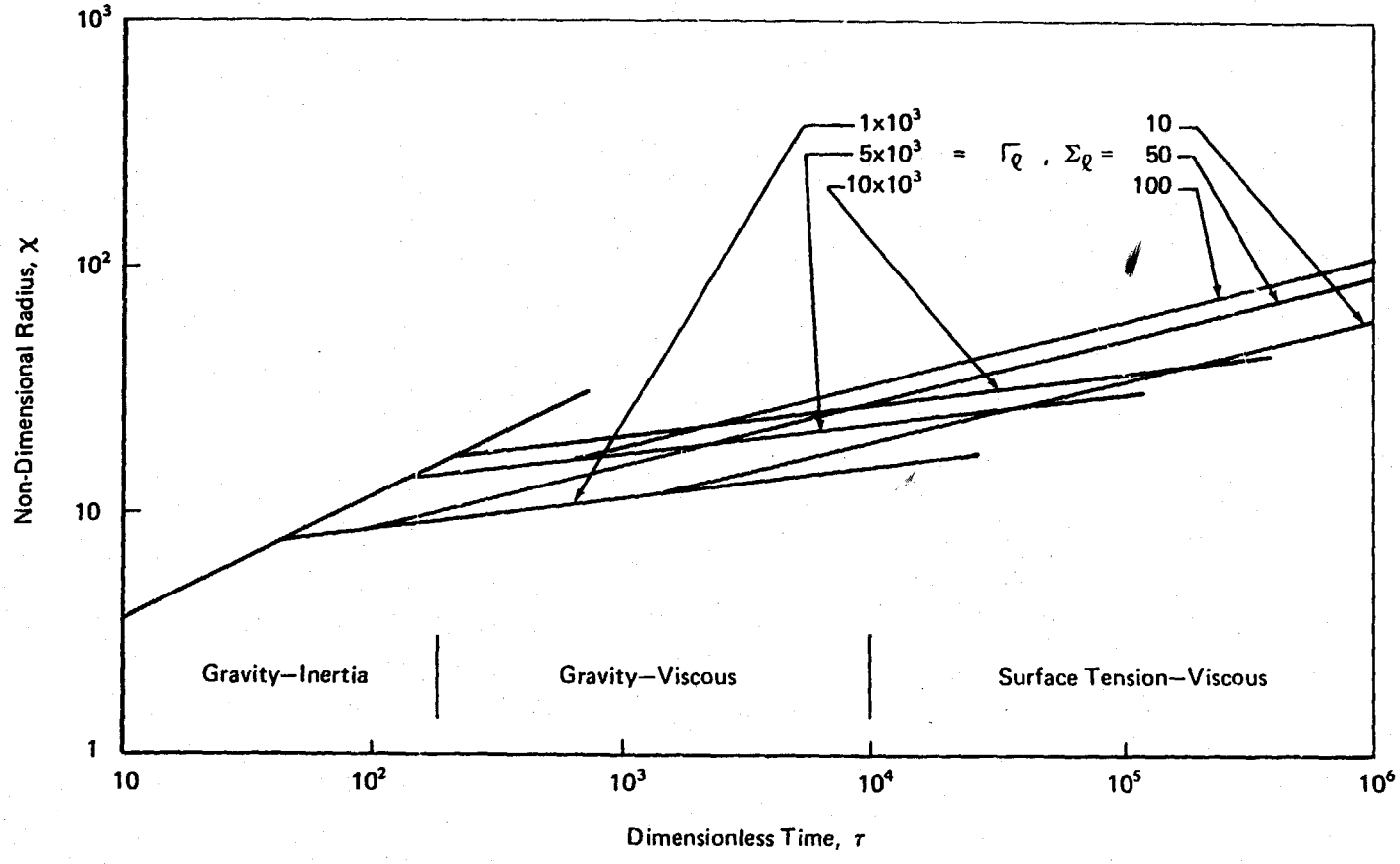

FIGURE 2.3 DIMENSIONLESS SPREAD RADIUS FOR VARIOUS REGIONS

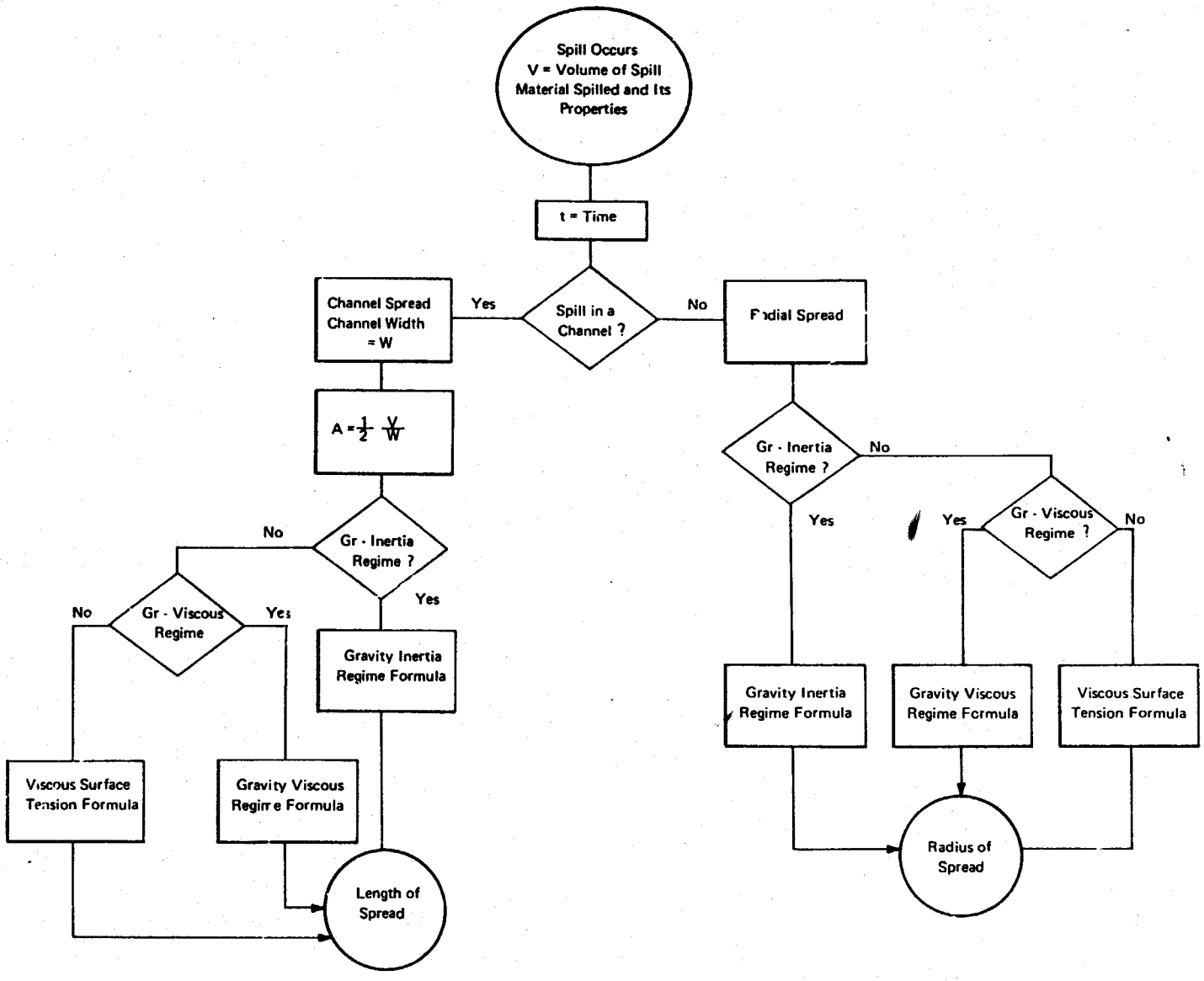

FIGURE 8.4 FLOW CHART FOR THE CALCULATION OF EXTENT OF SPREAD OF A LOW VISCOSITY LIQUID ON WATER

Type of Spread		= radial	
Volume of spill (assumed)	V	= 10^3	m^3
Properties:			
Density of the liquid spilled	ρ_ℓ	= 800	kg/m^3
Viscosity of liquid	μ_ℓ	= 5×10^{-4}	$N\,s/m^2$
Kinematic viscosity	ν_ℓ	= 6.25×10^{-7}	m^2/s
Interfacial tension with water	σ	= 3×10^{-2}	N/m
Density of water	ρ_w	= 10^3	kg/m^3
Viscosity of water	μ_w	= 10^{-3}	$N\,s/m^2$
Gravitation acceleration	g	= 9.8	m/s^2
Calculations:			
Effective gravity	G	= $(1 - \rho_\ell/\rho_\omega)\,g = 1.96$	m/s^2
Characteristic length	L	= $V^{1/3} = 10.0$	m
Characteristic time	T	= $(L/G)^{1/2} = 2.259$	s
Dimensionless viscosity	Γ_ℓ	= $(VG/\nu_\ell^2)^{1/4} = 0.8416 \times 10^4$	
Dimensionless surface tension	Σ_ℓ	= $\sigma/\mu_\ell\sqrt{GL} = 13.553$	

Noting that $\mu_\ell \ll \mu_\omega$ and using the results from Table 8.2, we have:

First change over time	τ_1	= 183.95	
i.e.,	t_1	= $T \times \tau_1 = 415.5$	s
Second cross over time	τ_2	= 6.5437×10^4	
i.e.,	t_2	= $\tau_2 \times T = 41.06$	hrs
Let the time at which the radius of spread is required be	t	= 10	hrs
i.e.,	τ	= 1.5936×10^4	
The value of τ indicates that the regime if viscous-gravity.			
Therefore radius of spread dimensionless (Eq. 8.22d)	χ	= $0.8412 \times [0.8416 \times 10^4]^{1/4} \times [1.5936 \times 10^4]^{1/8}$	
dimensional		= 27.01	
	R	= $\chi L = 270.1$	m.

8.8 DISCUSSIONS

Detailed derivations of the relationship between the extent of spread, the time, and the physical properties of the spreading liquid have been given for the case of the spread of a very low-viscosity liquid on another higher viscosity liquid (such as water). In those derivations, details such as the regime of spreading and the geometry of spreading were taken into consideration.

The derivations given in this chapter are *strictly* correct for the case of the spread of a liquid on a flat solid surface. The error involved in the application of these equations to the case of a liquid spread on another liquid becomes smaller and smaller when the ratio of the

viscosity of the spreading liquid to that of the other liquid becomes smaller and smaller. A cursory analysis of the actual problem of liquid-on-liquid spread indicates that the extent of spread depends, in addition to all of the above parameters, on the scale of the spill. In fact the analysis indicates that, in small spills, the solution tends toward the solution given in Chapter 3 ($\mu_\ell/\mu_\omega \gg 1$), even though $\mu_\ell/\mu_\omega < 1$. For larger size spills the time at which the solution starts tending toward Fay's solution (Chapter 3) increases. Because of the mathematical difficulties a complete solution could not be obtained for this liquid-on-liquid spread problem.

Figure 8.3 indicates the sensitivity of the spread model to the variation in physical parameters. As can be seen from the figure, the variations in viscosity and the surface tension (non-dimensional quantities) do not affect the spread radius very much. However, small changes in their values affect, to a large extent, the values of the crossover times at which the spread regime changes from one to another.

Another important feature of the results presented in Tables 8.1 and 8.2 is that the solutions do not depend on the water properties, except in the definition of the effective gravity G. This latter quantity is the only parameter that distinguishes between the spread on water and the spread on a solid surface.

8.9 CONCLUSIONS

Formulas have been derived for predicting the extent of spread of a suddenly released liquid spreading on another liquid. The viscosity of the spreading liquid is very low compared to the liquid on which it spreads. The derivations are strictly correct for the case of spread on a flat solid surface. However, the effects of buoyancy of the second liquid are also taken into account. The different regimes of spread and the two spread geometries (radial and one-dimensional) are considered. The solutions obtained are tabulated.

8.10 REFERENCE

1. Abramowitz, M., and Stegun, I.A., "Handbook of Mathematical Functions," Dover Publishing, N.Y. 1965, p. 258.

8.11 LIST OF SYMBOLS

Symbol	Description	Formula or Value	Units
A	half of the volume of spill per unit width of channel in 1-D spread		m^2
$f(\xi)$	a function representing the thickness profile of the spreading liquid		

Symbol	Description	Formula or Value	Units
F_σ	total spreading force due to surfact tension		N
F_ψ	total viscous resistive force against spreading		N
g	acceleration due to gravity	9.8	m/s^2
G	effective gravity	$g(1 - \rho_\ell/\rho_\omega)$	m/s^2
h (r,t) h (x,t)	Thickness of spreading liquid film		m
L	characteristic length scale		m
L_1	another characteristic length scale		m
p	hydrostatic pressure		N/m^2
r	radial coordinate		m
R (t)	radius to the spread front in radial spreading		m
S (t)	distance from the spill point to the spread front in 1-D spill		m
t	time		s
T	characteristic time	$\sqrt{L/G}$	s
T_1	another characteristic time	$12\,\nu_\ell/GL$	s
u (r,y,t) u (x,y,t)	particle velocity in the spreading liquid		m/s
U (r,t) U (x,t)	velocity of the top layer of the spreading liquid		m/s
U_R (t), U_S (t)	velocity of the spread front		m/s
v	non-dimensional particle velocity	UT/L	
V	volume of spill		m^3

Symbol	Description	Formula or Value	Units
W	width of channel		m
x	x coordinate in 1-D spill		m
y	a coordinate normal to plane of spread		m
z	dummy variable in integration		
Greek Letters			
Γ	non-dimensional viscosity (subscripted)	$(L^3 G/\nu^2)^{1/4}$	
$\delta(\xi,\tau)$	non-dimensional film thickness		
μ	viscosity (subscripted)		N s/m^2
ν	kinematic viscosity (subscripted)		m^2/s
ξ	non-dimensional distance in the spread direction	x/S or r/R	
ρ	density (subscripted)		kg/m^3
σ	interfacial tension between the two liquids		
Σ	non-dimensional surface tension (subscripted)	$\sigma T/\mu L$	
τ	non-dimensional time	t/T	
τ_1	another non-dimensional time	t/T_1	
$\Upsilon(\tau)$	a dimensionless function of time which indicates the time-wise behavior of the film thickness		
$\chi(\tau)$	non-dimensional distance to the spread front from the point of spill	S/L or R/L	
ψ	viscous shear stress between the two liquids		N/m^2

Subscripts

W	water
ℓ	liquid
$(\partial/\partial x)_t$	differential is performed maintaining "t" as a constant

8.12 APPENDICES

8.12.1 Solution of the following non-linear differential equation:

$$a\,\frac{1}{x}\,\frac{d}{dx}\left(x\,\frac{dy^4}{dx}\right) + 2y + x\,\frac{dy}{dx} = 0 \qquad \text{(A.1)}$$

with conditions

$$y(1) = 0 \qquad \text{(A.2)}$$

$$\frac{dy(0)}{dx} = 0 \quad ; \; y(0) = \text{finite} \qquad \text{(A.3)}$$

Multiplying Eq. (A.1) by x/a and then integrating, we have:

$$x\,\frac{dy^4}{dx} + 2\int\frac{x}{a}y\,dx + \int\frac{x^2}{a}\,\frac{dy}{dx}dx = B$$

where B is a constant of integration.

Integrating the second integral by parts, we have:

$$x\,\frac{dy^4}{dx} + \frac{x^2y}{a} - \cancel{\int\frac{x^2}{a}\,\frac{dy}{dx}dx} + \cancel{\int\frac{x^2}{a}\,\frac{dy}{dx}dx} = B$$

using the condition (A.3), we get B = 0

i.e.,

$$4xy^3\,\frac{dy}{dx} + \frac{x^2y}{a} = 0$$

Integrating:

$$y^3 + \frac{3}{8a}x^2 = c$$

using condition (A.2), we get the solution:

$$y^3 = \left[\frac{3}{8a}\right]^{\frac{1}{3}} \left[1 - x^2\right]^{\frac{1}{3}} \qquad \text{(A.4)}$$

8.12.2 Solution of the differential equation

$$b\frac{d^2y^4}{dx^2} + x\frac{dy}{dx} + y = 0 \qquad \text{(B.1)}$$

with boundary conditions

$$\left.\begin{aligned} \frac{dy}{dx} &= 0 \text{ at } x = 0 \\ y &= 0 \text{ at } x = 1 \end{aligned}\right\} \qquad \text{(B.2)}$$

Integrating Eq. (B.1) with respect to x , we have:

$$b\frac{dy^4}{dx} + \int x\frac{dy}{dx}\,dx + \int y\,dx = \text{constant}$$

The constant of integration is zero from the first boundary condition. Therefore,

$$4by^2\frac{dy}{dx} + x = 0 \qquad \text{(B.3)}$$

or

$$\frac{4b}{3}\frac{dy^3}{dx} + x = 0$$

Integrating we get:

$$y^3 = \frac{3}{8b}(c - x^2)$$

Now using the second boundary condition, we get:

$$y = \left[\frac{3}{8b}(1 - x^2)\right]^{\frac{1}{3}} \qquad \text{(B.4)}$$

TABLE 8.1

DIMENSIONAL EQUATIONS OF SPREAD

Regimes of Spread Geometry	Gravity–Inertia	Gravity–Viscous	Viscous–Surface Tension
One-dimensional	$t_1 = 0.644 \left[\frac{A^4}{G^2 \nu^3}\right]^{\frac{1}{7}}$		$t_2 = 0.645 \sqrt{\frac{G^3 A^4 \mu_\ell^5}{\nu_\ell^3}}$
	$t < t_1$	$t_1 \leqslant t \leqslant t_2$	$t > t_2$
	$S(t) = 1.39\,(GA)^{1/3}\, t^{2/3}$	$S(t) = 1.132 \left[\frac{GA^3}{\nu_\ell}\right]^{1/5} t^{1/5}$	$S(t) = 1.2 \left[\frac{\sigma A}{\mu_\ell}\right]^{1/8} t^{1/3}$
Radial	$t_1 = 0.4446 \left[\frac{V}{G \nu_\ell}\right]^{1/3}$		$t_2 = 0.1697 \left[\frac{GV \mu_\ell^2}{\sigma \nu_\ell}\right]$
	$t < t_1$	$t_1 \leqslant t \leqslant t_2$	$t > t_2$
	$R(t) = 1.14\,[GV]^{1/4}\, t^{1/2}$	$R(t) = 0.8412 \left[\frac{G V^3}{\nu_\ell}\right]^{1/8} t^{1/8}$	$R(t) = 1.05 \left[\frac{\sigma V}{\mu_\ell}\right]^{1/4} t^{1/4}$

TABLE 8.2

NON-DIMENSIONAL EQUATIONS OF SPREAD

Regimes of Spread Geometry	Gravity–Inertia	Gravity–Viscous	Viscous–Surface Tension
One-dimensional	$\tau_1 = 0.644\ \Gamma_\ell^{3/14}$ $\tau < \tau_1$ $\chi = 1.39\ \tau^{2/3}$	$\tau_1 \leqslant \tau \leqslant \tau_2$ $\chi = 1.132\ \Gamma^{1/10}\ \tau^{1/5}$	$\tau_2 = 0.645\ \frac{\Gamma_\ell^{3/4}}{\Sigma_\ell^{5/2}}$ $\tau > \tau_2$ $x = 1.2\ \Sigma_\ell^{1/3}\ \tau^{1/3}$
Radial	$\tau_1 = 0.4446\ \Gamma_\ell^{2/3}$ $\tau < \tau_1$ $\chi = 1.14\ \tau^{1/2}$	$\tau_1 \leqslant \tau \leqslant \tau_2$ $\chi = 0.8412\ \Gamma_\ell^{1/4}\ \tau^{1/8}$	$\tau_2 = 0.1697\ \frac{\Gamma_\ell^{2}}{\Sigma_\ell^{2}}$ $\tau >$ - $\chi = 1.05\ \Sigma_\ell^{1/4}\ \tau^{1/4}$

9.0 SIMULTANEOUS SPREADING AND EVAPORATION OF A CRYOGEN ON WATER

9.1 AIM

The aim of this chapter is to obtain the spread rate, the time for complete evaporation, and the maximum extent of spread of a cryogenic liquid spilled on a water surface.

9.2 INTRODUCTION

Many chemicals which are in gaseous state at ambient conditions are transported in ships as cryogenic liquids (e.g., natural gas, ammonia, nitrogen, etc.). If these liquids are released accidentally and spill on the water, they will vaporize and at the same time spread on the water surface. To assess the hazard caused by the liberation and subsequent dispersion of vapor, it is essential to know the rate of vapor liberation, the size of the source, and the total duration for which vapor will be released. In this chapter a model for the spreading, including the effects of evaporation, is worked out. It should be recalled that the spread models given in Chapter 3 assumed a constant mass of liquid in the slick at all times.

The heat necessary to evaporate the spreading cryogenic liquid comes from water. Depending on the boiling temperature of the cryogen at atmospheric pressure and the nature of the cryogen itself, the water may freeze and an ice sheet may form under the spreading liquid. In the model presented below this possibility is also included. The model, however, is predicated on all the liquid being spilled instantaneously (a Delta function initial condition). Of course, this can hardly represent the actual conditions, especially when the leak is slow. However, the results of this model would give the worst accident conditions and therefore help in overestimating the hazard – a conservative solution.

Equations are derived only for the case of the gravity-inertia regime of spread. In most cases most of the liquid is evaporated in this regime.

9.3 ASSUMPTIONS

The assumptions made in the derivation of the model follow:

- The liquid is lighter than water and immiscible with it.
- The heat for evaporation of liquid comes primarily from water.
- The spread area is a continuous mass of liquid at every instant.
- The spill occurs instantaneously.

- The properties of the liquids do not change during the spread.

Because of the violence associated with the boiling of a cryogenic liquid on water, the third assumption – the continuous slick – may not always be true in reality.

9.4 DATA REQUIRED

The following input data are necessary for obtaining the desired solution from this model:

- The physical properties of the cryogenic liquid, such as the density, boiling temperature (at atmospheric pressure), viscosity at boiling temperature, and the like.
- Data as to whether ice forms or not.
- Water (and/or ice) properties.
- Value of the boiling transfer coefficient between liquid and water (or liquid and ice), or equivalently the heat flow from water to the liquid.

9.5 MODEL DETAILS

Figure 9.1 shows a schematic view of the spreading of the liquid. For the purposes of the model, however, we use a mean film thickness "h." This is justifiable on the basis that the ultimate result needed is the time for evaporation and the extent of spread and not the detailed thickness profile at every instant of time. The error introduced by this uniform thickness assumption is minimized by the procedure illustrated below.

In deriving the equations of spread we again make use of the idea of the equilibrium of the spreading and resisting forces and the global continuity equation. First, we consider the radial spread case without and then with ice formation. In the second case we consider the one-dimensional spread.

9.5.1 Radial Spreading

(1) *Constant Boiling Heat Flux*

- **Gravity-Inertia Regime**

$$\text{Spreading force (gravitational)} = F_g = \pi \rho_\ell G R h^2 \qquad (9.1)$$

$$\text{Inertial resistance} = F_i = -C\,(\pi R^2 h \rho_\ell)\, d^2R/dt^2 \qquad (9.2)$$

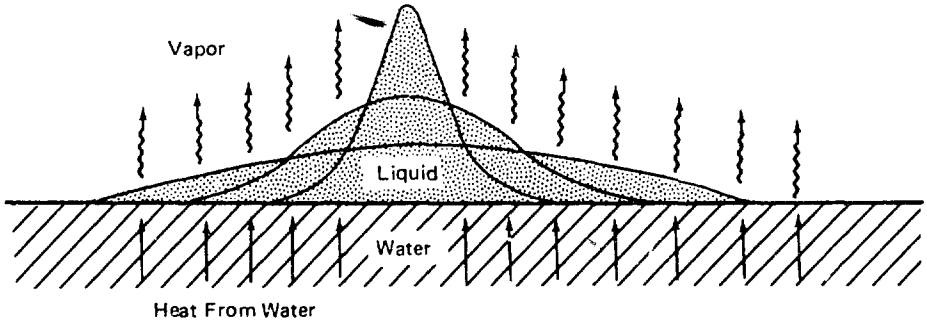

FIGURE 9.1a SPREADING AND EVAPORATING LIQUID – THICKNESSES OF THE FILM AT VARIOUS TIMES

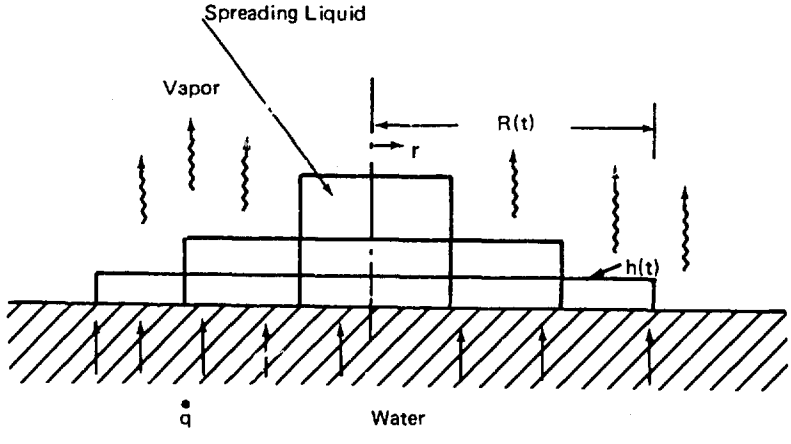

FIGURE 9.1b THE MEAN THICKNESSES OF THE LIQUID FILM USED IN THE MODEL AT VARIOUS TIMES

The factor C is introduced in Eq. (9.2) to take into account the fact that the inertia of the entire system is a fraction (C) of the inertia of the total mass, if the entire mass were being accelerated at the leading edge acceleration d^2R/dt^2. However, it is tacitly assumed that this fraction remains the same at all times, which may not be true in reality. This question can be answered conclusively only if the problem is solved in its entirety, starting from local continuity equation. However, this is an extremely difficult task.

Equating (9.1) and (9.2) and simplifying, we get the spread law:

$$h = -C \frac{R}{G} \frac{d^2R}{dt^2} \tag{9.3a}$$

The *mass conservation* equation is:

$$V\rho_\ell = V_i \rho_\ell - \pi \int_0^t \frac{\dot{q} R^2}{\lambda} dt \tag{9.4a}$$

where the integral on the RHS indicates the total mass lost by evaporation in a time duration t. $\dot{q}$ is the boiling heat flux.

Finally, we have the *geometric relation*

$$V = \pi R^2 h. \tag{9.5a}$$

The above equations are written in dimensionless form* as follows:

$$\eta = -c \chi \frac{d^2\chi}{d\tau^2} \tag{9.3b}$$

$$k = 1 - \pi \Delta \int_0^\tau \chi^2(\tau)\, d\tau \tag{9.4b}$$

$$k = \pi \eta \chi^2 \tag{9.5b}$$

We solve Eqs. (9.3b) through (9.5b) under the condition that the boiling heat flux from the water to the cryogen is a constant (i.e., $\Delta(\xi, \tau) = \Delta \equiv$ const). Substituting Eq.(9.3b) in Eq. (9.5b) for η and the resulting equation for k in Eq. (9.4b) and differentiating the resulting equation with respect to τ yields:

$$\frac{d}{d\tau}\left[\chi^3 \frac{d^2\chi}{d\tau^2}\right] = \frac{\Delta}{c} \chi$$

*For the definition of symbols see "Nomenclature" (9.11).

i.e.,

$$2\,\frac{d\chi}{d\tau}\,\frac{d^2\chi}{d\tau^2} + \left[\frac{d\chi}{d\tau}\,\frac{d^2\chi}{d\tau^2} + \chi\cdot\frac{d}{d\tau}\left(\frac{d^2\chi}{d\tau^2}\right)\right] = \frac{\Delta}{c}$$

or

$$\frac{d}{d\tau}\left[\left(\frac{d\chi}{d\tau}\right)^2 + \chi\,\frac{d^2\chi}{d\tau^2}\right] = \frac{\Delta}{c}$$

i.e.,

$$\frac{d}{d\tau}\left[\frac{d}{d\tau}\left(\chi\,\frac{d\chi}{d\tau}\right)\right] = \frac{\Delta}{c}$$

i.e.,

$$\frac{d^3}{d\tau^3}\left(\chi^2\right) = \frac{2\Delta}{c}$$

Integrating yields:

$$\chi^2 = \frac{\Delta}{c}\,\frac{\tau^3}{3} + A\,\tau^2 + B\,\tau + D \qquad (9.6)$$

Now using the condition $\chi\,(0) = 0$, we have $D = 0$. Also when there is no heat transfer, that is, when $\Delta = 0$, the solution should be the same as the solution given in Chapter 3 (Ref. Table 3.2) obtained by Fannelop and Waldman.

Hence:

$$A = 0$$

Another argument that can be proposed for A being zero is that the initial conditions of acceleration and velocity of the Delta-function release are such that the following holds:

$$\left(\frac{d\chi}{d\tau}\right)^2 + \chi\,\frac{d^2\chi}{d\tau^2} = 0 \quad \text{at} \quad \tau = 0$$

(Note, however, that both the acceleration and velocity have infinite magnitudes at time, $\tau = 0$)

Therefore:

$$\chi = \left[B\,\tau + \frac{\Delta}{3c}\,\tau^3\right]^{\frac{1}{2}} \qquad (9.7)$$

Differentiating χ w.r.t. τ and using Eq. (9.7) we can show that:

$$\frac{d\chi}{d\tau} = \frac{\left[B - \frac{\Delta}{C}\tau^2\right]}{2\left[B - \frac{\Delta}{3C}\tau^3\right]^{\frac{1}{2}}} \tag{9.8}$$

and

$$\frac{d^2\chi}{d\tau^2} = \frac{\frac{2\Delta}{C}\left[B\tau^2 + \frac{\Delta}{3C}\tau^4\right] - \frac{1}{2}\left[B + \frac{\Delta}{C}\tau^2\right]^2}{2\left[B\tau + \frac{\Delta}{3C}\tau^3\right]^{\frac{3}{2}}} \tag{9.9}$$

and using Eq. (8.3b):

$$\eta = -C\chi\frac{d^2\chi}{d\tau^2} = C\,\frac{\frac{1}{2}\left[B - \frac{\Delta}{C}\tau^2\right] - \left[\frac{2\Delta}{C}B\tau^2 + \frac{\Delta}{3C}\tau^4\right]}{2\left[B\tau + \frac{\Delta}{3C}\tau^3\right]} \tag{9.10}$$

using Eqs. (9.4b), (9.5b), and (9.10) yields:

$$(k)_{\tau=0} = 1 = \left[\pi\chi^2\eta\right]_{\tau=0} = \frac{\pi C B^2}{4}$$

Hence:

$$C = 4/\pi B^2 \tag{9.11}$$

The value of B is obtained from Table 3.2 for the radial spread in gravity inertia regime.

Hence:

$$B = (1.14)^2 = 1.2996.$$

Therefore:

$$C = 0.75386. \tag{9.12}$$

Eqs. (9.4b) and (9.7), after integration, yield:

$$k = 1 - \pi \Delta \left(\frac{B}{2} \tau^2 + \frac{\Delta}{3C} \frac{\tau^4}{4} \right) \tag{9.13a}$$

$$= 1 - 2.04 \Delta \tau^2 - 0.3473 \Delta^2 \tau^4 \tag{9.13b}$$

if

τ_e = time at which all the liquid evaporates, if the spreading continues in the gravity-inertia regime.

Then with $k = 0$ in Eq. (9.13) we get:

$$\tau_e = 0.68125 \sqrt{\frac{BC}{\Delta}} = \frac{0.6743}{\sqrt{\Delta}} \tag{9.14a}$$

The maximum radius at this time τ_e is:

$$\chi(\tau_e) = \chi_{max} = 1.0059/\Delta^{1/4} \tag{9.15a}$$

These are expressed in dimensional quantities as follows:

$$t_e = 0.6743 \left[\frac{V \rho_\ell^2 \lambda^2}{G \dot{q}^2} \right]^{\frac{1}{4}} \tag{9.14b}$$

$$R_{max} = 1.0059 \left[\frac{V^3 \lambda^2 \rho_\ell^2 G}{\dot{q}^2} \right]^{\frac{1}{8}} \tag{9.15b}$$

- **Gravity-Viscous Regime**

It can be shown that the viscous forces are of the same order of magnitude as the inertial forces when the mean film thickness in the liquid is of the order of magnitude as the mean viscous boundary layer thickness. The boundary layer thickness in this context refers to that in the liquid or water depending, respectively, on whether the liquid viscosity is much smaller than or very much greater than that of water; that is:

$$h \sim \sqrt{\nu t} \tag{9.16a}$$

or

$$\eta \sim \sqrt{\tau} / \Gamma. \tag{9.16b}$$

The model given below assumes that during the inertial spreading, as soon as the mean film thickness attains a value equal to the boundary layer thickness, the viscous forces start acting on the liquid and the inertial forces are neglected. We designate the time at which this occurs as "critical." This critical time is obtained from using Eqs. (9.16b), (9.5b), (9.7), and (9.13).

It is calculated from

$$\sqrt{\tau_c} = \Gamma \frac{\left[1 - 2.04\,\tau_c^2\Delta - 0.3473\,\tau_c^4\Delta^2\right]}{\pi\left[1.3\,\tau_c + 0.442\,\tau_c^3\right]} \qquad (9.17)$$

for given values of Γ and Δ.

An analysis similar to that indicated for the gravity inertia regime was attempted. However, because of the mathematical difficulties, an exact solution could not be obtained. The solution given below retains most of the physics of the phenomenon.

A "pseudo volume" is defined, and is assumed to remain constant during the viscous spread regime, even though the actual volume itself is decreasing due to evaporation. This method of approach is not new. Hoult[1] estimates the time for complete evaporation of a given volume of liquid, using the spread models with constant volume, but allowing for the evaporation rate based on the area of spread.

The radius at any instant in the gravity viscous spread regime for a constant-volume spread of a *low-viscosity* liquid is given by (Ref. Chapter 8, Eq. (8.22c)):

$$R(t) = 0.8412\,[GV^3/\nu_\ell]^{1/8}\,t^{1/8} \qquad (9.18)$$

At the critical time the two regimes of spread have the radius as common. Since this radius would be derived from Eq. (9.7) and the volume in the system by Eq. (9.13), these two numbers, together with the critical time, may not satisfy the Eq. (9.18) if V, the volume at that instant, is used. We therefore force the satisfaction of Eq. (9.18) by using a pseudo volume, V_s, which is then assumed to be an invariant with time.

If

$$V_s = \text{pseudo volume}$$

and

$$v_s = V_s/V_i = \text{dimensionless pseudo volume,}$$

we can show that, for the radius in the gravity-viscous regime (for $\mu_\ell \ll \mu_\omega$):

(9.19)

where V_s is evaluated from the equality of radii at τ_c.

Therefore:

$$0.8412\, V_s^{1/3}\, \Gamma_\ell^{1/4}\, \tau^{1/8} = [1.3\, \tau_c - 0.442\, \tau_c^3\, \Delta]^{1/2}, \tag{9.20}$$

and τ_c is obtained from solving Eq. (9.17).

To find the time for complete evaporation we have

$$dk/d\tau = -\pi \chi^2 \Delta$$

with condition

$$\chi = \chi_c \text{ and } k = k_c \text{ at } \tau = \tau_c.$$

Hence it can be shown that

$$\tau_e = \tau_c \left[1 + \frac{1.25\, k_c}{\pi \chi_c^2 \tau_c \Delta}\right]^{0.8} \tag{9.21}$$

Similar expressions can be derived for the case of $\mu_\ell \gg \mu_\omega$. All these results are given in Table 9.1 for the radial case.

(2) *Spread with Ice Formation*

In this section we consider the spreading of the cryogenic liquid on a sheet of ice that forms beneath it because of the freezing of water. As in the previous case we write the global continuity equation, the equation of the law of spread, and the geometric equation.

- **Gravity-Inertia Regime**

Geometric: $V = \pi R^2 h$ (9.5a)

Spread law: $h = -CR\, d^2R/dt^2$ (9.3a)

Global conservation: $$V\rho_\ell = V_i \rho_\ell - 2\pi \int_0^t \frac{dt}{\lambda} \int_0^{R(t)} r\, \dot{q}(r,t)\, dr \tag{9.4c}$$

where $\dot{q}$ (r,t) is the time and position-dependent heat flux from the water side (through the ice) to the cryogenic liquid.

It can be shown that the heat flux due to the formation of ice in water (because of the cryogenic liquid on the water surface) is (for infinite boiling heat-transfer coefficient):

$$\dot{q}\,(r,t) = k_{ice}\,(\theta_F - \theta_{cr}/y(r,t) \tag{9.22}$$

where y is the thickness of the ice layer at any instant at the radial location r. It can further be shown (based on one dimensional freezing problem analysis) that

$$y\,(r,t) = \sqrt{\frac{2\,K_{ice}(\theta_F - \theta_{cr})}{\rho_{ice}\;h_{fs}^{eff}}\,\bar{t}} \tag{9.23}$$

where

$\bar{t}$ = time for which ice has been formed at any particular location, r, and (9.24)

h_{fs}^{eff} = effective latent heat of fusion of ice =

$$= h_{fs} + c_w\,(\theta_w - \theta_F) + 0.5c_{ice}\,(\theta_F - \theta_{ice}) \tag{9.25}$$

We now assume a thickness distribution profile for the ice lens in the form* (refer to Figure 9.2):

$$y(r,t) = \sqrt{1 - \left(\frac{r}{R(t)}\right)^2}\;\;y_o(t) \tag{9.25}$$

where $y_o(t)$ is the maximum ice thickness at the center.

Substituting Eq. (9.23) in Eq. (9.25) and the resulting equation in Eq. (9.22) yields for the dimensionless heat flux:**

$$Q\,(\xi,\tau) = \frac{\dot{q}(r,t)}{\dot{q}_{ch}} = \frac{\alpha'}{\sqrt{(1-\xi^2)\,\tau}} \tag{9.26a}$$

*This elliptic profile is assumed to give the proper singularity at the leading edge for the heat flux and to satisfy the conditions of symmetry at r = 0.

**Since the spreading is now on a solid sheet of ice, G = g where g is the gravitational acceleration.

where

$$\alpha' = \left[\frac{K_{ice}(\theta_F - \theta_{cr})\, \rho_{ice}\, h_{fs}^{eff}}{\lambda^2 \rho_\ell^2 \sqrt{v_i\, g}} \right]^{\frac{1}{2}} \qquad (9.26b)$$

Substituting Eq. (9.26) in Eq. (9.4c) and first integrating w.r.t.ξ and simplifying yields:

$$k = 1 - \alpha \int_0^\tau \frac{\chi^2(\tau)}{\sqrt{\tau}}\, d\tau \qquad (9.27)$$

where

$$\alpha = 2\pi\, \alpha'$$

Equations (9.3b), (9.5b), and (9.27) now form three equations in three unknowns, viz: η, χ, and k. The value of C in Eq. (9.3b) is determined as before by considering the solution when there is no heat transfer. Since this solution would be identical to the one given in the earlier case of gravity-inertia spread without heat transfer, we have (from Eq. (9.12)):

$$C = 0.75386 \qquad (9.12)$$

Substituting Eq. (9.5b) in Eq. (9.3b) and the result in Eq. (9.27) and differentiating w.r.t.τ yields:

$$\frac{d}{d\tau}\left(\chi^3 \frac{d^2\chi}{d\tau^2}\right) = \frac{\alpha}{C}\, \frac{\chi^2}{\sqrt{\tau}}$$

After expanding the differential on the LHS and cancelling χ^2 terms throughout, and then simplifying and integrating, we can show that the above equation reduces to

$$\left(\frac{d\chi}{d\tau}\right)^2 + \chi \cdot \frac{d^2\chi}{d\tau^2} = \frac{2\alpha}{C}\, \tau + A \qquad (A = 0)$$

Assuming that the velocity and acceleration at time $\tau = 0$ are given to be such that the LHS of the above equation is zero, we have A = 0. Now the integration of the equation gives

$$\chi^2 = \frac{16}{15} \frac{\alpha}{C} \tau^{\frac{5}{2}} + B \tau$$

where use has been made of the condition $\chi(0) = 0$. The value of B is again obtained from Eq. (9.12).

Therefore:

$$\chi^2 (\tau) = 1.415 \alpha \tau^{5/2} + 1.3 \tau \tag{9.28b}$$

and from Eq. (9.27)

$$k(\tau) = 1 - 0.867 \alpha \tau^{3/2} + 0.4716 \alpha^2 \tau^3 \tag{9.29}$$

and τ_e is obtained by solving Eq. (9.29) with R = 0.

$$\tau_e = 0.864/\alpha^{2/3} \tag{9.30a}$$

In dimensional units:

$$t_e = 0.2537 \left[\frac{\lambda^2 \rho_\ell^2 V_i}{K_{ice} \rho_{ice} h_{fs}^{eff} (\theta_F - \theta_{cr}) g} \right]^{\frac{1}{3}} \tag{9.30b}$$

Similarly, substituting Eq. (9.30a) in Eq. (9.28b) yields:

$$\chi_{max} = 1.451/\alpha^{1/3}$$

or

$$R_{max} = 0.7864 \left[\frac{\lambda^2 \rho_\ell^2 g^{\frac{1}{2}}}{K_{ice} \rho_{ice} h_{fs}^{eff} (\theta_F - \theta_{cr})} \right] V_i^{\frac{1}{2}} \tag{9.31}$$

• **Gravity-Viscous Regime**

As before we assume that the viscous resistance becomes important when the mean film thickness is of the same order of magnitude as the mean viscous boundary layer thickness. Also using the idea of pseudo volume, enunciated in the previous section and using the equation for gravity-viscous spread formula for spreading on a solid surface (see Chapter 8, Eq. (8.22d)) we get the following equations:

$$\frac{dk}{d\tau} = -\pi \chi^2 \frac{\alpha}{\sqrt{\tau}} \tag{9.32}$$

$$\tau_c^{\frac{1}{2}} = \frac{\ell}{\pi} \frac{\left[1 - 0.867\alpha \tau_c^{\frac{3}{2}} + 0.4716 \alpha^2 \tau_c^3\right]}{\left[1.3\ \tau_c + 1.1415\ \alpha\ \tau^{5/2}\right]} \tag{9.33}$$

$$\chi = \chi_c \left[\frac{\tau}{\tau_c}\right]^{1/8} \tag{9.34}$$

$$k = k_c - \frac{4\pi\alpha\chi_c^2\tau_c^{\frac{1}{2}}}{3}\left[\left(\frac{\tau}{\tau_c}\right)^{\frac{3}{4}} - 1\right] \tag{9.35}$$

$$\tau_e = \tau_c \left[1 - \frac{3\ k_c}{4\pi\alpha\chi_c^2\tau_c^{1/2}}\right]^{\frac{4}{3}} \tag{9.36}$$

These equations are presented in Table 9.1.

9.5.2 One Dimensional Spreading

In this section the spread formulas for the spread of a cryogen in channel water are given. It is assumed that the release is instantaneous, like a Delta-function, uniform across the channel. All other assumptions made for the radial spreading are also assumed to apply.

(1) *Constant Boiling Heat Flux*

• **Gravity-Inertia Regime**

As before, by equating the gravitational spreading force to the inertial resistance yields:

$$\eta = -C\chi\, d^2\chi/d\tau^2; \tag{9.37}$$

also

$$k = \eta\chi \tag{9.38}$$

and the global conservation equation:

$$k = 1 - \Delta \int_0^{\tau} \chi(\tau)\, d\tau \tag{9.39}$$

with the initial conditions

$$k(0) = 1;\ \chi(0) = 0;\ \eta(0) = \infty \tag{9.40}$$

Substituting Eq. (9.38) in Eq. (9.39) and using Eq. (9.37) and differentiating the resulting equation with respect to τ and simplifying yields:

$$\frac{1}{2}\left(\frac{d\chi}{d\tau}\right)^2 + \chi\frac{d^2\chi}{d\tau^2} = \frac{\Delta}{C}\tau + \cancel{B}_{\,0} \tag{9.41}$$

where the constant of integration B is set to zero following the proper behavior of the infinities for velocity and acceleration at time $\tau = 0$.

Equation (9.41) has no exact solution. However, a perturbation solution has been obtained (because $\Delta \ll 1$, and $C \sim 1$ – see "Specific Example"). This solution to the lowest order in Δ is:

$$\chi(\tau) = A\tau^{\frac{2}{3}} + \frac{9}{40AC}\tau^{\frac{7}{3}}\Delta \tag{9.42}$$

where

$$A = 1.39$$

$$C = 4.5/A^3 = 1.67.$$

Also, the solution tends to the zero heat-transfer solution given in Chapter 3. Table 3.2 for $\Delta = 0$.

Hence:

$$k = 1 - \Delta\left[\frac{3A}{5}\,\tau^{\frac{5}{3}} + \frac{27}{400}\,\frac{\Delta}{AC}\,\tau^{\frac{10}{3}}\right] \tag{9.43}$$

and

$$\tau_e = \frac{\frac{20}{A}\left[-1+\sqrt{1+\frac{1}{6}}\right]}{\Delta^{0.6}} = \frac{1.0891}{\Delta^{0.6}} \tag{9.44}$$

Substituting Eq. (9.44) in Eq. (9.42) yields:

$$\chi_{max} = 1.5874/\Delta^{0.4} \tag{9.45}$$

- **Gravity-Viscous Regime**

Here also we utilize the ideas of pseudo volume and the results of Chapters 3 and 8 to get the following equation:

$$\tau_c = \Gamma\,\frac{\left[1 - 0.834\,\tau_c^{5/3}\Delta - 0.029\,\tau_c^{10/3}\Delta^2\right]}{\left[1.39\,\tau_c^{2/3} + 0\ 0966\,\tau_c^{7/3}\right]} \tag{9.46}$$

$$\chi = \chi_c\left[\frac{\tau}{\tau_c}\right]^a \tag{9.47}$$

and

$$k = k_c - \frac{\tau_c \chi_c \Delta}{1+a}\left[\left(\frac{\tau}{\tau_c}\right)^{1+a} - 1\right] \tag{9.48}$$

$$\tau_e = \tau_c \left[1 + \frac{(1+a)k_c}{\tau_c \chi_c \Delta} \right]^{\frac{1}{(1+a)}} \tag{9.49}$$

where

$$\left.\begin{aligned} a &= 1/5 \text{ for } \mu_\ell \ll \mu_\omega \\ a &= 3/8 \text{ for } \mu_\ell \gg \mu_\omega \end{aligned}\right\} \tag{9.50}$$

These results are indicated in Table 9.2

(2) *Spread with Ice Formation*

The analysis is similar to that in the radial case. Here also we assumed that ice formation follows the square root of time law (refer Eq. (9.23)). Also the elliptic profile for the ice thickness V_s x coordinate is assumed (see Figure 9.2). The analysis is extended to the gravity-viscous regime also, as shown in earlier cases, by the assumption of a pseudo volume. The results of these analyses are given in Table 9.2.

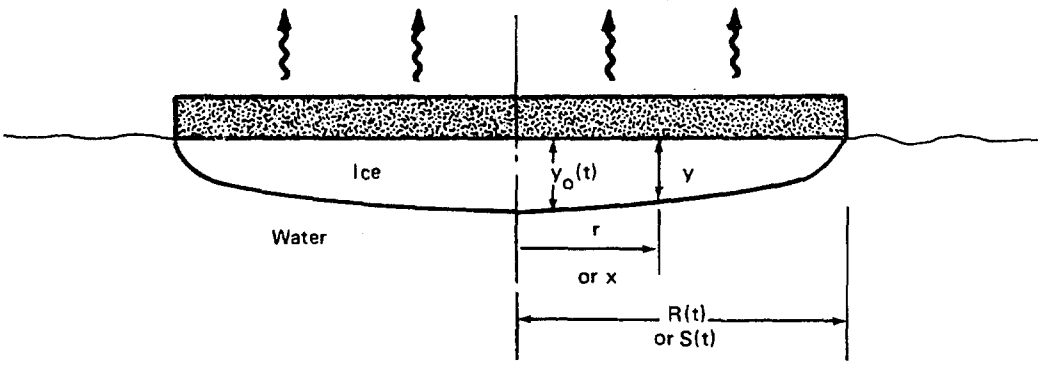

FIGURE 9.2 ELLIPTICAL PROFILE FOR ICE THICKNESS

9.6 COMPUTATIONAL ALGORITHM

The analyses discussed so far give equations which can be readily utilized to obtain the quantities of interest (such as spread extent, volume left in the system, and the like) at any time, provided the properties of the spreading liquid and water are known. The procedure for calculation is quite straightforward and is best illustrated by the example worked out below. A computer program has been written to give ready answers to various inputs. The flow chart for this program is shown in Figure 9.3.

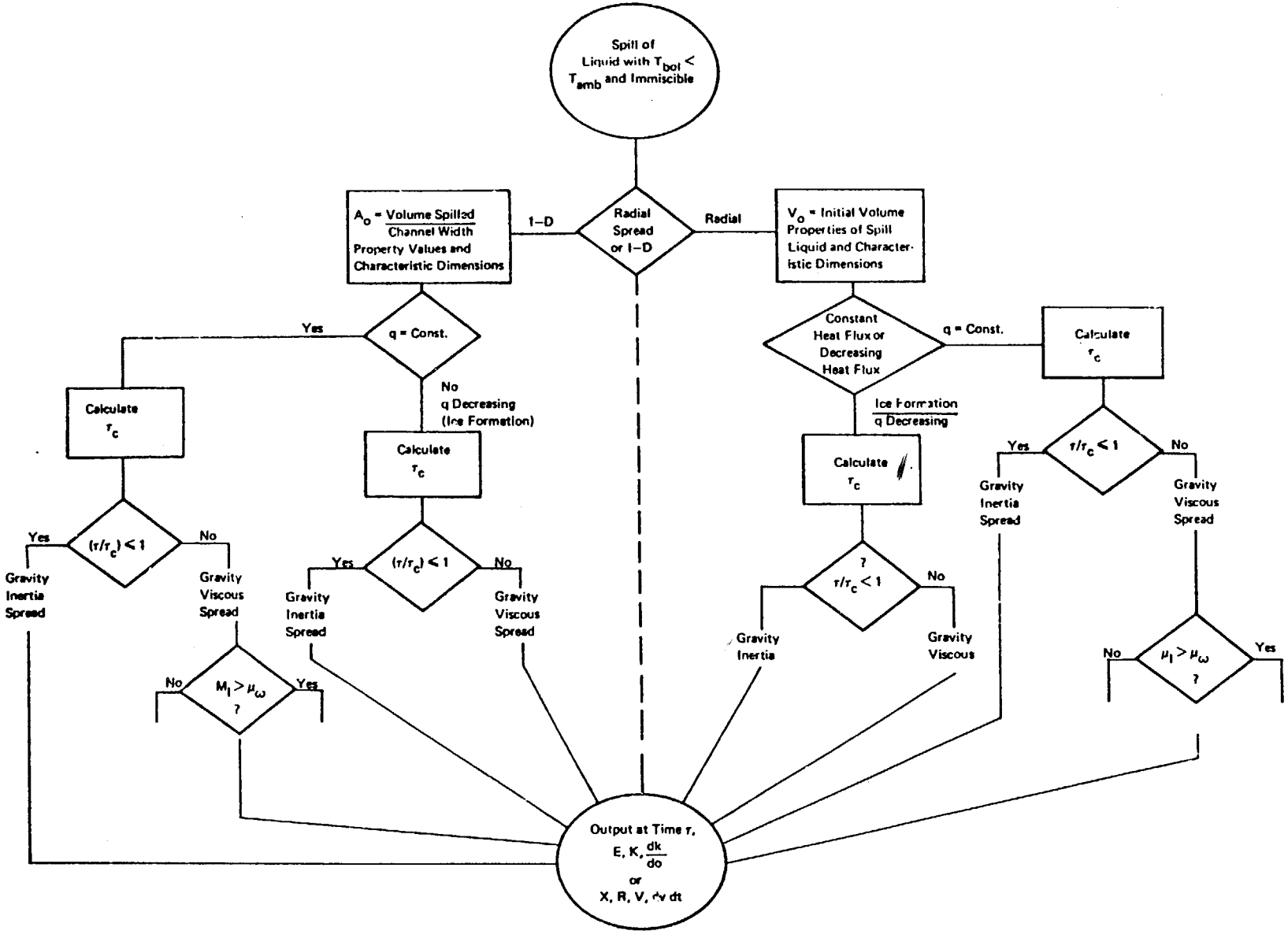

FIGURE 9.3 FLOW CHART OF COMPUTER PROGRAM

9.7 SPECIFIC EXAMPLE

The calculation procedure is illustrated by the following example:

Liquid Properties	Type of Spread		= Radial
Liquid spilled			= LNG
Mass spilled	M	$= 10^7$	kg
Density of liquid	ρ_ℓ	$= 425$	kg/m^3
Viscosity of liquid (at saturation)	μ_ℓ	$= 1.18 \times 10^{-4}$	N s/m^2
Kinematic viscosity	ν_ℓ	$= 2.776 \times 10^{-7}$	m^2/s
Latent heat of vaporization	λ	$= 510.8$	kJ/kg
Boiling temperature	θ_{cr}	$= 112$	K
Constant heat flux from water	q	$= 94.6$	kW/m^2
Water Properties			
Density	ρ_w	$= 10^3$	kg/m^3
Viscosity	μ_w	$= 10^{-3}$	N s/m^2
Calculations			
Volume spilled	V_i	$= 10^7/425 = 2.253 \times 10^4$	m^3
Characteristic length	L	$= 28.66$	m
Effective gravity	G	$= (1 - 425/1000) \times 9.8 = 5.635$	m/s^2
Characteristic time	T	$= (28.66/5.635)^{1/2} = 2.26$	s
Characteristic velocity	U_{ch}	$= 28.66/2.26 = 10.77$	m/s
Characteristic heat	$\dot{q}_{ch}$	$= 10.77 \times 510.8 \times 425$	
		$= 23.38 \times 10^5$	kW/m^2
	$\therefore$ Δ	$= 4.048 \times 10^{-5}$	
Dimensionless viscosity	Γ_ℓ	$= \left[\frac{2.353 \times 10^4 \times 5.635}{(2.776 \times 10^{-7})^2}\right]^{1/4} = 3.62 \times 10^4$	

Solving by an iterative method, Eq. (9.17) with $\Gamma = \Gamma_\ell$ yields:

Critical time	τ_c	$= 99.5$
Dimensionless volume at this time	k_c	$= 0.126$
Dimensionless radius	χ_c	$= 12.12$

If the spread were assumed to continue in the gravity-viscous regime itself, then the time for complete evaporation (see Eq. (9.14a)) and the maximum radius at this time (Eq. (9.15a)) are, respectively:

$$\tau_e = \frac{0.6743}{\sqrt{(4{,}048 \times 10^{-5})}} = 105.98$$

and

$$\chi_{max} = \frac{1.0059}{(4.048 \times 10^{-5})^{1/4}} = 12.61$$

However, if we do allow for the gravity-viscous spread, then:

Time to evaporate completely
(ref. Eq. (9.71)) $= \tau_e = 99.5$

$$= 99.5 \left[1 + \frac{1.25 \times 0.126}{\pi \times (12.12)^2 \times 9.5 \times \Delta} \right]^{0.8} = 106.19$$

and

radius $\chi_{max} = 12.12 \left(\frac{106.19}{99.5} \right)^{1/8} = 12.12$

The time history of volume and the radius of spread are plotted in non-dimensional units in Figure 9.4 for the property values chosen in this example.

9.8 DISCUSSIONS

The major assumptions made in the derivation of the equations were given in Section 9.3. It is noted that the assumptions of instantaneous release and that the spreading area is continuous are seldom valid in reality. Some experiments of release of LNG on water, conducted by the Bureau of Mines,[2] indicate that, because of the violence of boiling, the slick breaks up into a number of smaller puddles, especially toward the end of the spreading time. Also since the time of release from a barrel was comparable to the total time of evaporation, instantaneous release is not really occurring. Suffice it to say that the models presented here give a larger spread area and higher vaporization rates than observed and, therefore, the erring is on the correct side for hazard prediction. However, when better models become available, they should be used.

In one of the models we have assumed that the boiling heat flux to the liquid is a constant. It is known, however, that in the boiling phenomenon the heat flux depends on the local temperature difference between the boiling liquid and the "surface." Depending on the initial temperature difference, this heat flux may increase (film boiling to nucleate) or decrease (nucleate boiling), when the temperature difference is decreased. In the case of a cryogen spill on water, the water gets cooled progressively, thereby decreasing the temperature difference between the boiling liquid and the water. This results in a varying heat flux with time.

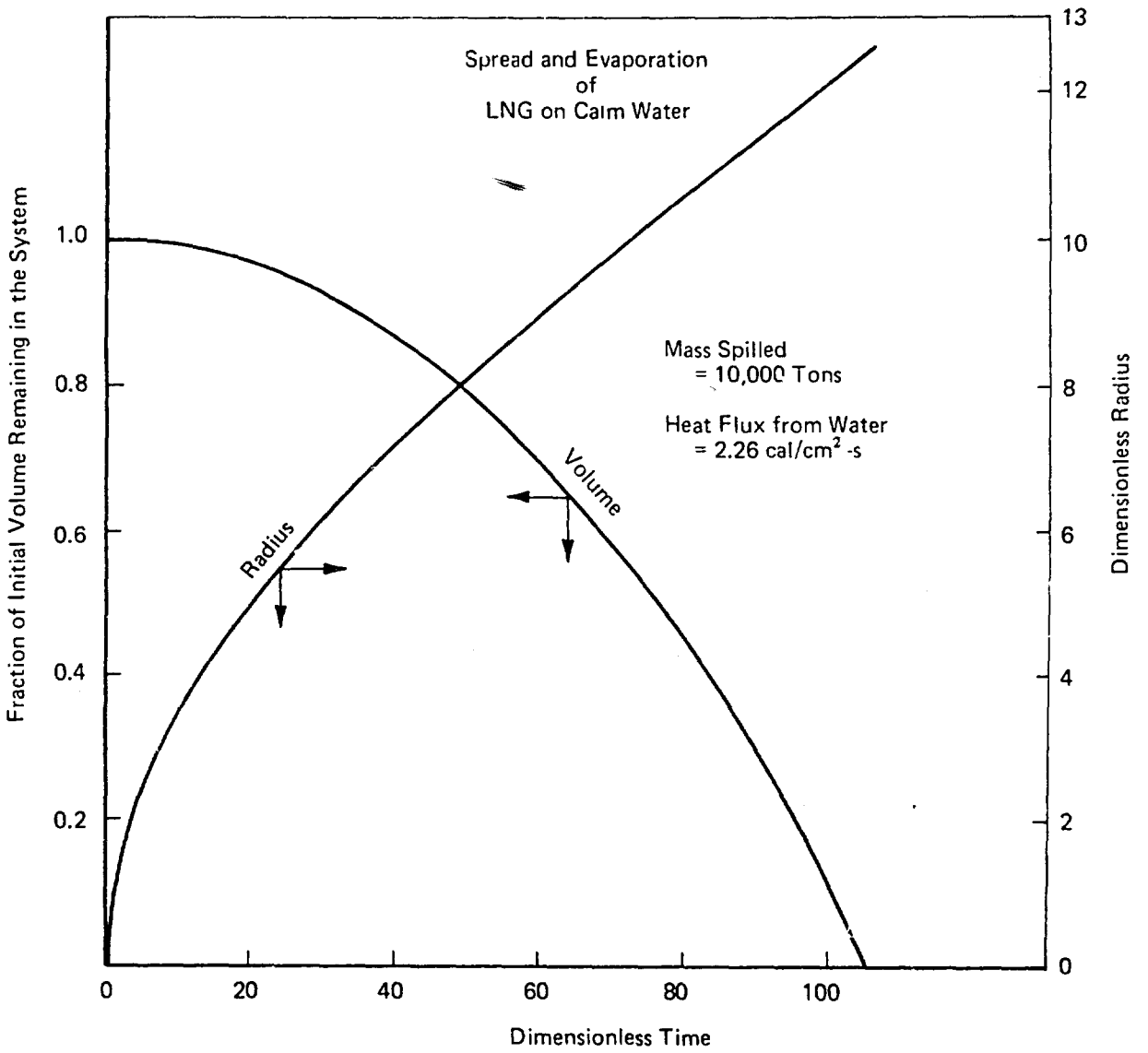

FIGURE 9.4 VOLUME & RADIUS OF LNG SPREADING ON WATER

The analysis based on the varying heat flux due to ice formation is correct to the extent that a similarity profile is assumed (elliptic) for the ice thickness. To execute the problem more exactly would involve horrendous mathematical difficulties. An *a posteriori* check on the accuracy of an elliptic profile assumption indicates a possible maximum error of about 15% in the heat flux estimation. Also a continuous sheet of ice formation may hardly occur in nature. Instead patches of ice sheets, or even tiny crystals of ice, may be formed.

Some other important factors not considered in the analysis are the effects of the dynamics of the release, the duration of release, initial flashing, and the like. Also not taken into account are the possibilities of a doughnut-shaped spread.

The example worked out shows the salient features of the models. It can be seen that most of the liquid evaporates in the gravity-inertia regime itself. This is because, by the time the viscous effects are important, the spread is over a large area (consequently high evaporation rate over the whole area) and a small volume of liquid is left over in the system (see Figure 9.4). However, if the heat flux is small, it is quite likely that the spread will proceed even in the gravity-viscous regime for a considerable length of time.

The effect of heat transfer on the spread radius is small (because of the small value of Δ). In fact, if one calculates the time to evaporate all the liquid, with the spread extent being calculated on the basis of constant volume, he will find that $\tau_e = 0.7/\Delta^{1/2}$ as opposed to actual value $\tau_e = 0.6743/\Delta^{1/2}$ (Eq. (9.14a)) for a specific case. It follows, therefore, that when the heat flux $\dot{q}$, due to boiling heat transfer, is much smaller than the characteristic heat flux $\dot{q}_{ch}$, the total time for evaporation can be calculated, without too much error, by obtaining the spread using constant volume formulas (Chapter 3) and using the area so determined to obtain the evaporation rate at every instant of time.

9.9 CONCLUSIONS

Equations have been derived to predict the evaporation rate, the extent of spread, and the total time for evaporation for the spread of a cryogenic liquid on water. The two regimes of spread, namely, the gravity-inertia and gravity-viscous regimes, are considered. Also considered are the cases wherein a thin sheet of ice forms under the spreading liquid caused by the freezing of water. One set of the equations (derived for the case of constant heat flux) could also be used to predict the movement and spreading of a slick burning.

The details of the models and their limitations are discussed. A specific example of LNG spread on water is worked out. It is found that most of the evaporation occurs in the gravity-inertia regime of spread alone.

The validity of all of the equations have not been proven because of the lack of experimental data, but are based on sound physical phenomena and theoretical solutions.

9.10 REFERENCES

1. Hoult, D.P., "The Fire Hazard of LNG Spilled on Water"; Presented at the Conference on LNG Importation and Terminal Safety, Boston, June 13-14, 1972.

2. Burgess, D., Biordi, J. and Murphy, J., "Hazards of Spillage of LNG into Water"; PMSCR Report No. 4177, September 1972; report prepared by the Bureau of Mines, U.S. Dept. of the Interior.

9.11 LIST OF SYMBOLS

Symbol	Description	Formula, Value or Defining Eq.	Units
A_i	half of the initial volume of spill per unit channel width in 1-D spread		m^2
c	specific heat (subscripted)		J/kg K
C	constant defined in Eq. (9.2)		
F	spreading or resisting force (subscripted)		N
g	acceleration due to gravity	9.8	m/s^2
G	effective gravity	$g(1-\rho_\ell/\rho_w)$	m/s^2
h (r,t)	mean thickness of the film		m
h_{fs}	latent heat of fusion of ice		J/kg
h_{fs}^{eff}	effective latent heat of ice		J/kg
k (τ)	dimensionless volume of liquid at any instant	V/V_i	
K_{ice}	thermal conductivity of ice		W/m K
L	characteristic length scale	$V^{1/3}$	m
$\dot{q}$ (r,t) $\dot{q}$ (x,t)	heat flux to the boiling liquid		W/m^2
$\dot{q}_{ch}$	characteristic heat	$\lambda\rho_\ell U_{ch}$	W/m^2
Q	dimensionless heat		

Symbol	Description	Formula, Value or Defining Eq.	Units
r	radial coordinate		m
R (t)	radius to the spread front		m
S (t)	distance to spread front from the spill point in 1-D spread		m
t	time		s
U_{ch}	characteristic velocity	L/T	m/s
T	characteristic time	$\sqrt{L/G}$	s
v_s	dimensionless pseudo volume		
V	volume of liquid at any instant of time		m^3
V_i	initial volume of spill of liquid		m^3
V_s	pseudo volume		m^3
x	X-coordinate		m
y (x,t)	thickness of ice layer		m
Greek Symbols			
α'	dimensionless ice heat flux	Eq. (9.26b)	
α	dimensionless ice heat flux	$= 2\pi\alpha'$	
β	dimensionless ice heat flux in 1-D spread	$=(\pi/2)\alpha'$	
Δ	ratio of heat flux to characteristic heat flux	$= \dot{q}/\dot{q}_{ch}$	
Γ	dimensionless viscosity (subscripted)	$= (V_i G/\nu^2)^{1/4}$	
η	dimensionless mean liquid film thickness	= h/L	
θ	temperature (subscripted)		°K
λ	heat of vaporization of the liquid at the boiling point at atmospheric pressure		J/kg

Greek Symbols

μ	viscosity (subscripted)		$N\ s/m^2$
ν	kinematic viscosity (subscripted)		m^2/s
ξ	dimensionless similarity variable in the direction of spread	x/S or r/R	
ρ	density of fluids (subscripted)		kg/m^3
τ	non-dimensional time	t/T	
$\chi(\tau)$	dimensionless spread front distance from the point of spill	S/L or R/L	

Subscripts

c	= critical – at which gravity-inertia regime changes to gravity-viscous regime
ch	= characteristic
cr	= cryogen
e	= end – at which time all the liquid has evaporated
F	= freezing – ice freezing
i	= initial
ice	= pertaining to ice properties
ℓ	= liquid that is spreading
max	= maximum value
w	= water

TABLE 9.1

RADIAL SPREAD OF A CRYOGENIC LIQUID ON WATER

Type of Heat Transfer	Gravity-Inertia Regime	Viscosity Ratio	Critical Time for Change of Regimes	Gravity-Viscous Regime	Remarks
Constant Flux from the Water	$\chi = [1.3\tau + 0.442\tau^3\Delta]^{1/2}$ $k = 1 - 2.04\tau^2\Delta + 0.347\tau^4\Delta^2$ $\eta = \frac{k}{\pi\chi^2}$ $\tau_e = \frac{0.6743}{\Delta^{1/2}}$ $\chi_{max} = \frac{1.0059}{\Delta^{1/4}}$	$\frac{\mu_\ell}{\mu_w} \gg 1$	$\tau_c^{1/2} = \Gamma_w \frac{(1 - 2.04\tau_c^2\Delta + .347\tau_c^4\Delta^2)}{\pi(1.3\tau_c + .442\tau_c^3\Delta)}$	$\chi = \chi_c(\tau/\tau_c)^{1/4}$ $k = k_c - \frac{\Delta\pi\chi_c^2\tau_c}{1.5}\left\{\left(\frac{\tau}{\tau_c}\right)^{1.5} - 1\right\}$ $\tau_e = \tau_c\left\{1 + \frac{1.5\,k_c}{\pi\chi_c^2\tau_c\Delta}\right\}^{2/3}$	χ_c and k_c are the radius and liquid volume calculated at time τ_c from the gravity-inertia regime formulas. τ_c is calculated from the equation given in terms of Γ and Δ
		$\frac{\mu_\ell}{\mu_w} \ll 1$	$\tau_c^{1/2} = \Gamma_\ell \frac{(1 - 2.04\tau_c^2\Delta + .347\tau_c^4\Delta^2)}{\pi(1.3\tau_c + .442\tau_c^3\Delta)}$	$\chi = \chi_c(\tau/\tau_c)^{1/8}$ $k = k_c - \frac{\Delta\pi\chi_c^2\tau_c}{1.25}\left\{\left(\frac{\tau}{\tau_c}\right)^{1.25} - 1\right\}$ $\tau_e = \tau_c\left\{1 + \frac{1.25\,k_c}{\pi\chi_c^2\tau_c\Delta}\right\}^{0.8}$	
"Ice Formation" Time and Position-Varying Heat Flux Due to the Water Freezing	$\chi = [1.415\alpha\tau^{5/2} + 1.3\tau]^{1/2}$ $k = 1 - 0.867\alpha\tau^{3/2} + 0.4716\alpha^2\tau^3$ $\eta = \frac{k}{\pi\chi^2}$ $\tau_e = \frac{0.864}{\alpha^{2/3}}$ $\chi_{max} = \frac{1.451}{\alpha^{1/3}}$		$\tau_c^{1/2} = \left\{\frac{\Gamma_\ell}{\pi}\frac{[1 - 0.867\alpha\tau_c^{3/2} + .4716\alpha^2\tau^3]}{[1.3\tau_c + 1.415\alpha\tau^{5/2}]}\right\}$	$\chi = \chi_c(\tau/\tau_c)^{1/8}$ $k = k_c - \frac{4\pi\alpha\chi_c^2\tau_c}{3}\left[\left(\frac{\tau}{\tau_c}\right)^{3/4} - 1\right]$ $\tau_e = \tau_c\left[1 + \frac{3\,k_c}{4\pi\alpha\chi_c^2\tau_c^{1/2}}\right]^{4/3}$	χ_c and k_c are the radius and liquid volume, respectively, calculated at time τ_c from the equations of gravity-viscous regime. τ_c is calculated from the equation given in terms of Γ and χ

TABLE 9.2

ONE-DIMENSIONAL SPREAD OF A CRYOGENIC LIQUID ON WATER SURFACE

Type of Heat Transfer	Gravity-Inertia Regime	Viscosity Ratio	Critical Time for Changeover Regimes	Gravity-Viscous Regime	Remarks
Constant Heat Flux from Water	$\chi = [1.39\,\tau^{2/3} + 0.0966\,\tau^{7/3}\Delta]$ $k = 1 - .834\,\tau^{5/3}\Delta - .029\,\tau^{10/3}\Delta^2$ $\eta = \frac{k}{\chi}$ $\tau_e = \frac{1.0891}{\Delta^{0.6}}$ $\chi_{max} = \frac{1.5874}{\Delta^{0.4}}$	$\frac{\mu_\ell}{\mu_w} \gg 1$	$\tau_c^{1/2} = \Gamma_w \frac{(1-0.834\,\tau_c^{5/3}\Delta - 0.029\,\tau_c^{10/3}\Delta^2)}{(1.39\,\tau_c^{2/3} + 0.0966\,\tau_c^{7/3}\Delta)}$	$\chi = \chi_c\,(\tau/\tau_c)^{3/8}$ $k = k_c - \frac{\tau_c \chi_c \Delta}{1.375}\left\{\left(\frac{\tau}{\tau_c}\right)^{1.375} - 1\right\}$ $\tau_e = \tau_c\left[1 + \frac{1.375\,k_c}{\tau_c\,\chi_c\,\Delta}\right]^{8/11}$	χ_c and k_c are the radius and volume calculated with $\tau = \tau_c$, using the gravity-inertia regime formulas. τ_c is calculated from the equations given
		$\frac{\mu_\ell}{\mu_w} \ll 1$	$\tau_c^{1/2} = \Gamma_\ell \frac{(\ell-0.834\,\tau_c^{5/3}\Delta - 0.029\,\tau_c^{10/3}\Delta^2)}{(1.39\,\tau_c^{2/3} + 0.069\,\tau_c^{7/3}\Delta)}$	$\chi = \chi_c\,(\tau/\tau_c)^{1/5}$ $k = k_c - \frac{\tau_c\,\chi_c\,\Delta}{1.2}\left[\left(\frac{\tau}{\tau_c}\right)^{1.2} - 1\right]$ $\tau_e = \tau_c\left[1 + \frac{1.2\,k_c}{\tau_c\,\chi_c\Delta}\right]^{5/6}$	
"Ice Formation" Time & Position Varying Heat Flux, Due to the Freezing of Water	$\chi = 1.39\,\tau^{2/3}$ $k = 1 - 1.19\,\beta\,\tau^{7/6}$ $\eta = k/\chi$ $\tau_e = \frac{0.859}{\beta^{6/7}}$		$\tau_c^{1/2} = \Gamma_\ell \frac{(1 - \beta\,1.19\,\tau_c^{7/6})}{1.39\,\tau^{2/3}}$	$\chi = \chi_c\,(\tau/\tau_c)^{1/5}$ $k = k_c - \frac{10\beta}{7}\,\chi_c\,\tau_c^{1/2}\left[\left(\frac{\tau}{\tau_c}\right)^{7/10} - 1\right]$ $\tau_e = \tau_c\left[1 + \frac{0.7\,k_c}{\beta\,\chi_c\,\tau_c^{1/2}}\right]^{10/7}$	Spreading on a sheet of ice.

10.0 SIMULTANEOUS SPREADING AND COOLING OF A HIGH VAPOR PRESSURE CHEMICAL

10.1 AIM

The aim of the analysis presented in Chapter 10 is to obtain the extent of spread and the vaporization rate at any instant of time after the instantaneous spill, of a high-vapor-pressure, lighter-than-water liquid on water.

10.2 INTRODUCTION

Several of the liquid chemicals, such as diethyl ether and ethyl acetate, have high vapor pressures at room temperature. When these liquids are spilled on water, they not only spread but they also evaporate. The heat for evaporation comes from the sensible heat of the liquid as well as from the water. The model presented here takes both these "heats" into account. The totality of the problem with all the phenomena of spreading, cooling, and evaporation is much too complicated to model mathematically and obtain solutions. However, some basic simplification is achieved, without losing the essential physics, if we assume that the spreading and evaporation are independent (see the discussions in Section 9.8). To this extent the analysis given below is approximate since many of the finer details are overlooked in favor of a quick answer.

The essential features of the model are schematically illustrated in Figures 10.1 and 10.2. The detailed derivations are given in Section 10.5 and an illustrative example in Section 10.7.

10.3 PRINCIPLES AND ASSUMPTIONS

The basic principle of the model is the vapor-pressure-difference-driven evaporation and the consequent cooling of the liquid. The liquid also spreads simultaneously. There is also heat addition to the liquid from water because of the thermal gradient in water. The other assumptions made in the derivation include:

- All of the liquid is spilled instantaneously.
- The spreading is independent of evaporation.
- Entire liquid mass is at a single temperature (mixed mean temperature) at every instant of time; that is, there are no thermal gradients in the liquid mass itself.
- Liquid and water properties are constant.
- The mass-transfer coefficient is constant.

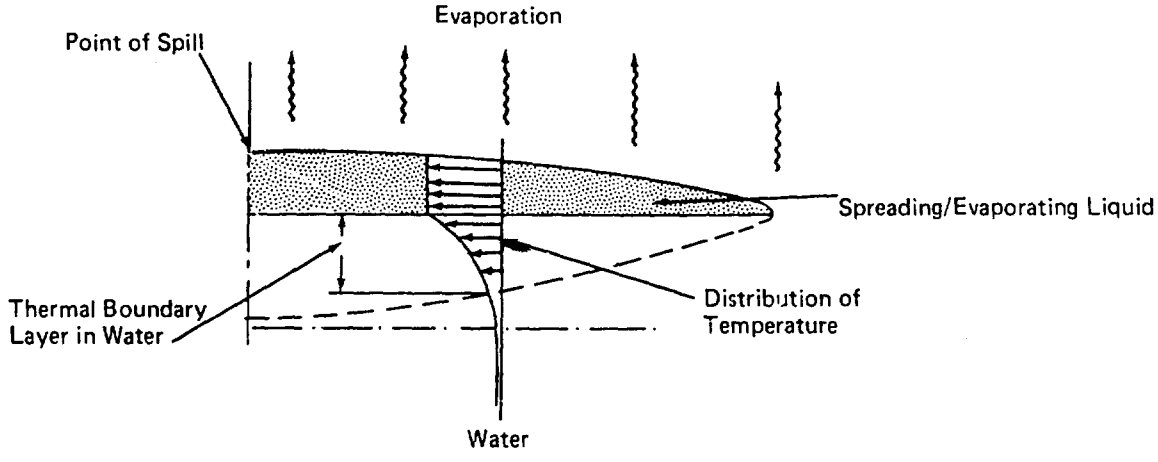

FIGURE 10.1 SCHEMATIC DIAGRAM ILLUSTRATING SPREADING AND EVAPORATION OF A LIQUID

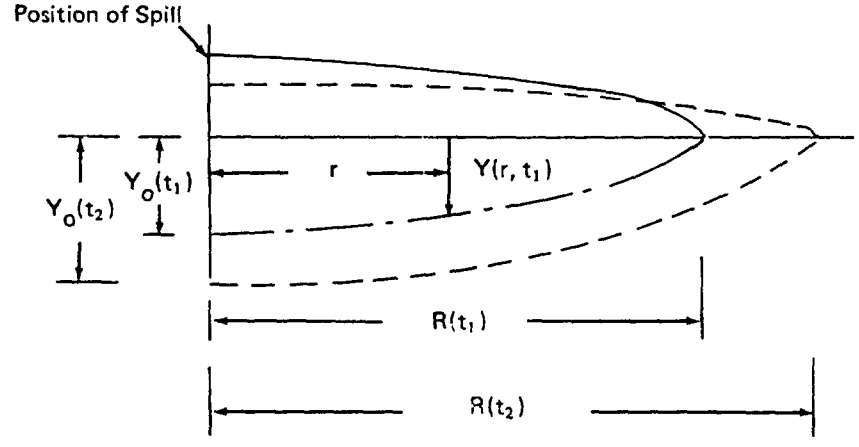

$$Y(r, t) = Y_o(t) \times \sqrt{1 - (\frac{r}{R(t)})^2}$$

FIGURE 10.2 SCHEMATIC DIAGRAM ILLUSTRATING THE ELLIPTIC THERMAL BOUNDARY LAYER IN WATER

- Evaporation is caused by a vapor concentration difference between the vapor just above the liquid surface and the vapor in the atmosphere. Also it is assumed that the vapor concentration in the atmosphere is zero.

- The temperature of the spilled liquid is the same as that of the water temperature.

The assumption of uniform liquid temperature is very idealistic. In fact, there will always be longitudinal and even thickness-wise thermal gradients in the liquid. However, in the interest of simplifying the problem this assumption is made. Also it is noted that the temperature so obtained gives a "mean" temperature. The assumption regarding the initial liquid temperature is questionable. If the liquid is hotter than water, it loses heat first to water and then starts cooling because of evaporation.

10.4 DATA REQUIRED

The following essential data are needed to utilize the results of the model presented:

- Physical and thermal properties of water,

- Physical properties and thermal properties of the liquid,

- Saturated vapor pressure-temperature relationship for the liquid, and

- A mass-transfer coefficient for evaporation. (This is given or calculated using heat mass-transfer analogy in which case the liquid vapor properties as well as the wind velocity should be given.)

This last item can be calculated approximately, using the heat and mass-transfer analogies and some forced correction heat-transfer results.

10.5 MODEL DETAILS

Figure 10.1 indicates the details of the model schematically. The liquid is spreading on the surface of water. The temperature of the liquid is less than that of water and consequently there exists a thermal boundary layer in water. The assumed elliptical profile for the variation of this boundary layer dimension along the radius (or length) is shown in Figure 10.2 for two different periods.

In the model below, first the energy conservation equation is written. This is solved simultaneously with the evaporation equation to obtain the temperature and the mass of the liquid in the system at any time.

10.5.1 Energy Equation

$$\frac{d}{dt}\left[M\,I_{liq}(T)\right] = Q - \dot{E}\,I_{vap}(T) \qquad (10.1)$$

Rate of change of enthalpy of the liquid system	Rate of heat coming into the system	Rate of heat loss by vapor leaving the system

Total evaporation rate $= \dot{E} = -\,dM/dt$ (10.2)

Also $\dot{E} = A\,\dot{E}''$ (10.3)

and $Q = \bar{q}\,A,$ (10.4)

where A is the area of the pool at any instant and $\dot{E}''$ and $\bar{q}$ are, respectively, the evaporation rate/unit area and mean heat flux from water at any instant of time. To calculate $\bar{q}$ we have:*

$$\bar{q} = c\,\frac{K_w(T_w - T)}{\sqrt{\pi \alpha_w t}} \qquad (10.5)$$

where

$$c = \begin{cases} 2\displaystyle\int_0^1 \frac{\xi\,d\xi}{\sqrt{1-\xi^2}} = 2 & \text{for radial spread} \\ \displaystyle\int_0^1 \frac{d\xi}{\sqrt{1-\xi^2}} = \frac{\pi}{2} & \text{for I - D spread} \end{cases} \qquad (10.6)\ (10.7)$$

also

$$\dot{E}'' = h_p\,P_{vap}(T) = a\,h_p\,e^{-\frac{b}{T}} \qquad (10.7a)$$

where the Clausius Clayperon equation has been used for the saturated pressure-temperature relationship.

Substituting Eq. (10.7a) in Eq. (10.3) and Eq. (10.5) in Eq. (10.4) and the resulting expressions in Eq. (10.1) and simplifying yields (after using $dI = C_{liq}\,dT$):

* $\bar{q}(t) = (2/R)\int_0^R r\,q(r,t)\,dr$ and using the elliptical profile for the thermal boundary layer yields

$$\bar{q}(t) = \left[K_w(T_w - T)/\sqrt{\alpha_w t}\right]\int_0^1 2\xi/\sqrt{(1-\xi^2)}\,d\xi$$

Substituting Eq. (10.7a) in Eq. (10.3) and Eq. (10.5) in Eq. (10.4) and the resulting expressions in Eq. (10.1) and simplifying yields (after using $dl = C_{liq}\,dt$):

$$M\,\frac{dT}{dt} = \frac{A}{C_{liq}}\left[c\,\frac{K_w(T_w - T)}{\sqrt{\pi \alpha_w t}} - \lambda h_p a e^{-\frac{b}{T}}\right] \qquad (10.8a)$$

and Eq. (10.2) yields in view of Eqs. (10.3 and 10.7):

$$dM/dt = -A\,h_p\,a\,e^{-b/T} \qquad (10.9a)$$

Initial conditions :

$$\text{at } t = 0;\ T = T_i;\ M = M_i \qquad (10.10a)$$

Equations (10.8a) and (10.9a) are two coupled, non-linear differential equations for the unknown M and T. These have to be solved with the given initial condition (10.10a). However, it is assumed that the area A is a known function of time (from the results of Chapter 3) and h_p, the mass-transfer coefficient, is a constant.

Analytical solution of the above equations is impossible. To obtain the numerical solution, we write Eqs. (10.8a) through (10.10a) in non-dimensional forms as follows, using the following definitions:

A_i = characteristic spill area $= (M_i/\rho_{liq})^{2/3}$

t_{ch} = characteristic evaporation time $= M_i/\dot{E}_i'' A_i$

where

$\dot{E}_i''$ = initial evaporation flux $= h_p\ ae^{-b/T_i}$

$\tau = t/t_{ch}$

$m = M/M_i$ (10.11)

T_{ch} = characteristic temperature $= \lambda/C_{liq}$

$\eta = \dot{E}''/\dot{E}_i''$

$\Gamma = A/A_i$

$$\theta = T/T_{ch}$$

$$\beta = b/T_{ch}$$

and

$$\Delta = c K_w T_{ch}/(\dot{E}''_i \lambda \sqrt{\pi \alpha_w t_{ch}})$$

where Δ represents physically the ratio of evaporation rate, caused by heat flow from water under a temperature difference T_{ch} and when the thermal boundary layer thickness is given by $\sqrt{\pi \alpha_w t_{ch}}$ to the initial evaporation rate caused by the vapor pressure difference.

Using Eq. (10.11), Eqs. (10.8a) and (10.9a) can be written as

$$\eta = e^{-\beta\left(\frac{1}{\theta} - \frac{1}{\theta_i}\right)} \tag{10.7b}$$

$$m \frac{d\theta}{d\tau} = \Gamma(\tau)\left[\Delta \frac{(\theta_w - \theta)}{\sqrt{\tau}} - \eta\right] \tag{10.8b}$$

$$\frac{dm}{d\tau} = -\Gamma(\tau)\,\eta \tag{10.9b}$$

and the initial conditions become

$$\tau = 0;\ m = 1;\ \theta = \theta_i \tag{10.10b}$$

Solution

The solution of Eqs. (10.7b) through (10.9b) are obtained by using the methods of numerical analysis for solving a set of simultaneous differential equations.[1] The solutions obtained are illustrated for a specific example in Section 10.7.

10.5.2 Evaluation of Mass-Transfer Coefficient

Reference 2 and the heat mass-transfer analogy yield the following equations for flow over a flat plate:

$$\frac{\overline{h}_D L}{D} = 1.328\ Sc^{\frac{1}{3}}\ Re_L^{\frac{1}{2}} \qquad (10.11a)$$

for $Re_L \leq 5 \times 10^5$

Laminar flow

and

$$\frac{\overline{h}_D L}{D} = 0.037\ Sc^{\frac{1}{3}}\ Re_L^{0.8} \qquad (10.11b)$$

for $Re_L > 5 \times 10^5$; turbulent flow

where L is the length of the flat plate.

$$\text{Also } h_p = h_D/RT \qquad (10.12)$$

We use the above equations to determine a mean mass-transfer coefficient. The characteristic length L used in this analysis is the length of spill and is defined by

$$L = (V_i)^{1/3}$$

where V_i is the initial spill volume. Also we assume that the mass-transfer coefficient does not change in spite of the fact that the pool is expanding (and so is the length of the liquid over which the air blows).

10.6 ALGORITHM FOR COMPUTATION

The algorithm for computing the spread extent, the evaporation rate, temperature, and the like, are shown in a flow chart (Figure 10.3). First, the mass-transfer coefficient is determined, and then the characteristic values are calculated. After that the subroutine to solve the system of differential equations is utilized to obtain the answers. The algorithm is best illustrated by an example.

10.7 SPECIFIC EXAMPLE

Liquid spilled	Diethyl Ether = $C_4H_{10}O$		
Volume of spill	V_i	1.27×10^3	m^3
Mass spilled	M_i	0.9×10^6	kg
Properties of liquid			
Density	ρ_ℓ	715	kg/m^3
Specific heat	C_ℓ	2200 at 0°C	J/kg °K

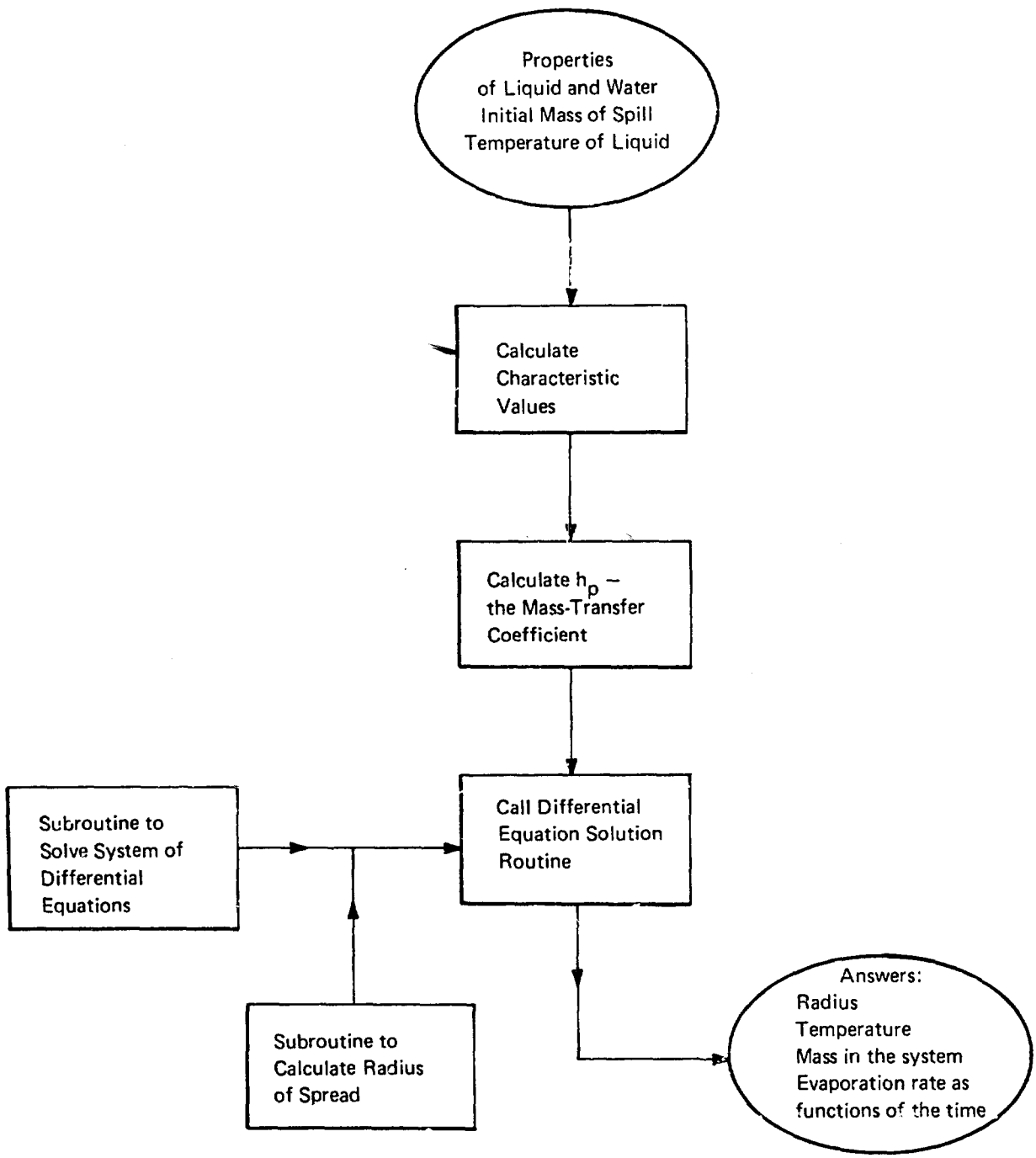

FIGURE 10.3 FLOW CHART FOR CALCULATING EVAPORATION RATE AND SPREAD EXTENT

Molecular weight	m	74.12	kg/kmole
Boiling temperature	T_B	307.8	°K
Freezing temperature	T_F	156.7	°K
Interfacial tension with water	σ	0.0107	N/m
Latent heat of vaporization	λ_{liq}	355.4×10^3	J/kg
Viscosity	μ_{liq}	0.2842×10^{-3}	N s/m^2
Diffusion coefficient[3]	D	8.9×10^{-6}	m^2/s
Saturated vapor pressure[3]	p_{sat}	$e^{(22.7522 - \frac{3494.736}{T})}$	N/m^2
Properties of water			
Density	ρ_w	10^3	kg/m^3
Viscosity	μ_w	10^{-3}	N s/m^2
Thermal conductivity	K_w	0.6	W/m °K
Thermal diffusivity	α_w	1.43×10^{-7}	m^2/s
Properties of air			
Kinematic viscosity	ν_{air}	15×10^{-6}	m^2/s
Wind velocity (assumed)	U_{wind}	5	m/s
Initial temperature	T_i	293	°K

Calculations

Schmidt number $Sc = \nu_{air}/D = 15/8.9 = 1.685$

Characteristic Length $L = (v_i)^{1/3} = (1.27 \times 10^3)^{1/3} = 10.83$ m

Reynolds number $Re_L = U_{wind} L/\nu_{air} = 5 \times 10.83/15 \times 10^{-6} = 3.61 \times 10^6$

Hence, the flow is turbulent in the boundary layer in the air stream. Therefore, using Eq. (10.11b) yields:

$$\bar{h}_D = [0.037 \times 1.685^{1/3} \times (3.73 \times 10^6)^{0.8}] \times 8.9 \times 10^{-6} / 10 = 6.906 \times 10^{-3} \text{ m/s}$$

Gas constant $R = 8.314 \times 10^3 / 74.12 = 112.174$ J/kg K

Using Eq. (10.12) $h_p = 6.906 \times 10^{-3} / 112.174 \times 293 = 2.101 \times 10^{-7}$ s/m

Characteristic Constants

Characteristic temperature	$T_{ch} = 355.4 \times 10^3 / 2200 = 161.55$	°K
Saturated vapor pressure at T_i	$P_{sat}(T_i) = 50250.4$	N/m²
Initial evaporation rate	$\dot{E}_i'' = h_p \, p_{sat}(T_i) = 1.056 \times 10^{-2}$	kg/m²
Characteristic area	$A_i = [V_i]^{2/3} = 125.15$	m²
Characteristic time	$t_{ch} = 1.27 \times 10^3 \times 715 / (1.056 \times 10^{-2} \times 125.15) = 7.33 \times 10^5$	s

Also

$$\Delta = 2 \times \frac{0.6 \times 161.55}{1.056 \times 10^{-2} \times 355.4 \times 10^3 \sqrt{\pi \times 1.43 \times 10^{-7} \times 7.33 \times 10^5}}$$

$$= 0.09$$

and

$$\beta = 3494.736 / 161.55 = 21.6325$$

The result obtained by using these values is indicated in Table 10.1.

10.8 DISCUSSIONS

The model given utilizes the basic ideas of spread and evaporation caused by a vapor pressure difference between the liquid surface and the atmosphere. The heat necessary to supply the latent heat of vaporization comes from the sensible heat of the liquid (which therefore cools) and also from the water on which the liquid is spreading. The analysis has not addressed itself to the relationship between the spread rate and evaporation. It is conceivable that very high evaporation rates may affect the spreading. However, as has already been demonstrated in Chapter 9, even in the case of rapid boiloff of cryogenic

liquids on water, the spreading rate is barely affected compared to a non-volatile liquid spreading. It is based on this knowledge that, in this model, the spread and evaporation mechanisms have been decoupled.

The weakness, if any, of the model lies in the assumption of uniform liquid temperature at every instant of time. This assumption may not be correct during the initial periods, because of the large film thickness, but toward the end when the film thickness is quite small, this assumption becomes better.

Analytical solutions of Eqs. (10.7b) through (10.9b) are impossible not only because of the coupling between the equations, but also their highly non-linear character (which is primarily from the vapor pressure term). Also the area of evaporation is changing continuously with time. A linearized version of the equations (with vapor pressure relation linearized) was tried but given up again because of mathematical difficulties.

The example worked out illustrates the utility of the model. The total evaporation time and the extent of spread during this time are easily obtained. The temperature of the liquid indicates the extent to which the liquid cools. As can be seen from the example, 1000 tons of diethyl ether evaporates in a rather short time of about 20 minutes. However, even though this number is small, it is about an order of magnitude greater than the time for evaporation of a cryogenic liquid spilled on water. It is also to be noted that the minimum temperature reached by the liquid is still well above its freezing temperature.

It is possible that the liquid temperature may fall below the water-freezing temperature (see Table 10.1). In this situation, ice may form beneath the spreading liquid surface. When this occurs (and if we assume ice formation as a continuous sheet formed over the whole area at the same time, we can use the conductivity of ice K_{ice} instead of K_w in Eq. (10.5)). In addition we now have to include the extra heat liberated due to the freezing of water. This increased heat transfer to the liquid will ensure that it will evaporate faster without further cooling.

10.9 CONCLUSIONS

A model has been developed to predict the rate of evaporation and the extent of spread of a high vapor pressure liquid spilled on water. Models derived for the spread of non-volatile liquids have been utilized. This model is based primarily on the heat transfer from water and the change of sensible heat of liquid (which cools) to supply the heat of evaporation. Solution to the governing equations are obtained by numerical methods.

10.10 REFERENCES

1) I.B.M. Applications Program, System 360, Scientific Subroutine Package (360A-CM-03X) Version III; Programmer's Manual; p. 343.

2) Eckert, E.R.G., and Drake, R.M., "Heat and Mass Transfer"; 2nd Edition, McGraw-Hill, N. Y., 1959.

3) Weast, Ed., "Hand Book of Chemistry and Physics"; 51st Edition; The Chemical Rubber Co., 1971.

10.11 LIST OF SYMBOLS

Symbol	Description	Equation	Unit
a	constant in the Clausius-Clayperon equation for the saturated vapor pressure	Eq. (10.7a)	N/m^2
b	constant in the Clausius-Clayperon equation for the saturated vapor pressure		°K
A (t)	pool area at any time		m^2
c	constant defined in Eq. (10.5)		
C_{liq}	specific heat of liquid		J/kg °K
D	diffusion coefficient of vapor in air		m^2/s
$\dot{E}$	total evaporation rate from pool		kg/s
$\dot{E}''$	specific evaporation rate		$kg/m^2 s$
$\dot{E}''_i$	initial specific evaporation rate		$kg/m^2 s$
h_p	mass-transfer coefficient		s/m
I	enthalpy (subscripted)		J/kg
L	characteristic length		m
m	dimensionless mass of liquid		kg

Symbols	Description	Equation	Unit
M (t)	mass of liquid remaining at any time		kg
$p_{sat}(t)$	saturated vapor pressure at temp. T		N/m^2
$\dot{q}''(t)$	heat flux at time t		$J/m^2 s$
Q	rate of total heat into liquid		J/s
R	gas constant of the vapor		J/kg °K
Re_L	Reynolds number	$U_{wind} L/\nu_{air}$	
Sc	Schmidt number	ν_{air}/D	
t	time		s
T	temperature (subscripted)		°K
U_{wind}	wind velocity		m/s
V(t)	volume of the liquid at any time t		m^3
Greek Letters			
α	thermal diffusivity		m^2/s
β	constant defined in Eq. (10.11)		
Γ	dimensionless area of pool		
Δ	characteristic heat flux		
η	dimensionless evaporation rate		
θ	dimensionless temperature (subscripted)		
λ	latent heat of vaporization of liquid		J/kg
μ	viscosity (subscripted)		$N\ s/m^2$
ν	kinematic viscosity (subscripted)		m^2/s

Symbols	Description	Equation	Unit
σ	interfacial tension between liquid and water		N/m
τ	dimensionless time		

Subscripts

b	boiling
liq	liquid
w	water

TABLE 10.1

EVAPORATION RATE AND TEMPERATURE OF A SPREADING POOL OF DIETHYL ETHER

Time (secs)	Temperature (°C)	Fraction of Initial Mass Remaining	Actual Mass Remaining (kg)	Specific Evaporation kg/s m^2	Pool Area m2
0.00	19.99	1.0000	0.90804E 06	0.89695E-02	0.00000E 00
59.99	19.31	0.9956	0.90412E 06	0.89689E-02	0.14589E 05
119.99	17.39	0.9827	0.89234E 06	0.89673E-02	0.29179E 05
179.99	14.43	0.9610	0.87272E 06	0.89649E-02	0.43768E 05
239.99	10.68	0.9308	0.84526E 06	0.89617E-02	0.58358E 05
299.99	6.36	0.8919	0.80996E 06	0.89579E-02	0.72947E 05
359.99	1.69	0.8445	0.76685E 06	0.89537E-02	0.87537E 05
419.99	-3.04	0.7898	0.71722E 06	0.89492E-02	0.94772E 05
479.99	-7.42	0.7328	0.66546E 06	0.89450E-02	0.97989E 05
539.99	-11.47	0.6740	0.61209E 06	0.89409E-02	0.10091E 06
599.99	-15.26	0.6136	0.55723E 06	0.89370E-02	0.10361E 06
659.99	-18.83	0.5517	0.50109E 06	0.89333E-02	0.10631E 06
719.99	-22.21	0.4884	0.44351E 06	0.89296E-02	0.10844E 06
779.99	-25.43	0.4237	0.38483E 06	0.89260E-02	0.11063E 06
839.99	-28.52	0.3579	0.32503E 06	0.89225E-02	0.11278E 06
899.99	-31.49	0.2909	0.26417E 06	0.89190E-02	0.11466E 06
959.99	-34.36	0.2228	0.20232E 06	0.89155E-02	0.11652E 06
1019.99	-37.15	0.1536	0.13952E 06	0.89121E-02	0.11837E 06
1079.99	-39.88	0.0834	0.75810E 05	0.89087E-02	0.12001E 06
1139.99	-42.55	0.0123	0.11234E 05	0.89052E-02	0.12164E 06

Time for Complete Evaporation = 1206.8 Seconds

11.0 MIXING AND DILUTION OF A HIGH-VAPOR-PRESSURE, HIGHLY WATER-SOLUBLE CHEMICAL

11.1 AIM

The objective of the model is to predict the vapor liberation rate as well as the area and the duration over which the vapor is liberated, when a highly water-soluble, high-vapor-pressure liquid is spilled on a water surface.

11.2 INTRODUCTION

When a chemical having extreme affinity for water is spilled on water, it rapidly dissolves. However, there are chemicals which are not only readily miscible with water, but also have high vapor pressures at ambient temperature. When such liquids are spilled, some vapor may be generated as well. The vapors of a large number of chemicals are toxic and therefore even in small dosages they may be harmful. Therefore, it becomes necessary to estimate the quantity of vapor released, when such a toxic chemical dissolves in water. The model presented below is derived with a view to obtaining such information.

The model basically is the mixing and dilution model in a uniform river (see Chapter 4). First, we assume that the entire liquid spilled goes into solution in water and, on this basis, estimate the liquid concentration in the water. With this information, the vapor pressure (on the water surface) of the toxic liquid can be estimated and the vaporization rate estimated. The model derived illustrates the method of vaporization prediction for only one situation of the several possible situations of mixing (see Chapter 4). The principle shown here can be readily used for other water regions.

11.3 PRINCIPLES AND ASSUMPTIONS

- Evaporation of the chemical takes place only at the water atmosphere interface and is a consequence of the difference in the concentration of the vapor (of the chemical) over the water surface and in the atmosphere.

- The chemical spilled reaches the temperature of the water instantly.

- The partial vapor pressure over water can be represented by $p = c_m p^{sat}_{vap}(T)$ where c_m is the molar fractional concentration in water.[1]

- To estimate the water dispersion (and hence surface concentration), we assume that the entire mass of the liquid spill goes into solution with water. It is, in effect, an *"a priori"* assumption for a very small mass of vapor liberation.

- Instantaneous spill at a point is assumed for calculating the water dispersion.

11.4 DATA REQUIRED

The following data are required to calculate the vapor liberation rate in a non-tidal river

- Mass of liquid spilled,
- Saturated vapor pressure at water temperature,
- Vapor pressure vs concentration of liquid data if the third assumption (above) is not valid,
- Characteristics of the river such as, the depth, width, mean stream velocity, roughness factor, and the like,
- Mass-transfer coefficient for surface evaporation. (This is either given or estimated from forced convection boundary layer theory – as has been enunciated in Chapter 10, Section 5.)

11.5 DETAILS OF THE MODEL

The following equation based on the water dispersion model (see Chapter 4), Eq. (4.1)) can be written, neglecting the contribution from image sources:

$$c(x,y,z,t) = \frac{2\,M_{liq}}{(4\pi t)^{3/2}\sqrt{e_x e_y e_z}} \exp -\left\{\frac{(x-ut)^2}{4e_x t} + \frac{y^2}{4e_y t} + \frac{z^2}{4e_z t}\right\} \tag{11.1}$$

where the x, y, z coordinate system is as shown in Figure 11.1.

Equation (11.1) can be utilized to obtain the concentration of the liquid on the water surface at any position at any time. It is to be noted that since the equation above is a solution to the diffusion equation (parabolic type), it gives finite concentrations at large distances from the point of spill in very short times. However, these can be neglected as their values will be exponentially small.

The molar fractional concentration in water is given by

$$c_m(x,y,z,t) = \frac{1}{\left[1 + \frac{\rho_w}{c}\frac{\mu_{liq}}{\mu_w}\right]} \tag{11.2}$$

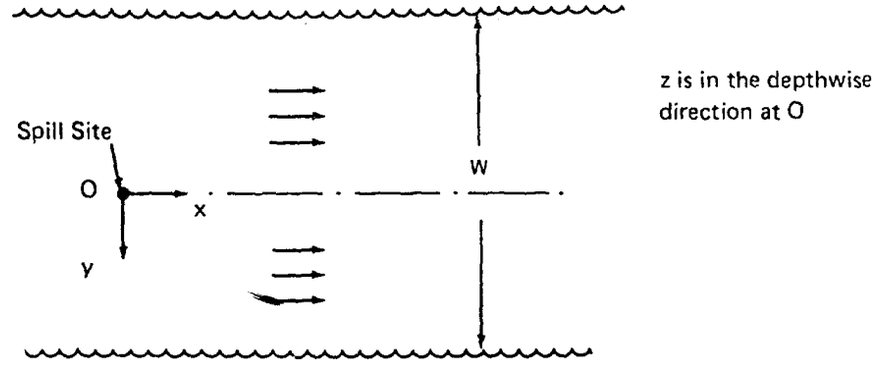

FIGURE 11.1 ILLUSTRATION OF THE WATER REGION WHERE THE SPILL OCCURS AND THE COORDINATE SYSTEM USED

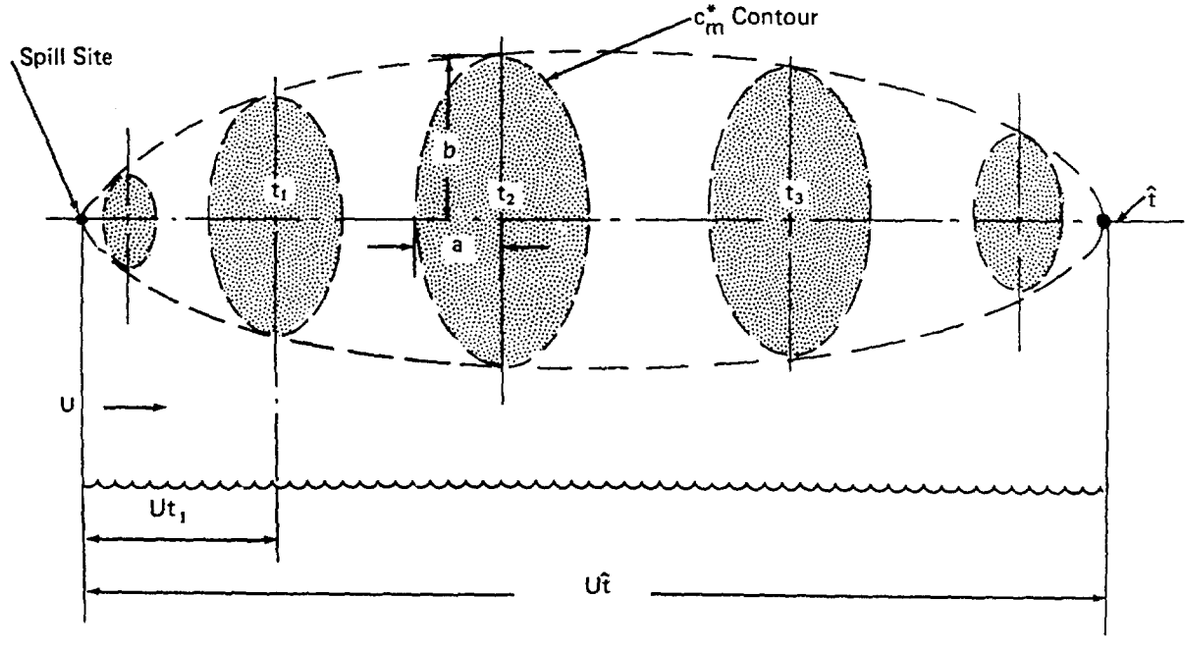

FIGURE 11.2 SCHEMATIC ILLUSTRATION OF THE EVAPORATION AREA

We now stipulate that the evaporation from water surface regions, having a molar concentration less than c_m^*, is negligibly small (the value of c_m^* is quite arbitrary and may have to be chosen properly for different chemicals; however a value between 0.1 and 0.05 may be reasonable). By choosing a value for c_m^* we are actually limiting the area from which evaporation can occur. It is estimated that the effect of evaporation from areas where the vapor pressure is less than 5% of the saturated vapor pressure is quite small.

Figure 11.2 indicates a time sequence picture of the evaporation area (on the water surface), at whose boundaries the concentration is c_m^*. The "slick" moves downstream with the stream velocity. The regions where the concentrations are greater than c_m^* are within the ellipses (the contours are circular if the x and y direction turbulent diffusion coefficients e_x and e_y are equal). The equation to these ellipses is obtained from Eq. (11.1). The semi-axis lengths for these elliptical areas are given by

$$a(t) = \sqrt{4 e_x t \ \ln\left\{\frac{2 M_{liq}}{C^* (4\pi t)^{3/2} \sqrt{e_x e_y e_z}}\right\}} \qquad (11.3a)$$

$$b(t) = \sqrt{4 e_y t \ \ln\left\{\frac{2 M_{liq}}{C^* (4\pi t)^{3/2} \sqrt{e_x e_y e_z}}\right\}} \qquad (11.3b)$$

where C* is the limiting concentration in units of mass/volume.

At the center of the elliptical area the concentration is a maximum and is given by

$$c^{max}(t) = \frac{2 M_{liq}}{(4\pi t)^{3/2} \sqrt{e_x e_y e_z}} \qquad (11.4)$$

If now,

$\hat{t}$ = time beyond which the concentration in water of the liquid spilled is below C* everywhere in the water, (11.5a)

then

$$\hat{t} = \frac{1}{4\pi}\left[\frac{2\,M_{liq}}{c^{*}\sqrt{e_x e_y e_z}}\right]^{\frac{2}{3}} \tag{11.5b}$$

Estimation of evaporation:

The rate of evaporation per unit area is given by

$$\dot{M}''_v = h_p \quad p \tag{11.6a}$$

where p is the partial pressure of the vapor of the liquid spilled, measured at the water surface.

Using the third assumption dealing with partial vapor pressure over water, we have,

$$\dot{M}''_v = c_m \; h_p \; P^{sat}_{vap}(T) \tag{11.6b}$$

Total evaporation rate at any instant:

$$\dot{M}_v(t) = h_p \; P^{sat}_{vap}(T) \int c_m \; dA \tag{11.7a}$$

over the elliptical area on on whose boundary the concentration is c^*_m

It can be shown that* (because of the Gaussian concentration distribution)

$$\int c_m \; dA = \pi \, a(t) \, b(t) \, c_m^{mean} \tag{11.8}$$

where

$$c_m^{mean} = \frac{(c_m^{max} - c_m)}{\ln\left\{\frac{c_m^{max}}{c_m^{*}}\right\}} \tag{11.9}$$

* See Appendix.

Combining Eqs. (11.7a) and (11.8) yields:

$$\dot{M}_v(t) = \pi\, h_p\, p_{vap}^{sat}(T)\, a(t)\, b(t)\, c_m^{mean} \tag{11.7b}$$

Defining the following characteristic values:

$$\left.\begin{aligned} \dot{M}_{ch} &= 4\pi\, \hat{t}\, \sqrt{e_x e_y}\; h_p\; p_{vap}^{sat}(T_i) \\ M_{ch} &= \dot{M}_{ch}\, \hat{t} \\ \tau &= \frac{t}{\hat{t}} \\ m &= \frac{M_v}{M_{ch}} = \frac{\text{Total mass of vapor liberated}}{\text{Characteristic mass of vapor}} \end{aligned}\right\} \tag{11.10a}$$

and noting that

$$\dot{m} = dm/d\tau = \dot{M}_v/\dot{M}_{ch} \quad , \tag{11.10b}$$

we write Eq. (11.7b), using Eqs. (11.3a), (11.3b), and (11.5b):

$$\dot{m}(\tau) = -\frac{3}{2}\, \tau\, \ln(\tau)\; c_m^{mean}(\tau) \tag{11.7c}$$

Therefore the total mass of vapor liberated up to time $\hat{t}$ is given by

$$m = \int_0^1 \dot{m}\, d\tau = -\frac{3}{2} \int_0^1 \tau\, \ln(\tau)\; c_m^{mean}(\tau)\, d$$

(11.11a)

where c_m^{mean} is defined in Eq. (11.9) (and use has to be made of Eqs. (11.2) and (11.4)).

In dimensional quantities we have:

$$M_v = m \quad M_{ch} \tag{11.11b}$$

The evaluation of the integral in Eq. (11.11a) has to be done numerically because of the complicated nature of the integrand (primarily due to the logarithmic and the c_m^{mean} terms). However certain observation can be made from the equation. It should be noted that $c_m^{mean} \geqslant c_m^*$ and, therefore, replacing the value of c_m^{mean} by c_m^* yields a minimum value for m, viz:

$$m_{min} = 3/8\ c_m^* \tag{11.12a}$$

Similarly the maximum value for m can be shown to be*

$$m_{max} = -\frac{3}{2} \int_0^1 \frac{\tau \ln(\tau)}{1 + \Gamma \tau^{3/2}} d\tau \tag{11.12b}$$

where

$$\Gamma = \frac{\rho_w \mu_{liq}}{c^* \mu_w} \tag{11.13}$$

Once the integral (11.11a) is evaluated, the total mass of vapor released is calculated from Eq. (11.11b).

*By replacing c_m^{mean} by c_m^{max} corresponding to the maximum molar concentration. However, if we replace c_m^{mean} by 1 which would be absolute maximum value for concentration, then *the* maximum evaporation m = 3/8.

11.6 COMPUTATIONAL ALGORITHM

The calculation procedure is simple. The required quantities are calculated from the appropriate equations. A computer program has been written to perform these calculations and the algorithm it follows is shown in the form of a flow chart in Figure 11.3. The calculation of the diffusion coefficient of vapor is effected by utilizing the formula derived from kinetic theory and given in Reference 2. The sequence of calculations is best illustrated by the example below.

11.7 SPECIFIC EXAMPLE

Properties of the Chemical Spilled:

Chemical spilled		= diethyl amine $[(CH_3CH_2)_2\ NH]$	
Molecular weight	μ_{liq}	= 73.14	kg/kmole
Boiling temperature at atmospheric pressure	T_b	= 56.3	°C
Vapor pressure equation (p in N/m^2 and T in °K)	$p_{vap}^{sat}(T)$	$= 10^{\left\{9.826621 - \frac{1596.68875}{T}\right\}}$	
Quantity spilled	M_{liq}	$= 10^6$	kg

Environmental Conditions

Width of river	w	= 31 m	
Depth of river	d	= 10 m	
Mean velocity of the river	U	= 1.5 m/s	
Manning roughness factor	n	= 0.03	
Density of water	ρ_w	= 10^3 kg/m^3	
Assumed mass-transfer coefficient	h_p	= 1.8×10^{-7} s/m	
Assumed limiting concentration	c_m^*	= 5%	
Water temperature	T_w	= 20°C.	

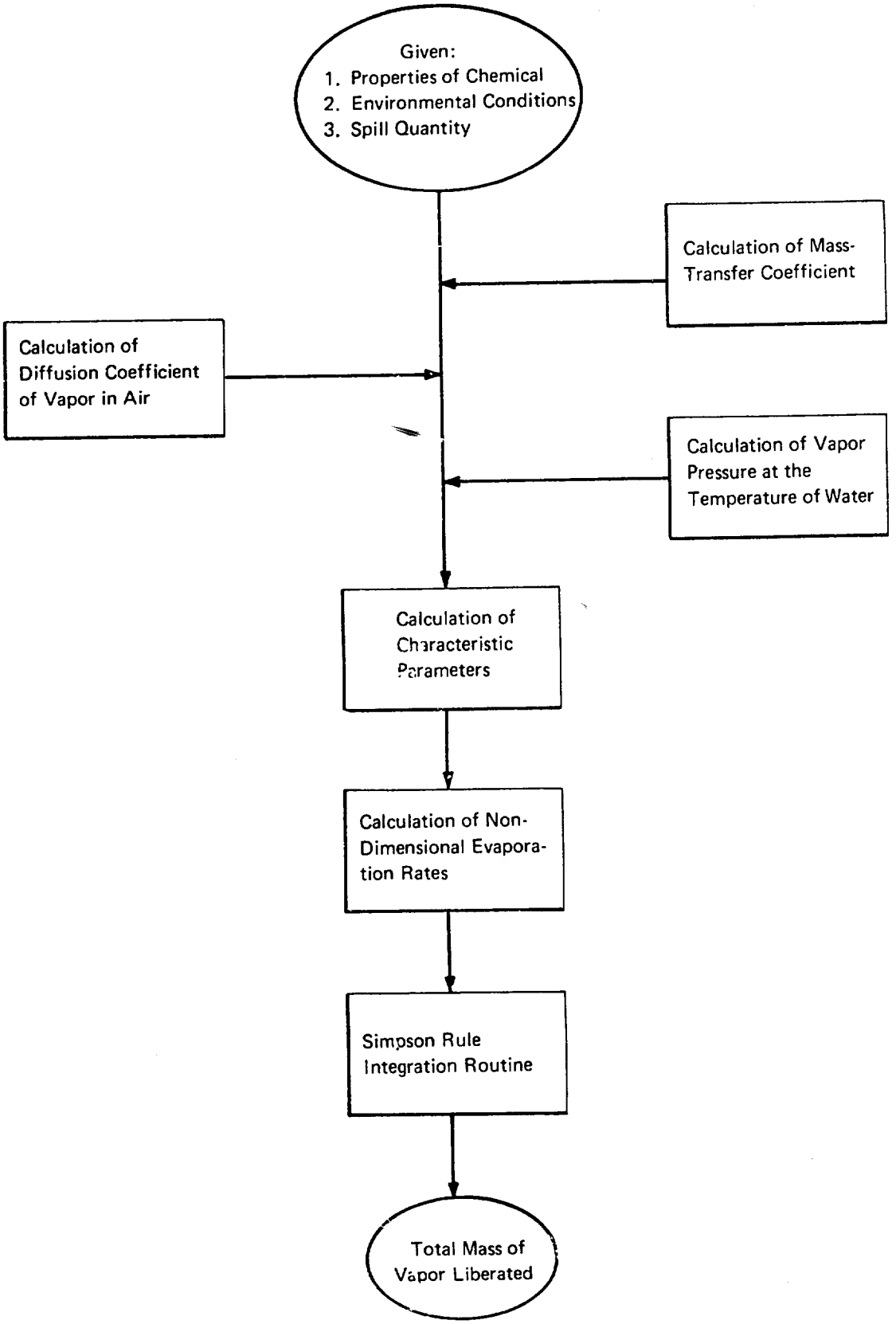

FIGURE 11.3 FLOW CHART FOR THE COMPUTATIONAL ALGORITHM

Calculation of Turbulent Diffusion Coefficients

Hydraulic radius for the river = R_h = $10 \times 30/[30 + 2 \times 10] = 6.0$ m

Shear velocity (refer to Section 3.11) = u^* = $3.115 \times 0.03 \times 1.5/6^{1/6} = 0.104$ m/s

Width-to-depth ratio = w/d = $3 \ll 100$

Hence the river is classified as a narrow river. Therefore:

Vertical diffusion coefficient (see Eq. 3, Chapter 3) $e_z = 0.067 \times .104 \times 6 = .0418$ m^2/s

Longitudinal diffusion coefficient (see Eq. 3, Chapter 3) $e_x = 0.0418 \times 0.1 = 0.0042$ m^2/s

Cross-stream diffusion coefficient (see Eq. 3, Chapter 3) $e_y = 0.23 \times 0.104 \times 6 = 0.1435$ m^2/s

Limiting concentration (in density units) using Eq. (11.2) $C^* = 213.86$ kg/m^3

Characteristic time (Eq. (11.5b)) $\hat{t} = \frac{1}{4\pi}\left[\frac{2 \times 10^6}{213.8\sqrt{.0418 \times .0042 \times .1435}}\right]^{2/3} = 1205$

Saturated vapor pressure at 20°C $p_{vap}^{sat} = 23832.6$ N/m^2

Hence:

Characteristic evaporation rate (Eq. (11.10))

$M_{ch} = 4\pi \times 1205 \times (0.1435 \times .0042)^{1/2} \times 1.8061 \times 10^{-7} \times 23832.4 = 1.591$ kg/s

Characteristic mass of vapor evaporated

$$M_{ch} = 1.591 \times 1205 = 1917.1 \text{ kg}$$

Maximum surface concentration at any time (Eq. (11.4))

$$c^{max} = \frac{8.996 \times 10^6}{t^{3/2}} \quad kg/m^3$$

The maximum possible evaporation* = 3/8 M_{ch} = 0.375 x 1917 = 719 kg.

% of spilled mass vaporized = $(719/10^6)$ x 100 = 0.072%

Maximum distance within which this evaporation occurs = S = Ut = 1.5 x 1205 = 1.807 km.

11.8 DISCUSSIONS

The model given is based essentially on two phenomena, viz., the mixing and dilution in water of a major portion of the spilled liquid and a small amount of evaporation caused by the difference of vapor concentration at the water surface and the atmosphere. In the derivation of equations used to predict the liquid concentration in water, it was assumed that all of the liquid would go into solution. The results obtained in the example prove – *"a posteriori"* – the accuracy of this assumption. The total vapor generated is such a small percentage of the mass spilled. This is because even though the evaporation is high (driven by a high partial pressure difference), the duration for which vaporization can occur is primarily determined by the rapidity of mixing of the liquid in water. That is, the more turbulent a stream is, the better the mixing, and the quicker the time in which the concentration everywhere in water is less than the critical. However, it should be noted that any possibility of vapor flash during the process of spilling is not considered in this model.

The assumption of partial pressure of vapor bearing a linear relationship with saturated vapor pressure (the constant of proportionality being the molar concentration) is quite close to the actual relationship for most chemicals. As in earlier chapters, the major assumption of instantaneous spill may not always be a correct representation of a spill. The model given can be suitably modified for continuous or intermittent spills. However, since even in the case of an instantaneous spill, the mass of vapor liberated is such a small fraction of the mass spilled, it is safe to guess that in the case of a long duration of spill of the same amount of mass, the total vapor mass liberated would still be a small fraction.

11.9 CONCLUSIONS

A method has been developed to predict both the rate of vapor release (and the total mass) and the area over which this release takes place, when a water-soluble, high vapor pressure liquid is spilled on water. The calculations for a typical case indicate that the mass of vapor liberated would be a very small fraction of the total mass of spill.

---

*By replacing c_m^{mean} by c_m^{max} corresponding to the maximum molar concentration. However, if we replace c_m^{mear} by 1 which would be absolute maximum value for concentration, then *the* maximum evaporation m = 3/8.

11.10 REFERENCES

1) Reid, R., "Partial Pressure of Compounds Dissolved in Water"; Arthur D. Little, Inc., Internal Memo, 1972.

2) Rohsenow, W. M., and Choi, H. Y., "Heat, Mass and Momentum Transfer"; Prentice-Hall, Inc., N. J., May 1963, p. 382.

11.11 LIST OF SYMBOLS

Symbol	Description	Value or definition	Units
a (t) b (t)	Semi-axis of the elliptic region on the water surface, within which the concentration of the chemical is greater than the limiting concentration	Eqs. (11.3a) and (11.3b)	m
A	area		m^2
c_m	concentration in molar fraction of the mixture of water and chemical		
c_m^*	limiting molar concentration		
C (t)	concentration of chemical in density units		kg/m^3 of mixture volume
$C^{max}(t)$	maximum concentration at any time		kg/m^3
d	river depth		m
e_x, e_y, e_z	turbulent diffusion coefficients in the downstream, cross-stream, and depth directions, respectively		m^2/s
h_p	mass-transfer coefficient		s/m
m	total mass of vapor liberated in dimensionless units		
$\dot{m}(\tau)$	dimensionless rate of vapor liberated dm/dt		
M_{liq}	mass of liquid spilled		kg
M_v	mass of vapor liberated		kg
M_{ch}	characteristic mass of vapor	Eq. 11.10	kg
p	partial vapor pressure of liquid at the surface of water		N/m^2

Symbol	Description	Value or definition	Units
$p_{vap}^{sat}(T)$	saturated vapor pressure at temperature T		N/m^2
S	distance downstream beyond which the concentration everywhere in water, is less than the limiting concentration		m
t	time		s
$\hat{t}$	time beyond which the concentration of chemical in the stream is everywhere is less than the limiting concentration		s
T	temperature (subscripted)		°K
U	mean stream velocity		m/s
w	width of river		m
x,y,z	coordinates in the downstream, cross-stream and depthwise directions		
Greek Letters			
Γ	A quantity defined in Eq. (11.13)		
μ	Molecular weight (subscripted)		kg/k mole
ρ	Density of liquids (subscripted)		kg/m^3
τ	Dimensionless time		
Superscripts			
"	= quantity per unit area		
•	= differentiation with respect to time (dimensional or non dimensional)		
sat	= saturated		
Subscripts			
b	= boiling		
ch	= characteristic		
liq	= liquid		
p	= based on pressure		
vap	= vapor		
w	= water		

11.12 APPENDIX

To evaluate:

$$\int c_m \, dA \tag{A-1}$$

over an elliptic area having semi-axis of length a and b. On the boundary of this ellipse the concentration is c_m^*.

Equal concentration contours within this area are all ellipses confocal with the given outer ellipse (see Figure A.1). Considering one such elemental elliptical area (on whose boundary the concentration is c_m) of semi-axis ra and rb, where $0 < r < 1$, we can represent:

$$c_m = c_m^{max} \; e^{-r^2 \ln\left(\frac{c_m^{max}}{c_m^*}\right)} \tag{A-2}$$

Now the area of the elemental ellipse is

$$dA = \pi \, a \, b \; 2r \, dr. \tag{A-3}$$

Therefore:

$$\int c_m \; dA = 2 \pi a b \int_0^1 c_m^{max} \, e^{-r^2 \ln\left(\frac{c_m^{max}}{c_m^*}\right)} \, r \, dr$$
$$= \pi a b \frac{(c_m^{max} - c_m^*)}{\ln\left(c_m^{max}/c_m^*\right)} \tag{A-4}$$

We can therefore define the mean concentration as:

$$c_m^{mean} = \frac{(c_m^{max} - c_m)}{\ln\left(\frac{c_m^{max}}{c_m^*}\right)} \tag{A-5}$$

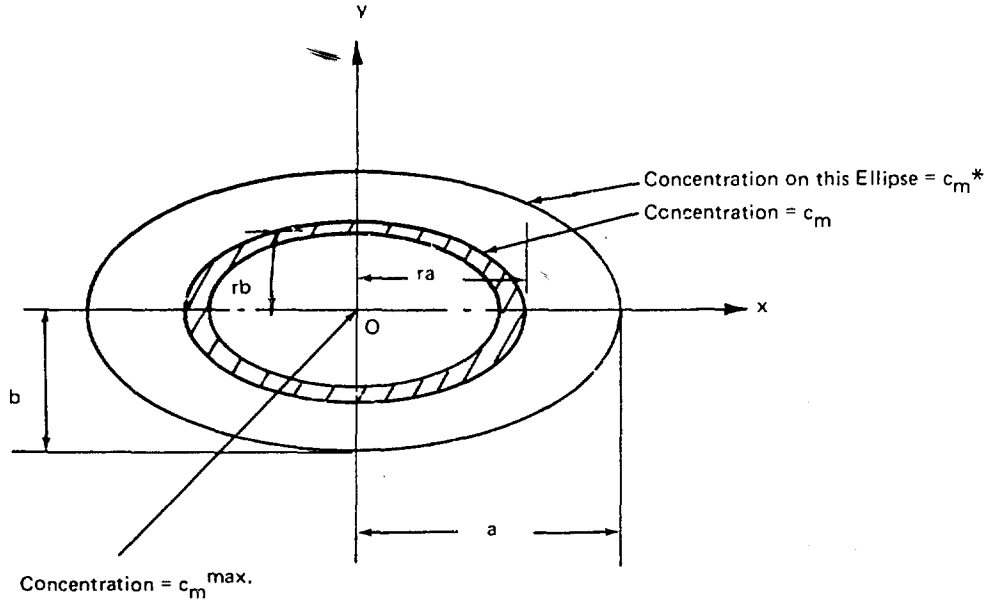

FIGURE 11-A-1: SCHEMATIC ILLUSTRATION OF CONCENTRATION DISTRIBUTION ON THE WATER SURFACE DUE TO THE SPILL OF A WATER SOLUBLE CHEMICAL ON WATER

12.0 BOILING RATE MODEL FOR HEAVY LIQUIDS WITH BOILING TEMPERATURES LESS THAN AMBIENT

12.1 AIM

The aim of the model presented below is to obtain the rate of evaporation and the total time for which a liquid will evaporate when it is spilled on water and sinks. The boiling point of the liquid is less than that of water.

12.2 INTRODUCTION

There are many liquids (chemicals) with densities greater than that of water whose boiling points at atmospheric pressure are less than the ambient temperature. When such liquids are spilled on water, they sink and vaporize at the same time because of their low boiling points. (It is assumed that the liquid is immiscible with water.) If the vapor of the chemical is toxic, its evaporation rate must be known, so that it can be fed into a vapor dispersion model to assess its hazard. The model presented here is derived with a view to obtaining such a quantity.

When a large mass ("blob") of a heavy liquid is spilled on the surface of water in a very short time, the liquid sinks *"en masse"* only for a short depth. The increasing sinking velocity of the blob results in a pressure force on the front face. When this pressure force exceeds the internal resistance of the blob the blob is broken into small sized drops. (This sequence of blob break-up and drop formation is schematically illustrated in Figure 12.1a through 12.1c.) The parameter which determines the stability of a blob (or a drop) or resistance to breaking is the Weber number, i.e., the ratio of the pressure force $\rho_m U^2$ to the surface tension force σ/R, where R is the characteristic radius of the blob. Experimental evidence indicates that most liquids tend to break up when the Weber number is above 8 to 10 [Kalelkar,[1] Levich,[2] Orr[3]]. Figure 12.2 shows the stability curve for a drop breakup. It can be shown easily that the duration over which a large mass (such as occurs in a spill) breaks up into smaller drops is indeed very short. Therefore, in the model presented it is assumed that the spill breaks up into small liquid drops instantaneously.

The cluster of drops so formed sinks at increasing velocities, accelerated by gravity. The motion of drop clusters has not been studied extensively. However, the motion of a single deformable drop has been treated quite extensively by Levich,[2] Kalelkar and Kung,[1] and Orr.[3] When a single drop sinks, it is accelerated by gravity, but is resisted by the drag due to motion in the medium (water). The drop reaches a terminal velocity (which is a function of drop size and medium properties) when the drag force and the effective weight force are equal. Expressions have been derived by Levich[2] and, in more detail, by Kalelkar and Kung[1] for the dependence of terminal velocity of a single drop on the surface tension, densities of the liquid and the medium, and the viscosity of the medium. The result from Reference 1 is plotted in Figure 12.3. These expressions are given in a later section.

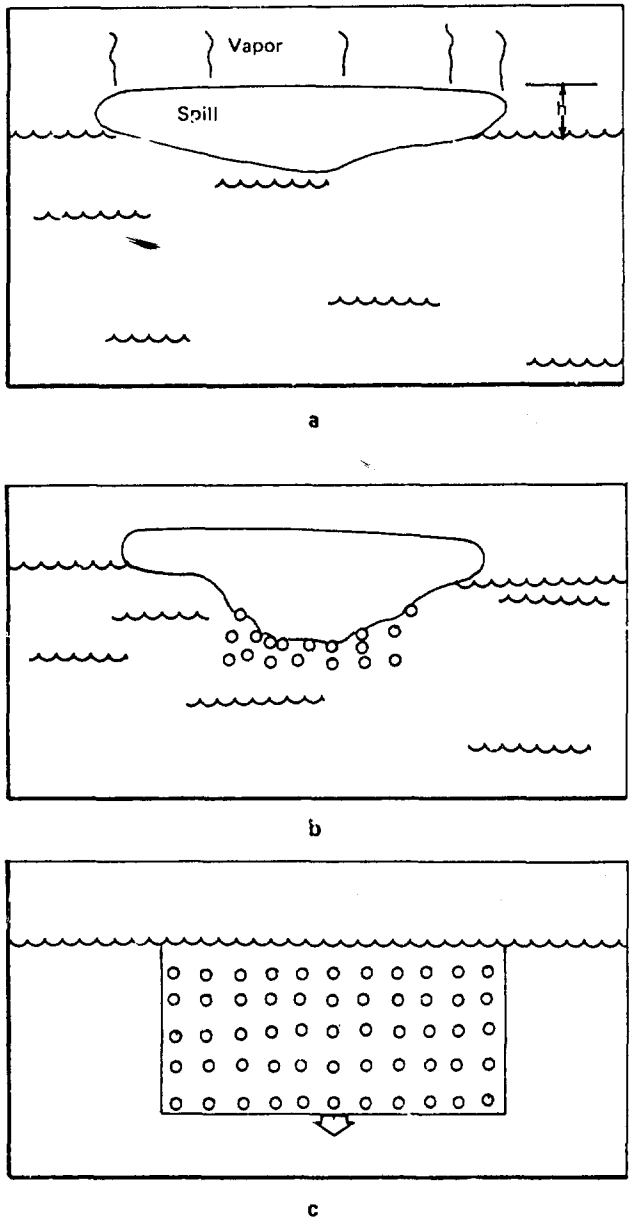

FIGURE 12.1: SCHEMATIC ILLUSTRATION OF THE SEQUENCE OF BLOB BREAKUP INTO DROPS

$5 < \delta < 500$ cm
$0.1 < \Delta p < 1$ gr/cm^3
$5 < ru^2 < 5000$

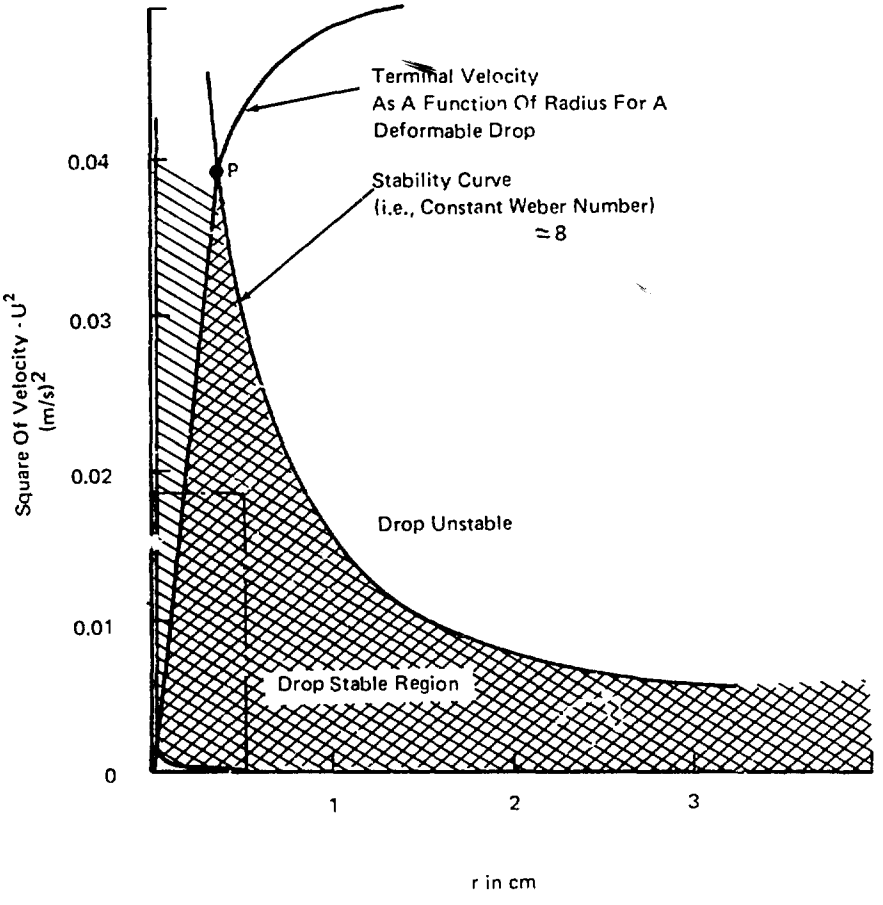

FIGURE I2.2: DROP STABILITY AND DROP TERMINAL VELOCITY AS FUNCTIONS OF DROP RADIUS

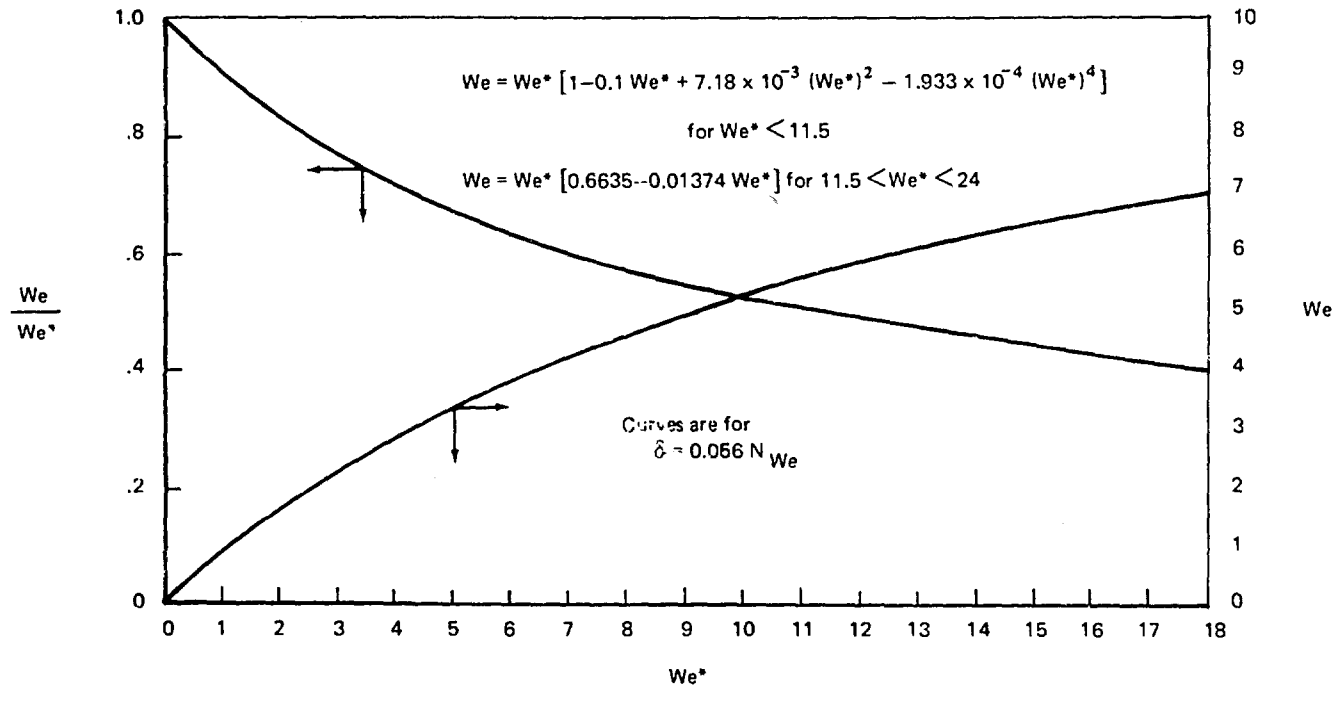

FIGURE 12.3 RELATIONSHIP BETWEEN THE TERMINAL VELOCITIES OF A DEFORMABLE DROP AND A NON-DEFORMABLE DROP, FALLING WITHIN A MEDIUM

Experiments indicate that, when a big blob breaks up, drops of various sizes are formed with the drop size distribution being a function of various physical parameters such as the properties of the liquid and the medium, the agency which causes the breakup, and others. However, in our analysis we assume that all the drops formed are of uniform size. Also this drop size is determined by satisfying both the stability criterion and the terminal velocity criterion simultaneously (point p in Figure 12.2). The details are given in Section 12.5.

To compute the rate of evaporation of the drop, we use the ideas of heat mass transfer (to a sphere in a forced flow) propounded by Spalding.[4] Essentially this analysis uses the Reynolds' analogy between heat and mass transfer and experimental correlations for the heat transfer coefficient.

Section 12.5 presents details of the derivations and their use in calculating the evaporation rate of drops and their total lifetime. A specific example is also worked out.

12.3 PRINCIPLES AND ASSUMPTIONS

The basic principle on which the derivation is based concerns the breakup of a large blob of heavy liquid into smaller drops and their subsequent evaporation due to heat transfer from the surrounding medium (in this case water). The assumptions made in deriving the model are given below:

- The blob of liquid spilled breaks up into small drops instantaneously, and these drops attain their terminal velocities in a very short time with very little evaporation.
- All the drops formed are of the same size.
- The drop cluster formed has high porosity; that is, the interdrop distances are large enough so that, as a first approximation, the effect of other drops on the motion of any single drop in the cluster can be neglected. In short, we assume that the motion of each drop is independent from all others.
- The critical Weber number is 8; that is, any drop moving at a velocity greater than that for which the Weber number is 8 breaks up.
- Forced convection heat and mass transfer results are assumed to apply.

12.4 DATA REQUIRED

The following input information is necessary for obtaining the results from this model:

- Density of the liquid,

- Surface tension of the liquid,
- Boiling temperature at atmospheric pressure,
- Latent heat of vaporization,
- Properties of water, such as its density, specific heat, viscosity, and Prandtl number, and
- Water temperature.

12.5 MODEL DETAILS

The drag force on a single, spherical, non-deformable body is given by

$$F_{DRAG} = C_D \pi R^2 \times \frac{1}{2} \rho_m U^2. \tag{12.1}$$

The accelerating force (by the weight) on a spherical liquid drop sinking in another fluid medium is:

$$F_{WEIGHT} = (\rho - \rho_m) \frac{4}{3} \pi R^3 g. \tag{12.2}$$

Therefore, for a *non-deformable spherical drop* the terminal velocity is obtained by equating the drag force to the accelerating force; that is, from Eqs. (12.1) and (12.2) we get for Re_D in the range $400 < Re_D < 5000$:

$$V = \left[\frac{8}{3} \frac{g}{C_D} \left(\frac{\rho}{\rho_m} - 1 \right) R \right]^{\frac{1}{2}} \tag{12.3}$$

with $C_D = 0.4$.

However, liquid drops falling in another medium do deform. Levich[2] gives the following result for the terminal velocity for a deformable drop:

$$U = \left[\frac{4g}{C_D} \left(\frac{\rho}{\rho_m} - 1 \right) \frac{\sigma}{\rho_m} \right]^{\frac{1}{4}} \tag{12.4}$$

It is noted that the terminal velocity given by Eq. (12.4) is independent of the size of the drop for a constant value of C_D. In reality, however, this is not so. Kalelkar and Kung[1] have derived the following result for the terminal velocity of a deformable spherical drop, based on the drag on a bean-shaped drop:

$$U = V \left[(1 - \delta) \frac{1 + A(1-\delta)^{\frac{3}{2}}}{1 + A} \right]^{\frac{1}{2}} \tag{12.5a}$$

and

$$\delta = 0.056 \, We \tag{12.6a}$$

$$We = \rho_m \, U^2 R/\sigma \tag{12.6b}$$

where

$$\delta = \frac{\text{Reduction in the radius of drop due to pressure forces}}{\text{Radius of drop}} \tag{12.7}$$

A = a constant = 1.778, and

U = terminal velocity of a drop of radius R given by Eq. (12.3).

It can be shown that Eq. (12.5a) (using Eq. (12.6a) and (12.6b)) reduces to:

$$We = We^* \left[1 - 0.1 \, We^* + 7.2 \times 10^{-3} \, (We^*)^2 - 1.93 \times 10^{-4} \, (We^*)^3 \right] \tag{12.8a}$$

$$\text{for } We^* < 11.5$$

and

$$We = We^* \left[0.6635 - 0.01374 \, We^* \right] \tag{12.8b}$$

$$\text{for } 11.5 < We^* < 24$$

where

$$We^* = V^2 \rho_m \, R/\sigma.$$

Equation (12.8a) is plotted in Figure 12.3.

If we assume the critical Weber number for drop breakup as

$$We_c = 8 = U_c^2 \rho_m R/\sigma, \tag{12.9}$$

then by substituting Eq. (12.9) in Eq. (12.6b), Eq. (12.6a), and the resulting Eq. (12.5a), we get:

$$U_c = 0.586\ V_c;$$

i.e.,

$$U_c^2 \rho_m R_i/\sigma = 8 = 0.3434 \left[V_c^2 \rho_m R_i/\sigma \right]$$

Now using Eq. (12.3) and simplifying, we get:

$$R_i = 1.87 \sqrt{\sigma/[g (\rho - \rho_m)]} \tag{12.10}$$

R_i represents the radius of the drops formed when the blob breaks up and their terminal velocity is given below.

Using Eqs. (12.9) and (12.10) the velocity (terminal) at break up is:

$$U_i = 2.07 \left[\frac{g\sigma}{\rho_m} \left(\frac{\rho}{\rho_m} - 1 \right) \right]^{\frac{1}{4}} \tag{12.11}$$

This equation is compared with Eq. (12.4) which gives, for $C_D = 0.4$, a factor of 1.77 on the RHS instead of 2.07 as in Eq. (12.11).

12.5.1 Heat Transfer

Because of the lower boiling point of the liquid compared to ambient temperature, heat is transferred from water to the liquid. This heat evaporates the liquid and therefore the drop size shrinks. The reduced drop size results in a larger drag and hence the drop velocity changes. These coupled effects are included in the following model to predict the evaporation rate.

Kays and London[5] give the following correlation for heat transfer to a packed bed of spheres:

$$St = 0.23\left([1.5(1-p)]^{0.3}/p\right)Re_d^{-0.3}\,Pr^{-2/3} \qquad 20 < Re_d < 5 \times 10^4 \qquad (12.12a)$$

where Re_d is the Reynolds' number based on the diameter of the drop and the free-stream velocity and p is the porosity of the bed.

McAdams[6] correlation for heat transfer for flow of a liquid over an isolated single sphere is of the form

$$St = 1.2\ Re_d^{-0.6}\ Pr^{-2/3}. \qquad (12.12b)$$

The drops formed from the blob form a cluster and sink *en masse*. This situation is similar to the flow of water through a bed of spheres. However, there is no way of calculating the "porosity" of the "bed" so formed by these drops. To give a conservative estimate of the vapor liberation rate we use Eq. (12.12a) in preference to Eq. (12.12b). Since the lowest porosity gives the highest transfer coefficient, and since the minimum porosity that can be achieved by a bed of uniform spheres is $p = 1/3$, we have, from Eq. (12.12a),

$$St = 0.69\ Re_d^{-0.3}\ Pr^{-2/3}. \qquad (12.12c)$$

12.5.2 Mass Transfer

Following Spalding[6] we write for the rate of evaporation:

$$\dot{m}'' = St\ G\ \ell n\ (1 + B) \qquad (12.13)$$

where

$$B = \text{transfer factor} = C_m\,(T_m - T)/\lambda \qquad (12.14)$$

$G = \rho_m U$ = mass flux of the mass transfer medium, and

$\dot{m}''$ = mass loss rate from a unit area of the spherical surface.

Now: $$\dot{m}'' = -\rho \, dR/dt \qquad (12.15a)$$

Combining Eqs. (12.12c), (12.13), and (12.15), we have:

$$dR/dt = -0.69 \, (\rho_m/\rho) \, U \, Re_d^{-0.3} \, Pr^{-2/3} \, \ell n \, [1 + B] \qquad (12.15b)$$

where U is the terminal velocity of a drop of radius R and is given by the Eq. (12.8a). To obtain the evaporation rate, solution has to be obtained for coupled Eqs. (12.8a) and (12.15b).

Defining the following quantities:

r = R/R_i = dimensionless drop radius

$$t_{ch} = \frac{R_i}{0.69 \, \frac{\rho_m}{\rho} \, Re_i^{-0.3} \, Pr^{-\frac{2}{3}} \, \ell n(1 + B)} = \frac{R_i \rho}{\dot{m}_i''} \qquad (12.16)$$

= time to evaporate a drop when the rate of evaporation is constant and equal to the initial value.

τ = dimensionless time = t/t_{ch}

u = U/U_i = terminal velocity ratio,

we can show that Eq. (12.15b) reduces to

$$dr/dt = -u^{0.7}/r^{0.3} \qquad (12.17)$$

with conditions

$$\tau = 0: \; r = 1, \; u = 1$$

In Eq. (12.16), u is a function of r given by Eqs. (12.8a) and 12.3). The relation between u and r can be shown to be

$$u = r^{0.5}\, v_i \left[(1 - 0.1\, r^2\, v^2{}_i\, We_i + 7.2 \times 10^{-3}\, (r^2\, v^2{}_i\, We_i)^2 + - 1.09 \times 10^{-4}\, (r^2\, v^2{}_i\, We_i)^3\right]^{1/2}$$

for $r < 0.4175$

$$= r^{0.5}\, v_i\, [0.6635 - 0.01374\, r^2\, v^2{}_i\, We_i] \qquad (12.18a)$$

for $1 > r > 0.4175$ (12.18b)

where

$$v_i = V_i / U_i$$

and (12.19)

$$We_i = R_i\, U_i^2\, \rho_m / \sigma = 8$$

R_i and U_i are defined in Eqs. (12.10) and (12.11).

The solution of Eqs. (12.17) and (12.18) is obtained numerically and is shown in the next section.

12.6 COMPUTATIONAL ALGORITHM

The algorithm involves first obtaining the initial drop size, the number of drops, and the initial terminal velocity. Using these values and Eqs. (12.16) and 12.16 yields the evaporation rate as a function of time. This procedure is illustrated in the flow diagram (Figure 12.4).

12.7 SPECIFIC EXAMPLE

To illustrate the calculation procedure the following example is worked out in detail.

Liquid spilled	Freon 114	($C\ell_2CFCF_3$)

Properties of Liquid

Mass of liquid spilled	$M = 10^6$	kg
Density of liquid spilled	$\rho = 1455$	kg/m^3
Surface tension	$\sigma = 2 \times 10^{-2}$	N/m
Heat of vaporization	$\lambda = 1.5 \times 10^{-5}$	J/kg
Boiling point at ambient pressure	$T = 3.8$	°C

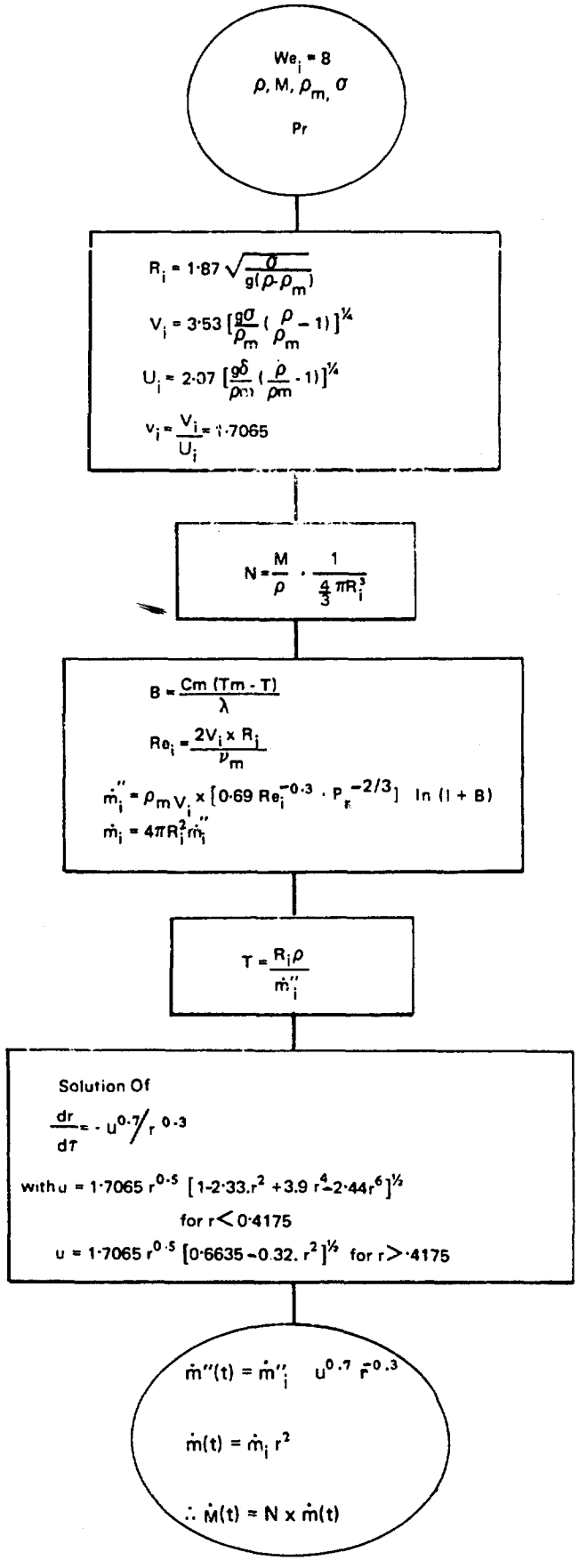

FIGURE 12.4 FLOW CHART FOR THE CALCULATION OF EVAPORATION RATE OF A LIQUID SINKING IN WATER

Properties of Water

Temperature of water (assumed)	$T_m = 20$	°C
Density of water	$\rho_m = 10^3$	kg/m^3
Specific heat of water	$C_m = 4186$	J/kg °K
Kinematic viscosity	$\nu_m = 10^{-6}$	m^2/s
Prandtl number	$Pr = 7$	

Assuming that the critical Weber number = 8,

the size of drip formed = $R_i = 1.87\sqrt{2 \times 10^{-2}/9.8\,(1455 - 1000)} = 3.96 \times 10^{-3}$ m

Terminal velocity of a non-deformable drop of the above size

$$V_i = 3.35 \left[\frac{9.8 \times 2 \times 10^{-2}}{10^3} \quad (1.455\text{-}1)\right]^{1/4} = 0.341 \quad \text{m/s}$$

Terminal velocity of a deformable drop of the above size

$$U_i = 0.586 \times .341 = 0.2 \text{ m/s}$$

Number of drops formed	$N = 2.64 \times 10^9$
Mass transfer factor	$B = 0.452$
Initial Reynolds number	$Re_i = 1584$
Initial rate of evaporation	$\dot{m}_i'' = 1.543$ kg/m^{2}s
Total initial vaporization rate	$\dot{M}_i = 8.0273 \times 10^5$ kg/s

Characteristic time for evaporation $t_{ch} = 1455 \times 3.96 \times 10^{-3}/1.543 = 3.73$ s.

The results of the integration are shown in Table 12.2. The table gives the radius of the drop and the total evaporation rate as a function of time. Table 12.1 is the same result using the "single sphere in an infinite stream" correlation for heat transfer (Eq. (12.12b).

12.8 DISCUSSIONS

The model given is based on the ideas of drop motion and the evaporation of the drop caused by convective heat transfer between the water and the lower temperature liquid that is sinking. It has been assumed that the initial blob of liquid breaks up into uniform and same size drops because of pressure forces and the instability. Experimental evidence indicates that a whole range of drop sizes exist. We have also used the formulas for the drag on a single drop and assume the same to hold good for a drop in an ensemble. While this

approximation is bad for a closely packed ensemble, it may be quite adequate for describing the drag on the individual drops when the inter-drop distances are more than two diameters. However, there is no information in the literature which predicts the "porosity" of the drop ensemble formed by the sinking of a blob of liquid. The assumption of single-sphere drag leads to increased drop velocity and therefore higher vaporization rates, thus giving a conservative estimate for the vapor-generation rate.

The heat transfer model is based on the similarity between convective heat and mass transfers. The heat transfer coefficient (alternatively the Stanton number) correlation depends on the effect of the neighboring drops. Two kinds of correlations are presented: (1) the closely packed spheres with $p = 1/3$ correlations obtained with air as the working fluid are presented, and (2) the single sphere in a liquid correlation. The results obtained using these two heat transfer correlations for the specific example worked out in Section 12.7 are shown in Tables 12.2 and 12.1. It is seen that the use of packed bed correlation leads to a very high evaporation rate and all of the spilled liquid is vaporized in a very short duration (about 3 seconds). The single-sphere heat transfer correlations for the same problem lead to a lower vaporization rate and a larger duration for evaporation. However, even this duration is short (15 seconds). The question of which correlation is more appropriate is of academic interest only, as in both cases the times are short. It may be therefore valid to use, the spill rate itself as the evaporation rate in the case of continuous spills. From the point of view of hazard analysis, therefore, it may be more appropriate to use the closely packed sphere correlations.

In describing the motion of the deformable drops in water, the phenomenon of drop deformation – and consequently the increased drag -- has been taken into account. It is also seen that the terminal velocity in water is much smaller (0.2 m/s compared to 5 to 10 m/s in air) than in air. Based on this and the duration of evaporation, one can say that the liquid does not sink deeply into the water (where the effect of the hydrostatic pressure starts to influence the boiling temperature of the liquid). However, this statement assumes that the liquid temperature is well below the ambient temperature.

Experimental evidence is not available to test the results of this theory. It is possible that the results of this model are off by factors of 3 or 4. The most serious question might be the assumption of the instantaneous break up of the blob to tiny drops – especially in light of the short periods of drop life predicted for the specific example worked out. It may be safe, however, to say that the vapor liberation rate predicted by this model will be definitely higher than the actual value that might be obtained in an experiment. In short, more work – especially experimental – should be done to solve this problem.

12.9 CONCLUSIONS

An evaporative model has been worked out based on the assumption of drop formation when a blob of heavy, low-boiling-point liquid is spilled on a water surface. The details of drag on a deformable drop have been included in the analysis to calculate the terminal velocity of drops. A heat-mass similarity model is used to predict the vaporization rate. It is found that to obtain a conservative vapor hazard estimate, the packed sphere bed heat transfer correlations should be used. To predict the evaporation rate in the case of continuous spill, the rate of spill itself can be used for the vapor liberation rate.

12.10 REFERENCES

1) Kalelkar, A. S., and Kung, H. C., "Generalized Terminal Velocities of Large Drops," Report RC70-T-10,, Factory Mutual Res. Corp. Norwood, Mass.

2) Levich, V.G., "Physicochemical Hydrodynamics," Prentice Hall, Inc., 1962, Section 79.

3) Orr, C., "Particulate Technology," McMillan and Co., New York, 1966.

4) Spalding, D. B., "Convective Mass Transfer," McGraw-Hill, Inc., 1963.

5) Kays, W. M., and London, A. L., "Compact Heat Exchangers," 2nd edn., McGraw-Hill, 1964, p. 131.

6) McAdams, "Heat Transmission," McGraw-Hill, Inc., 1954.

12.11 LIST OF SYMBOLS

Symbol	Description	Value	Units
C_D	drag coefficient for a single sphere in an infinite stream of fluid		
C_m	specific heat of the medium (water)		J/kg °K
d	diameter of a spherical drop		m
F	force (drag or weight)		
g	acceleration due to gravity	9.8	m/s^2
G	mass flux of the medium	$= \rho U$	
h	heat transfer coefficient		$J/m^2 s\ °K$
K_m	thermal conductivity of the medium		J/m s °K
Nu	Nusselt number		
p	porosity of the drop ensemble		
Pr	Prandtl number of the medium =	$\mu_m\ C_m / K_m$	

Symbol	Description	Value	Units
r	ratio of drop size at any instant to the initial size		
R	radius of the drop		m
Re_d	Reynolds number = $U\ d/\nu_m$		
St	Stanton number = $h/C_m\ G$		
t	time		s
t_{ch}	characteristic time (Eq. (12.16))		s
T	boiling temperature of the liquid at ambient pressure		°K
T_m	temperature of the medium		°K
u	dimensionless terminal velocity = U/U_i		
U	terminal velocity of the deformable drops		m/s
v	dimensionless terminal velocity of a rigid drop = V/U_i		
V	erminal velocity of a non-deformable drop (Eq. (12.3))		m/s
We	Weber number = $\rho_m\ U^2\ R/\sigma$		
We*	Weber number [based on velocity V] = $\rho_m\ V^2\ R/\sigma$		
Greek Letters			
δ	fractional decrease in the drop radius caused by pressure forces		
λ	heat of vaporization of liquid		J/kg
μ	viscosity		N s/m^2
ν	kinematic viscosity		m^2/s
ρ	density		kg/m^3
σ	surface tension		N/m

Symbol	Description	Value	Units
τ	non-dimensional time = t/t_{ch}		N/m

Subscripts

c	= critical
ch	= characteristic
d	= based on diameter as the characteristic's dimension
i	= initial
m	= medium

TABLE 12.1

VARIATION OF DROP RADIUS AND EVAPORATION RATE WITH TIME DURING THE SINKING OF A BLOB OF LIQUID IN WATER USING $St = 1.2\ Re_d^{-0.6}\ Pr^{-2/3}$

Time	Drop Radius	Evaporation Rate
Secs	meters	kg/m^2 s
0.00	0.39300E-02	0.15300E 06
0.97	0.37304E-02	0.14223E 06
1.94	0.35242E-02	0.13135E 06
2.91	0.33105E-02	0.12033E 06
3.89	0.30882E-02	0.10917E 06
4.86	0.28558E-02	0.97852E 05
5.83	0.26115E-02	0.86336E 05
6.81	0.23534E-02	0.73979E 05
7.78	0.20808E-02	0.61297E 05
8.75	0.17905E-02	0.48583E 05
9.72	0.14715E-02	0.37081E 05
10.70	0.11088E-02	0.24151E 05
11.67	0.67825E-03	0.11241E 05

$$St = 1.2\ Re_d^{-0.6}\ Pr^{-\frac{2}{3}}$$

TABLE 12.2

VARIATION OF DROP RADIUS AND EVAPORATION RATE WITH TIME DURING THE SINKING OF A BLOB OF LIQUID IN WATER USING $St = 0.69\ Re_d^{-0.3}\ Pr^{-2/3}$

Time	Drop Radius	Evaporation Rate
secs	meters	kg/m^2 s
0.00	0.39300E-02	0.80273E 06
0.18	0.37319E-02	0.73519E 06
0.37	0.35307E-02	0.66908E 06
0.55	0.33260E-02	0.60447E 06
0.74	0.31174E-02	0.54145E 06
0.93	0.29046E-02	0.48012E 06
1.11	0.26869E-02	0.42057E 06
1.30	0.24641E-02	0.36070E 06
1.49	0.22384E-02	0.30041E 06
1.67	0.20109E-02	0.24414E 06
1.86	0.17821E-02	0.19264E 06
2.05	0.15479E-02	0.15426E 06
2.23	0.13017E-02	0.11146E 06
2.42	0.10508E-02	0.73869E 05
2.61	0.79663E-03	0.42844E 05
2.79	0.54134E-03	0.19746E 05
2.98	0.28863E-03	0.54996E 04
3.17	0.46442E-04	0.13051E 03

$$St = 0.69\ Re_d^{-0.3}\ Pr^{-\frac{2}{3}}$$

13.0 RADIATION VIEW FACTOR BETWEEN AN INCLINED FLAME AND AN ARBITRARILY ORIENTED SURFACE IN SPACE

13.1 AIM

The aim of the derivations in this chapter is to obtain analytically the value of the radiation view factor between a cylindrical flame and a plane in space having an arbitrary orientation.

13.2 INTRODUCTION

There are many instances in which it is necessary to calculate the radiant heat flux to a building or some other structure from a nearby flame. The radiant energy received by the object depends on many factors and these are discussed in detail in Chapter 7. Of these, one of the important ones is the "radiation view factor" which is purely a geometric shape parameter. The view factor indicates the extent to which the two objects can "see" each other.

Since the view factor is purely a geometric parameter it can be calculated, at least in principle, once the shapes of the objects, their relative positions, and relative orientations are known. However, but for the simplest of geometries (such as planar objects) and positions, the calculation of the view factor by analytical methods is impossible.

The thermal radiation from a flame to a plane object in space has been modeled by considering the flame as a cylinder with a possible inclination of the axis to the ground ("wind tilt"). The view factor calculations have been done numerically by Rein et al.[1] and Merriam[2] by subdividing the cylinder into a number of sections, calculating the contribution from each section to the view factor, and then summing the results to obtain the overall factor. It has been observed that in this numerical method the accuracy of the result depends on the number of sections, being better for a larger number of sections. However, the computation time increases as the square of the number of sections. Also large errors occur in the final result when the distance between the observer and the flame is small. To overcome all of the above shortcomings in the numerical scheme, the following analytical method was developed. It is expected that this method will result in a large saving in computer time, while at the same time providing a more accurate result.

For the purposes of this analysis, the flame is considered to be a right circular cylinder. The analysis is itself based primarily on the methods of contour integration. The analysis is in two parts. Part A deals with the coordinate transformations, so that in the redefined coordinate system the flame is normal to the "ground" and the object plane is on one of the axes on the ground. In Part B analytical expressions are derived to calculate the view factor for different orientations of the object plane. Details are discussed in Section 13.5. A computer program has been written to do the calculations. The algorithm is given in Section 13.6.

13.3 PRINCIPLES AND ASSUMPTIONS

The view factor for radiation exchange between an infinitesimal plane of area dA_1 and another plane of A_2 is given by Hottel and Sarofim[3] (see Section 13.11 for the definition of symbols).

$$F_{dA_1 \to A_2} = \frac{1}{\pi} \int_{A_2} \frac{\cos\theta_1 \cos\theta_2}{r^2} \, dA_2 \tag{13.1}$$

where θ_1 and θ_2 are, respectively, the angles made by the outward normals to the planes dA_1 and dA_2 with the line joining the two elemental areas, and r is the distance between the two elemental areas.

The heat flux received by the elemental area dA_1 is given by

$$Q = F \epsilon \tau \sigma T_f^4 \tag{13.2}$$

It has been shown[4] that Eq. (13.1) can be written as

$$\begin{aligned} F_{dA_1 \to A_2} = {} & l_1 \oint_c \frac{(z_2 - z_1)\, dy_2 - (y_2 - y_1)\, dz_2}{2\pi r^2} \\ & + m_1 \oint_c \frac{(x_2 - x_1)\, dz_2 - (z_2 - z_1)\, dx_2}{2\pi r^2} \\ & + n_1 \oint_c \frac{(y_2 - y_1)\, dx_2 - (x_2 - x_1)\, dy_2}{2\pi r^2} \end{aligned} \tag{13.3}$$

where l_1, m_1, n_1, are the direction cosines of the outward normal to the plane of observation and c is the closed contour on the cylinder enveloping an area that is "visible" from the elemental area dA_1.

The basic principle of the model presented below involves, first, the determination of the contour c and then evaluation of the integrals of Eq. (13.3) on this contour, for each of the many possible orientations of the elemental area dA_1.

The primary assumptions made in the model are

- The flame is a right circular tilted cylinder.
- The contributions to the view factor from the end surfaces of the cylinder are small and therefore not included in the analysis.

13.4 DATA REQUIRED

- The radius and length of the cylinder,
- The inclination of the cylinder (with respect to a suitably defined cartesian coordinate system),
- The distance of the plane of observation from the base of the cylinder,
- The orientation of (i.e., the direction cosines of the normal to) the plane.

13.5 DETAILS OF THE MODEL

A cartesian coordinate system X, Y, and Z, is defined such that the axis of the cylinder is in the Y-Z plane and is inclined to the Z axis at an angle α. The position of the observation plane is at P(X, Y, Z), an arbitrary point in space. The direction cosines of the normal to this plane (on the face of interest) are L, M, and N, respectively, with respect to the X, Y, and Z axes. These are shown in Figure 13.1.

13.5.1 Part A: Coordinate Transformations

In this part we reduce the problem by coordinate transformations, such that, with respect to a new system of cartesian coordinates, the flame axis is vertical and the observation point P is on one of the other axes (say, the y axis). To do this we have to find;

1) The coordinates of a point Q(u,v,w) which is the foot of the perpendicular drawn from the point P onto the cylinder axis;
2) The direction cosines of a line passing through Q and normal to both the cylinder axis and the line QP. [Let this line be the new x axis, line QP be the y axis and the cylinder axis QT, the new z axis.]
3) The direction cosines of the normal to the observation plane at P with respect to this new coordinate system (whose origin is Q); and
4) The coordinates of point P with respect to the new coordinate system.

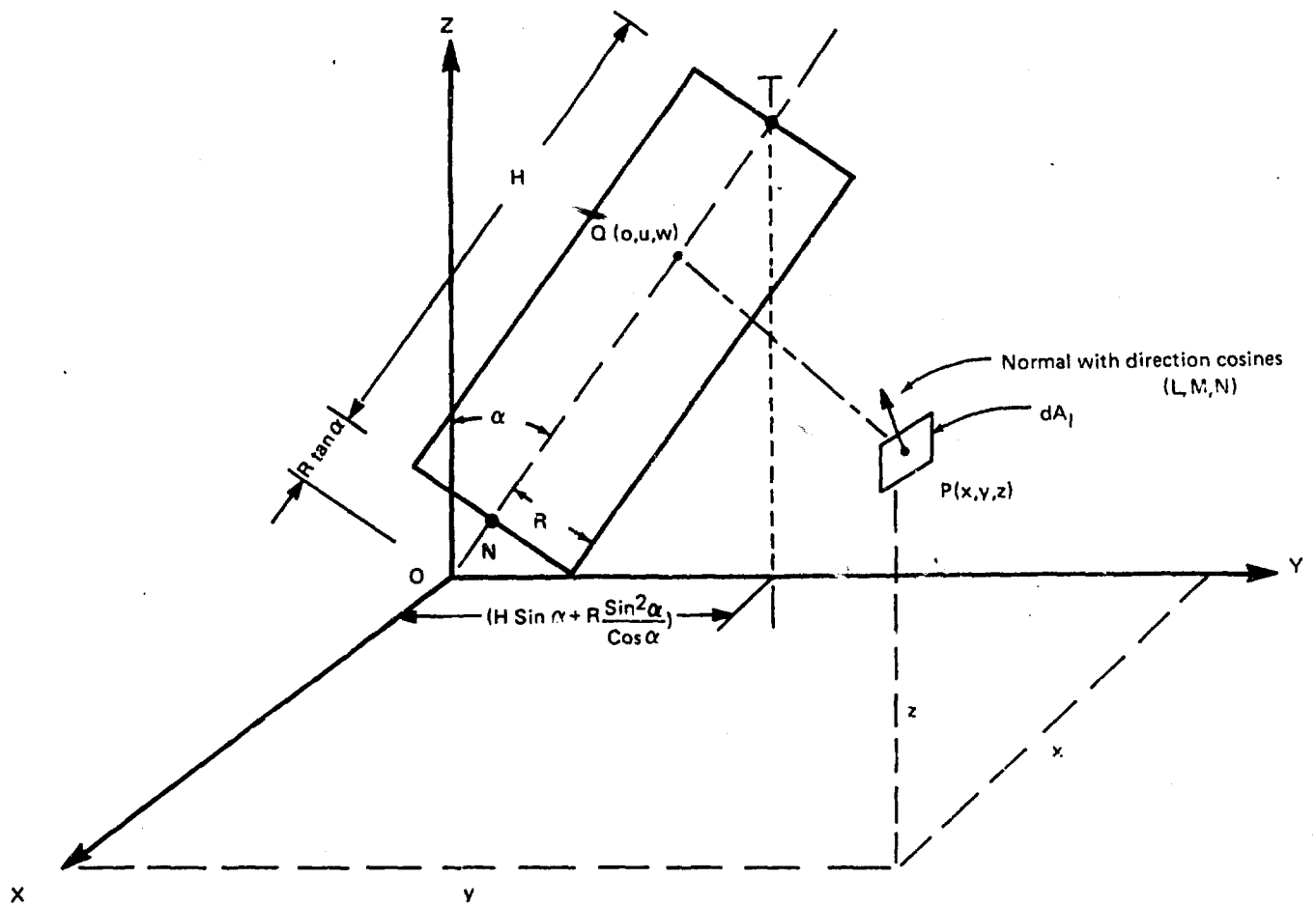

FIGURE 13.1 ILLUSTRATION OF THE RELATIVE POSITIONS AND ORIENTATIONS OF THE CYLINDER AND THE OBSERVATION PLANE

Solution:

Since Q is on the axis of the cylinder and since the axis itself is in the Y-Z plane, the X coordinate of Q is zero.

Let $\vec{i}, \vec{j}, \vec{k}$ represent unit vectors in the X, Y, and Z directions, respectively. Then,

$$\left.\begin{aligned} \vec{r}_Q &= 0\,\vec{i} + v\,\vec{j} + w\,\vec{k} \\ \text{and} \\ \vec{r}_P &= X\,\vec{i} + Y\,\vec{j} + Z\,\vec{k} \end{aligned}\right\} \tag{13.4}$$

$$\vec{r}_{QP} = (\vec{r}_P - \vec{r}_Q) = \vec{i}\,X + \vec{j}\,(Y - v) + \vec{k}\,(Z - w) \tag{13.5}$$

Since line PQ is normal to the axis, we have:

$$\vec{r}_{QP} \cdot \vec{r}_Q = 0$$

i.e.,

$$(Y - v)\,v + (Z - w)\,w = 0 \tag{13.6a}$$

and

$$\tan \alpha = v/w \tag{13.6b}$$

Substituting Eq. (13.6b) in Eq. (13.6a) yields:

$$\left.\begin{aligned} u &= 0 \\ v &= \frac{Z + Y \tan\alpha}{1 + \tan^2\alpha} \tan\alpha \\ w &= \frac{Z + Y \tan\alpha}{1 + \tan^2\alpha} \end{aligned}\right\} \tag{13.7}$$

Therefore:

$$Q \equiv Q\left(0, \frac{Z + Y \tan\alpha}{1 + \tan^2\alpha}\tan\alpha, \frac{Z + Y \tan\alpha}{1 + \tan^2\alpha}\right)$$

Hence $\vec{r}_{QP} X \vec{r}_Q$ gives a vector which is normal to both $\vec{r}_{QP}$ and $\vec{r}_Q$ vectors.

i.e.,

$$\vec{r}_{QP} \times \vec{r}_Q = \vec{i}(Y w - Z v) - \vec{j} w X + \vec{k} v X \qquad (13.8)$$

Let us define a new coordinate system centered at Q and defined by the x, y, and z axes (see Figure 13.2). x is in the direction of $r_{QP} \times r_Q$ vector, y is in the direction of QP vector, and z is in the direction of OQ vector.

Now the length $PQ = \sqrt{X^2 + (Y - v)^2 + (Z - w)^2}$ (13.9a)

and length $OQ = \sqrt{v^2 + w^2}$ (13.9b)

The direction cosines of the x, y, z coordinates axes are therefore (from Eqs. (13.8) and (13.9)) with respect to X, Y, Z axes are

x axis:	$\ell_1' = (Yw - Zv)/(PQ \cdot OQ)$	$m_1' = -Xw/(PQ \cdot OQ)$	$n_1' = Xv/(PQ \cdot OQ)$
y axis:	$\ell_2' = X/PQ,$	$m_2' = (Y - V)/PQ$	$n_2' = (Z - w)/PQ$
z axis:	$\ell_3' = 0,$	$m_3' = \sin\alpha$	$n_3' = \cos\alpha$

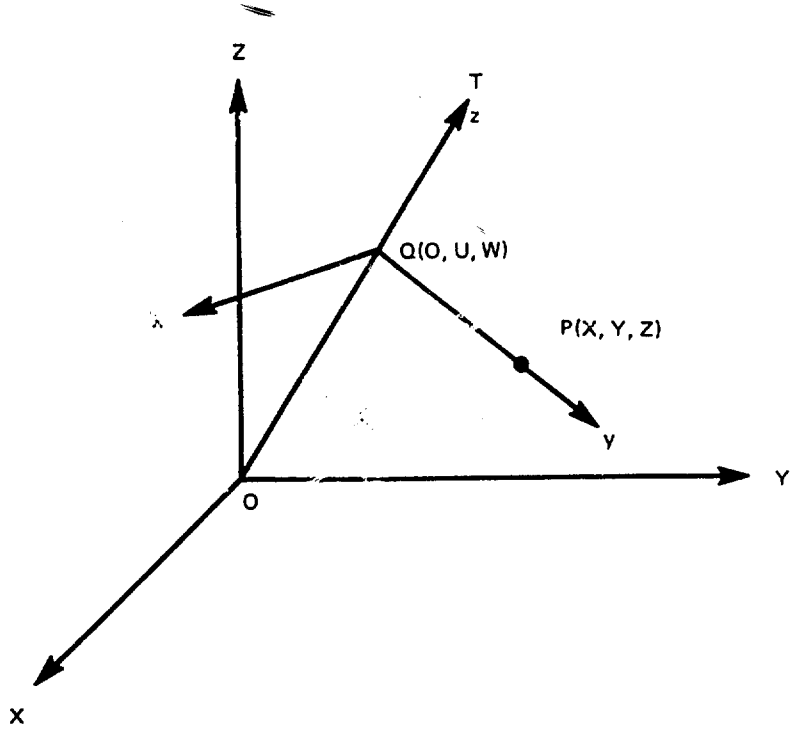

FIGURE 13.2 FIGURE INDICATES THE TRANSFORMED COORDINATE SYSTEM

If ℓ, m, and n are the direction cosines of the plane with respect to the new system of coordinates, then we have:

$$\begin{bmatrix} \ell \\ m \\ n \end{bmatrix} = \begin{bmatrix} \ell_1' & m_1' & n_1' \\ \ell_2' & m_2' & n_2' \\ \ell_3' & m_3' & n_3' \end{bmatrix} \begin{bmatrix} L \\ M \\ N \end{bmatrix} \tag{13.11}$$

where the first matrix, on the right hand side, is the transformation matrix whose elements are the direction cosines of the new coordinate system with respect to the original coordinate system. The second matrix, on the right hand side, contains the direction cosines of the normal of the plane with respect to the original set of axes.

Any point $c(X,Y,Z) \equiv c(x,v,z)$ in space has the coordinate equivalence given by

$$\begin{bmatrix} x \\ y \\ z \end{bmatrix} = \begin{bmatrix} \ell_1' & m_1' & n_1' \\ \ell_2' & m_2' & n_2' \\ \ell_3' & m_3' & n_3' \end{bmatrix} \begin{bmatrix} X \\ Y \\ Z \end{bmatrix} + \begin{bmatrix} O \\ -v \\ -w \end{bmatrix} \tag{13.12}$$

Now the coordinates of point P with respect to the new coordinate system x,y,z (Figure 13.2) become:

$$P \equiv P\ (0, PQ, 0)$$

where PQ the length is given in Eq. (13.9).

The problem of finding the view factor is now simplified (relatively speaking), because in the x,y,z coordinates, we have an infinitesimal plane with its normal having direction cosines ℓ,m,n, and plane located on the y axis at a distance PQ (say equal to S). The cylinder axis is vertical. However, it should be noted that the cylinder extends in the negative z axis also (below the ground) in some cases depending on the position of point Q. There are, therefore, three cases to consider (see Figure 13.1):

a) point Q is beyond the top of the cylinder (i.e., point T). i.e., $w \geq (H + R \tan \alpha) \cos \alpha$.

b) Q is below the cylinder (i.e., point N). i.e., $w \leq R \sin \alpha$.

c) Q is inside the cylinder (in between N and T). i.e., $R \sin \alpha \leq w \leq (H \cos \alpha + R \sin \alpha)$.

(13.13)

In case "a" the cylinder is entirely under the ground in the x,y,z coordinates. In this case, the view factor from the cylinder, together with its extension, is to be found first and then the view factor due to the extension alone is to be subtracted. A similar "break-up" technique is to be used to evaluate the correct view factors in both cases b and c. This is illustrated below.

- **View Factor Calculation**

Let the function f(R,H,S,ℓ,m,n) be the view factor for a cylinder that is entirely above ground, of radius R and height H when the observation plane is S away from the axis of the cylinder. The terms ℓ,m, and n, as usual, represent the direction cosines of the normal to the observation plane (see Figure 13.3).

Going back to the cases represented in Eq. (13.13), we have:

Case a:

$$\text{i.e., } w > (H \cos \alpha + R \tan \alpha)$$

$$\text{View Factor} = f(R, H_1, PQ, -\ell, +m, -n) - f(R, H_2, PQ, -\ell, m, -n) \qquad (13.14a)$$

where

$$H_1 = \sqrt{v^2 + w^2} - R \tan \alpha,$$

$$H_2 = H - H_1$$

and

PQ = the length of line joining P and Q (Eq. (13.9)).

ℓ,m,n = direction cosines of normal to plane (Eq. 13.11)).

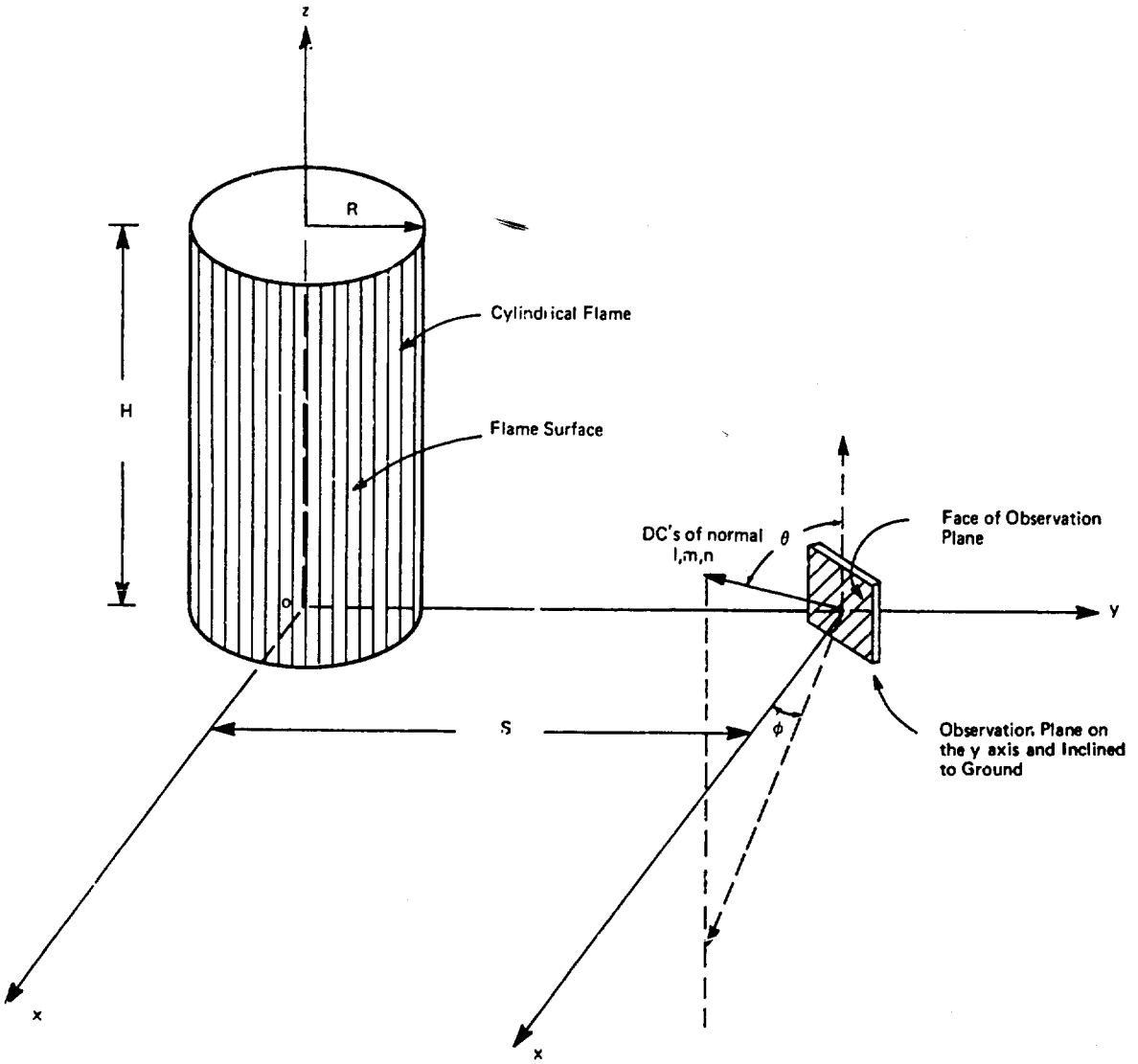

FIGURE 13.3 FIGURE ILLUSTRATING THE RELATIVE POSITIONS OF THE CYLINDER AND THE OBSERVATION ELEMENT

Case b:

$$w \leqslant R \sin \alpha$$

$$\text{View Factor} = f(R, H_1, PQ, \ell,m,n) - f(R,H_2, PQ, \ell,m,n) \qquad (13.14b)$$

where

$$H_1 = (H + R \tan \alpha - w/\cos \alpha)$$

$$H_2 = (H_1 - H)$$

Case c:

$$R \sin \alpha \leqslant w \leqslant (H \cos \alpha + R \tan \alpha)$$

$$\text{View Factor} = f(R,H_1, PQ, \ell,m,n) + f(R, H_2, PQ, -\ell,m, -n) \qquad (13.14c)$$

where

$$H_1 = H + R \tan \alpha - w/\cos \alpha$$

$$H_2 = w/\cos \alpha - R \tan \alpha..$$

In Part B we discuss the analytical solutions for the evaluation of the function f(R,H,S,ℓ,m,n).

13.5.2 Part B: View Factor Calculation for an Upright Cylinder Viewed from a Point on the Ground

In this part expressions for the view factor are derived for the case, when the cylinder axis is vertical and the observation plane is on the y axis at a distance S from the center of the cylinder on the ground. The cylinder is of height H and radius R. Also the direction cosines of the normal to the observation plane are ℓ, m, and n.

We define the following non-dimensional quantities

$$h = H/R$$

$$s = S/R \qquad (13.15a)$$

and the radius of the cylinder in dimensionless units is unity.

To evaluate the view factor, Eq. (13.3) is used, together with contour integrations. The contours in this case are the lines of intersection of the observation plane and the cylinder. Depending on the orientation of this plane, only fractional areas of the cylinder surface are "seen." The different possible orientations of the plane are given in Table 13.1. Each possible orientation is considered as a "case." The direction cosines of the normal to the plane always satisfy the relation:

$$\ell^2 + m^2 + n^2 = 1 \qquad (13.16)$$

Based on Table 13.1 and noting the constraint of Eq. (13.16), there are 26 possible cases (see Table 13.2). However, the number of cases to be actually worked out in detail is small because of symmetry considerations and complementary cases. In the latter category each set of the cases has a common contour and by finding the view factor for one case the other can be calculated easily. This is shown below (also see the Lemma):

Let

I_F = view factor when the maximum of area (A_{max}) of the flame is seen by the observation plane [this is worked out in Appendix 13.1];

I_2 = view factor between dA_1 and an area A_2 on the flame having a common contour c with another complementary area A_2' [note $A_2 + A_2' = A_{max}$),

I_2' = view factor between A_2' on the flame and dA_1.

Then it can be shown (see Lemma):

$$I_2' = I_F - I_2 \qquad (13.17)$$

The actual cases worked out are shown in Table 13.2 and are given below.

- **View Factor Calculations for Selected (primary) Cases**

The general nomenclature used in the derivations are indicated in Figure 13.4. Their definitions are:

$$\left.\begin{aligned} \alpha &= \sin^{-1}(1/s) \\ \beta &= \tan^{-1}[h/(s-1)] \\ \beta' &= \tan^{-1}[h\,s/(s^2-1)] \end{aligned}\right\} \qquad (13.18)$$

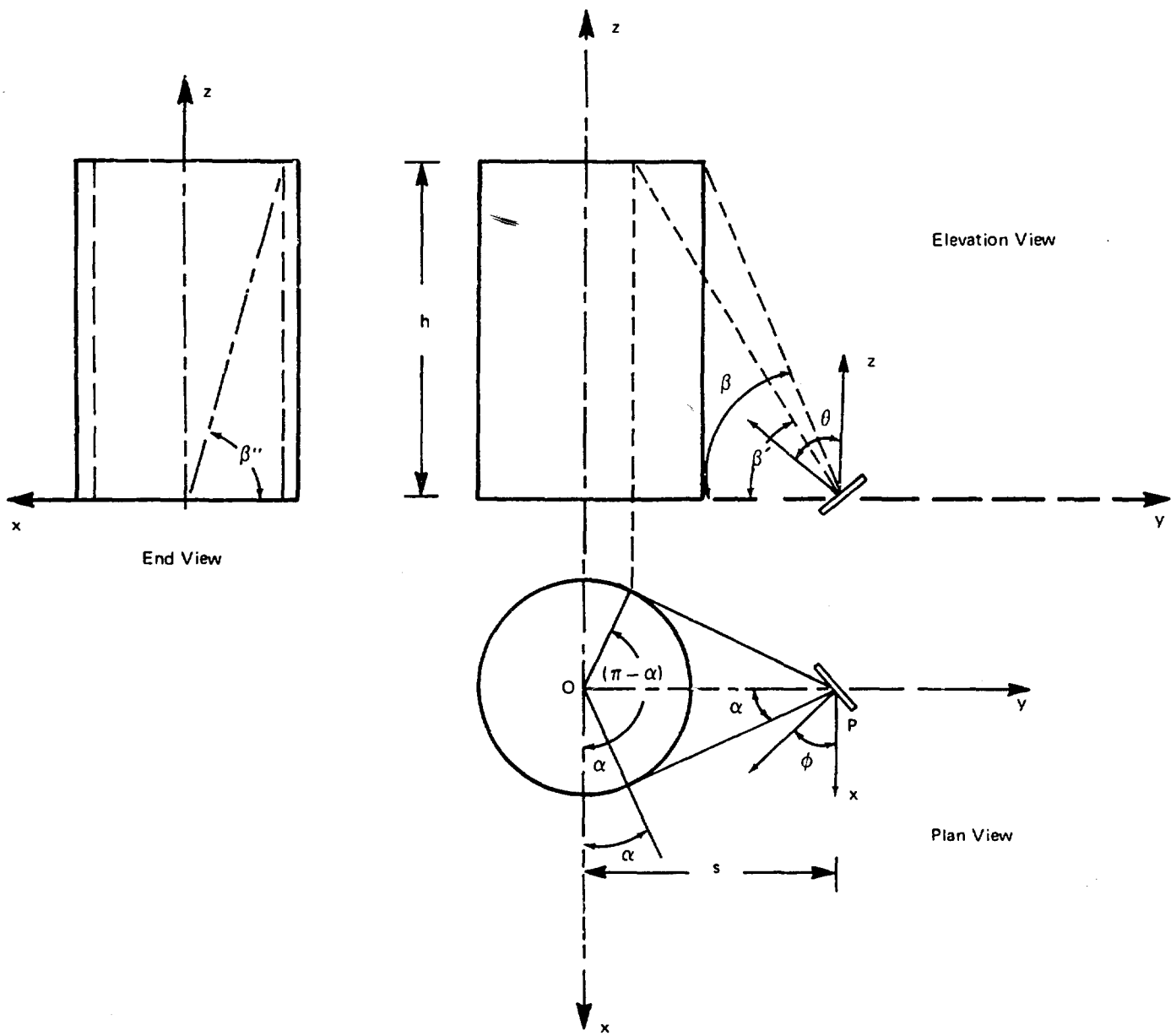

FIGURE 13.4 FIGURE ILLUSTRATING THE DEFINITION OF THE VARIOUS PARAMETERS

$$\left.\begin{aligned} \beta'' &= \tan^{-1}[h\, s/\sqrt{s^2-1}] \\ \theta &= \cos^{-1}|n| \\ \phi &= \cos^{-1}[|\ell|/\sin\theta] \end{aligned}\right\} \qquad (13.18)$$

The definitions of the functions I(1,---), I(2,---)--- used below are given in the Appendix. Each "I" represents the result obtained by integrating Eq. (13.3) over specific contours.

Case 1.3.3 $\quad n = -1,\ m = 0,\ \ell = 0$

The face of the plane is looking away from the cylinder.

Hence:

$$VF = 0 \qquad (13.19)$$

Case 2.2.2 $\quad -1 < n < 0,\ -1 < m < 0,\ -1 < \ell < 0$

The plane is inclined to all three axes. There are five subcases to consider. These are given below.

2.2.2.a

$$\phi \leqslant \alpha \text{ and } \bar{h} = h.$$

$$\bar{h} = [\cos(\alpha+\phi) + s\sin\phi]\tan\theta = \sqrt{s^2-1}\tan\theta\sin(\alpha+\phi)$$

Referring to Figure 2.2.2.a [see footnote below*], we have

$$\nu_1 = \cos^{-1}(PC\sin\phi)$$

where

$$PC = PD - DC = s\cos\phi - \sqrt{1 - s^2\sin^2\phi}$$

$$\nu_2 = \pi - \alpha.$$

*The figure numbers are not preceded by 13 in this section to facilitate the correspondence between the case numbers and the figure numbers.

and

$$VF = I(2, \ell, m, n, s, 0, \nu_1, \nu_2) + I(3, \ell, m, n, s, \nu_2, 0, \bar{h}) - I(6, \ell, m, n, s, 0, \phi, \theta, \nu_1, \nu_2) \quad (13.20a)$$

2.2.2.b

$$\phi < \alpha, \bar{h} \geq h.$$

ν_1 is the same as given before (2.2.2.a) referring to Fig. 2.2.2.b we have,

$$\begin{aligned} \nu_2 &= \phi + \pi/2 + A\hat{O}E \\ &= \phi + \pi/2 + \text{Sin}^{-1} AE \\ &= \phi + \pi/2 + \text{Sin}^{-1} [AB - OC] \quad (13.20b) \\ \nu_2 &= \phi + \pi/2 + \text{Sin}^{-1} \left[\frac{h}{\tan\theta} - s \sin\phi\right] \end{aligned}$$

$$\therefore VF = I(2, \ell, m, n, s, 0, \nu_1, \pi-\alpha) + I(3, \ell, m, n, s, (\pi-\alpha), 0, h) - I(6, \ell, m, n, s, 0, \phi, \theta, \nu_1, \nu_2)$$

2.2.2.c

$$\phi > \alpha \text{ and } h_2 < h$$

Referring to Fig. 2.2.2.c we have

$$\begin{aligned} h_1 &= CE \tan\theta \\ &= PC \sin(\phi - \alpha) \tan\theta \\ &= \sqrt{s^2 - 1} \sin(\phi - \alpha) \tan\theta \\ h_2 &= \sqrt{s^2 - 1} \sin(\phi + \alpha) \tan\theta \end{aligned}$$

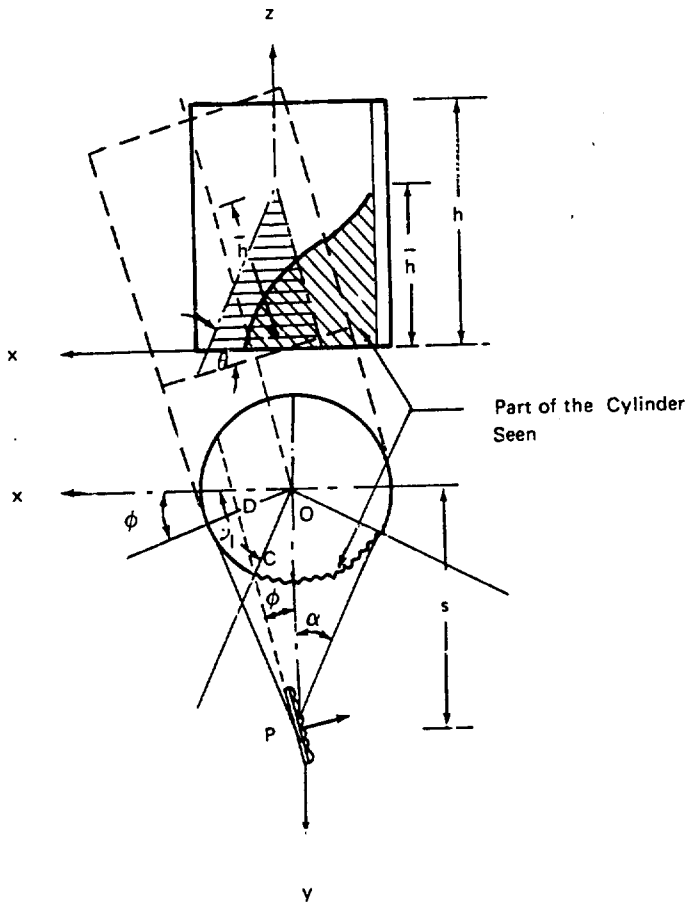

FIGURE 2.2.2a

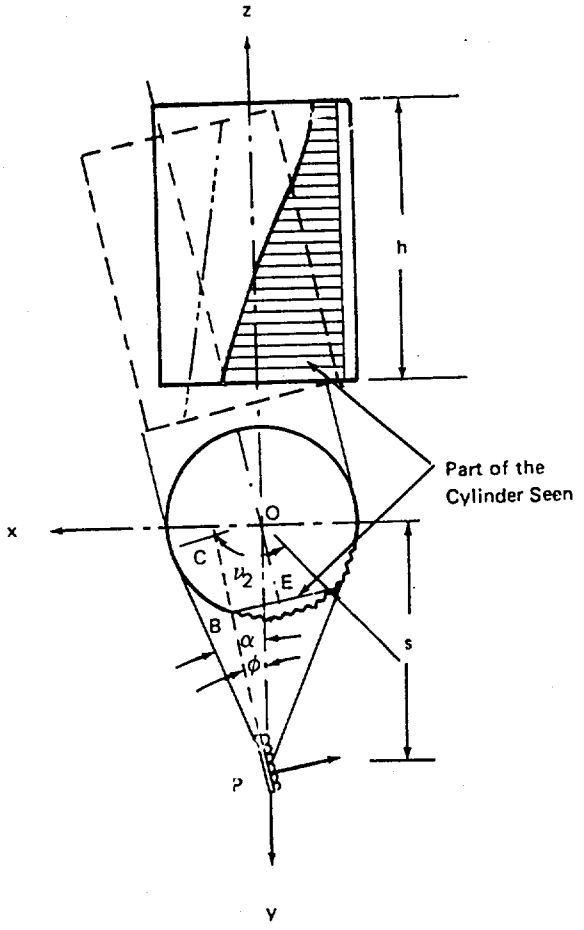

FIGURE 2.2.2b

$\nu_1 = \alpha, \quad \nu_2 = \pi - \alpha$

$\therefore$ VF = I (2, ℓ, m, n, s, 0, ν_1, $\pi - \alpha$) + I (3, ℓ, m, n, s, $(\pi - \alpha)$, 0, $\frac{h}{2}$)

$- I (6, \ell, m, n, s, h_1, \phi, \theta, \nu_1, \nu_2)$ (13.20c)

2.2.2.d

$$\phi > \alpha, h_2 > h$$

$\nu_1 = \alpha$

$\nu_2 = \phi + \pi/2 + \sin^{-1} (\frac{h}{\tan\theta} - s \sin \phi)$

$h_1 = \sqrt{s^2 - 1} \sin (\phi - \alpha) \tan\theta$

$h_2 = h$

VF = I (2, ℓ, m, n, s, 0, ν_1, ν_2) + I (3, ℓ, m, n, s, ν_2, 0, h)

$- I (6, \ell, m, n, s, h_1, \phi, \theta, \nu_1, \nu_2)$ (13.20 d)

2.2.2.e

$$\phi > \alpha, \quad h_1 > h$$

VF = I (1, ℓ, m, n, s, h) (13.20e)

Case 2.2.3 $-1 < n < 0, \quad -1 < m < 0, \quad \ell = 0$

2.3.2.a

$$\theta > \beta$$

VF = I (1, ℓ, m, n, s, h) (13.21a)

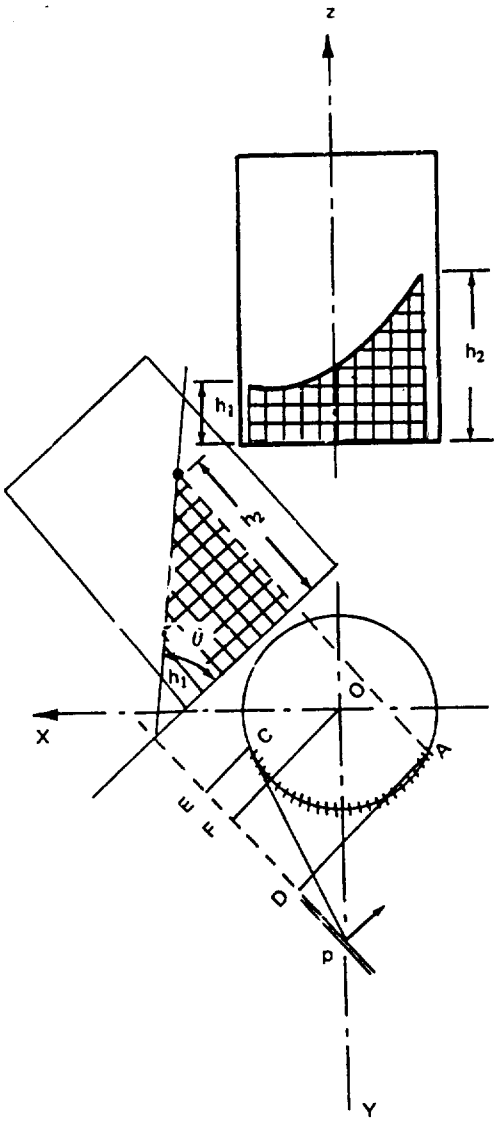

FIGURE 2.2.2c

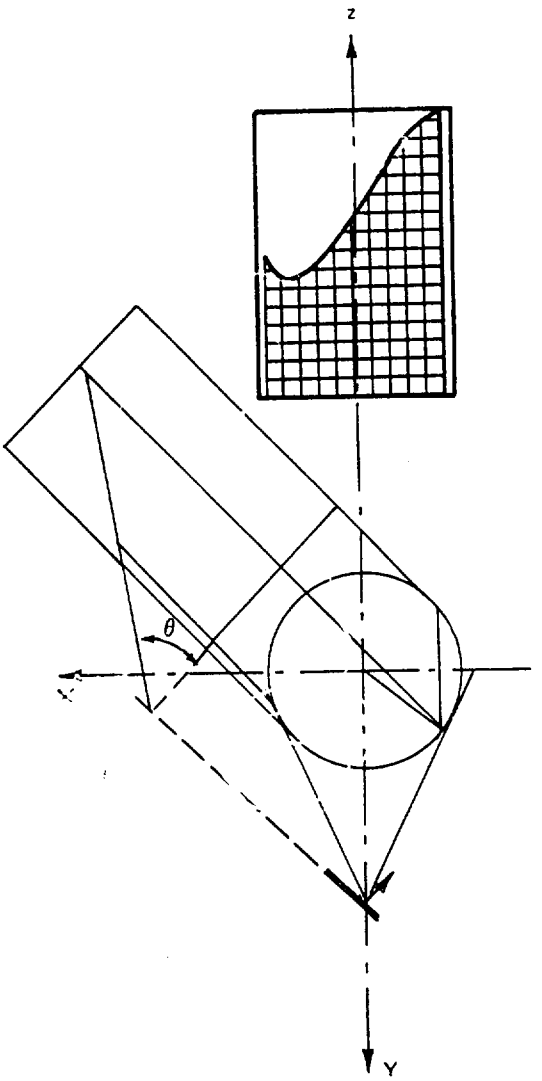

FIGURE 2.2.2d

2.2.3.b

$$\beta' < \theta < \beta$$

$$\nu_1 = \sin^{-1}\left[s - \frac{h}{\tan\theta}\right]$$

and $\nu_2 = \pi - \nu_1$

$$VF = I(2, \ell, m, n, s, 0, \alpha, \pi - \alpha) + I(3, \ell, m, n, s, \pi - \alpha, 0, h) + I(2, \ell, m, n, s, h, \pi - \alpha, \nu_2) - I(4, \ell, m, n, s, \theta, \nu_1, \nu_2) - I(2, \ell, m, n, s, h, \alpha, \nu_1) - I(3, \ell, m, s, \alpha, 0, h) \quad (13,21b)$$

2.2.3.c

$$\theta < \beta'$$

$$\nu_1 = \alpha$$

$$\nu_2 = \pi - \alpha$$

$$\bar{h} = (s - \sin\alpha)\tan\theta = \frac{(s^2 - 1)}{s}\tan\theta$$

$$VF = I(2, \ell, m, n, s, 0, \nu_1, \nu_2) + I(3, \ell, m, n, s, \nu_2, 0, \bar{h}) - I(4, \ell, m, n, s, \theta, \nu_1, \nu_2) - I(3, \ell, m, n, s, \nu_1, 0, \bar{h}) \quad (13.21c)$$

Case 2.3.4 $\quad -1 < n < 0,\ m = 0,\ 0 < \ell < 1$

2.3.4.a

$$\theta \leq \beta''$$

$$\bar{h} = \cos\alpha\tan\theta$$

$$= \frac{\sqrt{s^2 - 1}}{s}\tan\theta$$

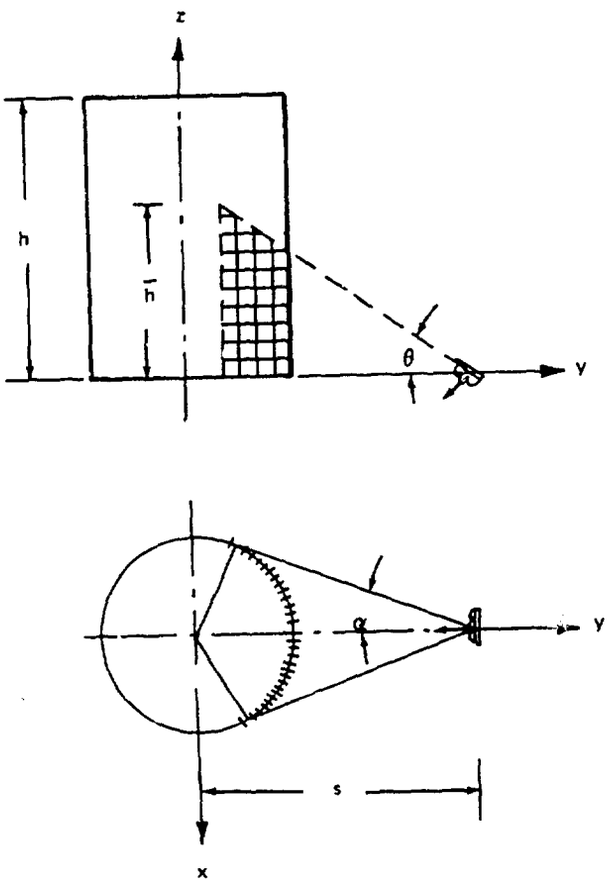

FIGURE 2.2.3c

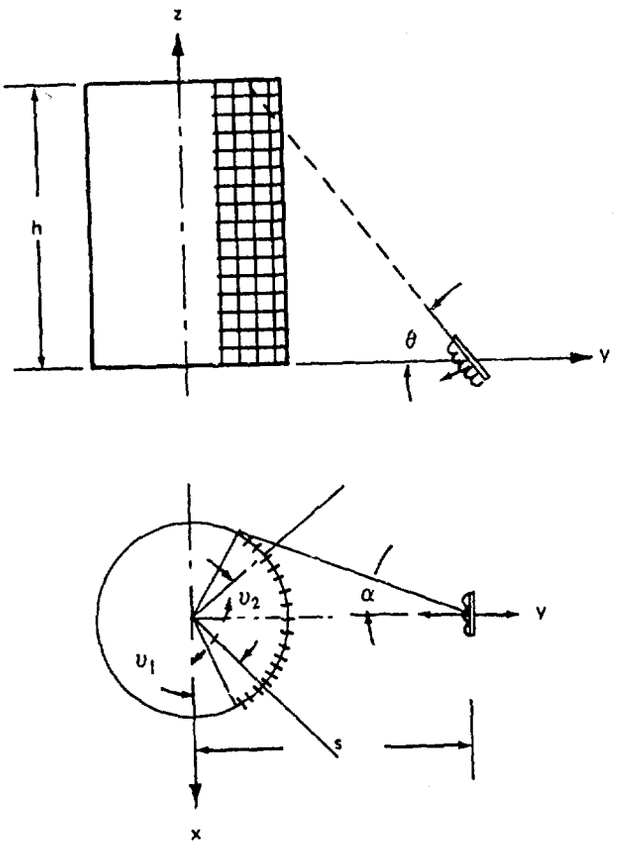

FIGURE 2.2.3b

then $VF = I(2, \ell, m, n, s, 0, \alpha, \pi/2) + I(5, \ell, m, n, s, \theta, \alpha)$

$- I(3, \ell, m, n, s, \alpha, 0, \bar{h})$

(13.22a)

2.3.4.b

$$\theta > \beta''$$

$$\nu_1 = \cos^{-1}\left(\frac{h}{\tan\theta}\right)$$

$VF = I(2, \ell, m, n, s, 0, \alpha, \pi/2) + I[5, \ell, m, n, s, \theta, \nu_1]$

$- I(2, \ell, m, n, s, h, \alpha, \nu_1) - I(3, \ell, m, n, s, \alpha, 0, h)$

(13.22b)

Case 2.4.3 $\quad -1 < n < 0,\ 0 < m < 1,\ \ell = 0$

Since no part of the plane is seen by the flame,

$$VF = 0$$

(13.23)

Case 2.4.4 $\quad -1 < n < 0,\ 0 < m < 1,\ 0 < \ell < 1$

2.4.4.a

$$\phi < \alpha,\ \bar{h} < h$$

where

$$\bar{h} = \sqrt{s^2 - 1}\ \sin(\alpha - \phi)\ \tan\theta$$

Referring to Figure 2.4.4.a we have

$$\nu_1 = \cos^{-1}(PC \sin\phi)$$

$$PC = PD - DC$$

$$= s\cos\phi - [\sqrt{1 - OD^2}]$$

$$= s\cos\phi\ [\sqrt{1 - s^2\sin^2\phi}]$$

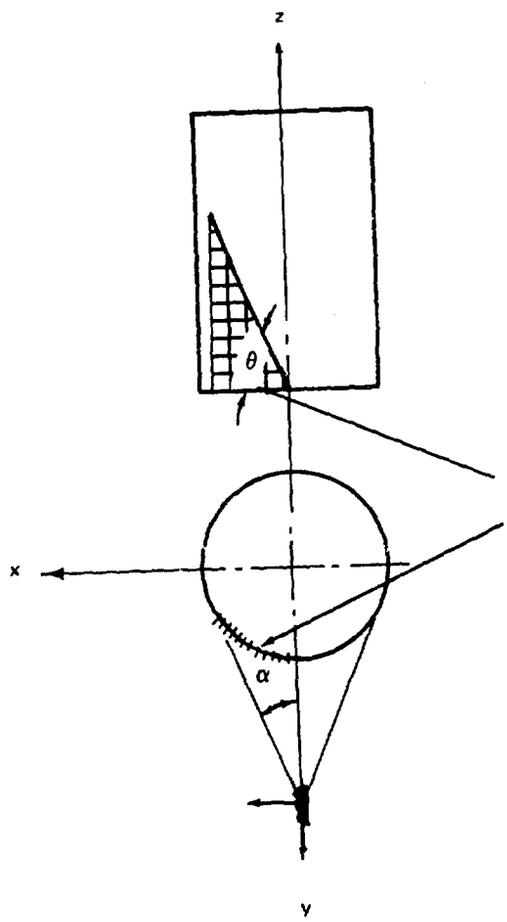

FIGURE 2.3.4a

part of the
cylinder seen

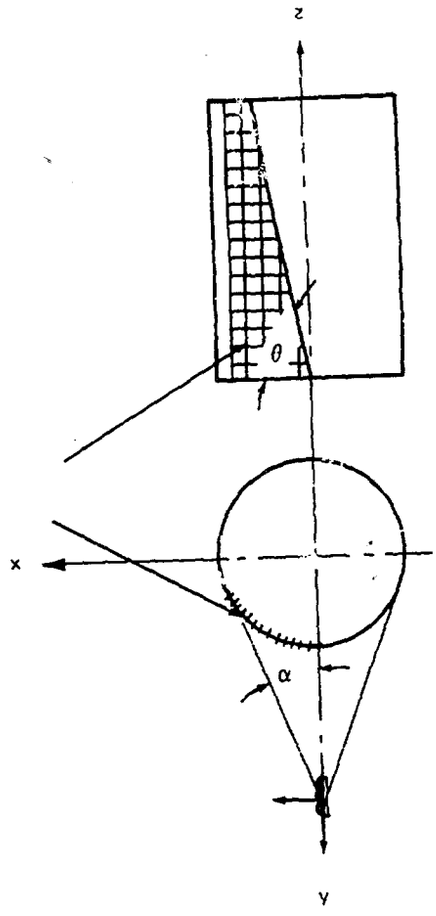

FIGURE 2.3.4b

$$\nu_1 = \cos^{1} [s \cos\phi \quad \sin\phi - \sin\phi \sqrt{1 - s^2 \sin^2\phi}]$$

$$\nu_2 = \alpha$$

$$VF = I\ (2, \ell, m, n, s, 0, \alpha, \nu_1)$$
$$+ I\ (7, \ell, m, n, s, 0, \phi, \theta, \nu_1, \nu_2)$$
$$- I\ (3, \ell, m, n, s, \alpha, 0, \bar{h})$$

(13.24a)

2.4.4.b $\qquad \phi < \alpha,\ \bar{h} \geq h$

$$\nu_1 = \cos^{-1} (PC \sin\phi)$$

$$\nu_2 = \phi + \cos^{-1} \left[\frac{h}{\tan\theta} + s \sin\phi\right]$$

note $\nu_2 < \nu_1$

$$VF = I\ (2, \ell, m, n, s, 0, \alpha, \nu_1)$$
$$+ I\ (7, \ell, m, n, s, 0, \phi, \theta, \nu_1, \nu_2)$$
$$- I\ (2, \ell, m, n, s, h, \alpha, \nu_2)$$
$$- I\ (3, \ell, m, n, s, \alpha, 0, h)$$

(13.25b)

2.4.4.c

$$\phi \geq \alpha$$

Since the flame is not seen

$$VF = 0$$

(13.25c)

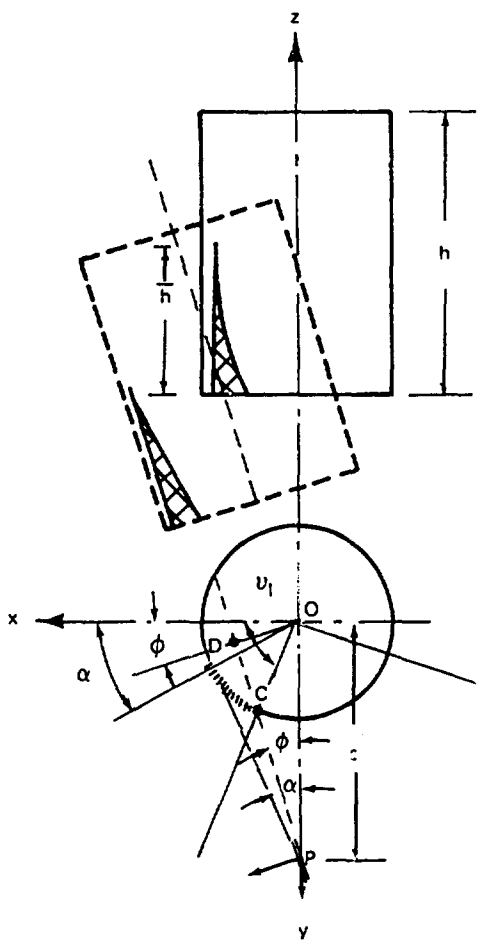

FIGURE 2.4.4a

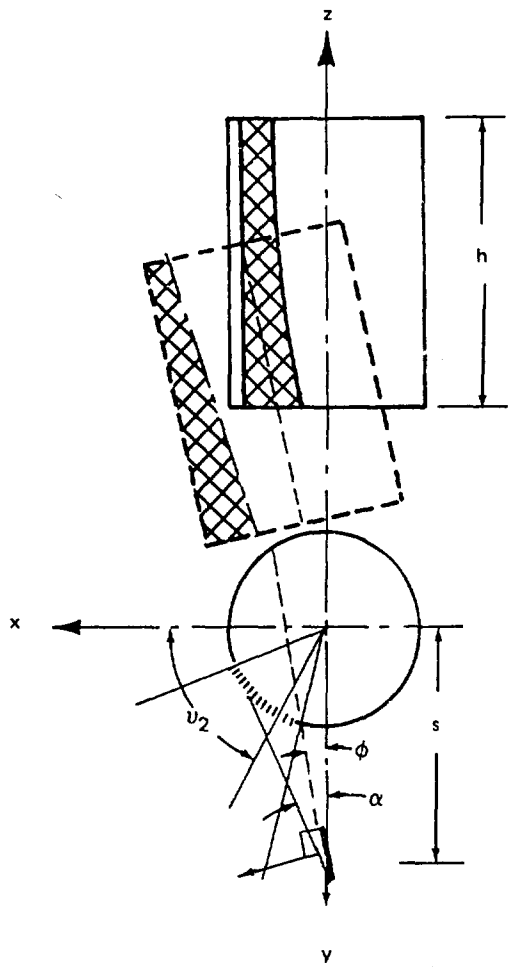

FIGURE 2.4.4b

Case 3.1.3 $n = 0,\ m = -1,\ \ell = 0$

The entire flame is seen, hence

$$VF = I\ (1,\ \ell,\ m,\ n,\ s,\ h) \qquad (13.26)$$

Case 3.2.2 $n = 0,\ -1 < m < 0,\ -1 < \ell < 0$

3.2.2.a

when $\phi \geq \alpha$

$$VF = I\ (1,\ \ell,\ m,\ n,\ s,\ h) \qquad (13,27a)$$

3.2.2.b

$$\phi < \alpha$$

Referring to Figure 3.2.2.b we have,

$$1 = s^2 + PC^2 - 2PC\ s\ \cos\phi$$

$$PC = s\ \cos\ \phi - \sqrt{s^2\ \cos^2\phi - (s^2 - 1)}$$

$$= s\ \cos\phi - \sqrt{1 - s^2\ \sin^2\phi}$$

$$\text{and } \nu_1 = \cos^{-1}\ (PC\ \sin\phi)$$

$$= \cos^{-1}\ [\sin\phi\ (s\ \cos\phi - \sqrt{1 - s^2\ \sin^2\phi})]$$

$$VF = I\ (2,\ \ell,\ m,\ n,\ s,\ 0,\ \nu_1,\ \pi-\alpha)$$

$$+ I\ (3,\ \ell,\ m,\ n,\ s,\ \pi-\alpha,\ 0,\ h)$$

$$- I\ (2,\ \ell,\ m,\ n,\ s,\ h,\ \nu_1,\ \pi-\alpha)$$

$$- I\ (3,\ \ell,\ m,\ n,\ s,\ \nu_1, 0,\ h) \qquad (13,27b)$$

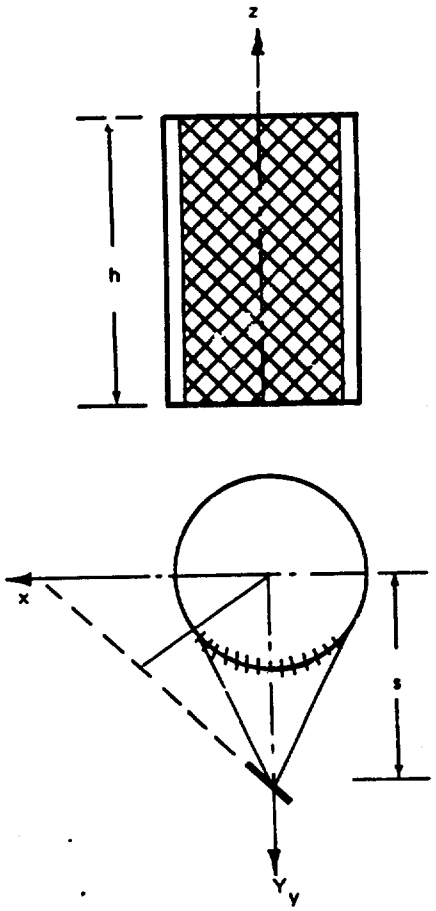

FIGURE 3.2.2a

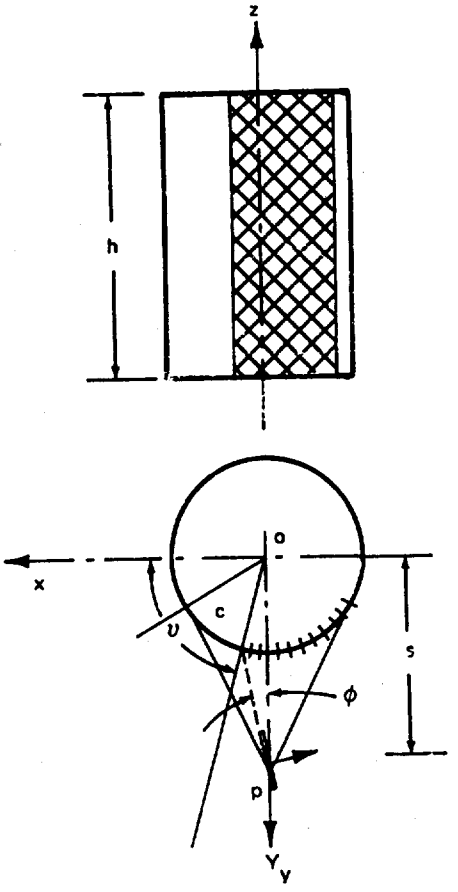

FIGURE 3.2.2b

Case 3.3.5 $n = 0, m = 0, \ell = 1$

Only half the flame is seen

$$VF = (1/2)\, I\ (1, \ell, m, n, s, h) \qquad (13.28)$$

The rest of the cases can be calculated using the Lemma derived.

13.6 COMPUTATIONAL ALGORITHM

The algorithm involves first the transformation of coordinates so that the cylinder is vertical with respect to the newly defined set of coordinate axes. The total view factor is then calculated by summing the contributions from (or taking the difference of) the two parts into which the cylinder is divided by the plane containing the line of normal to the axis from the observer and which is also normal to the cylinder axis. This procedure is shown very concisely as a flow chart in Figure 13.5.

To calculate the view factor to a vertical cylinder the following procedure is employed:

1. Based on the values of the direction cosines (l m n) of the observation plane, the proper case number (see Table 13.2) is decided.

2. Then the view factor is calculated using the formula appropriate to that case number. These formulas have been given already in Section 13.5.

Some of the cases have symmetry or can be calculated from other cases. These are shown in Table 13.2. A flow chart is also given in Table 13.2. A computer program is written based on the above algorithm.

13.7 SPECIFIC EXAMPLE

To illustrate the computational procedure, a specific example is worked out:

- **Cylinder Data**

Diameter	D = 5 m
Length	L = 15 m
Tilt with respect to vertical	α = 45 deg.

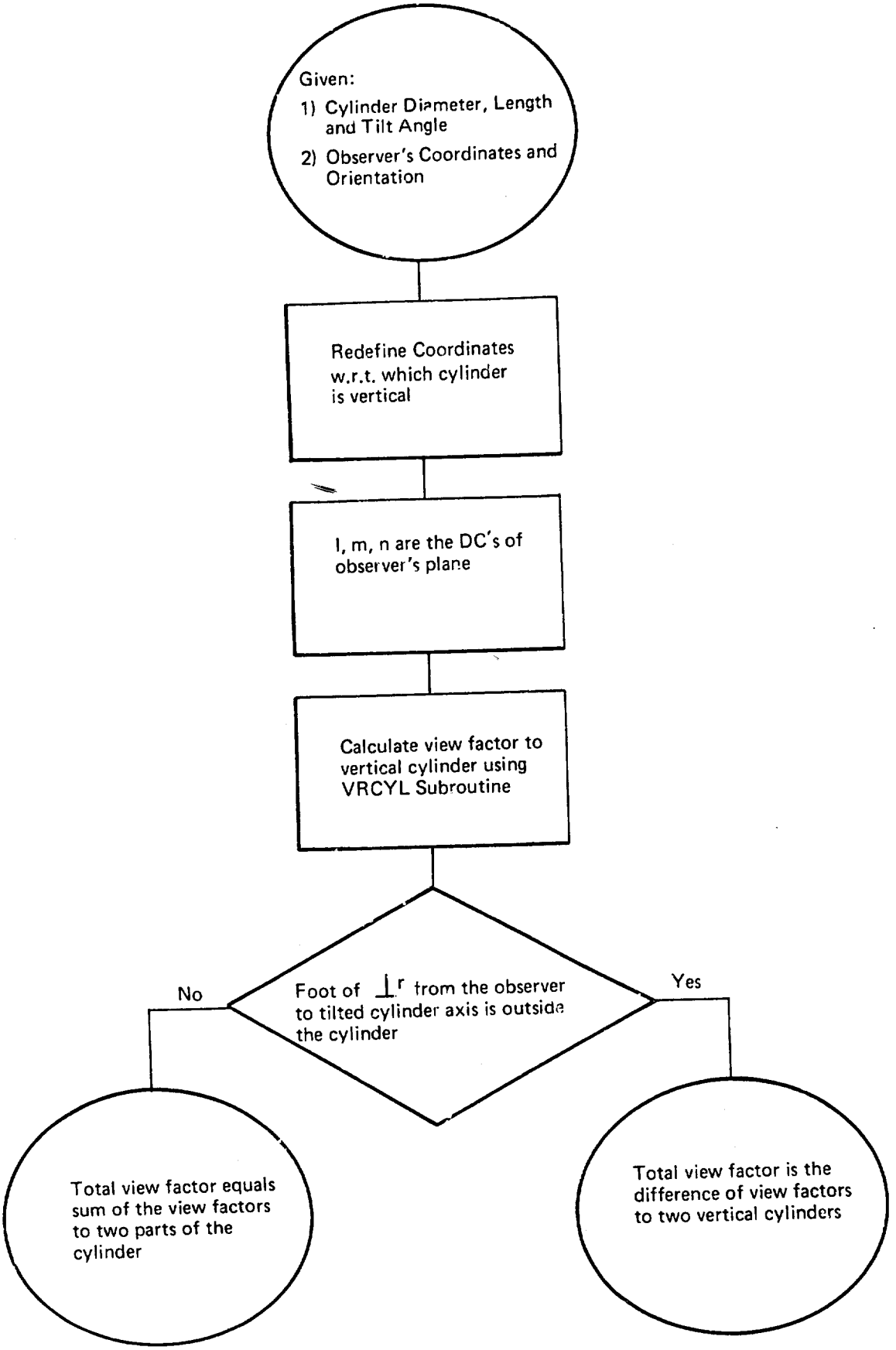

FIGURE 13.5 FLOW CHART FOR VIEW FACTOR CALCULATION

- **Observer Details**

Plane is on the ground, on the Y-axis, is vertical, and facing the cylinder. The view factors to the plane and at distances 1, 2, 3, ... and 20 diameters are calculated. The distances are measured from the point of intersection of the cylinder axis and the ground. The result is given in Table 13.3 and is also plotted in Figure 13.6.

13.8 DISCUSSIONS

The methods so far available in the literature for calculating the view factor between a cylinder and a plane, utilize the definition of the view factor (Eq. (13.1)) and a numerical integration procedure. This procedure involves the subdivision of the cylinder surface into a number of small areas, calculating the view factors between these subdivision areas and the observation plane, and summing up all the results to obtain the final view factor. The disadvantages of this method are that:

a. The accuracy of the result depends on the number of subdivisions, and

b. The computational time increases as the square of the number of subdivisions. To overcome these difficulties the analytical method given in Section 13.5 was undertaken.

The method presented is based on the fact that the view factor area integral (Eq.(13.1)) can be converted to a line integral (Eq. (13.3)) based on Stokes' theorem. The contour of integration is the line bounding the area on the cylinder that can be "seen" by the observation plane. The methods presented in Section 13.5 identify the contours for the different cases of orientation of the observation plane and indicate the final results after integration. Except in two cases (when numerical integration of the line integrals are essential), all other integrals have been solved in terms of the standard mathematical functions.

The specific example shown in Section 13.6 indicates that the computational time, using the results of the above analysis, is about one-tenth of the time for the same results using a 6 x 12 subdivision of the cylinder and the numerical integration of the Eq. (13.1)).

It is expected that the results of this analysis will be useful in plotting contours of constant heat flux on the ground surface around a pool fire.

13.9 CONCLUSIONS

An analytical method for calculating the view factor between a right circular cylinder and an elemental plane area has been presented. The method is based on contour integrals and is a very general method. The main feature of the method is that it is applicable to a cylinder of any size, any inclination, and for arbitrary position and orientation of the observer.

Because of the straightforward nature of the calculations the computational time is an order of magnitude less than other numerical procedures.

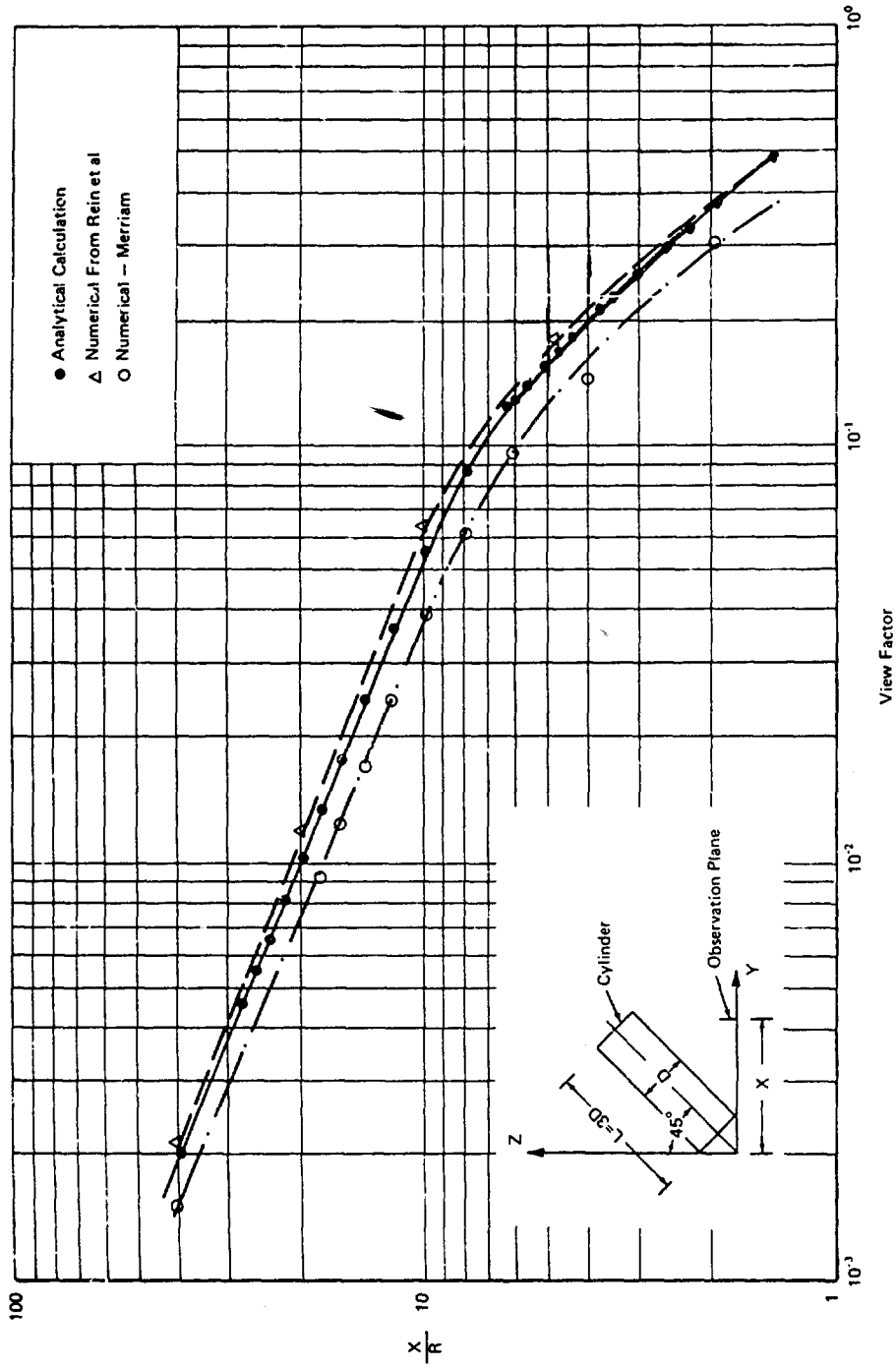

FIGURE 13.6 COMPARISON OF VIEW FACTORS OBTAINED BY ANALYTICAL AND NUMERICAL METHODS FOR A PARTICULAR CASE

13.10 REFERENCES

1) Rein, R. G., Sliepcevich, C. M., and Welker, J. R., "Radiation View Factors for Tilted Cylinders," J. Fire and Flammability; n1, 1970, pp. 140-153.

2) Merriam, R. L., View Factor between an Inclined Cylinder and a Plane – A Numerical Method," Arthur D. Little, Inc., internal report, 1972.

3) Hottel, H. C., and Sarofim, A. F., "Radiative Transfer," McGraw-Hill, Inc., 1967, p. 39.

4) Wiebelt, J. A., "Engineering Radiation He Transfer"; Holt, Rinehart, and Winston, Inc. New York, 1966, pp. 82-84.

13.11 LIST OF SYMBOLS

Symbol	Description	Units
A_1	area of the observation plane	m^2
A_2	area on the cylinder surface seen by plane of area A_1	m^2
D	diameter of the cylinder	m
dA_1	elemental area of plane at position 1	m^2
$F_{dA_1 \longrightarrow A_2}$	view factor between dA_1 and cylinder	
H	height of an upright cylinder	m
h	dimensionless height of cylinder = H/R	
$\vec{i},\vec{j},\vec{k}$	unit vectors in X,Y, and Z directions	
L,M,N	direction cosines of the normal to plane dA_1, measured with respect to original coordinates X,Y,Z	
ℓ,m,n	direction cosines of the normal to plane dA_1 measured with respect to transformed coordinates x,y,z	
Q	heat flux received by a unit area at the position A_1 (Eq. (13.2))	W/m^2

Symbol	Description	Units
R	radius of the cylinder	m
$\vec{r}$	a vector joining any two points in space. When only one subscript is used, it represents the radius vector from the origin to the point. When two subscripts are used, the direction of the vector is from the first point to the second.	
r	magnitude of vector $\vec{r}$	
S	distance to the observation point 1 from the origin of coordinates	m
s	non-dimensional distance = S/R	
T_f	flame temperature	°K
X.Y.Z	coordinates of the observation point with respect to the original system of coordinates	m
x.y.z	coordinates of the observation point with respect to the transformed axes	m
Greek Letters		
α	tilt of the cylinder axis with respect to the Z coordinate. Also used as the angle that the tangent from the observation point on the ground to the cylinder circle makes with the negative y axis (Eq. (13.18))	radian
β	angle with the ground made by a plane, passing through the point of observation and at the same time being tangent to the top of the cylinder (see Figure 13.4)	radian
β'	angle defined in Figure 13.4 and Eq. (13.18)	radian
β''	angle defined in Figure 13.4 and Eq. (13.18)	radian
ϵ	emissivity of the cylinder surface	radian

θ	principal value of the angle made by the normal to the observation plane, with the z axis	radian
ν	any arbitrary angle with respect to the x axis	radian
σ	Stefan-Boltzmann constant	
τ	transmissivity of the medium in between the cylinder and the observation plane	
ϕ	principal value of the angle made with respect to the x axis, by the projection of the normal to the observation plane on the x-y plane	radian

Note: principal value of an angle is the value that lies between 0 and $\pi/2$ radians

Subscript

1	refers to the point of observation
2	refers to any point on the surface of the cylinder
max	equals maximum

LEMMA

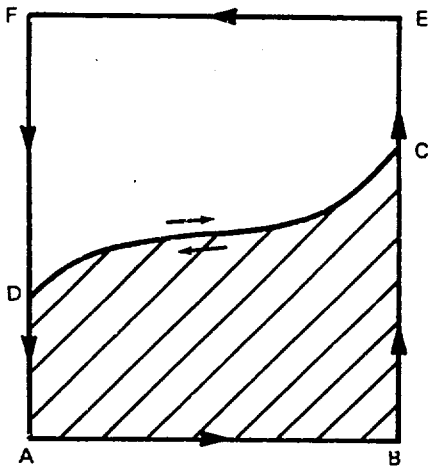

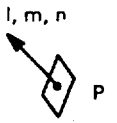

Suppose we know the view factor from region ABCD of the cylinder to an observer at P and also the view factor from ABEF (the total view) then to show that

$$F_{DCEF} = E_{ABEF} - F_{ABCD} \tag{1}$$

Now

$$F = \sum_{\ell,m,n} \ell \oint \frac{(z_2 - z_1)\, dy_2 - (y_2 - y_1)\, dz_2}{\pi\, r^2} \tag{2}$$

(3)

$$F_{ABEF} = \sum_{\ell,m,n} \ell \oint_{ABEF} (-------)$$

$$= \sum \ell \left\{ \int_{AB}(\cdots) + \int_{BE}(\cdots) + \int_{EA}(\cdots) + \int_{FA}(\cdots) \right\}$$

By representing the integrals on different contours I_s we have

$$F_{ABEF} = I_{AB} + I_{BE} + I_{EF} + I_{FA} \tag{4}$$

Noting that $I_{BE} = I_{BC} + I_{CE}$

and $I_{FA} = I_{FD} + I_{DA}$ (5)

Also noting $I_{DC} = -I_{CD}$

Substituting Eq. (5) in (4) we have

$$F_{ABEF} = (I_{AB} + I_{BC} + I_{CD} + I_{DA}) + (I_{CE} + I_{FE} + I_{FD} + I_{DC})$$

$$= F_{ABCD} + F_{DCEF}$$

Hence $F_{DCEF} = F_{ABEF} - F_{ABCD}$ QED

TABLE 13.1

CASE NOMENCLATURE TABLE

The following nomenclature is used to denote each of the different cases of orientation of the observation plane.

Case: N.M.L

Value of N	Value of n	Value of M	Value of m	Value of L	Value of ℓ
1	$= -1$	1	$= -1$	1	$= -1$
2	$-1 < n < 0$	2	$-1 < m < 0$	2	$-1 < \ell < 0$
3	$= 0$	3	$= 0$	3	$= 0$
4	$0 < n < 1$	4	$0 < m < 1$	4	$0 < \ell < 1$
5	$= 1$	5	$= 1$	5	$= 1$

All cases are not possible because of the restriction

$$\ell^2 + m^2 + n^2 = 1$$

Case 1.3.3 is a possible case

Case 1.1.1 is impossible

TABLE 13.2

FLOW CHART FOR CALCULATING THE VIEW FACTORS FOR DIFFERENT ORIENTATIONS OF THE OBSERVATION PLANE

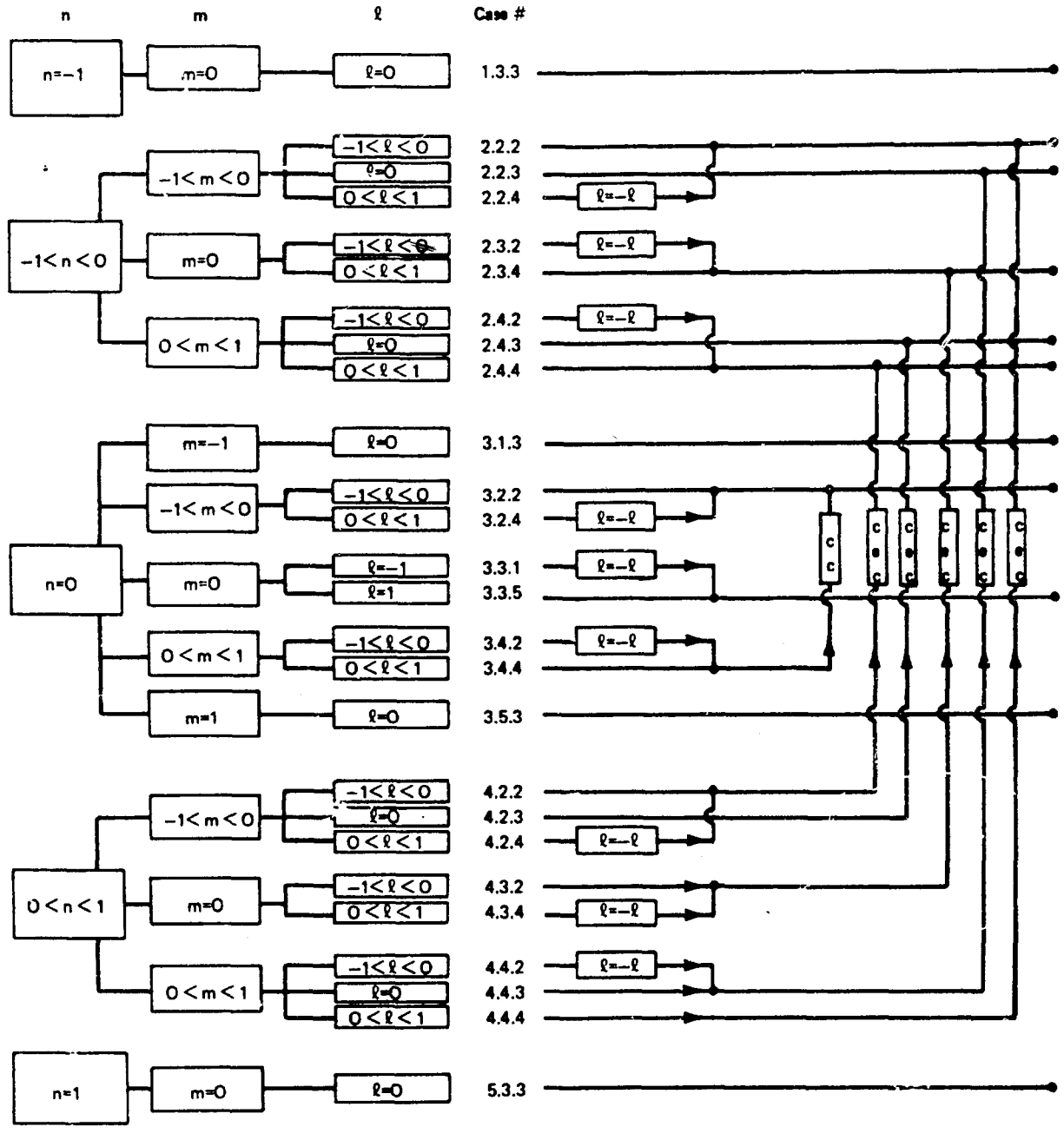

TABLE 13.3

VIEW FACTOR BETWEEN A PLANE ON THE GROUND AND A CYLINDER TILTED AT 45 DEGREES TO THE VERTICAL AND OF LENGTH THRICE THE DIAMETER

Distance s = S/R	View Factor
2.0	0.392153
4.0	0.210337
6.0	0.132977
8.0	0.087764
10.0	0.055170
12.0	0.035729
14.0	0.024411
16.0	0.017542
18.0	0.013143
20.0	0.010186
22.0	0.008113
24.0	0.006608
26.0	0.005483
28.0	0.004620
30.0	0.003946
32.0	0.003408
34.0	0.002973
36.0	0.002616
38.0	0.002319
40.0	0.002070

View factor between a plane on the ground and a cylinder tilted at 45 degrees to the vertical and of length thrice the diameter.

14.0 SENSITIVITY ANALYSIS

In this section the sensitivity of the results obtained in each model to the various input parameters is discussed. The main input parameters are listed and the effect of each on the final answer is studied, with the results given quantitatively wherever possible. In such cases where this is not possible, qualitative analyses are made.

14.1 VENTING RATE (Chapter 2.0)

The important input parameters are:

- The tank wall condition (isothermal or adiabatic)
- The tank initial pressure, and
- The size of the hole.

The rate of mass flow (either liquid or gas) is directly proportional to the diameter of the hole. For gas release the wall condition of the tank is quite important. Based on the analysis of the problem, the following statements can be made.

1. For a 100% change of the initial pressure drop there is only a 50% change in the initial mass flow rate, provided the pressure drop is still below the critical pressure drop for sonic condition at the orifice. For pressure above critical, the mass flow rate is insensitive to tank pressure changes.

2. The time to empty the gaseous contents of the tank, when the wall is adiabatic, is at least an order of magnitude greater than the time to empty when the wall is isothermal.

For liquid venting:

1. The rate of mass flow is fairly insensitive to initial tank pressure, provided the depth of liquid is large. For example, for a 20-foot depth of a liquid of density equal to that of water, and for a change of tank initial pressure ranging from 15 to 20 psig (i.e., a 33% increase in gauge pressure), the increase in the initial flow rate is about 15%. If the liquid depth above hole center were 2 feet (instead of 10 feet), then, for the same increase in tank pressure, the increase in initial mass flow would be 15.4%. Even if the initial depth of liquid were 50 feet, and the change in pressure were 33%, the change in initial flow rate would be only 14%. This shows that the fractional change in mass flow rate is about one-half the fractional change in pressure, and this is insensitive to the initial liquid depth. However, for a 100% change in the depth there is a 50% change in the flow rate when the pressure is maintained the same.

2. The liquid discharge rate is unaffected by the wall condition.

3. The total mass flow from the tank is orders of magnitude larger for liquid venting than for gas venting.

14.2 SPREADING OF A LIQUID ON WATER (Chapter 3.0)

The important input parameters for this model are the volume of spill, the density of the liquid, and the surface tension of the liquid. The result obtained is the radius (or length in channel spill) as a function of time. The result is insensitive to the viscosity of the liquid so long as it is very much (at least one order of magnitude) larger than the viscosity of water. For radial spreading we can make the following observations:

1. In the gravity-inertia regime, the radius of spread changes only by 19% for a 100% change in spilled volume (when the radius is evaluated at the same time).

2. In the gravity-viscous regime for a 100% change in the spill volume, the change in the value of the radius calculated (for identical times) is about 23%.

3. In the viscous-surface tension regime the radius of spread is independent of the volume of spill, but is a square root function of the surface tension; i.e., for a two-fold increase in surface tension, the increase in radius is about 40%.

A similar analysis can also be carried out very easily for one-dimensional spreads.

14.3 MIXING AND DILUTION

The result obtained in this model is the concentration of the chemical in the water as a function of spatial position, time, and geometry of the water region. The concentration predicted is directly proportional to the quantity of mass spilled (or rate of mass spill); that is, a 1% change in mass spilled causes a 1% change in concentration. The dependence of the maximum concentration on the velocity and the geometry is more complicated.

In the case of a river (non-tidal) the maximum concentration predicted, close to the spill point, at a particular instant is inversely proportional to the square root of the velocity cubed; that is, a 1% change in the velocity causes a 1.5% change in concentration. For tidal rivers approximately the same results also hold. However, the velocity considered should be the tidal velocity instead of the stream velocity.

The dependence of the concentration on the geometry is very complicated. The rougher the surface of the channel, the greater is the turbulence and the smaller the concentration. The concentration is also inversely proportional to the cross-sectional area for large distances from the point of spill. For shallow rivers the near-field concentration

varies as $(\text{depth})^{1.25}$; that is, for a 1% change in depth, the change in concentration is − 1.25%. The far field concentration varies inversely with depth; that is, for a 1% change in depth, − 1% change in the concentration results, with the other parameters remaining the same.

14.4 VAPOR DISPERSION

The principal factors that influence the concentration of vapor in the atmosphere (after the spill of a cryogenic liquid) are:

1. The mean wind velocity,
2. The atmospheric condition (unstable, stable, neutral, etc.), and
3. The mass of the vapor liberated (or alternatively the rate of vapor liberation).

In the case of an instantaneous spill, the maximum concentration at any instant of time is affected by the wind velocity only in an indirect way. The wind velocity determines the distance (from the spill point) at which the peak concentration occurs at any given instant of time and, depending upon this, X the dispersion parameters σ_y and σ_z will be affected. These dispersion parameters can be represented by (approximately):

$\sigma_y \sim X^{0.9}$	for all weather conditions,
$\sigma_z \sim X^{2.5}$	for extremely unstable conditions (atmosphere A in Figure 4.2b),
$\sigma_z \sim X^{0.8}$	for neutral conditions (atmosphere D), and
$\sigma_z \sim X^{0.5}$	for stable conditions (atmosphere F).

Considering an *instantaneous* spill and any given instant after the spill, we can show that:

$$X = Ut$$

$$dc/C = -[2d\sigma_y/\sigma_y + d\sigma_z/\sigma_z]$$

$$= -2 \times 0.9\, dx/x + n\, dx/x$$

$$= -[1.8 + n]\, dU/U$$

where n depends on the type of the atmospheric condition. Therefore, we see that the fractional change in the concentration of vapor with the velocity depends on the type of the atmosphere.

For a 1% change in the wind velocity the percent change in the concentration value predicted is:

– 4.3% for an unstable atmosphere,

– 2.6% for a neutral atmosphrere, and

– 2.3% for a stable atmosphere.

The above numbers also hold good for a constant velocity, but for change of concentration with 1% change in the downwind distance. The concentration and the vapor mass are in direct proportions; that is, for a 1% change in spilled mass, a 1% change in the concentration results.

14.5 FLAME SIZE

In discussing the sensitivity of flame size to the various physical input parameters, distinction has to be made between the flame size in a jet issuing from a hole in a tank and the flame size of a burning pool.

14.5.1 Jet Flame

The important input parameters that have great influence on the length of the jet flame are the nature of the chemical and the chemical formula of the substance burning (which directly gives the air/fuel ratio and reactants to the product's molar ratio), its molecular weight, and the adiabatic flame temperature. The diameter of the hole is also an important parameter.

It can be shown (see Eq. (5.1)) that for a high air/fuel ratio (i.e., >), and with the molecular weights of air and fuel being of the same order, that

$$dL/L \sim dr/r;$$

that is, a 1% change in the air/fuel ratio produces a 1% change in the length of flame. Similarly it can be shown that for r > 10 and r held constant

$$dL/L \sim (-3/2)\, dMf/Mf \;\; dM_f/M_f;$$

that is, a 1% change in the molecular weight of the fuel (which is assumed to be close to that of air) would result in a –1.5% change in the length. In exactly the same way the length is dependent in direct proportion of the diameter and approximately as the square root of the adiabatic flame temperature. Suffice it to say that the length of the jet flame is most sensitive to the molecular weight of the fuel.

14.5.2 Pool Burning

The important parameters on which the flame height depends are the burning rate and the pool diameter. From Thomas' correlation (see Eq. (5.4)) we can show that, with a constant-diameter pool, a 1% change in specific burning rate results in a 0.6% change in the length of the flame. Similarly, for a constant burning rate per unit area, a 1% increase in pool diameter gives an 0.7% increase in flame length; that is the flame height (or length) is sensitive more or less equally to both the burning rate and the diameter of the pool.

The flame tilt is quite insensitive to the Reynolds number of the wind but is quite sensitive to the wind velocity and the pool diameter, considered separately. Based on the Welker-Sleipcevich correlation (see Eq. (6.6)) the rate of change of angle with respect to wind velocity is given by

$$\theta\ (1 + 2\ \tan^2\ \theta)/\tan\theta\ d\theta/\theta = 1.6\ dU/U;$$

i.e., for a maximum rate of change of angle (as $\theta \longrightarrow 0$) a 1% change of velocity yields a 1.6% change of angle. Similarly with velocity constant, a 1% change in pool diameter results in a −0.8% change in angle for maximum variation. Hence, the angle of tilt is more sensitive to the wind velocity than to the pool diameter.

14.6 THERMAL RADIATION FROM FLAMES

The important input parameters for this model that have much influence on the result (heat flux) are the size and inclination of the flame and the position and orientation of the receiving element. The ambient conditions and the flame temperature and emissivity also have great influence on the heat flux received.

The sensitivity of the result to the variation of each of the parameters is considered separately and discussed below.

14.6.1 Flame Temperature

The heat flux received by the element varies as the fourth power of the absolute temperature of the flame. For a 1% variation in the flame temperature (absolute value), a 4% change in the heat flux results. As a further example, if the flame temperature changes from, say, 1500°F to 1800°F (i.e., a 15.3% increase in absolute temperature), the heat flux radiated from the flame would change by 77%. This example shows that, except for small changes (in the temperature of the flame), the percentage change in radiative heat flux received by the element is always greater than four times the percentage change in absolute temperature of the radiating body.

14.6.2 Flame Emissivity

The heat flux from the flame varies directly as the emissivity; that is, for a 1% change in emissivity there is a corresponding 1% change in heat flux.

14.6.3 Atmospheric Transmissivity

Water vapor in the atmosphere absorbs thermal radiation. The total absorption is a function of distance for which the radiation passes through the atmosphere and the water vapor partial pressure (a function of ambient temperature and humidity). The transmissivity is less sensitive to temperature for temperatures below 20°C than to the relative humidity. For distances less than 500 feet, a 100% increase in temperature (from 10°C to 20°C) results in a maximum change of transmissivity of −20% (from 0.6 to 0.5). However, no general sensitivity relationships can be given, since the dependence of atmospheric absorption on water vapor partial pressure and temperatures (of the source and the ambient) is quite complicated.

14.6.4 View Factor

The view factor depends entirely on the geometrical positions of the observer and the flame. A detailed analysis of the variation in view factor value with observer position and orientation is deferred to a later section (14.12).

Based on the above discussions, it is seen that the thermal flux from a flame (received by an observer) is most sensitive to the flame temperature.

14.7 SPREADING OF A LOW-VISCOSITY LIQUID ON A HIGH-VISCOSITY LIQUID

The result of this model, namely, the radius (or the length) of spread depends on the properties of the liquid spilled and the mass spilled. In discussing the sensitivity of the answer to various input parameters, we consider the different regimes of spread. Only radial spread is considered.

14.7.1 Gravity-Inertia Regime:

1. For a 100% change in the volume of spill, the radius calculated (at identical times) changes by only 19%. However, for much smaller changes in the spill volume, say 1%, the change in the radius is 0.25%; that is, the change of radius obtained for small changes in volume of spill is more sensitive than for large variations in volume.

2. The sensitivity of radius predicted to the density difference between the liquids is very small. Again for a 1% change in density difference, only 0.25% change in radius is obtained.

3. The duration for which the gravity-inertia regime lasts depends on the cube root of the spill volume.

14.7.2 Gravity-Viscous Regime:

1. The radius of spread is slightly more sensitive to the volume of spill than in the previous case, a 1% change in volume producing a 0.375% change in radius.

2. The spread extent is almost independent of the density difference between the two liquids because of the 1/8th power dependence (refer to Table 8.1).

3. The duration of which the gravity-viscous regime lasts is directly proportional to the volume; that is, an increase in spill volume correspondingly stretches the time for which the spreading is in the gravity-viscous regime.

4. The above duration is also a 1-to-1 function of the spreading liquid viscosity-density product; that is, a 100% increase in this product stretches this time by 100%.

5. The viscosity of water has no influence on the spreading. The radius of spread in this regime is very weak (−1/8 power) function of the kinematic viscosity of liquid; i.e., an eight-fold increase in kinematic viscosity has the same effect as a decrease of spilled volume by a factor of one-half.

14.7.3 Viscous-Surface Tension

1. The radius is quite insensitive to the volume, surface tension, and the liquid viscosity. A 4% increase in volume increases the radius by only 1%. Similarly, 4% increase in surface tension or a 4% decrease in absolute viscosity produces only a 1% increase in the radius.

The above analysis indicates that the radius is most sensitive to the volume of spill only in the gravity-viscous regime and even there its dependence cannot be considered strong.

14.8 SIMULTANEOUS SPREADING AND EVAPORATION OF A CRYOGEN ON WATER

The quantity of interest in this model is the rate of evaporation and the total duration for which the liquid evaporates. The main variables that influence these parameters, in addition to the mass of spill, are:

1. The difference in temperature between the water temperature and the cryogen boiling temperature; and

2. The boiling heat transfer coefficient for heat transfer between the water and the liquid.

It has already been shown in Chapter 9 that the radius of spread (in the gravity-inertia regime) is quite independent of the evaporation rates, even for material such as LNG (which evaporate quite rapidly). All of the discussions on the sensitivity of radius to both the volume of spill and the density of the liquid given in the previous sections apply to this also. The sensitivity of other results to the various inputs are discussed below.

14.8.1 Radial Spread without Ice Formation

1. The time for complete evaporation increases as the 1/4th power of the initial volume of spill; i.e., a 16-fold increase in volume will evaporate in only twice the time. Thus, the total time for which the cryogen is on the water is quite insensitive to the volume of spill.

2. The evaporation time is more sensitive to the change in the heat of vaporization. The larger the heat of vaporization, the larger is the time for evaporation. A 4-fold increase in latent heat results in a 2-fold increase in time. Similarly, a 100% increase in heat flux from water (or, alternatively, a 100% increase in heat transfer coefficient for the same temperature difference) results in a 30% decrease in the time for evaporation.

3. The time of evaporation is insensitive to the viscosity of the liquid. However, for very low heat fluxes (for $\Delta < 10^{-6}$, see Eq. (9.21)) this may not be true, as the evaporation will proceed in the gravity-viscous regime also. However, for most cryogens the statement is true.

4. The maximum pool radius depends more strongly on the initial spill volume. For a 1% increase in volume of spill the radius increases by a maximum of 0.355%. The dependence of this maximum radius is less sensitive than above for variations with heat flux, liquid density, and latent heat (see Eq. (9.15b)).

14.8.2 Radial Spreading with Ice Formation

1. The time for complete evaporation varies as the cube root of the volume of spill; that is, for an 8-fold increase in volume, the time for evaporation increases by twice the previous value. This dependence is stronger than in the constant heat flux (no ice) case.

2. A 1% increase in latent heat results in a 0.67% increase in the time of evaporation. However, a 1% increase in the difference in temperature between water and the cryogen results in a 0.33% decrease in time of evaporation. This is contrasted with a 0.5% decrease for the case of constant heat flux (and constant heat transfer coefficient).

3. The maximum radius of spread is proportional to the square root of volume; that is, a 1% increase in volume results in a 0.5% increase in radius.

The above analysis shows that both the time for evaporation and the maximum extent of spread are more sensitive to the volume of spill in the case when the ice forms than in the case where there is no ice formation.

A similar analysis can also be carried out for one-dimensional spreads (see Table 9.2).

14.9 SIMULTANEOUS SPREADING AND COOLING OF A HIGH VAPOR PRESSURE CHEMICAL

The main input parameters of the model are the mass of spill and the vapor pressure-temperature relationship for the liquid spilled. The results obtained from the model are the evaporation rates as functions of time and the total time for complete evaporation of the chemical. The spreading of the chemical is quite independent of the evaporation (see the discussion in Section 9.8) and, as such, all the relations on sensitivity of radius to the volume of spill and the liquid properties hold (discussed in previous sections). In this section the sensitivity of the evaporation time value and the evaporation rate to the various physical parameters are discussed.

1. The time for complete evaporation varies approximately as the cube root of the mass spilled; that is, for a 3% increase in mass spilled, the time increase is 1%.

2. Increasing the initial liquid temperature results in a smaller time for complete evaporation. The sensitivity of the result to this initial temperature change depends on the nature of the chemical (through the saturation pressure-temperature relationship). As an example, for diethyl ether spilled on water at 20°C, we find that increasing the spill tempaeraute from 20°C to 25°C (about 2% increase based on absolute temperature) results in a 17%

decrease in time for complete evaporation. For a 10°C rise in spill temperature (from 20°C to 30°C), i.e., a 3.3% increase, the resultant decrease in time for total evaporation is about 28%. It is noted that a small increase in temperature results in a large decrease in time (a 1% temperature rise results in a 12% decrease in time).

The above analysis indicates that the effect of initial temperature is more pronounced than the effect of spill mass on the time for complete evaporation.

14.10 MIXING AND DILUTION OF A HIGH VAPOR PRESSURE, HIGHLY WATER-SOLUBLE CHEMICAL

The main input parameters to the model are:

- The mass spilled,
- Geometrical information of the water region,
- The velocity of the stream, and so forth.

For calculating the concentration of the pollutant in water, the mixing and dilution theory discussed in Chapter 4 is used. The sensitivity of this concentration to various input parameters has been discussed in an earlier section. In this section the sensitivity of the quantity of vapor liberated to various inputs is discussed.

For spill in a non-tidal river, the following results hold good:

1. The duration for which vapor liberation occurs from the water surface is inversely proportional to the mean stream velocity; that is, a 1% increase in stream velocity results in a 1% decrease in the time for which vapor is liberated.

2. A 1% increase in spill mass results in a 0.67% increase in the time during which vapor is liberated.

3. The rate of evaporation is independent of the stream velocity, and it increases as the 2/3 power of the mass spilled.

4. The rate of evaporation is very sensitive to the temperature of the water. As an example, a water temperature change from 20°C to 21°C (0.35% based on the absolute temperature) results in 4.36% change in the evaporation rate. However, for a temperature change from 20°C to 30°C (3.3%) the corresponding change in evaporation is 51%.

5. The evaporation rate is dependent on the wind velocity over the water surface. This dependence is through the mass transfer coefficient. A 1% change in wind velocity results in about a 0.8% change in the evaporation rate.

14.11 BOILING RATE MODEL FOR HEAVY LIQUIDS WITH THE BOILING TEMPERATURE LESS THAN THE AMBIENT TEMPERATURE

The results obtained in this model are the evaporation rate as a function of time and the total time for all the spilled liquid to evaporate. The most important input parameters that have great influence on the final results are:

1. The surface tension,

2. The density of the liquid, and

3. The liquid-water temperature difference.

The effect of change in value of each of the above input parameters is considered below:

1. The time for complete evaporation varies almost as the square root function of the surface tension. For a 1% change in the value surface tension the total time of evaporation varies by 0.475%.

2. The rate of evaporation is an extremely weak function of the surface tension. For a 100% change in the surface tension, the change in evaporation rate is approximately 2.5%.

3. The size of the drops formed is an inverse square root function of the difference in density between the liquid and water; that is, of 1% increase in density difference causes a 0.5% decrease in the diameter of the drops formed.

4. A 1% change in density difference causes a 0.3% change in the evaporation rate. The time for evaporation is almost a direct inverse function of the density difference. A 1% increase in density decreases the time by 0.825%.

5. If all other parameter values are held constant, a 1% change in temperature difference between water and liquid causes a 1% change in the evaporation rate and a --1% change in the total time.

It is seen therefore, that the temperature difference has the greatest influence on the final results. Also the effect of surface tension on the evaporation rate is minimal.

14.12 RADIATION VIEW FACTOR BETWEEN AN INCLINED FLAME AND AN ARBITRARILY ORIENTED SURFACE IN SPACE

The result of this model is a unique value for the view factor. The input parameters are the size of the flame (diameter and length), the inclination of the flame, and the position and orientation of the observation plane.

It is extremely difficult to make a general sensitivity analysis for the whole problem. There are too many geometric variables to consider. However, for the purposes of a sensitivity study, we assume a vertical observation surface on the ground and consider only the variations in the flame length and flame tilt. Thus:

1. Irrespective of the angle of tilt, at large distances from the flame the view factor falls off an inverse square function of the distance; that is, a 1% increase in distance decreases the view factor by 2%.

2. For an angle of tilt less than 45 degrees, the above inverse square law holds for distances greater than about 5 flame diameters from the flame center.

3. For distances less than this, the view factor varies approximately as the inverse of the distance; that is, a 1% change in distance causes −1% change in the view factor.

4. For a fixed distance ($x/d \cong 5$) and small inclination angles (less than 30 degrees) the increase in length-to-radius ratio of the flame correspondingly increases the view factor. A 1% increase in length causes a 1% increase in the view factor.

5. For fixed distance and a L/D ratio, the view factor is insensitive to a change in the flame angle (for $0 < \theta < 45$ degrees) for distances greater than 5 diameters. Below this distance the view factor is weakly dependent on the angle.